AFRL-PR-ED-TR-2004-0041,
Vol. 2 of 2

AFRL-PR-ED-TR-2004-0041,
Vol. 2 of 2

Volume 2: History of the AFRL/USC DARPA Program on Polynitrogen Chemistry

Karl O. Christe*
Ashwani Vij

Edited by Ronald E. Channell

*** ERC, Inc.**
10 E. Saturn Blvd.
Edwards AFB, CA 93524-7680

AFRL/PRSP
10 E. Saturn Blvd.
Edwards AFB, CA 93524-7680

October 2004

Final Report

AIR FORCE RESEARCH LABORATORY
AIR FORCE MATERIEL COMMAND
EDWARDS AIR FORCE BASE CA 93524-7048

REPORT DOCUMENTATION PAGE

Form Approved
OMB No. 0704-0188

1. REPORT DATE *(DD-MM-YYYY)*	2. REPORT TYPE	3. DATES COVERED *(From - To)*
08-03-2004	Final Technical Report, Vol. 2	20 Feb 2002 to 30 Mar 2004

4. TITLE AND SUBTITLE

Volume 2: History of the AFRL/USC DARPA Program on Polynitrogen Chemistry

5a. CONTRACT NUMBER

5b. GRANT NUMBER

5c. PROGRAM ELEMENT NUMBER
63765E

6. AUTHOR(S)

Dr. Karl O. Christe* and Dr. Ashwani Vij

Edited by Dr. Ronald E. Channell

5d. PROJECT NUMBER
DARP

5e. TASK NUMBER
A205

5f. WORK UNIT NUMBER
549718

7. PERFORMING ORGANIZATION NAME(S) AND ADDRESS(ES)

*ERC, Inc.
10 E. Saturn Blvd.
Edwards AFB CA 93524-7680

AFRL/PRSP
10 E. Saturn Blvd.
Edwards AFB CA 93524-7680

8. PERFORMING ORGANIZATION REPORT NO.

9. SPONSORING / MONITORING AGENCY NAME(S) AND ADDRESS(ES)

Air Force Research Laboratory (AFMC)
AFRL/PRSP
10 E. Saturn Blvd.
Edwards AFB CA 93524-7680

10. SPONSOR/MONITOR'S ACRONYM(S)
XC

11. SPONSOR/MONITOR'S REPORT NUMBER(S)
AFRL-PR-ED-TR-2004-0041, Vol. 2

12. DISTRIBUTION / AVAILABILITY STATEMENT

Approved for public release; distribution unlimited.

13. SUPPLEMENTARY NOTES
This report is Volume 2 of 2 volumes. Vol 1 is entitled, "The Solid Gas Singlet Delta Oxygen Generator."

14. ABSTRACT

In the course of the High Energy Density Matter (HEDM) Program, which was initiated in 1986 by the Air Force, the potential of polynitrogen compounds for HEDM was recognized by numerous theoretical studies. However, no systematic efforts were undertaken to synthesize any of the potential candidates predicted by the theoreticians. This changed in 1998, when Dr. Oestmark from the Swedish Defense Research Agency proposed to DARPA an experimental study to prepare tetrahedral N_4. In response to this proposal and upon urging from the Air Force Research Laboratory, DARPA issued a broad solicitation for experimental efforts and funded eight programs in the polynitrogen area. One of these programs was the effort at the Air Force Research Laboratory at Edwards Air Force Base. This effort was led by Karl Christe, who is also a Research Professor at the Loker Research Institute of the University of Southern California in Los Angeles, CA, and was expanded one year later to include a program at USC. Because of the overlap and close cooperation between these two programs, the results are summarized in a single report.

15. SUBJECT TERMS
high energy density matter; HEDM; polynitrogen; chemistry; tetrahedral N4

16. SECURITY CLASSIFICATION OF:			17. LIMITATION OF ABSTRACT	18. NUMBER OF PAGES	19a. NAME OF RESPONSIBLE PERSON
a. REPORT	b. ABSTRACT	c. THIS PAGE			Ashwani Vij
Unclassified	**Unclassified**	**Unclassified**	A	143	19b. TELEPHONE NO *(include area code)* (661) 275-6278

Standard Form 298 (Rev. 8-98)
Prescribed by ANSI Std. 239.18

NOTICE

When U.S. Government drawings, specifications, or other data are used for any purpose other than a definitely related Government procurement operation, the fact that the Government may have formulated, furnished, or in any way supplied the said drawings, specifications, or other data, is not to be regarded by implication or otherwise, or in any way licensing the holder or any other person or corporation, or conveying any rights or permission to manufacture, use or sell any patented invention that may be related thereto.

FOREWORD

This Final technical report, entitled "History of the AFRL/USC DARPA Program on Polynitrogen Chemistry," presents Volume 2 of the results of a DARPA-funded study performed under JON DARPA205 by AFRL/PRSP, Edwards AFB CA. The Principal Investigator/Project Managers for the Air Force Research Laboratory were Dr. Robert Corley and Dr. Ashwani Vij.

This report has been reviewed and is approved for release and distribution in accordance with the distribution statement on the cover and on the SF Form 298.

/ s /
ASHWANI VIJ
Project Manager

/ s /
RONALD E. CHANNELL
Chief
Propellants Branch

/ s /
PHILIP A. KESSEL
Technical Advisor
Space & Missile Propulsion Division

This Page Intentionally Left Blank

TABLE OF CONTENTS

TABLE OF CONTENTS (CONT'D)

LIST OF FIGURES

Figure No. **Page**

LIST OF TABLES

Table No. **Page**

GLOSSARY

AFRL	Air Force Research Laboratory
CID	collision induced dissociation
DARPA	Defense Advanced Research Projects Agency
ESI-MS	electrospray ionization mass spectrometry
FT-IR	Fourier transform infrared
HEDM	High Energy Density Matter
HF	hydrogen fluoride
HOPG	highly oriented pyrolytic graphite
IP	ionization potential
ISU	Iowa State University
LDI	laser desorption ionization
NMR	nuclear magnetic resonance
PI	Principle Investigator
PNNL	Pacific Northwest National Laboratory
TOF	time-of-flight
USC	University of Southern California

EXECUTIVE SUMMARY

1. Discovery of the N_5^+ Cation and its Compatibility Studies with Energetic Anions

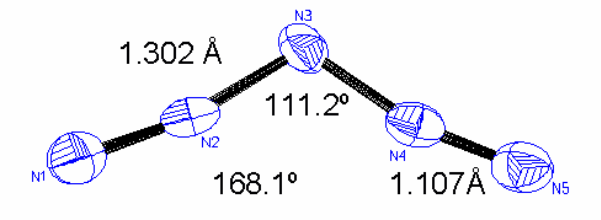

The experimental work at the Air Force Research Laboratory, Edwards AFB CA, was begun in the Fall of 1998. The following system was chosen for our first reaction:

$$N_2F^+AsF_6^- \quad + \quad HN_3 \xrightarrow[-78\ C]{HF} N_5^+AsF_6^- \quad + \quad HF \qquad (1)$$

Using both known starting materials, the reaction succeeded on the first attempt, and a white solid was obtained that was marginally stable at room temperature. The observed vibrational spectrum was in accord with the frequencies and intensities predicted for $N_5^+AsF_6^-$, and was further confirmed by ^{15}N substitution experiments, which showed the correct isotopic shifts, and by low-temperature $^{14}N/^{15}N$ NMR spectroscopy. The full scientific paper on N_5AsF_6 was published in the July 1999 issue of *Angewandte Chemie* [A].

The next major goals of synthesizing a more stable N_5^+ salt, $N_5^+SbF_6^-$, and the development of a scalable process for its safe production were subsequently achieved. Complementing this success were the process improvements for the starting materials, reducing the cost and time required for the synthesis of $N_2F^+SbF_6^-$ by about 80 %. The V-shaped geometry of the N_5^+ cation was confirmed by the crystal structure of $N_5Sb_2F_{11}$ [B]. During these studies, crystal structures of numerous N-F containing cations; i.e., ONF_2^+ [C], H_3NF^+, N_2F^+, $N_2F_3^+$, and NF_4^+, were determined.

The ready availability of stable N_5SbF_6 enabled study of its reaction chemistry and development of methods for converting it into other N_5^+ salts. Combination of the N_5^+ cation with anions, such as ClO_4^-, NO_3^-, N_3^-, was not successful due to lack of sufficient lattice energies. Two highly energetic salts, $N_5^+[B(N_3)_4^-]$ and $N_5^+[P(N_3)_6^-]$, containing >90 weight % nitrogen, were prepared, but are highly shock sensitive and thermally unstable. Since the discovery of the N_5^+ cation in 1998, a total of 12 N_5^+ salts have been isolated and characterized.

Of these 12 salts, $N_5B(CF_3)_4$, $N_5Sb_2F_{11}$, N_5SbF_6, and N_5SnF_5 are stable above room temperature, $(N_5)_2SnF_6$, N_5AsF_6, N_5PF_6, N_5BF_4, and N_5SO_3F are marginally stable at ambient temperature, while $N_5P(N_3)_6$, $N_5B(N_3)_4$, and $N_5HF_2 \cdot nHF$ are stable only at low temperatures [D]. The existence of FN_5 as a possible starting material for polynitrogen compounds was also investigated [E].

During our attempts to explore solvent compatibility with the azide ion, the new azido species, $(SO_2)_2N_3^-$, $SO_2N_3^-$ and $SO_3N_3^-$, were isolated and structurally characterized [F,G].

2. The Pentazolate Anion, *cyclo* - N_5^-

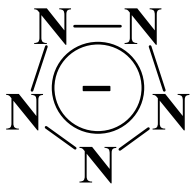

Although the existence and stability of substituted pentazole ring compounds was demonstrated successfully more than 40 years ago by Huisgen and Ugi, and substituted pentazoles have been well characterized, attempts to prepare either the parent HN_5 molecule or its anion, N_5^-, had been unsuccessful. In our pursuit of the N_5^- anion, the following strategy was employed: (i) the use of Ugi-Huisgen-type, substituted phenylpentazoles as starting materials; (ii) the transfer of maximum negative charge to the pentazole ring by the use of highly electron donating substituents on the phenyl ring in *para*-position to the pentazolyl substituent to increase the aromaticity and stability of the pentazole ring, while at the same time weakening the connecting C-N bond; (iii) the selective cleavage of the C-N bond while keeping the N-N bonds of the pentazole ring intact; and (iv) the use of an analytical method that is ideally suited for the generation and detection of anions. In the electrospray ionization mass spectrometry (ESI-MS) cleavage experiments, the desired negative ion peaks were mass-selected and subjected to product ion mass analysis following collision induced dissociation (CID) at variable collision

voltages using N_2 or Ar as the collision gases. An unambiguous proof for the formation of *cyclo*-N_5^- anions was obtained using normal and ^{15}N substituted starting materials. [H]. The bulk-synthesis of stable N_5^- salts is an important objective of this program which has not been accomplished so far. The possible existence of N_5^+ N_5^- and N_5^+ N_3^- was studied computationally. It was found that both compounds are unstable by large margins with respect to decomposition to $N_3^{\cdot}$ radicals and N_2. This conclusion was experimentally confirmed for N_5^+ N_3^- [I].

3. Synthesis and Characterization of the $FN(O)N_3^+$ Cation

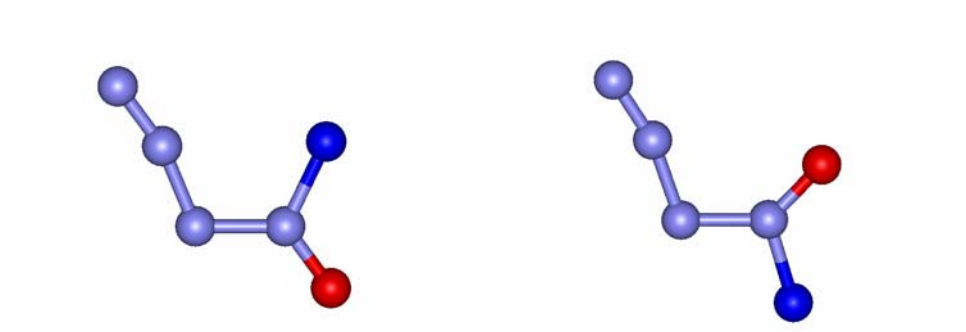

The *e*- and *z*- isomers of $FN(O)N_3^+$
red = oxygen, dark blue = fluorine.

Since the reaction of a nitrogen fluoride cation with HN_3 is an excellent synthetic tool for the formation of N-N bonds, this approach was applied to other systems, such as ONF_2^+, $N_2F_3^+$, and NF_4^+. The reaction of ONF_2^+ with HN_3 was successful and allowed us to isolate and characterize the novel $FN(O)N_3^+$ cation. Depending on the orientation of the oxygen/fluorine atoms with respect to the azide group, the structure can exist as either the *z*- or *e*-isomer, which was confirmed by vibrational and NMR spectroscopy and theoretical calculations.

4. Polyazides

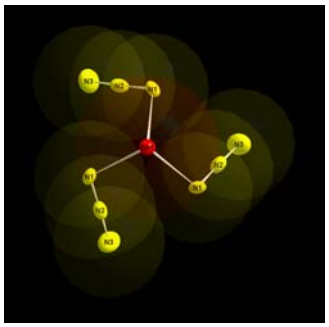

The azide group is highly energetic and adds ~ 70 kcal/mol endothermicity to a compound. Consequently, polyazides offer a unique opportunity to prepare nitrogen rich, highly energetic materials. Of particular interest to this program were polyazido anions, which might be useful as energetic counter-ions to polynitrogen cations, such as N_5^+. A large number of binary metal azides were characterized using vibrational and NMR spectroscopy, and x-ray crystallography [J]. Furthermore, an important issue about N-N bond distance anomalies in the case of mixed metal azide/chlorides was addressed. Since most of the metathetical reactions require anhydrous metal azide salts, a novel method was demonstrated to prepare cesium azide [K].

5. Azidamines

Azidamines represent an attractive class of HEDM materials, and only two azidamines were reported in the literature, about four decades ago. After carefully reexamining these reports, we were unable to duplicate the previous claims. The only covalent azide isolated from one of these systems was $CH_2(N_3)_2$, formed from the reaction of the solvent with NaN_3. Furthermore, condensation reactions involving $(CH_3)_2NCl$, one of the starting materials, gave rise to two novel compounds that were isolated and identified by their crystal structures. They are dimethylamino-methyltetrazole and an interesting 1-methylated 1,3,5-triazinium dication. Therefore, the previous claims of the existence of azidamines should be discredited.

As spin-off chemistry from the reaction of $(CH_3)_2$(t-butyl)$SiNCl_2$ with $N(CH_3)_4^+F^-$ in CHF_3 solution at low temperature, a solid product was isolated which, on warm-up to room temperature, yielded $(CH_3)_4N^+$ NCl_2^-, N_2 and NCl_3. Additional work is required to positively identify the expected intermediate $(CH_3)_4N^+$ NCl_2^-. The novel NCl_2^- anion would provide an ideal precursor for exploring the possible synthesis of the $N(N_3)_2$- anion.

Another interesting new compound was obtained when $[(CH_3)_3Si]_2NCl$ was reacted with HF and Lewis acids, such as BF_3, AsF_5, or SbF_5. In all cases, stable salts containing the novel NH_3Cl^+ cation were obtained. These salts develop, on exposure to moisture, NH_2Cl, a powerful disinfectant and biocide. The salts could serve as ideal safe solid storage media for NH_2Cl and might be used as gas generators for disabling chemical warfare agents, such as Anthrax.

References for Program Highlights

Appendix A: "N_5^+: A Novel Homoleptic Polynitrogen Ion as a High Energy Density Material," Angew. Chem. Int. Ed. 38, 2004 (1999)

Appendix B: "Polynitrogen Chemistry. Synthesis, Characterization, and Crystal Structure of Surprisingly Stable Fluoroantimonate Salts of N_5^+," J. Am. Chem. Soc., 123, 6308 (2001)

Appendix C: "Crystal Structure of $F_2NO^+AsF_6^-$ and Method for Extracting Meaningful Geometries from Oxygen/Fluorine Disordered Crystal Structures," Inorg. Chem., 40, 416 (2001)

Appendix D: "Polynitrogen Chemistry: Preparation and Characterization of $(N_5)_2SnF_6$, N_5SnF_5, and $N_5B(CF_3)_4$," Chemistry – A European Journal, 9, 2840 (2003)

Appendix E: "On the Existence of FN_5, a Theoretical and Experimental Study," J. Phys. Chem. A, 107, 6638 (2003)

Appendix F: "Synthesis and Characterization of the $SO_2N_3^-$, $(SO_2)_2N_3^-$, and $SO_3N_3^-$ Anions," Inorg. Chem., 41, 4275 (2002)

Appendix G: "The $(SO_2)_2N_3^-$ Anion," Inorg. Chem., 42, 419 (2003)

Appendix H: "Experimental Detection of the Pentaazacyclopentadienide (Pentazolate) Anion, *cyclo*-N_5^-," Angew. Chem. Int. Ed., 41, 3051 (2002)

Appendix I: "Enthalpies of Formation of Gas Phase N_3, N_3^-, N_5^+, and N_5^- from *Ab Initio* Molecular Orbital Theory, Stability Predictions for $N_5^+N_3^-$ and $N_5^+N_5^-$, and Experimental Evidence for the Instability of $N_5^+N_3^-$," J. Am. Chem. Soc., 126, 834 (2004)

Appendix J: "First Structural Characterization of Binary As(III) and Sb(III) Azides," Chemistry – A European Journal, 10, 508 (2004)

Appendix K: "Improved Synthesis of CsN_3," Z. Anorg. Allg. Chem., 628, 909 (2002)

BACKGROUND

In the course of the High Energy Density Matter (HEDM) Program, which was initiated in 1986 by the Air Force [Ref. 1], the potential of polynitrogen compounds for HEDM was recognized by numerous theoretical studies [Ref. 2]. However, no systematic efforts were undertaken to synthesize any of the potential candidates predicted by the theoreticians. This changed in 1998, when Dr. Oestmark from the Swedish Defense Research Agency proposed to the Defense Advanced Research Projects Agency (DARPA) an experimental study to prepare tetrahedral N_4. In response to this proposal and upon urging from the Air Force Research Laboratory (AFRL), DARPA issued a broad solicitation for experimental efforts and funded eight programs in the polynitrogen area. One of these programs was the effort at the Air Force Research Laboratory at Edwards Air Force Base. This effort was led by Karl Christe, who is also a Research Professor at the Loker Research Institute of the University of Southern California (USC) in Los Angeles, and was expanded one year later to include a program at USC. Because of the overlap and close cooperation between these two programs, the results are summarized in a single report. The following scientists were associated with this program and are shown in Figures 1 and 2:

Responsible Scientist (PI): Karl O. Christe

Senior Investigators at AFRL: William W. Wilson, Ashwani Vij, Vandana Vij, Jerry Boatz (Computational Chemistry), Jeff Mills (Computaional Chemistry), Jeff Sheehy (Computational Chemistry)

Air Force Program Managers: Pat Carrick, Jessica Harper, Jeff Sheehy, Robert Corley, Ashwani Vij

Senior Investigators at USC: Ross Wagner, Thorsten Schroer, Stefan Schneider, Michael Gerken, Ralf Haiges

Fig. 1. Members of the AFRL Group

From left to right: Ashwani Vij, Vandana Vij, Karl Christe, William Wilson, Robert Corley, Jerry Boatz, and Angelo Alfano (A. Alfano worked with Karl Christe on a DARPA-sponsored program for singlet delta oxygen generation).

Fig.2. Members of the USC Group

From left to right: Ralf Haiges, Thorsten Schroer, Ross Wagner, Stefan Schneider, Karl Christe, and Michael Gerken.

Collaborators: David Dixon (PNNL), David Feller (PNNL), Mark Gordon (ISU, Ames), Heather Netzloff (ISU, Ames), Ryan Olson (ISU Ames), Fook Tham (UC Riverside), James Pavlovich (UC Santa Barbara), Robert Bau (USC), Irena Tsyba (USC), Eduard Bernhardt (University Duisburg, Germany), Don Jenkins (University of Warwick, UK). The Program was guided by Drs. Art Morrish and Don Woodbury from DARPA.

I. Discovery of the N_5^+ Cation

The experimental work at the Air Force Research Laboratory, Edwards AFB CA, was begun in the Fall of 1998. Because N-N single and double bonds exhibit bond energies that are significantly smaller than one-third and two-thirds, respectively, of that of the N-N triple bond in dinitrogen, all polynitrogen compounds are highly endothermic with respect to decomposition to N_2. Therefore, very few reactions are known for the formation of N-N bonds, and multi-step syntheses are practically impossible. For these reasons, this research team's first target was a catenated rather than a cyclic or polycyclic compound. Furthermore, researchers realized that the fragments to be coupled had to already contain most of the desired energy; the coupling reaction had to be exothermic to proceed readily at low-temperatures; and a suitable solvent had to be used to provide a heat sink for the energy released in the coupling reaction. The synthesis of a polynitrogen cation also had to incorporate the use of one cation in the starting materials because the first ionization potentials of nitrogen compounds are around 300 kcal/mol. Final prerequisites were that the starting materials had to be readily accessible and that the desired product had to be resonance stabilized and could not contain any weak N-N single bonds. After some deliberation, the following system was chosen for the first reaction:

$$N_2F^+AsF_6^- \quad + \quad HN_3 \xrightarrow[-78\ C]{HF} N_5^+AsF_6^- \quad + \quad HF \qquad (1)$$

Both starting materials were known compounds, and there was still some $N_2F^+AsF_6^-$ on hand from previous work [Ref. 3]. With considerable luck and experimental skill (Fig. 3), the reaction succeeded on the first attempt, and a white solid was obtained that was marginally stable at room temperature and, most encouragingly, reacted explosively with water or organic materials. It was characterized by low-temperature Raman spectroscopy. The observed spectrum was in qualitative accord with expectations for a V-shaped N_5^+ cation, and *ab initio* calculations of the frequencies and intensities proved beyond doubt that we had indeed prepared $N_5^+AsF_6^-$.

This was further confirmed by ^{14}N substitution experiments which showed the correct ^{14}N-^{15}N isotopic shifts. Final proof for the presence of N_5^+ was obtained at Christmas 1998, with the help of Alan Kershaw at USC, by low-temperature nitrogen NMR spectroscopy which showed the

Fig. 3. Bill Wilson Shown Carrying Out a Typical $N_5^+AsF_6^-$ Preparation

predicted chemical shifts. A theoretical calculation for N_5^+ had been published by Pyykkoe and Runeberg in 1991 as part of a systematic study of the isoelectronic dicyanamide series, but little emphasis was given to N_5^+ as a possible new species [Ref. 4] and, therefore, it had escaped attention.

The successful synthesis of $N_5^+AsF_6^-$ was reported in January 1999 at the 14th ACS Winter Fluorine Conference in St. Petersburg, FL, and was an instant hit. It was only the second stable polynitrogen ever made, the first one being the azide anion, N_3^-, discovered by Curtius in 1890. Furthermore, a mishap during low-temperature Raman characterization, in which a few milligrams of material destroyed the recording apparatus (Fig. 4), caught the public's eye. Within one week, the discovery was highlighted in Chemical & Engineering News [Ref. 5]; and from there it spread like wildfire around the world. It was covered in the New York Times, the London Times, the New Scientist, the Hindu, Chemistry in Britain, the CPIA Bulletin, Nature, Aviation Week, Popular Mechanics, Chemistry & Industry, the Rheinische Post, etc, etc. It was also selected by Chemical & Engineering News as one of Chemistry's five top achievements in 1999 [Ref. 6].

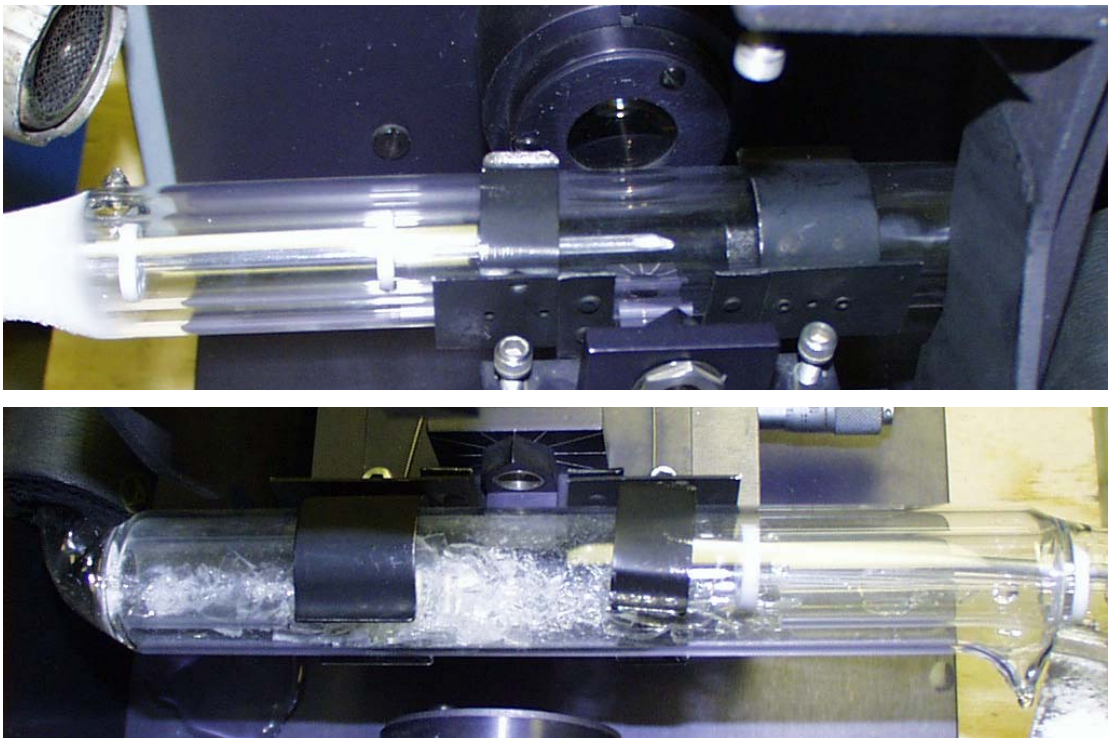

Fig. 4. Raman Apparatus Before (Upper Picture) and After (Lower Picture) the Mishap

The full scientific paper on N_5AsF_6 was published in the July 1999 issue of *Angewandte Chemie* [Ref. 7] and highlighted on the cover of this prestigious journal (see Fig. 5). This discovery was also covered by a US Patent in 2001 [Ref. 8].

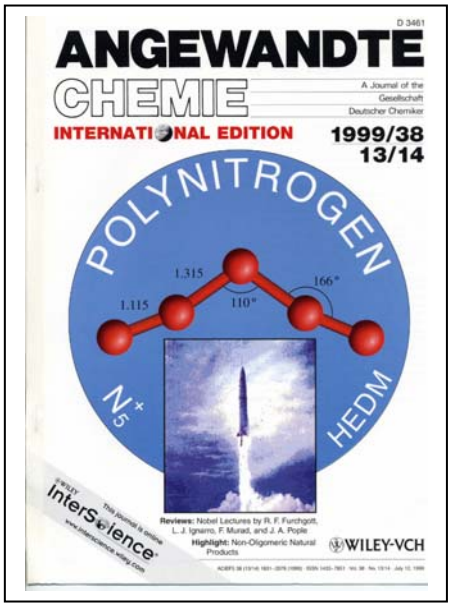

Fig. 5. Cover page of *Angewandte Chemie* with article on N_5AsF_6

This success with N_5AsF_6 prompted DARPA to increase the support of the work. The research team was able to hire two new colleagues, Dr. Ashwani Vij and his wife Vandana Vij, at AFRL and to set up a second laboratory at the University of Southern California in Los Angeles. With DARPA support, two old laboratories were completely rebuilt, which the late Prof. Anton Burg had generously made available for this program, and equipped for polynitrogen and HEDM work (Fig. 6). Dr. Ross Wagner, a retired former colleague from Rocketdyne, and four young German scientists, Drs. Thorsten Schroer, Stefan Schneider, Michael Gerken, and Ralf Haiges, who had come to USC as post-docs, joined the program.

Fig. 6. One Of The Six Walk-In Fume Hoods of the New USC Laboratory
Each fume hood is equipped with a custom-built stainless-steel/Teflon™ and glass vacuum line.

II. Synthesis and Scale-up Production of $N_5^+SbF_6^-$, a Stable N_5^+ Salt

The next major goals of the program were the synthesis of a more stable N_5^+ salt and the development of a scalable process for its safe production. These goals were accomplished at AFRL/Edwards by the synthesis of $N_5^+SbF_6^-$ according to Eq. 2.

$$N_2F^+SbF_6^- + HF \xrightarrow[-78 \text{ to } 20\ C]{HF} N_5^+SbF_6^- + HF \qquad (2)$$

Because SbF_5 is a stronger Lewis acid than AsF_5 [Ref. 9], N_5SbF_6 is considerably more stable than N_5AsF_6. It is stable up to about 60 °C and, surprisingly, is insensitive to mechanical shock

(as demonstrated by negative drop weight tests at 300 kg-cm). It was thoroughly characterized [Ref. 10], and the crystal structure of $N_5Sb_2F_{11}$ was determined (see Fig. 7). The experimental structure was in excellent agreement with earlier structure predictions, which were based on the good match between calculated and observed spectroscopic properties [Ref. 7].

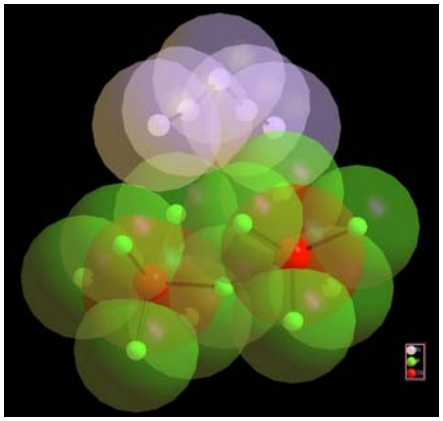

Fig. 7. Crystal Structure of $N_5^+Sb_2F_{11}^-$ Shown as a Space-Filling Model

The synthesis of N_5SbF_6 was successfully scaled up to the 5 gram level. During this sale-up, the handling of large amounts of shock-sensitive pure HN_3, generated from NaN_3 and stearic acid, had led to numerous explosions with significant damage to equipment (see Fig. 8). This problem was overcome by the generation of HN_3 from NaN_3 and a large excess of anhydrous HF and co-distillation of the HN_3 and HF, thus avoiding the handling of pure HN_3. This approach provided a very safe and scalable synthesis for N_5SbF_6.

Fig. 8. Typical Damage Caused by an HN_3 Explosion
One trap of the glass line is missing, and parts of it have penetrated the safety glass of the door.

The preparation of the $N_2F^+SbF_6^-$ precursor was a time-consuming, multi-step synthesis and involved the following individual reactions:

- Reduction of N_2F_4 to N_2F_2

$$\text{Graphite} + AsF_5 \longrightarrow C_{12}^{\bullet}AsF_5 \quad (3)$$

$$2C_{12}^{\bullet}AsF_5 + N_2F_4 \longrightarrow 2C_{12}^{+}AsF_6^{-} + \textit{trans}\text{-}N_2F_2 \quad (4)$$

- *trans-cis* isomerizatio of N_2F_2:

$$\textit{trans}\text{-}N_2F_2 + AsF_5 \xrightarrow{T/P} N_2F^+AsF_6^- \quad (5)$$

$$N_2F^+AsF_6^- + NaF \xrightarrow{HF} NaAsF_6 + \textit{cis}\text{-}N_2F_2 \quad (6)$$

- Formation of $N_2F^+SbF_6^-$:

$$\textit{cis}\text{-}N_2F_2 + SbF_5 \xrightarrow{HF} N_2F^+SbF_6^- \quad (7)$$

- If N_2F_4 is not available,

$$H_2NCONH_2 \longrightarrow F_2NCONH_2 \longrightarrow NHF_2 \longrightarrow N_2F_4 \quad (8)$$

These steps were significantly improved by replacing expensive highly oriented pyrolytic graphite (HOPG) with cheap mineral graphite flakes, and by replacing stoichiometric amounts of expensive AsF_5 in the tricky *trans-cis* isomerization of N_2F_2 with catalytic amounts of re-usable solid AlF_3. The latter improvement also eliminated the previously required displacement step between $N_2F^+AsF_6^-$ and NaF. Using these improvements, the cost and time required for the synthesis of $N_2F^+SbF_6^-$ were reduced by about 80 %.

III. N_5^+ Chemistry and Metathetical Syntheses of Other N_5^+ Salts

The availability of sufficient amounts of stable N_5SbF_6 enabled the research team to study its reaction chemistry and to develop methods for converting it into other N_5^+ salts. For example, its potential use as a reagent for introducing N_5 groups into aromatic rings by electrophilic substitution reactions was investigated at USC but was unsuccessful because of the high electron affinity and oxidizing power of N_5^+. Its electron affinity was experimentally determined [Ref. 10] using bracketing methods and substrates with known first ionization potentials. In this manner, researchers were able to show that N_5^+ is capable of oxidizing NO, NO_2, and Br_2 to NO^+, NO_2^+, and Br_2^+, respectively, but not Cl_2, O_2, or Xe.

Table 1. First Ionization Potential of Substrate (eV)

	Ionization Potential
$N_5^+SbF_6^- + NO \longrightarrow NO^+SbF_6^- + 2.5\,N_2$	9.26
$N_5^+SbF_6^- + NO_2 \longrightarrow NO_2^+SbF_6^- + 2.5\,N_2$	9.75
$N_5^+SbF_6^- + Br_2 \longrightarrow Br_2^+SbF_6^- + 2.5\,N_2$	10.52
$N_5^+SbF_6^- + Cl_2 \not\longrightarrow Cl_2^+SbF_6^- + 2.5\,N_2$	11.48
$N_5^+SbF_6^- + O_2 \not\longrightarrow O_2^+SbF_6^- + 2.5\,N_2$	12.07
$N_5^+SbF_6^- + 2\,Xe \not\longrightarrow Xe_2^+SbF_6^- + 2.5\,N_2$	12.13

Therefore, the electron affinity of N_5^+ must fall between 10.52 and 11.48 eV. This result is in excellent agreement with theoretical calculations [Ref. 11], which gave a value of 10.55 eV (243.3 kcal/mol) for the adiabatic electron affinity of N_5^+.

For the conversion of N_5SbF_6 into other N_5^+ salts, metathetical approaches were chosen that were similar to those used in the past to prepare many novel NF_4^+ salts [Ref. 12]. In this approach, the ions in two salts were exchanged. It required a compatible solvent in which both starting materials are soluble, and one of the products is soluble while the other one is insoluble, as shown schematically in Equation (9).

$$N_5^+SbF_6^- + A^+B^- \longrightarrow N_5^+B^- + ASbF_6\downarrow \qquad (9)$$

Because $CsSbF_6$ has a low solubility in anhydrous HF, and $NaSbF_6$ has a low solubility in SO_2 solution, these two solvents were studied extensively. It was found that HF works well in cases where the B^- anion is derived from an acid stronger than HF, and HF does not displace B^- from its salt. In this manner, the novel $(N_5^+)_2SnF_6^{2-}$ salt was successfully prepared (Eq. 10) and characterized at AFRL/Edwards [Ref. 13].

$$2\,N_5SbF_6 + Cs_2SnF_6 \xrightarrow[-78\ ^\circ C]{HF} (N_5)_2SnF_6 + 2CsSbF_6\downarrow \qquad (10)$$

This salt was a white solid that was marginally stable at room temperature and was somewhat friction sensitive. The successful isolation of this compound was particularly noteworthy,

because it demonstrated that salts with touching polynitrogen ions can be isolated. This achievement allows hope for the eventual synthesis of an ionic solid consisting exclusively of polynitrogen ions. Normally, large inert counterions, which can serve as spacers, are required to separate highly energetic ions and, thus, suppress propagation and spontaneous explosive decomposition. Another interesting aspect of this compound was its thermal decomposition. Under carefully controlled conditions, this compound was successfully stepwise decomposed and $N_5^+SnF_5^-$ was isolated (Eq. 11).

$$(N_5)_2SnF_6 \xrightarrow{25 - 30\ ^\circ C} N_5SnF_5 + \text{“}FN_5\text{”} \qquad (11)$$

The N_5SnF_5 salt was a white solid and had a thermal stability comparable to that of N_5SbF_6 (50 – 60 °C). The structure of the SnF_5^- anion in this compound is interesting and was shown by ^{119}Sn NMR spectroscopy to be a mixture of tetrameric and dimeric polyanions (see Fig. 9).

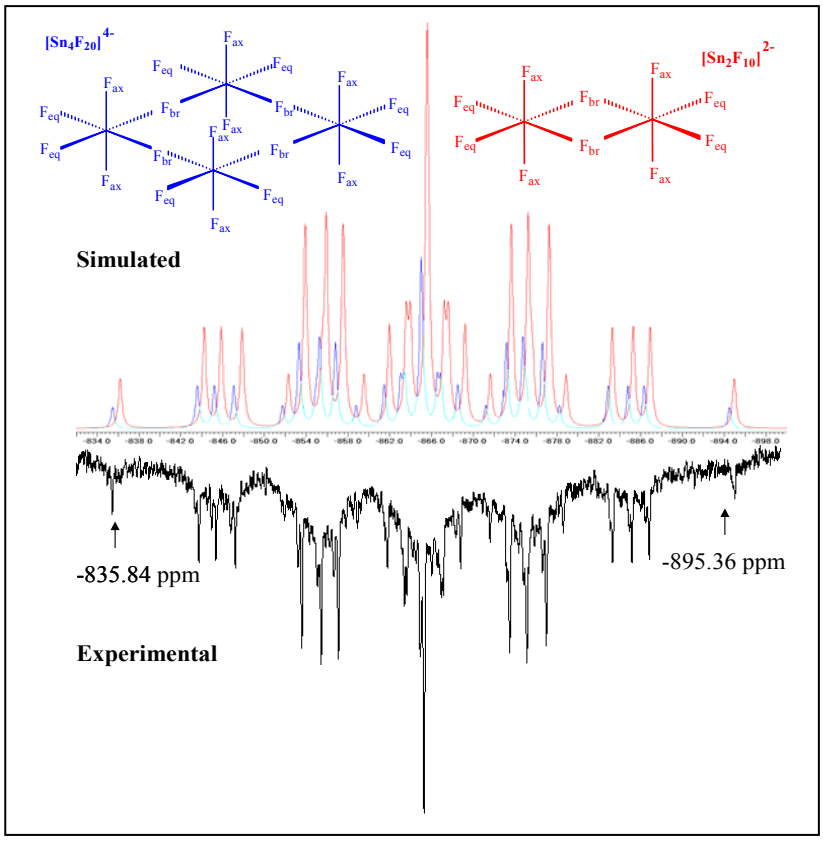

Figure 9. Observed (Black Trace) and Simulated ^{119}Sn NMR Spectra of $Sn_2F_{10}^{2-}$ (Red Trace) and $Sn_4F_{20}^{4-}$ (Blue Trace) in a 2 : 1 Mole Ratio

Attempts were made to detect the expected “FN_5” by-product by dynamic FT-IR spectroscopy; however, only its expected decomposition products, FN_3, N_2F_2, and NF_3, were observed. These

results prompted the research team to carry out, in collaboration with Mark Gordon's group, a theoretical study on the stability and lifetime of FN_5 [Ref. 14]. This study identified at least six vibrationally stable isomers of FN_5 but, in accord with experimental results, the predicted lifetimes of these species were in the nanosecond range.

Yet another N_5^+ salt, $N_5^+B(CF_3)_4^-$, was prepared by the metathetical route [Ref. 13]. For the synthesis of this compound, the use of anhydrous HF did not result in a good separation of the products, because their solubilities in HF were too similar. Therefore, SO_2 was used as a solvent (Eq. 12), and good product separation was achieved.

$$N_5SbF_6 + KB(CF_3)_4 \xrightarrow[-64\ ^\circ C]{SO_2} N_5B(CF_3)_4 + KSbF_6\downarrow \qquad (12)$$

The resulting $N_5B(CF_3)_4$ salt was a white stable solid which also decomposed between 50 and 66 °C. It appears that the thermal stabilities of most of the N_5^+ salts are similar and are governed by the stability of the N_5^+ cation itself.

In the course of working with the azide ion in SO_2 solution, an interesting observation was made. When colorless azide ions are dissolved in colorless liquid SO_2, bright yellow solutions are formed. To clarify this startling observation, the SO_2/azide system at USC was thoroughly characterized. It was found [Ref. 15, 16] that SO_2 forms well-defined 2:1 and 1:1 adducts with the N_3^- anion. In addition, crystals of the $SO_3N_3^-$ anion were obtained, and its crystal structure was determined (see Fig. 10).

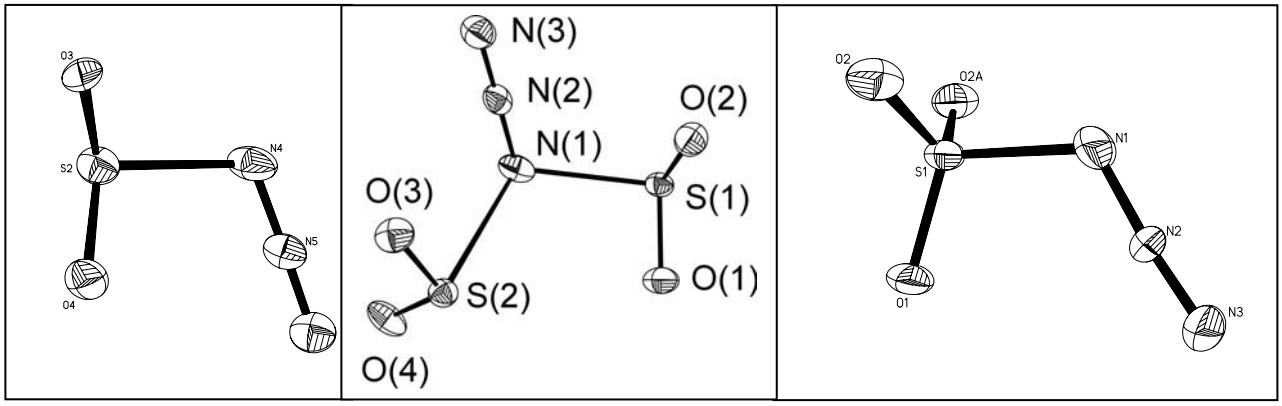

Fig. 10. Crystal Structures of the $SO_2N_3^-$, $(SO_2)_2N_3^-$, and $SO_3N_3^-$ Anions

The thermal instability of these SO_2/N_3^- adducts and their facile decomposition to CsN_3 and SO_2 was exploited at USC for the development of an improved synthesis of pure anhydrous

CsN_3 [Ref. 17]. Furthermore, the requirement for anhydrous cesium salts in metathetical reactions prompted researchers to develop at USC a general method for the syntheses of anhydrous cesium salts. It was based on the fact that NH_4^+ salts are usually non-hygroscopic and are readily available, whereas the corresponding cesium salts are highly hygroscopic and difficult to come by. Using a clever metathesis, in which the undesired by-product is thermally unstable and decomposes to volatile compounds, affords anhydrous cesium salts free of any impurities [Ref. 18]. The process can be exemplified by the generic Equations 13 and 14.

$$NH_4X + CsOCH_3 \longrightarrow CsX + [NH_4^+CH_3O^-] \qquad (13)$$

(X = Cl, CH_3CO_2, $N(NO_2)_2$, ClO_4)

$$[NH_4^+CH_3O^-] \xrightarrow{20\ C} NH_3 + CH_3OH \qquad (14)$$

$$N_5SbF_6 + CsN(CF_3)_2 \xrightarrow[-78\ C]{HF} N_5N(CF_3)_2 + CsSbF_6\downarrow \qquad (15)$$

In the course of an attempt to prepare $N_5^+N(CF_3)_2^-$ according to Eq. 15, an unexpected result was obtained. After removal of all volatile products at -64 °C, a clear colorless liquid was isolated. Its low-temperature Raman spectrum (Fig. 11) exhibited, in addition to some weak bands due to the Teflon™ container and a trace of SbF_6^- from the starting material, only bands due to N_5^+. This situation was reminiscent of a situation encountered many years ago with $NF_4^+HF_2^-\cdot nHF$ [Ref.

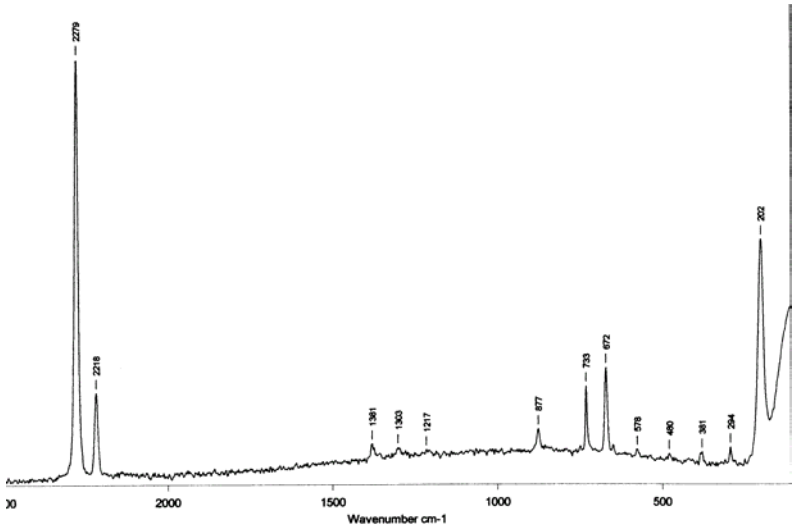

Fig. 11. Raman spectrum of $N_5^+HF_2^-\cdot nHF$

12c] and, indeed, the counter-ion in the present case was also polybifluoride. It was formed because a large excess of HF can displace $N(CF_3)_2^-$ from its salts with formation of $HN(CF_3)_2$ (Eq. 16).

$$N_5SbF_6 + CsN(CF_3)_2 + (n+1)\ HF \xrightarrow[-78]{HF} N_5HF_2{\cdot}nHF + CsSbF_6\downarrow + HN(CF_3)_2 \qquad (16)$$

On warm-up to room temperature, the $N_5^+HF_2^-{\cdot}nHF$ salt decomposes; however, like $NF_4^+HF_2^-{\cdot}nHF$, it is an extremely useful reagent for the synthesis of other salts derived from Lewis acids stronger than HF. This principle was demonstrated for the syntheses of $N_5^+BF_4^-$, $N_5^+PF_6^-$, and $N_5^+SO_3F^-$ (Eq. 17). All these new N_5^+ salts were white, marginally stable solids that were characterized by vibrational and NMR spectroscopy.

$$N_5HF_2{\cdot}nHF \ + \ BF_3 \xrightarrow[-78]{HF} N_5^+BF_4^- \ + \ (n+1)\ HF \qquad (17)$$

IV. N_5^+ Salts with Energetic Counter-Ions

Whereas the N_5^+ cation is a highly energetic ion with a calculated endothermicity of 351.6 kcal/mol [Ref. 11], all of the above-described counter-ions were non-energetic. Although the use of a doubly charged anion in $(N_5)_2SnF_6$ had allowed doubling of the N_5^+ and energy content, an energetic anion would be required for a true HEDM. For this reason researchers investigated the possibilities of combining the N_5^+ cation with energetic anions, such ClO_4^-, NO_3^-, N_3^-, and $P(N_3)_6^-$ by metathetical reactions in solvents, such as HF, SO_2, CHF_3, or CH_3CN (typical desired reactions are shown in Eq. 18-20).

$$N_5SbF_6 + CsNO_3 \xrightarrow[-64 \text{ to } 20°C]{SO_2} N_5NO_3 + CsSbF_6\downarrow \qquad (18)$$

$$N_5SbF_6 + CsClO_4 \xrightarrow[-78°C]{HF} N_5^+ClO_4^- + CsSbF_6\downarrow \qquad (19)$$

$$N_5SbF_6 + CsN_3 \xrightarrow[-64°C]{SO_2} N_5N_3 + CsSbF_6\downarrow \qquad (20)$$

The $CsNO_3$ reaction did not proceed as desired, because $CsNO_3$ is less soluble in SO_2 than $CsSbF_6$. Furthermore, there was not sufficient lattice energy available to stabilize the salt. Born-

Haber cycle calculations showed that stabilization would require 154 kcal/mol, while the estimate for the lattice energy of $N_5^+NO_3^-$ was only 129 kcal/mol. In the case of the perchlorate salt, the reaction proceeded but $NO^+ClO_4^-$ and N_2 were formed, and again the available lattice energy would have been insufficient (by 13 kcal/mol) to stabilize the salt. In the case of the azide ion, many reactions were carried out under different conditions, but only explosive decompositions were observed upon melting of the solvent containing the frozen reactants. The lattice energy deficit in this case was estimated to be 53 kcal/mol. A more thorough theoretical analysis, carried out in collaboration with Dave Dixon, Dave Feller, Don Jenkins, and Mark Gordon, showed that, after inclusion of entropy corrections, $N_5^+N_3^-$ was unstable by 76 kcal/mol with respect to spontaneous decomposition to N_3 and N_2, and that any experimental efforts in this direction would be doomed [Ref. 11]. Highly energetic N_5^+ salts have been successfully synthesized. $N_5^+[P(N_3)_6^-]$ was prepared (Eq. 21) and identified by low-temperature Raman spectroscopy (Fig. 12).

$$N_5^+SbF_6^- + Na^+[P(N_3)_6^-] \xrightarrow[-64\ C]{SO_2} N_5^+[P(N_3)_6^-] + NaSbF_6\downarrow \qquad (21)$$

It was, however, extremely shock sensitive and exploded with the slightest provocation with great violence (see Fig. 13). In addition to its high energy content, this salt is remarkable for its high nitrogen content of 91 weight %. $N_5^+[B(N_3)_4^-]$ was also prepared in a similar fashion, but again the salt was extremely shock sensitive and exploded on warm-up towards room temperature. Attempts to carry out this reaction with $Cs[B(N_3)_4]$ in HF solution were unsuccessful because HF reacts with $Cs[B(N_3)_4]$ to give $CsBF_4$.

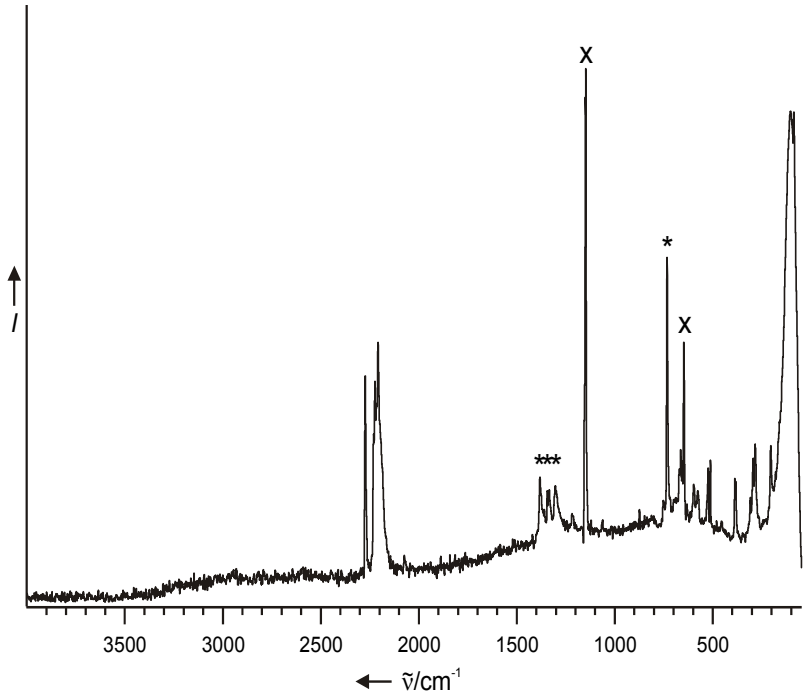

Fig. 12. Low-Temperature Raman Spectrum of $N_5^+[P(N_3)_6^-]$

Fig. 13. Typical Damage Caused by the Explosions of About 0.5 mmol of $N_5^+P(N_3)_6^-$
In the left picture, the explosion destroyed the heavy ceramic plate of a stirring plate. The right picture shows the close-up of an exploded Teflon™ reaction tube.

Researchers also attempted to prepare the tetrazolate salt, $N_5^+CHN_4^-$, from both the Cs^+ salt in HF solution and the Na^+ salt in SO_2 solution. In HF solution, the tetrazolate anion was displaced with evolution of the free tetrazole, while in SO_2 solution the solubilities were unfavorable for a metathesis. The syntheses of N_5^+ salts with anions derived from halogen

fluorides were also attempted using $NF_4^+HF_2^-\cdot nHF$ and halogen fluorides, such as ClF_3, as displacing agents, but the corresponding N_5^+ salts could not be isolated.

Since the discovery of the N_5^+ cation in 1998 a total of 12 N_5^+ salts have been isolated and characterized. All this work was carried out either at AFRL/Edwards or USC. Of these 12 salts, $N_5B(CF_3)_4$, $N_5Sb_2F_{11}$, N_5SbF_6, and N_5SnF_5 are stable above room temperature; $(N_5)_2SnF_6$, N_5AsF_6, N_5PF_6, N_5BF_4, and N_5SO_3F are marginally stable at ambient temperature; while $N_5P(N_3)_6$, $N_5B(N_3)_4$, and $N_5HF_2\cdot nHF$ are stable only at low temperatures.

V. Synthesis and Characterization of the $FN(O)N_3^+$ Cation

Because the reaction of a nitrogen fluoride cation with HN_3 had turned out to be such an excellent synthetic tool for the formation of N-N bonds, this approach was applied at AFRL/Edwards to other systems, such as ONF_2^+, $N_2F_3^+$, and NF_4^+. Whereas the NF_4^+ cation acted only as a fluorinating agent, fluorinating HN_3 to FN_3, followed by subsequent decomposition reactions of FN_3 (Eq. 22-25), the $N_2F_3^+$ and ONF_2^+ cations underwent F-N_3 exchange.

$$NF_4SbF_6 + HN_3 \xrightarrow{HF/-78\ C} NF_3 + HF + FN_3 + SbF_5 \qquad (22)$$

$$2\ FN_3 \longrightarrow 2\ N_2 + \textit{trans}\text{-}N_2F_2 \qquad (23)$$

$$HN_3 + HF + SbF_5 \longrightarrow H_2N_3SbF_6 \qquad (24)$$

$$3\ \textit{trans}\text{-}N_2F_2 \longrightarrow 2\ N_2 + 2\ NF_3 \qquad (25)$$

While in the case of $N_2F_3^+$, the desired $F_2NNN_3^+$ intermediate could not be isolated, and only the expected secondary reaction products were observed (Eq. 26-30), the reaction of ONF_2^+ with HN_3 allowed researchers to isolate and characterize the novel $FN(O)N_3^+$ cation (Eq. 31). This compound is a white solid that is stable up to -20 °C.

$$F_2NNF^+SbF_6^- + HN_3 \longrightarrow [F_2NNN_3^+SbF_6^-] + HF \qquad (26)$$

$$[F_2NNN_3^+SbF_6^-] \longrightarrow [F_2NNN^+SbF_6^-] + N_2 \qquad (27)$$

$$[F_2NNN^+SbF_6^-] \longrightarrow [F_2N^+SbF_6^-] + N_2 \quad (28)$$

$$[F_2N^+SbF_6^-] \longrightarrow NF_3 + SbF_5 \quad (29)$$

$$HN_3 + HF + SbF_5 \longrightarrow H_2N_3^+SbF_6^- \quad (30)$$

$$ONF_2^+SbF_6^- + HN_3 \xrightarrow{HF/-78\ C} FN(O)N_3^+SbF_6^- + HF \quad (31)$$

Depending on the orientation of the FN(O)- group, it can exist as either the *z*- or *e*-isomer (Fig.14). The compound was characterized by vibrational spectroscopy and, based on a comparison to the calculated spectra, was shown to contain both isomers in about the same ratio. Attempts to replace the second fluorine atom by another N_3 group were unsuccessful because, below its decomposition point, $FN(O)N_3^+$ did not react with HN_3.

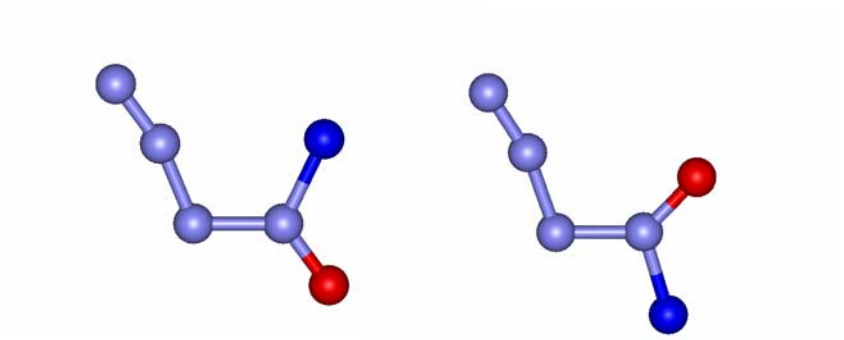

Fig. 14. The *e*- and *z*- Isomers of $FN(O)N_3^+$
Red = oxygen; dark blue = fluorine.

VI. Crystal Structures and Theoretical Calculations

A crystal structure determination constitutes definitive proof of the existence of a novel compound and provides exact information about its structure. Consequently, whenever possible, attempts were made to obtain crystal structures for both the novel compounds and crucial intermediates or starting materials. Because, in the beginning, the research team did not have its own diffractometer, a collaboration was formed with Dr. Fook Tham of UC Riverside. Since the transport and handling of highly energetic, sensitive, and unstable materials can present serious problems, the research team acquired its own diffractometer and now possesses excellent in-house capabilities at AFRL/Edwards. At USC, there are also excellent X-ray diffraction

facilities, with a new Department diffractometer at the team's disposition and technical support from Prof. Bob Bau. Many important crystal structures were determined in the course of this program, including those of $N_5^+Sb_2F_{11}^-$ [Ref. 10], $ONF_2^+AsF_6^-$ [Ref. 19], H_3NF^+, N_2F^+, $N_2F_3^+$, and NF_4^+ salts, numerous polyazides, triphenylmethylsulfinylamine [Ref. 20], $(SO_2)_2N_3^-$ [Ref. 16], and $SO_2N_3^-$, $SO_3N_3^-$ [Ref. 15].

Other crucial elements of the research are theoretical calculations. This program has, from the very beginning, heavily relied on the synergism between theory and synthesis. Because many possible target compounds are vibrationally unstable and, therefore, cannot exist, it is very important to carry out stability calculations before investing time and effort into experimental work. Furthermore, the availability of predicted vibrational and NMR spectra and isotopic shifts greatly facilitates the identification of new compounds. This approach has served very well during this program and has greatly contributed to its success. We were fortunate to have an outstanding computational chemistry capability at AFRL/Edwards. There were also collaborations with outsiders in the computational area. Main contributors included Drs. David Dixon, David Feller, Don Jenkins, and Mark Gordon. Efforts in computational chemistry have produced numerous spin-offs, which have made significant contributions to the general field of chemistry. A few typical examples are the development of the first quantitative scale for Lewis acidity [Ref. 9], a quantitative measure for the nakedness of fluoride ion sources [Ref. 21, 22], and structure rules for a model of attracting points on a sphere.

VII. Azidamines

Azidamines represent an attractive class of HEDM materials [Ref. 23]. However, only one azidamine has been reported in the literature [Ref. 24]. Because this report was 40 years old and the results were questionable, this work was repeated at USC. In the previous work, it was claimed that the reaction of $(CH_3)_2NCl$ with NaN_3 in CH_2Cl_2 solution affords $(CH_3)_2NN_3$, but the compound was not well characterized. Researchers at USC carefully repeated this work and obtained surprising results. The only covalent azide isolated from this system was $CH_2(N_3)_2$, formed from the reaction of the solvent with NaN_3. Furthermore, condensation reactions involving $(CH_3)_2NCl$ gave rise to two novel compounds that were isolated and identified by their crystal structures. They are dimethylaminomethyltetrazole and an interesting 1-methylated 1,3,5-triazinium dication. Therefore, the previous claim for the existence of an azidamine should be discredited.

A number of systems that might lead to azidamines was also studied. For example, the reaction of Select Fluor (1-chloromethyl-4-fluoro-1,4-diazoniabicyclo-[2.2.2]octane bis (tetra-fluoro-borate)) with trimethylsilylazide was studied in CH_3CN solution. At -40 °C, no reaction occurred; while at higher temperatures N_2 evolution and the formation of brown tacky products were observed. Reactions of silylchloramines, such as $(CH_3)_2$(t-but)$SiNCl_2$, $(C_6H_5)_3SiNCl_2$, or $[(CH_3)_3Si]_2NCl$, with trimethylsilylazide or NaN_3 were also unsuccessful. However, some interesting spin-off chemistry was obtained. For example, in the reaction of $(CH_3)_2$(t-butyl)$SiNCl_2$ with $N(CH_3)_4^+F^-$ in CHF_3 solution at low temperature, a solid product was isolated which, on warm-up to room temperature, evolved NCl_3. The low-temperature Raman spectrum of the solid before the decomposition showed the presence of the tetramethyl ammonium cation and a new nitrogen chloride species. The species exhibited more bands than predicted for the hoped-for novel NCl_2^- anion and resembled more NCl_3, but with major frequency and intensity deviations. Additional work will be required to positively identify this novel species. The NCl_2^- anion would provide an ideal precursor for exploring the possible synthesis of the $N(N_3)_2$- anion. Another interesting new compound was obtained when $[(CH_3)_3Si]_2NCl$ was reacted with HF and Lewis acids, such as BF_3, AsF_5, or SbF_5. In all cases, stable salts containing the novel NH_3Cl^+ cation were obtained. These salts developed, on exposure to moisture, NH_2Cl, a powerful disinfectant and biocide. The salts could serve as ideal safe solid storage media for NH_2Cl and might be used as gas generators for disabling chemical warfare agents, such as Anthrax.

VIII. The Pentazolate Anion, *cyclo* - N_5^-

One of the drawbacks of the N_3^- anion is its low first ionization potential of 61.2 kcal/mol (2.66 eV), thus making it very vulnerable to electron loss when combined with a powerful oxidizer, such as N_5^+ (electron affinity of 243.3 kcal/mol) [Ref. 11]. It was, therefore, of interest to pursue the synthesis of alternate polynitrogen anions that might possess higher ionization potentials. A promising candidate, *cyclo* - N_5^-, (Fig. 15), had been identified by numerous theoretical calculations, some of them dating back to the last century [Ref. 2b,c, 25-33]. This anion is isoelectronic with the cyclopentadienide anion, $C_5H_5^-$ and possesses a highly aromatic ring system. Its barrier towards decomposition to $N_3^- + N_2$ is predicted to be 28 kcal/mol (see Fig. 16).

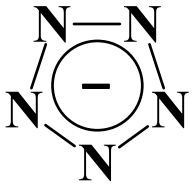

Fig. 15. The Calculated Structure of the Pentazolate Anion.

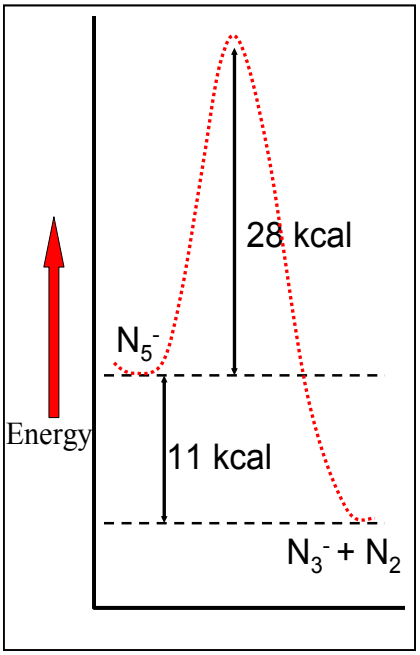

Fig. 16. Energy Profile For The Decomposition of N_5^- to N_3^- + N_2 Along The Reaction Coordinate
Showing a predicted barrier of 28 kcal/mol and an exothermicity of 11 kcal/mol.

Although the existence and stability of substituted pentazole ring compounds had been demonstrated successfully more than 40 years ago by Huisgen and Ugi [Ref. 34-37] and substituted pentazoles had been well characterized [Ref. 38-44], attempts to prepare either the parent HN_5 molecule or its anion, N_5^- [Ref. 37, 45], had been unsuccessful. In our pursuit of the N_5^- anion, the following strategy was employed: (i) the use of Ugi-Huisgen-type, substituted phenylpentazoles as starting materials; (ii) the transfer of maximum negative charge to the pentazole ring by the use of highly electron donating substituents on the phenyl ring in *para*-position to the pentazolyl substituent to increase the aromaticity and stability of the pentazole ring, while at the same time weakening the connecting C-N bond; (iii) the selective cleavage of

the C-N bond while keeping the N-N bonds of the pentazole ring intact; and (iv) the use of an analytical method that is ideally suited for the generation and detection of anions. Similar approaches had been described in the literature, but attempts to cleave the C-N bond by ozonolysis were unsuccessful [Ref. 37, 45]. The reasons, outlined above, prompted researchers to choose the well-known *para*-oxophenyl-pentazolate anion [Ref. 35, 45] and *para*-dimethylaminopentazole [Ref. 35, 36, 38, 39] as starting materials and negative-ion electrospray ionization mass spectrometry (ESI-MS) [Ref. 46-49] as the analytical tool.

The arylpentazoles and the corresponding diazonium salt precursors were prepared and characterized at AFRL using literature methods [Ref. 35, 36, 38, 39, 45, 50] and multinuclear NMR spectroscopy [Ref. 38-43]. The ESI-MS cleavage experiments were carried out by Dr. James Pavlovich at UC Santa Barbara. For these experiments, the pentazoles were dissolved in strongly polar solvents, such as CH_3CN or a mixture of CH_3OH and CH_2Cl_2. The desired negative ion peaks were mass-selected and subjected to product ion mass analysis following collision induced dissociation (CID) at variable collision voltages using N_2 or Ar as the collision gases.

The best results were obtained with pyridinium *para*-pentazolylphenolate in CH_3CN solution, and unambiguous proof for the formation of *cyclo*-N_5^- anions was obtained using normal and ^{15}N substituted starting materials (see Fig. 17).

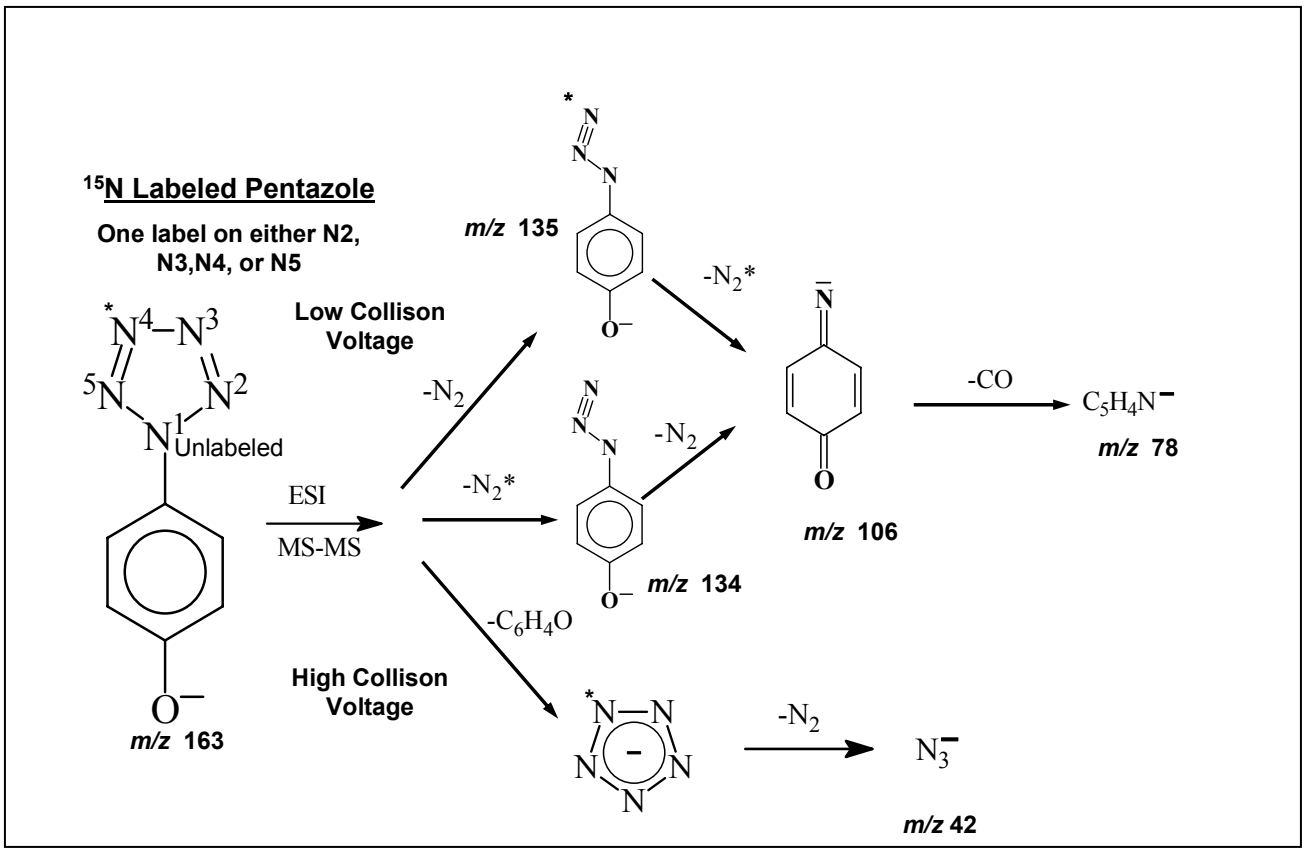

Fig. 17. ESI-MS Fragmentation Observed for the Mass-Selected ^{15}N Singly Labeled 4-Pentazolylphenolate Anion At Low And High Collision Voltages.

These results were published in *Angewandte Chemie* as a "hot paper" [Ref. 51] and received considerable public attention [Ref. 52]. They also stimulated the publication of numerous theoretical papers predicting all kinds of adducts analogous to the well-known ferrocene-type compounds. The research team's report of a successful cleavage of an arylpentazole to N_5^- stimulated reports by other groups that had independently pursued the same problem. One year after this team's report, the Swedish group of Oestmark and coworkers published a paper on the detection of *cyclo*-N_5^- by laser desorption ionization (LDI) time-of-flight (TOF) mass spectroscopy of solid *p*-dimethylaminophenylpentazole [Ref. 53], in which they quoted a previous report from their group at a meeting [Ref. 54] dealing with an ESI-MS and LDI-TOF study of the same system. However, the results presented in that report were inconclusive.

The cleavage of arylpentazoles to give the *cyclo*-N_5^- anion has also been observed by ^{15}N NMR spectroscopy at AFRL/Edwards and by Prof. Butler's group in Ireland [Ref. 55]. Although the observation of N_5^- by NMR implies the presence of higher concentrations of N_5^- than in the

mass spectroscopic experiments, all attempts to isolate N_5^- salts in bulk have so far been unsuccessful. Extensive efforts in this direction are being made in our and other laboratories. For example, at USC considerable amounts of time were spent on attempts to prepare aliphatic [Ref. 56] or silyl-substituted diazonium salts for eventual conversion to the corresponding pentazoles. However, all these attempts were unsuccessful. We have also explored at great length the possible bulk-synthesis of N_5^- from arylpentazoles and alkali metals in liquid ammonia at low temperatures. One of the major obstacles is the preference of N_5^- for forming with the counter-ion σ-complexes, which results in a strong polarization of the bonds in N_5^-, accompanied by loss of aromaticity and increased ease of N_2 elimination. This was established through model calculations, and efforts are under way at USC to eliminate the competing σ-complexation. Clearly, the bulk-synthesis of stable N_5^- salts is an important objective of this program which still needs to be accomplished.

An important question which needed a conclusive answer was whether N_5^-, if available in bulk, would offer an opportunity to prepare a stable $N_5^+N_5^-$ salt. While we were actively pursuing the actual syntheses of N_5^+ and N_5^-, Bartlett and coworkers [Ref. 33] and Gagliardi and coworkers [Ref. 31] published theoretical papers on this subject, implying that $N_5^+N_5^-$ might exist as a stable compound. Their conclusions are in stark contrast to the results from our own studies which were carried out in collaboration with David Dixon, David Feller, and Mark Gordon [Ref. 11]. We showed that the use of vertical instead of adiabatic ionization potentials and electron affinities can cause very large errors in stability predictions when the formed radicals are not vibrationally stable. As a result, we predicted that $N_5^+N_5^-$ is expected to be unstable by about 88 kcal/mol with respect to decomposition to N_3 radicals and N_2 and that this decomposition does not involve a significant activation energy barrier [Ref. 11]. In spite of predicted instability of $N_5^+N_5^-$, the bulk-syntheses of N_5^- salts remain a very desirable goal because of the many potential uses one could foresee for this interesting new class of compounds.

IX. Polyazides

The azide group is highly energetic and adds ~ 70 kcal/mol endothermicity to a compound. Consequently, polyazides offer a unique opportunity to prepare nitrogen rich, highly energetic materials [Ref. 57]. Of particular interest to this program were polyazido anions which

might be useful as energetic counter-ions to polynitrogen cations, such as N_5^+. Most of the research in this area was carried out at USC. Many of the compounds are extremely shock-sensitive and often are also thermally unstable. Their handling requires outstanding preparative skills and courage. Because of the high energy content and high detonation velocities of these azides, these explosions are particularly violent and can cause, even on a one mmol scale, significant damage (see Figs. 8, 13, and 18). The wearing of heavy leather welding suits, leather gloves, safety glasses, face shields, and ear plugs is mandatory when working with these compounds (see Fig. 19).

Fig. 18. Before And After Pictures
of a 10 mm o.d. Teflon™-FEP tube (left picture)
and a 45 mm o.d. heavy wall Pyrex™ waste trap (right picture),
destroyed by about 0.5 mmol of typical polyazides.

Fig. 19. Mandatory Safety Gear for Work with Polynitrogens or Polyazides, (modeled By Ashwani Vij)

The following families of polyazides were studied by this research team.

***Phosphorus, arsenic, and antimony compounds*:** The $P(N_3)_6^-$ anion had been known since 1967 [Ref. 58], and was prepared as its Na^+ salt. It was successfully converted into $N_5^+P(N_3)_6^-$ by metathesis in SO_2 solution. The properties of this compound have already been discussed above and do not need to be reiterated. Attempts to characterize $P(N_3)_5$ in the solid state were abandoned because of handling problems. Whereas the crystal structure of $As(N_3)_6^-$ had been known [Ref. 59], the structures of $Sb(N_3)_6^-$, $Sb(N_3)_3$, and $As(N_3)_3$ were unknown. Crystal structures for all three compounds were obtained. The very interesting structures of $Sb(N_3)_3$ and $As(N_3)_3$ were described in a paper [Ref. 60] and garnered the cover page of *Chemistry – A European Journal* (see Fig. 20).

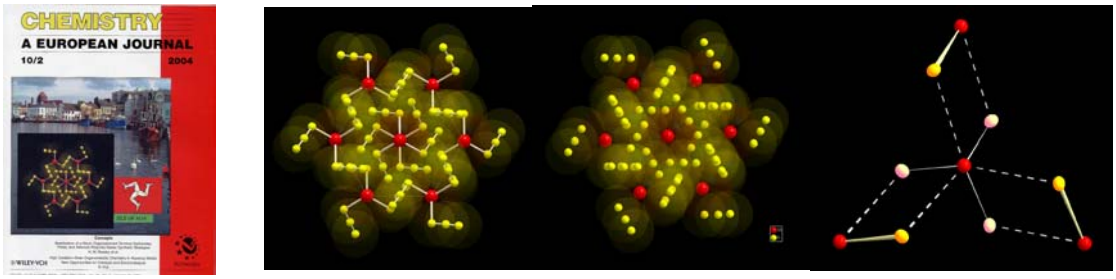

Fig. 20. Cover Page from *Chemistry –A European Journal*
Highlighting our polyazide work, and three packing diagrams of $Sb(N_3)_3$ and $As(N_3)_3$ taken from this paper.

The structure of $Sb(N_3)_6^-$ also turned out to exhibit very interesting features, because during recrystallization from CH_2Cl_2 some of the azido groups were replaced by chlorine; and the structures of a series of mixed azides / chlorides were obtained. Furthermore, partial occupancy of azide positions by chloride gives the appearance of azide groups with unusual N-N bond distances. This effect has previously been observed by others, but was misinterpreted in terms of either unusal azido ligands or so-called *trans*-effects. It will be the subject of a forthcoming paper.

***Tellurium and selenium compounds**:* Three new binary tellurium polyazides, $Te(N_3)_4$, $Te(N_3)_5^-$, and $Te(N_3)_6^{2-}$ were prepared and characterized (see Fig. 21). The work was published in *Angewandte Chemie* [Ref. 61] and highlighted in *Chemical and Engineering News* [Ref. 62]. Attempts to prepare Te(+VI) compounds were unsuccessful and resulted in reduction of Te(+VI) to Te(+IV) by azide. Attempts to combine N_5^+ with $Te(N_3)_6^{2-}$ were unsuccessful because of solubility and sensitivity problems.

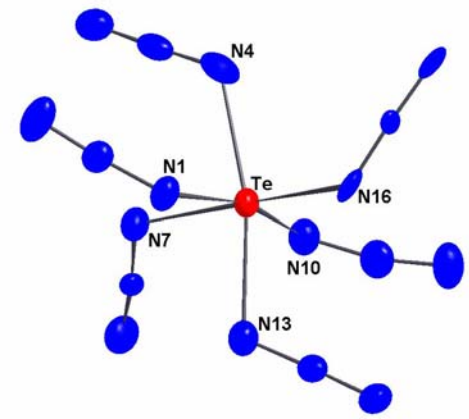

Fig. 21. Crystal Structure of the $Te(N_3)_6^{2-}$ Anion
showing the distortion from perfect octahedral symmetry
by the presence of a sterically active free valence electron pair on Te.

Attempts to prepare so-far unknown neutral binary Se(+VI) azides resulted in the formation of polyazides; however, the compounds were too sensitive and could not be characterized.

***Boron compounds**:* $B(N_3)_4^-$ salts had been known since 1954 [Ref. 63]. The sodium salt was prepared from $NaBH_4$ and HN_3 in ether. Its conversion to the N_5^+ salt has already been described above and is not reiterated here.

Titanium compounds. Binary titanium azides are unknown. Recently, they received much attention through a theoretical paper by Gagliardi and Pyykkoe [Ref. 64]. These authors predicted that $Ti(N_3)_4$ should exhibit perfect T_d symmetry with unprecedented linear Ti-N-N bond angles (see Fig. 22). This structure was confirmed by theoretical calculations and they also predicted that both $Ti(N_3)_5^-$ and $Ti(N_3)_6^{2-}$ should possess conventional, strongly bent Ti-N-N bond angles.

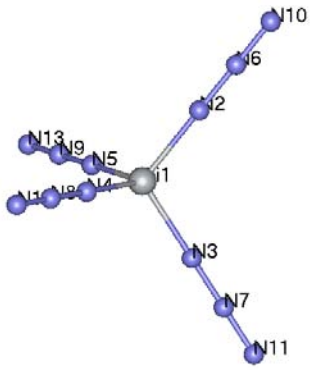

Fig. 22. Predicted Tetrahedral Structure of $Ti(N_3)_4$ with Linear Ti-N-N Bonds

All three compounds were synthesized and characterized by vibrational and NMR spectroscopy. Attempts to obtain a crystal structure for $[P(C_6H_5)_4]_2[Ti(N_3)_6]$ were also successful, confirming the predicted bent nature of the Ti-N-N bond angles (see Fig.23).

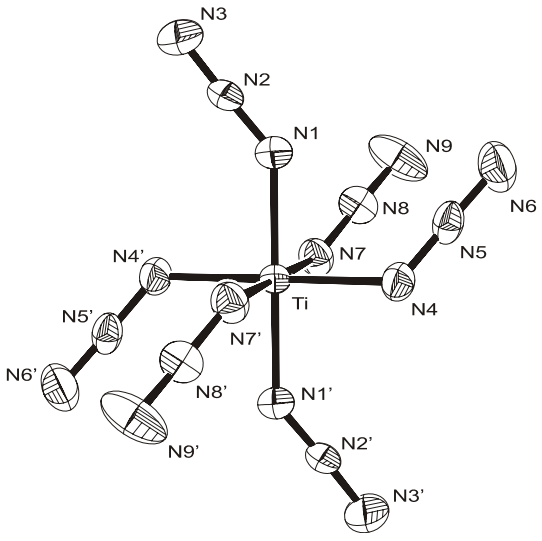

Fig. 23. Crystal Structure of $Ti(N_3)_6^{2-}$
Showing the Bent Ti-N-N Bond Angles

Attempts to obtain single crystals of $Ti(N_3)_4$ by either sublimation or recrystallization failed, but the vibrational spectra prove beyond doubt that solid $Ti(N_3)_4$ is polymeric, having a

coordination number higher than 4 and bent Ti-N-N bond angles. Our theoretical analysis of the bonding in free gaseous $Ti(N_3)_4$ resulted in a plausible explanation for the linearity of its Ti-N-N groups. It is due to a tridentate donation of electron density from the three free valence electron pairs on each nitrogen atom into the empty *d*-orbitals of Ti. This assumption also explains why for coordination numbers higher than 4 the spatial arrangements of the free nitrogen pairs and the d-orbitals are no longer suitable for tridentate bonding, resulting in bent Ti-N-N bond angles. A structure determination of free gaseous $Ti(N_3)_4$ will be required to confirm the theoretical predictions. This, however, could be a difficult task, because studies showed that $Ti(N_3)_4$ could not be sublimed *in vacuo* without decomposition.

X. Possible Synthesis of the N_3^+ Cation

The N_3^+ cation holds substantial promise as a novel polynitrogen that might exhibit good kinetic stability. Furthermore, a potential route exists for its synthesis. It should be possible to transfer a fluoride ion from the known [Ref. 65] FN_3 molecule to a strong Lewis acid, such as SbF_5 (Eq. 32).

$$FN_3 + SbF_5 \longrightarrow N_3^+SbF_6^- \qquad (32)$$

This approach had previously been investigated unsuccessfully by Willner's group in Germany, using infrared matrix isolation techniques [Ref. 66]. When weaker Lewis acids, such as BF_3 or AsF_5, were used, only nitrogen-bridged donor-acceptor adducts were formed. When FN_3 and the stronger Lewis acid SbF_5 were co-condensed on a cold window, explosions were always observed on warm-up. Clearly, the used reaction conditions were unsuitable. Using a suitable solvent, it should be possible to better control this reaction and to avoid the explosions.

The preparation and handling of FN_3 is extremely tricky. Pure FN_3 is one of the most shock-sensitive materials and violently explodes when exposed to the slightest mechanical shock or rapid temperature changes. Furthermore, its thermal half-life time at room temperature is on the order of 30 minutes. Its reported synthesis involves the reaction of HN_3 with gaseous F_2 at room temperature using steel surfaces as a catalyst. The yields of FN_3 under these conditions are only about 50 %, and product purification is very difficult. To avoid all of these problems, a better synthesis and safer handling techniques are being developed for FN_3 at AFRL/Edwards. Our approach involves the use of a suitable solvent for the preparation and safe handling of FN_3.

Although, at first look, anhydrous HF appeared an ideal solvent, it turned out that HF protonates HN_3 (Eq. 33), and that the resulting $H_2N_3^+$ cation is no longer fluorinated by F_2.

$$HN_3 + n\,HF \longrightarrow H_2N_3^+HF_2^-\cdot(n-2)HF \qquad (33)$$

Therefore, the use of Freons was checked as possible solvents. It was found that HN_3 is very soluble in $CFCl_3$ and that HN_3 can be fluorinated in this solvent to FN_3 in quantitative yield and high purity. Unfortunately, it was found that $CFCl_3$ rapidly reacts with SbF_5, undergoing fluorine/chlorine exchange forming $SbCl_4^+$ salts. Now $(CF_3)_2CFH$ appears to be a good solvent for HN_3, can be used for the fluorination of HN_3 to FN_3, and is compatible with SbF_5. The crucial experiment (i.e., the combination of FN_3 and SbF_5 solutions in $(CF_3)_2CFH$) is imminent.

XI. Conclusions and Recommendations

This research team's effort on Polynitrogen Chemistry is an impressive showpiece for a highly successful DARPA Program. Through DARPA's sponsorship, major breakthroughs in a technically very difficult area were achieved, research in this field was stimulated on a worldwide scale, and much public and scientific acclaim (2000 Prix Moissan, 2003 ACS Award in Inorganic Chemistry, coverage in major news media, etc) was received. Because DARPA is not a long-term, basic research funding agency, it is hoped that these efforts and DARPA's investment were not in vain and that other agencies will enthusiastically step in to take over the sponsorship of this winning program.

References

[1] "Proceedings of the High Energy Density Matter (HEDM) Conference," Air Force Astronautics Laboratory, Rep. No. AFAL CP-87-002, W. J. Lauderdale and W. A. Sowell, Editors, Sept. 1987, and subsequent reports.

[2] In view of the many publications in this area, only a few selected references are listed here which contain many of the pertinent references: (a) W. J. Lauderdale, J. F. Stanton, R. J. Bartlett, *J. Phys. Chem.* **1992**, *96*, 1173; (b) M. N. Glukhovtsev, H. Jiao, P. v. R. Schleyer, *Inorg. Chem.* **1996**, *35,* 7124; (c) M. T. Nguyen, *Coord. Chem. Rev*. **2003**, *244*, 93.

[3] K. O. Christe, R. D. Wilson, W. W. Wilson, R. Bau, S. Sukumar, D. A. Dixon, *J. Am. Chem*. *Soc*. **1991**, *113*, 1991.

[4] P. Pyykkoe, N. Runeberg, *J. Mol. Struct. (Theochem.)* **1991,** *234,* 279.

[5] R. Rawls, *Chem. & Eng. News*, Jan. 25 issue, **1999**, pg. 7.

[6] P. Zurer, *Chem. & Eng. News*, Nov. 29 issue, **1999**, pg. 38.

[7] K. O. Christe, W. W. Wilson, J. A. Sheehy, J. A. Boatz, *Angew. Chem., Int.Ed. Engl.* **1999,** *38,* 2004.

[8] K. O. Christe, W. W. Wilson, "Pentanitrogen(1+) Cation and Salt Containing the Same," U. S. Patent 6,224,696, May 1, 2001.

[9] K. O. Christe, D. A. Dixon, D. McLemore, W. W. Wilson, J. A. Sheehy, J. A. Boatz *J. Fluor. Chem.* **2000,** *101,* 151.

[10] A. Vij, W. W. Wilson, V. Vij, F. S. Tham, J. A. Sheehy, K. O. Christe, *J. Am. Chem. Soc.* **2001,** *123*, 6308.

[11] D. A. Dixon, D. Feller, K. O. Christe, W. W. Wilson, A. Vij, V. Vij, H. D. B. Jenkins, R. M. Olson, M. S. Gordon, *J. Am. Chem. Soc.* **2004,** *126*, 834.

[12] a) K. O. Christe, J. P. Guertin, A. E. Pavlath, *Inorg. Nucl. Chem. Lett.* **1966**, *2,* 83; b) W. W. Wilson, K. O. Christe, *J. Fluorine Chem.* **1980**, *15,* 83; c) K. O. Christe, W. W. Wilson, R. D. Wilson, *Inorg. Chem.* **1980**, *19,* 1494; d) K. O. Christe, W. W. Wilson, R. D. Wilson, *Inorg. Chem.* **1980**, *19,* 3254; e) W. W. Wilson, K. O. Christe, *J. Fluorine Chem.* **1982**, *19,* 253.

[13] W. W. Wilson, A. Vij, V. Vij, E. Bernhardt, K. O. Christe, *Chemistry – A European Journal,* **2003**, *9*, 2840.

[14] H. M. Netzloff, M. S. Gordon, K. O. Christe, W. W. Wilson, A. Vij, V. Vij, J. A. Boatz, *J. Phys. Chem. A* **2003**, *107*, 6638.

[15] K. O. Christe, J. A. Boatz, M. Gerken, R. Haiges, S. Schneider, T. Schroer, F. S. Tham, A. Vij, V. Vij, R. I. Wagner, W. Wilson, *Inorg. Chem.* **2002**, *41*, 4275.

[16] K. O. Christe, M. Gerken, R. Haiges, S. Schneider, T. Schroer, I. Tsyba, R. Bau, *Inorg. Chem.* **2003**, *42*, 416.

[17] M. Gerken, S. Schneider, T. Schroer, R. Haiges, K. O. Christe, *Z. Anorg. Allg. Chem*. **2002**, *628*, 909.

[18] R. Haiges, K. O. Christe, *Z. Anorg. Allg. Chem*. **2002,** *628*, 1717.

[19] A. Vij, X. Zhang, K. O. Christe, *Inorg. Chem*. **2001**, *40*, 416.

[20] K. O. Christe, M. Gerken, R. Haiges, S. Schneider, T. Schroer, F. S. Tham, A. Vij, *Solid State Sciences*, **2002**, *4*, 1529.

[21] M. Gerken, J. A. Boatz, A. Kornath, R. Haiges, S. Schneider, T. Schroer, K. O. Christe, *J. Fluor. Chem*. **2002**, *116*, 49.

[22] K. O. Christe, H. D. B. Jenkins, *J. Am. Chem. Soc*. **2003**, *125*, 9457.

[23] H.H. Michels, J.A. Montgomery, Jr., K. O. Christe, D.A. Dixon, *J. Phys. Chem*., **1995**, *99*, 187.

[24] H. Bock, K. Kompa, *Z. Anorg. Allg. Chem*. **1964**, *332*, 238.

[25] M. T. Nguyen, M. Sana, G. Leroy, J. Elguero, *Canad. J. Chem.* **1983,** *61,*1435.

[26] M. T. Nguyen, M. A. McGinn, A. F. Hegarty, J. Elguero, *Polyhedron* **1985,** *4,*1721.

[27] M. N. Glukhovtsev, P. v. R. Schleyer, C. Maerker, *J. Phys. Chem*., **1993**, *97*, 8200.

[28] V. A. Ostrovskii, G. B. Erusalimskii, M. B. Shcherbinin, *Russ. J. Org. Chem.* **1995,** *31,* 1284.

[29] R. J. Bartlett, *Chem. Ind.* **2000,** 140, and references cited therein.

[30] M. T. Nguyen, T. K. Ha, *Chem. Phys. Lett.* **2001,** *335,* 311.

[31] L. Gagliardi, G. Orlandi, S. Evangelisti, B. O. Ross, *J. Chem. Phys.* **2001,** *114,* 10733.

[32] M. Lein, J. Frunzke, A. Timoskin, G. Frenking, *Chem. Eur. J.* **2001,** *7,* 4155.

[33] S. Fau, K. J. Wilson, R. J. Bartlett, *J. Phys. Chem. A* **2002,** *106,* 4639.

[34] R. Huisgen, I. Ugi, *Angew. Chem.* **1956**, *68,* 705; *Chem. Ber.* **1957**, *90,* 2914.

[35] I. Ugi, R. Huisgen, *Chem. Ber.* **1958**, *91,* 531.

[36] I. Ugi, H. Perlinger, L. Behringer, *Chem. Ber.* **1958**, *91,* 2324.

[37] I. Ugi, *Angew. Chem.* **1961**, *73,* 172.

[38] J. D. Wallis, J. D. Dunitz, *J. Chem. Soc., Chem. Commun.* **1983**, 910.

[39] M. Witanowski, L. Stefaniak, H. Januszewski, K. Bahadur, G. A. Webb, *J. Cryst. Mol. Struct.* **1975**, *5,* 137.

[40] R. Mueller, J. D. Wallis, W. v. Philipsborn, *Angew. Chem.* **1985**, *97,* 515; *Angew. Chem. Int. Ed.* **1985**, *24,* 513.

[41] R. N. Butler, S. Collier, A. F. M. Fleming, *J. Chem. Soc., Perkin Trans. 2* **1996**, 801.

[42] a) R. N. Butler, A. Fox, S. Collier, L. A. Burke, *J. Chem. Soc., Perkin Trans. 2* **1998**, 2243; b) L. A. Burke, R. N. Butler, J. C. Stephens, *J. Chem. Soc., Perkin Trans. 2* **2001**, 1679.

[43] A. Hammerl, T. M. Klapoetke, *Inorg. Chem.* **2002**, *41,* 906.

[44] F. Biesemeier, U. Mueller, W. Massa, *Z. Anorg. Allg. Chem.* **2002,** *628,* 1933.

[45] V. Benin, P. Kaszynski, J. G. Radziszewski, *J. Org. Chem.* **2002**, *67,* 1354.

[46] M. Yamashita, J. B. Fenn, *J. Chem. Phys.* **1984**, *88,* 4451.

[47] C. M. Whitehouse, R. N. Dreyer, M. Yamashita, J. B. Fenn, *Anal. Chem.* **1985**, *57,* 675.

[48] R. B. Cole (ed), *Electrospray Ionization Mas Spectrometry* (Wiley-Interscience, New York, NY, **1997**).

[49] B. H. Lipshutz, K. L. Stevens, B. James, J. G. Pavlovich, J. P. Snyder, *J. Am. Chem. Soc.* **1996**, *118,* 6796.

[50] C. Colas, M. Goeldner, *Eur. J. Org. Chem.* **1999,** 1357.

[51] A. Vij, J. G. Pavlovich, W. Wilson, V. Vij, K. O. Christe, *Angew. Chem. Int. Ed*. **2002**, 41, 3051.

[52] See for example: R. Dagani, *Chem. & Eng. News*, Aug. 19 issue, **2002**, pg. 8.

[53] H. Oestmark, S. Wallin, T. Brinck, P. Carlqvist, R. Claridge, E. Hedlund, L. Yudina, *Chem. Phys. Lett.* **2003,** *379,* 539.

[54] A. Hahma, E. Holmberg, N. Hore, R. Tryman, S. Wallin, H. Bergman, H. Oestmark, paper 62, presented at the 33rd International Annual Conference of ICT, Karlsruhe, 2002.

[55] R. N. Butler, J. C. Stephens, L. A. Burke, *J. Chem. Soc. Chem. Commun.* **2003,** 1016.

[56] A typical example for one of the approaches towards aliphatic diazonium salts involved the synthesis of triylsulfinylamine: K. O. Christe, M. Gerken, R. Haiges, S. Schneider, T. Schroer, F. S. Tham, A. Vij, *Solid State Sciences,* **2002,** *4,* 1529.

[57] For recent reviews, see: (a) W. Fraenk, T. M. Klapötke, in *Inorganic Chemistry Highlights* (Eds.: G. Meyer, D. Naumann, L. Wesemann), Wiley-VCH, Weinheim, **2002;** (b) A. Kornath, *Angew. Chem. Int. Ed.* **2001,** *40,* 3135.

[58] H. W. Roesky, *Angew. Chem. Int. Ed.* **1967,** *6,* 637.

[59] T. M. Klapoetke, H. Noeth, T. Schuett, M. Warchhold, *Angew. Chem. Int. Ed.* **2000,** *39,* 2108.

[60] R. Haiges, A. Vij, J. A. Boatz, S. Schneider, T. Schroer, M. Gerken, K. O. Christe, *Chem. Eur. J.* **2004,** *10,* 508.

[61] R. Haiges, J. A. Boatz, A. Vij, M. Gerken, S. Schneider, T. Schroer, K. O. Christe, *Angew. Chem. Int. Ed.*. **2003,** *42,* 5847.

[62] *Chem. & Eng. News*, Dec. 15 issue, **2003**, pg. 22.

[63] E. Wiberg, H. Michaud, *Z. Naturforsch.* **1954,** *96,* 497.

[64] L. Gagliardi, P. Pyykkoe, *Inorg. Chem.* **2003,** *42,* 3074.

[65] J. F. Haller, Ph.D. Thesis, Cornell University, Ithaca, NY, 1942.

[66] G. Schatte, H. Willner, *Z. Naturforsch.* **1991,** *46b,* 483.

This Page Intentionally Left Blank

APPENDIX A

"N_5^+: A Novel Homoleptic Polynitrogen Ion as a High Energy Density Material"
Angew. Chem. Int. Ed. 38, 2004 (1999)

This Page Intentionally Left Blank

Harteneck et al.[22] The antibodies used are directed against the C-terminal peptide of the α_2 subunit (KKVSYNIGTTMFLRETSL).

Received: December 23, 1998 [Z 12821 IE]
German version: *Angew. Chem.* **1999**, *111*, 2180 – 2184

Keywords: molecular recognition · peptides · peptide – peptide interactions

[1] P. Bork, J. Schultz, C. P. Ponting, *Trends Biochem. Sci.* **1997**, *22*, 296 – 298.
[2] P. Bork, E. V. Koonin, *Curr. Opin. Struct. Biol.* **1996**, *6*, 366 – 376.
[3] a) J. K. Scott, G. P. Smith, *Science* **1990**, *249*, 386 – 390; b) S. Fields, O. Song, *Nature* **1989**, *340*, 245 – 246.
[4] a) K. O. Cho, C. A. Hunt, M. B. Kennedy, *Neuron* **1992**, *9*, 929 – 942; b) C. P. Ponting, C. Phillips, *Trends Biochem. Sci*. **1995**, *20*, 102 – 103; c) C. P. Ponting, C. Phillips, K. E. Davies, D. J. Blake, *BioEssays* **1997**, *19*, 469 – 479.
[5] J. E. Brenman, S. S. Chao, S. H. Gee, A. W. McGee, S. E. Craven, D. R. Santillano, Z. Wu, F. Huang, H. Xia, M. F. Peters, S. C. Froehner, D. S. Brendt, *Cell* **1996**, *84*, 757 – 767.
[6] J. Saras, C. Heldin, *Trends Biochem. Sci.* **1996**, *21*, 455 – 458.
[7] a) R. Frank, *Tetrahedron* **1992**, *48*, 9217 – 9232; b) R. Frank, H. Overwin, *Methods Mol. Biol*. **1996**, *66*, 149 – 169; c) A. Kramer, J. Schneider-Mergener, *Methods Mol. Biol*. **1998**, *87*, 25 – 39.
[8] a) R. S. Kania, R. N. Zuckermann, C. K. Marlowe, *J. Am. Chem. Soc*. **1994**, *116*, 8835 – 8836; b) M. Lebl, V. Krchnak, N. F. Sepetov, V. Nikolaev, A. Stierradova, P. Safar, B. Seligmann, P. Stop, P. Thorpse, S. Felder, D. F. Lake, K. S. Lam, S. E. Salmon in *Innovation and Perspectives in Solid Phase Synthesis* (Ed.: R. Epton), Mayflower Worldwide, Oxford, **1994**, p. 233.
[9] M. E. Adams, T. M. Dwyer, L. L. Dowler, R. A. White, S. C. Froehner, *J. Biol. Chem.* **1995**, *270*, 25859 – 25865.
[10] J. Schultz, U. Hoffmüller, G. Krause, J. Ashurst, M. Macias, P. Schmieder, J. Schneider-Mergener, H. Oschkinat, *Nat. Struct. Biol*. **1998**, *5*, 19 – 24.
[11] S. H. Gee, R. Madhavan, S. R. Levinson, J. H. Caldwell, R. Sealock, S. C. Froehner, *J. Neurosci*. **1998**, *18*, 128 – 137.
[12] a) L. Fu, G. Wallukat, A. Hjalmarson, J. Hoebeke, *Clin. Exp. Immunol*. **1994**, *97*, 146 – 151; b) A. H. Ahn, C. A. Freener, E. Gussoni, M. Yoshida, E. Ozawa, L. M. Kunkel, *J. Biol. Chem.* **1996**, *271*, 2724 – 2730.
[13] D. Koesling, J. Herz, H. Gausepohl, F. Niroomand, K. D. Hinsch, A. Mulsch, E. Böhme, G. Schultz, R. Frank, *FEBS Lett*. **1988**, *239*, 29 – 34.
[14] D. S. Chao, F. Silvagno, H. Xia, T. L. Corwell, T. M., Lincoln, D. S. Bredt, *Neuroscience* **1997**, *76*, 665 – 672.
[15] T. C. Liang, W. Luo, J. T. Hsieh, S. H. Lin, *Arch. Biochem. Biophys.* **1996**, *329*, 208 – 14
[16] M. Davies, M. Bradley, *Angew. Chem.* **1997**, *109*, 1135 – 1138; *Angew. Chem. Int. Ed. Engl.* **1997**, *36*, 1097 – 1099.
[17] R. Volkmer-Engert, B. Hoffmann, J. Schneider-Mergener, *Tetrahedron Lett*. **1997**, *38*, 1029 – 1032.
[18] M. B. Wilson, P. K. Nakane in *Immunofluorescence Related Staining Techniques* (Eds.: W. Knapp, K. Hlubar, G. Wick), Elsevier, Amsterdam, **1978**, pp. 215 – 224.
[19] B. Friguet, A. F. Chaffotte, L. Djavadi-Ohaniance, M. E. Goldberg, *J. Immunol. Methods* **1985**, *77*, 305 – 319.
[20] M. Russwurm, S. Behrends, C. Harteneck, D. Koesling, *Biochem. J.* **1998**, *335*, 125 – 130.
[21] M. M. Bradford, *Anal. Biochem*. **1976**, *72*, 248 – 254.
[22] C. Harteneck, B. Wedel, D. Koesling, J. Malkewitz, E. Böhme, G. Schultz, *FEBS Lett.* **1991**, *292*, 217 – 222.
[23] M. Michalak, M. Opas, *Curr. Opin. Neurol*. **1997**, *10*, 436 – 42.
[24] A. Castello, V. Brocheriou, P. Chafey, A. Kahn, H. Gilgenkrantz, *FEBS Lett*. **1996**, *383*, 124 – 128.

N_5^+: A Novel Homoleptic Polynitrogen Ion as a High Energy Density Material**

Karl O. Christe,* William W. Wilson, Jeffrey A. Sheehy, and Jerry A. Boatz

Dedicated to Professor George Olah

Polynitrogen compounds are of significant interest as high energy density materials (HEDM) for propulsion or explosive applications.[1–3] In spite of numerous theoretical studies predicting that certain all-nitrogen compounds might be stable, only a few unsuccessful experimental studies aimed at their actual synthesis have been undertaken.[4] Presently, only two homoleptic polynitrogen species are known that can be prepared on a macroscopic scale: dinitrogen, N_2, which was independently isolated in pure form from air in 1772 by Rutherford, Scheele, and Cavendish, and the azide anion, N_3^-, discovered in 1890 by Curtius.[5] Other species such as $N_3^{\bullet}$, N_3^+, and N_4^+ have been observed only as free gaseous or matrix-isolated ions or radicals.[6–8] In view of the extensive theoretical studies indicating that molecules such as N_4, N_8, $N(N_3)_2^-$, $N(N_3)_3$, and $N(N_3)_4^+$ are vibrationally stable,[4] the lack of a single successful synthesis of a new species on a macroscopic scale is surprising and may be a testament to the great experimental difficulties resulting from their high endothermicities, which give rise to instability and unpredictable explosiveness.

The high energy content of polynitrogen candidates stems from the N–N single and double bonds they possess. The average bond energies of 160 and 418 kJ mol^{-1}, respectively, are much less than one-third or two-thirds the N_2 triple bond energy of 954 kJ mol^{-1}.[9] Therefore, any transformation of a polynitrogen compound to N_2 molecules is accompanied by a very large energy release, and any new metastable polynitrogen compound will be isolable and manageable only if it possesses a sufficiently large energy barrier to decomposition.

In view of the dearth of potential synthetic pathways for the construction of homoleptic polynitrogen rings or polycycles, and because many chain- or branch-type polynitrogen compounds are calculated to be lower in energy than their cyclic or polycyclic isomers,[3] our efforts are focused on the synthesis of catenated polynitrogen species, which may be more readily accessible. The weakest link in a chain always

[*] Dr. K. O. Christe, Dr. W. W. Wilson, Dr. J. A. Sheehy, Dr. J. A. Boatz
Propulsion Sciences and Advanced Concepts Division
Air Force Research Laboratory (AFRL/PRS)
Edwards Air Force Base, CA 93524 (USA)
Fax: (+1) 661-275-5471
E-mail: karl.christe@ple.af.mil
and
Loker Hydrocarbon Research Institute
University of Southern California
Los Angeles, CA 90089 (USA)

[**] This work was funded predominantly by the Defense Advanced Research Projects Agency, with additional support from the Air Force Office of Scientific Research and the National Science Foundation. We thank A. Kershaw for recording the NMR spectra, Dr. M. Fajardo for the mass spectra, Prof. J. Stanton for calculating the nitrogen NMR shifts, and Dr. P. Carrick, Dr. S. Rodgers, Dr. M. Berman, and Dr. A. Morrish for continuing encouragement and support.

  1433-7851/99/3813-2004 $ 17.50+.50/0

determines the overall strength, so it is imperative to search for target compounds devoid of any isolated N–N single bonds that cannot gain partial multiple bond character through resonance with neighboring bonds.

The building principle and unique resonance stabilization of the well-known and exceptionally stable azide anion (**1**, Scheme 1), in which each N–N bond has full double bond

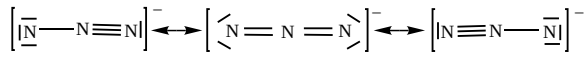

Scheme 1. Resonance structures of N_3^- (**1**).

character, might be further extended by the addition of nitrogen atoms containing only four valence electrons, that is, N^+ ions. This leads first to neutral N_4 (**2**) and then to the N_5^+ cation (**3**, Scheme 2).

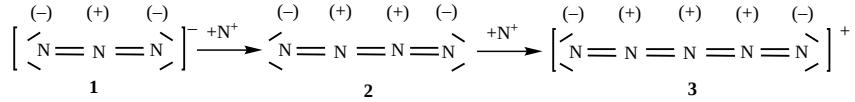

Scheme 2. Addition of N^+ to N_3^- (**1**) to form N_4 (**2**) and N_5^+ (**3**) as well as the electronic charge distrubutions in **1**–**3**.

Although **2** and **3** contain, like azide, only cumulated linear N=N bonds, the electronic charge distributions shown in Scheme 1 are only favorable for N_3^-, whereas the neighboring positive charges render structures **2** and **3** energetically unfavorable. However, the problem of neighboring equal-sign charges can be remedied for N_5^+ with the resonance structures shown in Scheme 3, which result in a bent structure of C_{2v} symmetry with a bond order of 1.5 for the central N–N bonds. For linear N_4, analogous structures cannot be written, and therefore N_5^+ was chosen as the prime target of our synthesis program.

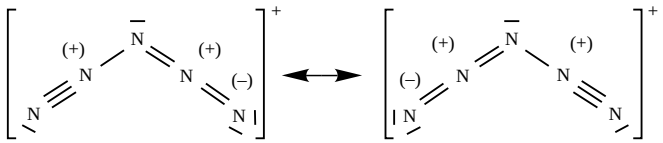

Scheme 3. Resonance structures of N_5^+ (**3**).

Only one previous report on N_5^+ was found in the literature, a theoretical study of a series of ABCBA-type compounds by Pyykkö and Runeberg.[10] Based on MP2/6-31G* calculations, they predicted a planar C_{2v}-symmetric structure with a B-C-B angle of 110.7°. The possible synthesis of N_5^+ was considered in 1992 by G. Rasul in his Ph.D. proposal at the University of Southern California, but it was not pursued.[11] Theoretical calculations were used to predict whether the candidate is vibrationally stable, and IR, Raman, and NMR spectra were calculated to aid in the identification and characterization. For N_5^+, these calculations predict the stable C_{2v} structure depicted in Figure 1. We report now the synthesis and characterization of $N_5^+AsF_6^-$, which constitutes only the third known compound containing a homoleptic polynitrogen moiety that is preparable on a macroscopic scale.

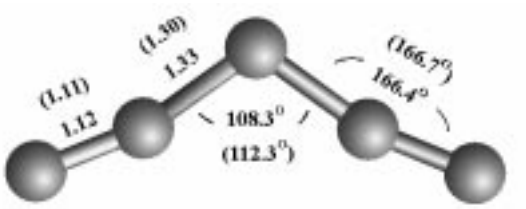

Figure 1. Optimized structures of N_5^+ calculated at the B3LYP (values given in parentheses) and CCSD(T)/6–311 + G(2d) levels of theory.

In designing a synthesis, it is useful to find energetic starting materials that already possess the energy-enhancing weakened bonds, the required formal charges, and suitable ligands that allow for an exothermic and facile coupling reaction. If the target molecule is a cation such as N_5^+, the presence of a formal positive charge in one of the starting materials is very important in view of the high first ionization potential of N_2 (1503 kJ mol^{-1}). Equation (1) shows that the N_2F^+ cation and HN_3 are ideal starting materials for the synthesis of N_5^+ because they already possess the desired types of bonds, N_2F^+ provides the formal positive charge, and, in view of the weak N–F and strong H–F bond, the HF elimination reaction is expected to be exothermic.

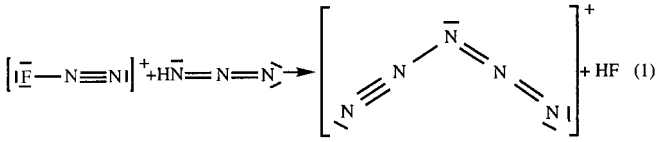

(1)

A final important point is the need for a reaction medium that offers good solubility at low temperatures, can act as a heat sink for the exothermic reaction, and can stabilize a product that is potentially very shock sensitive. For N_5^+, anhydrous HF was chosen because of its high dipole moment, low melting point (−80 °C), and high volatility.

Application of these principles led to a surprisingly straighforward synthesis of N_5^+ according to Equation (2). A

$$N_2F^+AsF_6^- + HN_3 \xrightarrow[-78\,^\circ C]{HF} N_5^+AsF_6^- + HF \quad (2)$$

$$HN_3 + HF + AsF_5 \xrightarrow{HF} H_2N_3^+AsF_6^- \quad (3)$$

$$4\,N_5^+AsF_6^- + 2\,H_2O \longrightarrow 4\,HF + 4\,AsF_5 + 10\,N_2 + O_2 \quad (4)$$

small excess of HN_3 was used to ensure complete conversion of the $N_2F^+AsF_6^-$. The only detectable by-product was less than 20 mol% of protonated HN_3,[12] formed according to Equation (3). The AsF_5 required for the protonation of HN_3 to proceed could have formed by decomposition of some $N_5^+AsF_6^-$, or less likely by hydrolysis of $N_5^+AsF_6^-$ with traces of water in the system [Eq. (4)].

For the synthesis of ^{15}N-labeled N_5^+, ^{15}N-labeled HN_3 was prepared from stearic acid and ^{15}N-labeled $Na^+N_3^-$ [Eq. (5)].

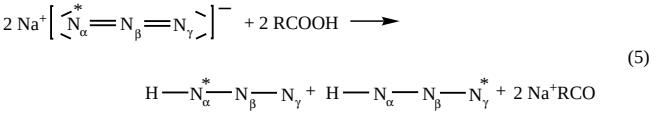

(5)

The reaction of labeled HN_3 with $N_2F^+AsF_6^-$ produced a roughly equimolar mixture of N_5^+ with ^{15}N in either the 1- or 3-position [Eqs. (6), (7)].

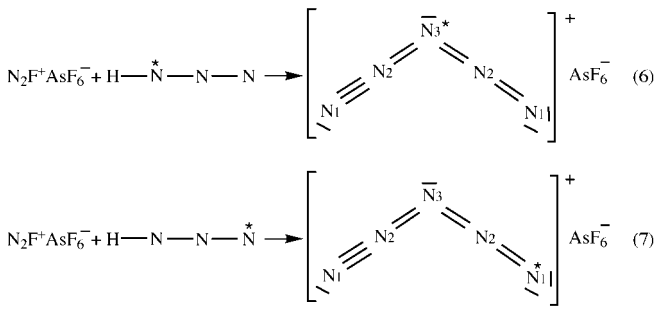

The $N_5^+AsF_6^-$ salt is a white solid that is sparingly soluble in anhydrous HF. It is marginally stable at 22 °C and can be stored for weeks at −78 °C without noticeable decomposition. It can be handled both in HF solution or as a solid and, in our experience, has not exploded during careful normal handling or when squashed with a stainless steel spatula at −196 °C. It has survived numerous exposures to a focused 488-nm Ar-ion laser beam (1.5 watt) at −130 °C, although a 5-mg sample did explode on one occasion with sufficient force to destroy our low-temperature Raman device. It is a powerful oxidizer, capable of igniting organic substances such as foam rubber even at low temperatures. The reaction of $N_5^+AsF_6^-$ with water is violently explosive and should be avoided. This is not surprising in view of the facts that O_2^+ is a powerful oxidizer and the first ionization potential of N_2 (1503 kJ mol^{-1}) is significantly higher than that of O_2 (1206 kJ mol^{-1}); the electron affinity of N_5^+ is the subject of a further computational study. The high energy density of N_5^+ was also confirmed by a calculation using the G2 method[13] that gave formation enthalpies of $\Delta H_f^0 = 1478$ and $\Delta H_f^{298} = 1469$ kJ mol^{-1} for free gaseous N_5^+.

Solid ^{15}N-labeled $N_5^+AsF_6^-$ in a quartz tube (3 mm outer diameter) was warmed in a stepwise manner from −78 to +22 °C under a vacuum of 10^{-7} Torr while monitoring the volatile products with a mass spectrometer; the principal decomposition product detected was N_2. After pumping at 22 °C for 20 min, however, most of the solid remained and was identified by low-temperature Raman spectroscopy as $N_5^+AsF_6^-$, thus demonstrating that the compound has reasonable stability at room temperature. In samples prepared from an excess of HN_3 and containing some $H_2N_3^+AsF_6^-$[12] as a by-product, HN_3 and its fragments, HF, and AsF_5 were also observed in the mass spectra.

The ^{14}N and ^{15}N NMR spectra of N_5^+ labeled in either the 1- or 3-position and the ^{14}N NMR spectrum of unlabeled N_5^+ were recorded at −63 °C in anhydrous HF solution that was acidified with about 2 mol % of AsF_5 to slow down a potential exchange between the cation and the solvent.[14] The spectra of the ^{15}N-labeled mixture are shown in Figure 2, and the observed and calculated chemical shifts are compared in Table 1.

The signals due to N1 and N3 were observable in the ^{15}N spectra at $\delta = -237.3$ and −100.4, respectively, in excellent agreement with the calculated values of $\delta = -235$ and −95. The signal-to-noise ratio of the ^{15}N spectrum was low due to the poor solubility of $N_5^+AsF_6^-$ in HF at −63 °C, and a long delay time (60 s) was needed because of the slow relaxation rates. The area ratio of the two signals was about 1:1, indicating that the synthesis of HN_3 from end-labeled N_3^- and stearic acid had resulted in about equimolar quantities of N_α- and N_γ-labeled HN_3. In addition to the two N_5^+ signals, two weaker signals at $\delta = -312.0$ (t, $^1J(^1H,^{15}N) = 100.7$ Hz) and −111.4 (s) were observed in the ^1H-coupled ^{15}N NMR spectrum that are attributable to N_α and N_γ, respectively, of $[H_2N_\alpha N_\beta N_\gamma]^+$.[12] This was verified by recording the spectrum of a known sample of $H_2N_3^+AsF_6^-$ in HF solution.

In the ^{14}N spectrum of labeled and unlabeled $N_5^+AsF_6^-$ a single resonance at $\delta = -165.3$ was observed and assigned to

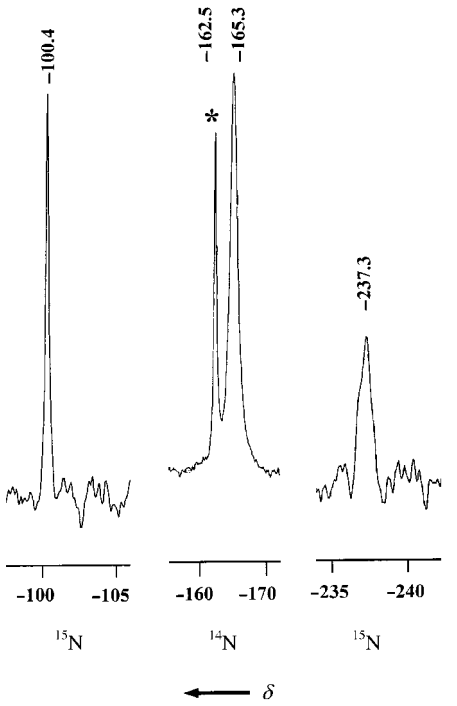

Figure 2. Sections of ^{14}N and ^{15}N NMR spectra for an equimolar mixture of singly ^{15}N-labeled $[^{15}N^{14}N^{14}N^{14}N^{14}N]^+$ and $[^{14}N^{14}N^{15}N^{14}N^{14}N]^+AsF_6^-$ recorded at −63 °C in anhydrous HF solution that was acidified with 2 mol % AsF_5. The resonance marked by an asterisk is due to $H_2N_3^+$ (see text for details).

Table 1. Observed and calculated ^{15}N and ^{14}N NMR data for N_5^+.

	δ[a] observed[b]		calculated[c]		
	^{15}N	^{14}N	N1	N2	N3
$[^{15}N1\text{-}^{14}N2\text{-}^{14}N3\text{-}^{14}N2'\text{-}^{14}N1']^+$	−237.3				
		−165.3[d]	−235	−166	−95
$[^{14}N1\text{-}^{14}N2\text{-}^{15}N3\text{-}^{14}N2'\text{-}^{14}N1']^+$	−100.4				

[a] Chemical shifts are given relative to that of neat CH_3NO_2 as external standard. [b] The spectra were recorded ^1H-coupled at −63 °C in anhydrous HF solution which was acidified with AsF_5. [c] Calculated at the CCSD(T)/QZP level of theory. An empirical correction of −20 ppm was applied to all calculated values, based on a comparison between the calculated and observed shifts of a number of closely related molecules and ions. [d] The other two resonances are badly broadened owing to exchange and were not detected in the ^{14}N spectrum.

  1433-7851/99/3813-2006 $ 17.50+.50/0

N2 of N_5^+ based on the calculated value of $\delta = -166$. The signals due to N1 and N3 could not be observed in the ^{14}N spectra under these conditions due to excessive quadrupole broadening. The N_β signal of $[H_2N_\alpha N_\beta N_\gamma]^+$ was also observable in the ^{14}N spectra of the labeled and unlabeled cations as a sharp resonance at $\delta = -162.5$, while signals for N_α and N_γ were strongly quadrupole broadened. It is fortunate that N2 of N_5^+ gives rise to a sharp ^{14}N signal and that the single ^{15}N substitution provided us with an equal mixture of ^{15}N labels on N1 and N3, thus allowing the unambiguous observation of all three signals of N_5^+. Their excellent agreement with the calculated values provides positive proof for the presence of a C_{2v}-symmetric N_5^+ cation.

Additional unambiguous proof for the presence of C_{2v}-N_5^+ was provided by the vibrational spectra of $N_5^+AsF_6^-$ and the $^{14}N-{}^{15}N$ isotopic shifts observed for the mixture of $^{15}N1$- and $^{15}N3$-labeled $N_5^+AsF_6^-$. The low-temperature Raman spectra of unlabeled and a mixture of labeled $N_5^+AsF_6^-$ are shown in Figures 3 and 4, respectively, and the observed frequencies are summarized in Tables 2 and 3. The vibrational assignments for octahedral AsF_6^- in Table 2 are well established[15] and do not require any further discussion; those for N_5^+ are based on our calculations. As can be seen, the four N–N stretching modes were observed with the predicted frequencies and intensities.

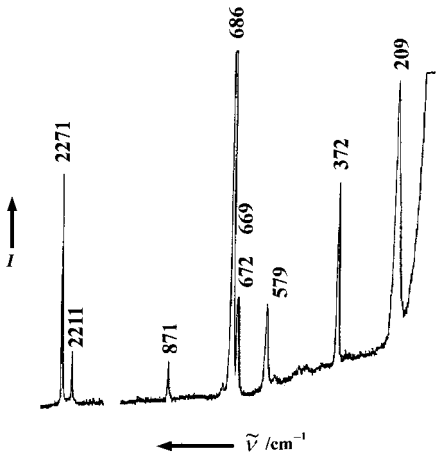

Figure 3. Low-temperature Raman spectrum of unlabeled solid $N_5^+AsF_6^-$.

The spectra of $^{15}N1$- and $^{15}N3$-labeled N_5^+ allowed accurate measurements of the isotopic shifts for modes $\nu_2(A_1)$, $\nu_7(B_2)$, and $\nu_1(A_1)$. Again, the agreement between experiment and theory is very good and confirms the validity of the predicted structure given in Figure 1. Since the observed frequencies of N_5^+ are intermediate between those predicted at the CCSD(T) and the B3LYP levels of calculation, the actual geometry of N_5^+ is probably also intermediate between the CCSD(T) and B3LYP values of Figure 1. Therefore, the following geometry is interpolated for $[N1\text{-}N2\text{-}N3\text{-}N2\text{-}N1]^+$: $r(N1{-}N2) = 1.11$ Å, $r(N2{-}N3) = 1.315$ Å, $\sphericalangle(N1\text{-}N2\text{-}N3) = 166.6°$, and $\sphericalangle(N2\text{-}N3\text{-}N2) = 110.3°$.

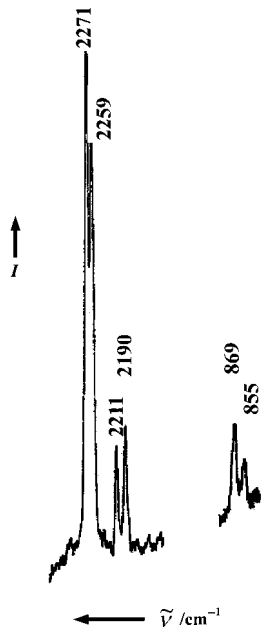

Figure 4. Low-temperature Raman spectrum of an equimolar mixture of solid $[^{15}N^{14}N^{14}N^{14}N^{14}N]^+AsF_6^-$ and $[^{14}N^{14}N^{15}N^{14}N^{14}N]^+AsF_6^-$.

The results from a normal coordinate analysis of N_5^+ are summarized in Table 4. They show that the A_2, B_1, and B_2 vibrations and $\nu_1(A_1)$ are all highly characteristic, but that $\nu_2(A_1)$ is a mixture of stretches and bends.

The internal force constants of greatest interest are the stretching force constants f_r and f_R of the terminal and the central N–N bonds, respectively. Interpolation of the data in Table 4 and adjustments for the observed frequencies give values of 20.08 and 6.59 mdyn Å^{-1} for the terminal and the central N–N stretching force constants, respectively. The

Table 2. Low-temperature Raman and IR bands of solid $^{14}N_5^+AsF_6^-$ and their assignments based on the calculated harmonic frequencies of free gaseous N_5^+.

Obsd frequencies [cm^{-1}][a]		Assignment (point group)		Calcd frequencies [cm^{-1}][b]	
Raman[c]	IR[d]	$^{14}N_5^+(C_{2v})$	$AsF_6^-(O_h)$	B3LYP	CCSD(T)
2271 [44]	2270 (m)	$\nu_1(A_1)$		2336 (22)	2229 (13) [215][e]
2211 [8]	2210 (s)	$\nu_7(B_2)$		2282 (147)	2175 (105) [42]
	1088 (s)	$\nu_8(B_2)$		1167 (141)	1032 (138) [2]
871 [7]	872 (w)	$\nu_2(A_1)$		850 (4)	818 (0.5) [5]
	704 (vs)		$\nu_3(F_{1u})$		
686 [100]	680 (sh)		$\nu_1(A_{1g})$		
672 [17], 669 [18]		$\nu_3(A_1)$	or part of $\nu_1(A_{1g})$ or $\nu_3(F_{1u})$	678 (1)	644 (2) [1]
579 [16]	575 (w)		$\nu_2(E_g)$		
		$\nu_5(A_2)$		502 (0)	475 (0) [1]
	420 (sh)	$\nu_6(B_1)$		424 (7)	405 (6) [0]
		$\nu_9(B_2)$		436 (0.6)	399 (1) [0.5]
	394 (vs)		$\nu_4(F_{1u})$		
372 [32]	360 (sh), 380 (sh)		$\nu_5(F_{2g})$		
209 [44]		$\nu_4(A_1)$		193 (0.5)	181 (0.3) [6]
127 [55]		lattice vibration			

[a] Relative IR and Raman intensities given in parentheses and brackets, respectively. [b] Frequencies calculated using a 6–311 + G(2d) basis set. IR intensities given in parentheses [km mol^{-1}], and Raman intensities given in brackets [Å^4 amu^{-1}]. [c] $T = -130$ °C. [d] $T = -196$ °C. [e] The Raman intensities were calculated at the RHF level.

  1433-7851/99/3813-2007 $ 17.50+.50/0

Table 3. Comparison of the calculated (B3LYP) and observed ^{15}N isotopic shifts for N_5^+.

N_5^+ isotopomer	Calcd frequencies (shifts) [cm^{-1}]								
	$\nu_4(A_1)$	$\nu_9(B_2)$	$\nu_6(B_1)$	$\nu_5(A_2)$	$\nu_3(A_1)$	$\nu_2(A_1)$	$\nu_8(B_2)$	$\nu_7(B_2)$	$\nu_1(A_1)$
$^{14}N1$-$^{14}N2$-$^{14}N3$-$^{14}N2$-$^{14}N1$	193.1(0)	424.1(0)	436.3(0)	502.4(0)	678.1(0)	850.0(0)	1116.9(0)	2281.7(0)	2336.3(0)
$^{14}N1$-$^{14}N2$-$^{15}N3$-$^{14}N2$-$^{14}N1$	191.8(1.3)	422.0(2.1)	436.0(.2)	502.4(0)	677.5(.7)	833.3(16.7)	1138.0(28.9)	2281.2(.5)	2336.3(.1)
$^{15}N1$-$^{14}N2$-$^{14}N3$-$^{14}N2$-$^{14}N1$	190.8(2.2)	422.3 (1.8)	434.7(1.5)	500.7(1.7)	674.4(3.7)	847.4(2.6)	1163.4(3.5)	2259.8(21.9)	2324.5(11.9)

N_5^+ isotopomer	Obsd frequencies (shifts) [cm^{-1}][a]					
	$\nu_2(A_1)$, IR	$\nu_2(A_1)$, RA	$\nu_7(B_2)$, IR	$\nu_7(B_2)$, RA	$\nu_1(A_1)$, IR	$\nu_1(A_1)$, RA
$^{14}N1$-$^{14}N2$-$^{14}N3$-$^{14}N2$-$^{14}N1$	872(0)	871(0)	2210(0)	2211(0)	2271(0)	2271(0)
$^{14}N1$-$^{14}N2$-$^{15}N3$-$^{14}N2$-$^{14}N1$	858(14)	855(16)	2209.8	2211(1)	2270.8	2271(0)
$^{15}N1$-$^{14}N2$-$^{14}N3$-$^{14}N2$-$^{14}N1$	870(2)	869(2)	2189.0(21)	2190(21)	2259.0(12)	2259(12)

[a] RA = Raman.

Table 4. Results from the normal coordinate analysis[a] of N_5^+.

Approx. mode in point group C_{2v}			Frequency [cm^{-1}]		Symmetry force constants[b] CCSD(T) (B3LYP)				Potential energy distribution[a] [%]
			obsd	calcd CCSD(T) (B3LYP)					CCSD(T)
A_1	ν_1	in-phase terminal stretches	2270	2229 (2336)	F_{11}	19.573(21.314)			93(1) + 6(2)
	ν_2	sym. central stretch	872	818 (850)	F_{22}	0.702(0.843)	5.546(6.952)		62(2) + 23(3) + 13(4) + 2(1)
	ν_3	central bending		644 (678)	F_{33}	−0.085(−0.137)	1.377(1.535)	1.540(1.427)	39(3) + 33(2) + 23(4) + 5(1)
	ν_4	in-phase terminal bends	209	181 (193)	F_{44}	0.167(0.171)	0.204(0.312)	0.120(0.108)	0.373(0.425) 64(4) + 37(3) − (2)
A_1	ν_5	torsion		475 (502)	F_{55}	0.0266(0.0281)			100(5)
B_1	ν_6	torsion		405 (424)	F_{66}	0.0236(0.0246)			100(6)
						F_{77}	F_{88}	F_{99}	
B_2	ν_7	out-of-phase term stretch	2210	2175 (2282)	F_{77}	19.491(21.272)			96(7) + 4(8)
	ν_8	asym. central stretch	1088	1032 (1167)	F_{88}	1.197(1.359)	4.780(5.927)		95(8) + 4(7)
	ν_9	out-of-phase terminal bends		399 (436)	F_{99}	0.200(0.195)	0.085(0.159)	0.358(0.423)	99(9) + 1(8)

[a] The following symmetry coordinates were used for $[N1\text{-}N2\text{-}N3\text{-}N2'\text{-}N1']^+$: $S_1 = \nu(1-2) + \nu(1'-2')$; $S_2 = \nu(2-3) + \nu(2'-3)$; $S_3 = \delta(2-3-2')$; $S4 = \delta(1-2-3) + \delta(1'-2'-3)$; $S_5 = \tau(1-2-3-2') + \tau(2-3-2'-1')$; $S_6 = \tau(1-2-3-2') - \tau(2-3-2'-1')$; $S_7 = \nu(1-2) - \nu(1'-2')$; $S_8 = \nu(2-3) - \nu(2'-3)$; $S_9 = \delta(1-2-3) - \delta(1'-2'-3)$. [b] The two most important internal force constants, estimated from the calculated symmetry force constants and the observed frequencies are $f_{(1-2)} = 20.08$ mdyn Å^{-1} and $f_{(2-3)} = 6.59$ mdyn Å^{-1}. Streching constants in mdyn Å^{-1}, deformation constants in mdyn Å^{-1} rad^{-2}, and stretch-bend interaction constants in mdyn rad^{-1}.

former value is significantly lower than the 22.4 mdyn Å^{-1} found for the N≡N bond in N_2,[15] whereas the latter value is between those found for typical N–N single (f_{N-N} = 3.6 mdyn Å^{-1}) and double bonds (f_{N-N} = 10.2 mdyn Å^{-1}).[15] The strengthening of the N–N central bonds at the expense of the terminal bonds, as suggested by the resonance structures, explains the relative stability of N_5^+ toward N_2 elimination. Reliable calculations of the energy barrier for N_2 elimination from N_5^+ will be the subject of a separate study.

Experimental Section

Caution! $N_5^+AsF_6^-$ is a highly energetic, strongly oxidizing material that can detonate violently. It should be handled only on a very small scale while using appropriate safety precautions (face shields, leather gloves, and protective clothing).

The $N_2F^+AsF_6^-$ was prepared from *cis*-N_2F_2 and AsF_5 as previously described.[16a–c] The HN_3 was generated by heating NaN_3 with a threefold excess of stearic acid to about 80 °C under a dynamic vacuum and collecting the evolved HN_3 in a trap cooled with liquid N_2. The HN_3 was purified by fractional condensation through a series of traps at −64, −95, and −196 °C, with the material retained at −95 °C being used. Singly ^{15}N-labeled NaN_3 (Cambridge Isotope Laboratories, 99 % ^{15}N label) was used for the preparation of a roughly 50:50 mixture of HN_3 that was singly ^{15}N-labeled in either the α or γ position. The HF (Matheson Co.) was dried by storage over BiF_5.[17]

The HN_3 was generated and handled on a Pyrex glass vacuum line equipped with grease-free Kontes glass-Teflon valves. The HF was handled on a previously described[18] stainless steel-Teflon FEP vacuum line. The $N_5^+AsF_6^-$ samples were handled at −196 °C in the dry N_2 atmosphere of a glove box.

Low-temperature Raman spectra were recorded on a Cary Model 83GT spectrometer using the 488-nm line of an Ar-ion laser for excitation, a previously described cooling device,[19] and quartz tubes (3 mm outer diameter) as sample containers. For measurements of the $^{14}N - ^{15}N$ isotopic shifts, the signal was scale expanded on an external strip chart recorder. The low-temperature IR spectra were recorded on a Mattson Galaxy FTIR

  1433-7851/99/3813-2008 $ 17.50+.50/0

spectrometer using a demountable low-temperature cell equipped with CsI windows. The ^{14}N and ^{15}N NMR spectra were recorded at 36.13 and 50.69 MHz, respectively, on a Bruker AMX 500 spectrometer using saturated solutions of $N_5^+AsF_6^-$ in HF/AsF_5 at $-63\,^\circ C$ and heat-sealed 5-mm Teflon-FEP liners (Wilmad Glass Co.) as sample containers, delay times of 60–120 s for the recording of the ^{15}N spectra, and neat CH_3NO_2 and aqueous ^{15}N-labeled urea referenced as $\delta = -305.0$ relative to CH_3NO_2 as external standards. The spectra were recorded both ^1H-coupled and ^1H-decoupled to determine if there was a nuclear Overhauser effect.

Preparation of $N_5^+AsF_6^-$: In a typical experiment, $N_2F^+AsF_6^-$ (1.97 mmol) was loaded in the drybox into a Teflon-FEP ampule (1.9 cm outer diameter) that was closed by a stainless steel valve. On the metal vacuum line, anhydrous HF (≈3 mL) was added at $-196\,^\circ C$, and the mixture was warmed to room temperature to dissolve the $N_2F^+AsF_6^-$. The ampule was connected to the glass line, and HN_3 (2.39 mmol) was added at $-196\,^\circ C$. The ampule was reconnected to the metal line and allowed to warm to $-78\,^\circ C$, where it was kept for three days with occasional gentle agitation. The ampule was then cooled to $-196\,^\circ C$ to check for the presence of volatile products. Nitrogen (0.76 mmol) was identified by mass spectrometry. All material volatile at $-64\,^\circ C$ was pumped off for 8 h, leaving behind a white solid residue that was identified by low-temperature vibrational and ^{14}N and ^{15}N NMR spectroscopy as a mixture of $N_5^+AsF_6^-$ (≈80 mol %) and $H_2N_3^+AsF_6^-$ (≈20 mol %).

Preparation of ^{15}N-labeled $N_5^+AsF_6^-$: The procedure was identical to that used for the synthesis of unlabeled $N_5^+AsF_6^-$, except for the use of a mixture of HN_3 that was ^{15}N-labeled in either the N_α or N_γ position.

Computational Methods. Hartree–Fock (HF), density functional theory (DFT), and single- and double-excitation coupled cluster calculations[20] that include a noniterative treatment of connected triple excitations (denoted CCSD(T))[21] were carried out employing several atomic basis sets. The DFT calculations employed the B3LYP functional.[22] Geometries, IR and Raman spectra, and nuclear magnetic resonance shieldings were calculated for N_5^+ as well as (for calibration purposes) N_2F^+, $H_2N_3^+$, and the standard CH_3NO_2, the geometries and NMR parameters of which are experimentally known.[12, 14, 16] The vibrational spectra reported in this work were computed using the 6-311 + G(2d) atomic basis set.[23] The NMR shieldings were computed at the CCSD(T)/6-311 + G(2d) geometries employing the gauge-including atomic orbital (GIAO) solution to the gauge-invariance problem[24] and density matrices obtained from second-order many-body perturbation theory [MBPT(2)], CCSD, or CCSD(T) calculations.[25–27] The results reported in this work used quadruple-zeta plus polarization (QZP) atomic basis sets derived from the QZ sets of Schäfer et al.,[28] supplemented with a d function with exponent 1.0. As discussed by Gauss and Stanton,[25–27] the accurate calculation of nitrogen NMR shieldings frequently requires an extensive electron correlation treatment such as that provided by the CCSD(T) method. Hartree–Fock and even MBPT(2) shielding calculations for species such as N_5^+ with many free valence electron pairs yield extremely poor results. The GAMESS,[29] Gaussian,[30] and ACES II[31] program systems were used for these calculations on IBM RS/6000 work stations.

Received: March 9, 1999 [Z 13131 IE]
German version: *Angew. Chem.* **1999**, *111*, 2112–2118

Keywords: density functional calculations · isotopic labeling · nitrogen · NMR spectroscopy · vibrational spectroscopy

[1] See, for example, *Proceedings of the High Energy Density Matter Conference* (New Orleans, LA) **1989**, available from the Defense Technical Information Center, Fort Belvoir, VA, as report no. ADA212314.
[2] W. J. Lauderdale, J. F. Stanton, R. J. Bartlett, *J. Phys. Chem.* **1992**, *96*, 1173.
[3] M. N. Glukhovtsev, H. Jiao, P. v. R. Schleyer, *Inorg. Chem.* **1996**, *35*, 7124.
[4] For a recent summary of previous experimental and theoretical studies, see the citations given in reference [3], and M. T. Nguyen, T. K. Ha, *Chem. Ber.* **1996**, *129*, 1157.
[5] a) T. Curtius, *Ber. Dtsch. Chem. Ges.* **1890**, *23*, 3023; b) N. N. Greenwood, A. Earnshaw, *Chemistry of the Elements*, Pergamon, Oxford, **1984**, p. 466.
[6] For a recent summary of previous work, see J. Wasilewski, *J. Chem. Phys.* **1996**, *105*, 10969.
[7] a) R. Tian, J. C. Facelli, J. Michl, *J. Phys. Chem.* **1988**, *92*, 4073; b) J. A. Guthrie, R. C. Chaney, A. J. Cunningham, *J. Chem. Phys.* **1991**, *95*, 930.
[8] a) W. E. Thompson, M. E. Jacox, *J. Chem. Phys.* **1990**, *93*, 3856; b) E. Bieske, *J. Chem. Phys.* **1993**, *98*, 8537; c) K. Sohlberg, *J. Mol. Struct. (Theochem.)* **1995**, *339*, 195; d) T. Ruchti, T. Speck, J. P. Connelly, E. J. Bieske, H. Linnartz, J. P. Maier, *J. Chem. Phys.* **1996**, *105*, 2591.
[9] F. A. Cotton, G. Wilkinson, *Advanced Inorganic Chemistry*, 3rd ed., Interscience, New York, **1972**, p. 113.
[10] P. Pyykkö, N. Runeberg, *J. Mol. Struct. (Theochem.)* **1991**, *234*, 279.
[11] G. Rasul, private communication.
[12] K. O. Christe, W. W. Wilson, D. A. Dixon, S. I. Khan, R. Bau, T. Metzenthin, R. Lu, *J. Am. Chem. Soc.* **1993**, *115*, 1836.
[13] L. A. Curtiss, K. Raghavachari, G. W. Trucks, J. A. Pople, *J. Chem. Phys.* **1991**, *94*, 7221.
[14] K. O. Christe, J. F. Hon, D. Pilipovich, *Inorg. Chem.* **1973**, *12*, 84.
[15] a) H. Siebert, *Anwendungen der Schwingungsspektroskopie in der Anorganischen Chemie, Anorganische und Allgemeine Chemie in Einzeldarstellungen VII*, Springer, Heidelberg, **1996**; b) J. Weidlein, U. Müller, K. Dehnicke, *Schwingungsspektroskopie*, Georg Thieme, Stuttgart, **1982**.
[16] a) D. Moy, A. R. Young, *J. Am. Chem. Soc.* **1965**, *87*, 1889; b) K. O. Christe, R. D. Wilson, W. Sawodny, *J. Mol. Struct.* **1971**, *8*, 245; c) K. O. Christe, R. D. Wilson, W. W. Wilson, R. Bau, S. Sukumar, D. A. Dixon, *J. Am. Chem. Soc.* **1991**, *113*, 3795; d) J. Mason, K. O. Christe, *Inorg. Chem.* **1983**, *22*, 1849.
[17] K. O. Christe, W. W. Wilson, C. J. Schack, *J. Fluorine Chem.* **1978**, *11*, 71.
[18] K. O. Christe, R. D. Wilson, C. J. Schack, *Inorg. Synth.* **1986**, *24*, 3.
[19] F. A. Miller, B. M. Harney, *Appl. Spectrosc.* **1970**, *24*, 291.
[20] G. D. Purvis III, R. J. Bartlett, *J. Chem. Phys.* **1982**, *76*, 1910.
[21] K. Raghavachari, G. W. Trucks, J. A. Pople, M. Head-Gordon, *Chem. Phys. Lett.* **1989**, *157*, 479.
[22] A. D. Becke, *J. Chem. Phys.* **1993**, *98*, 5648.
[23] M. J. Frisch, J. A. Pople, J. S. Binkley, *J. Chem. Phys.* **1984**, *80*, 3265.
[24] R. Ditchfield, *Mol. Phys.* **1974**, *27*, 789.
[25] J. Gauss, *J. Chem. Phys.* **1993**, *99*, 3629.
[26] J. Gauss, J. F. Stanton, *J. Chem. Phys.* **1995**, *103*, 3561.
[27] J. Gauss, J. F. Stanton, *J. Chem. Phys.* **1996**, *104*, 2574.
[28] A. Schäfer, H. Horn, R. Ahlrichs, *J. Chem. Phys.* **1992**, *97*, 2571.
[29] GAMESS, M. W. Schmidt, K. K. Baldridge, J. A. Boatz, S. T. Elbert, M. S. Gordon, J. J. Jensen, S. Koseki, N. Matsunaga, K. A. Nguyen, S. Su, T. L. Windus, M. Dupuis, J. A. Montgomery, *J. Comput. Chem.* **1993**, *14*, 1347.
[30] Gaussian 94, Revision E.2, M. J. Frisch, G. W. Trucks, H. B. Schlegel, P. M. W. Gill, B. G. Johnson, M. A. Robb, J. R. Cheeseman, J. Keith, G. A. Petersson, J. A. Montgomery, K. Raghavachari, M. A. Al-Laham, V. G. Zakrzewski, J. V. Ortiz, J. B. Foresman, J. Cioslowski, B. B. Stefanov, A. Nanayakkara, M. Challacombe, C. Y. Peng, P. Y. Ayala, W. Chen, M. W. Wong, J. L. Andres, E. S. Replogle, R. Gomperts, R. L. Martin, D. J. Fox, J. S. Binkley, D. J. Defress, J. Baker, J. P. Stewart, M. Head-Gordon, C. Gonzalez, J. A. Pople, Gaussian, Inc., Pittsburgh, PA, **1995**.
[31] ACES II, Quantum Theory Project, University of Florida. Authors: J. F. Stanton, J. Gauss, J. D. Watts, M. Nooijen, N. Oliphant, S. A. Perera, P. G. Szalay, W. J. Lauderdale, S. R. Gwaltney, S. Beck, A. Balkova, D. E. Bernholdt, K. K. Baeck, P. Rozyczko, H. Sekino, C. Hober, R. J. Bartlett; integral packages included are VMOL (J. Almlöf, P. R. Taylor), BPROPS (P. R. Taylor), and ABACUS (T. Helgaker, H. J. Aa. Jensen, P. Jorgensen, J. Olsen, P. R. Taylor).

  1433-7851/99/3813-2009 $ 17.50+.50/0

APPENDIX B

"Polynitrogen Chemistry. Synthesis, Characterization, and Crystal Structure of Surprisingly Stable Fluoroantimonate Salts of N_5^+"
J. Am. Chem. Soc., 123, 6308 (2001)

This Page Intentionally Left Blank

Polynitrogen Chemistry. Synthesis, Characterization, and Crystal Structure of Surprisingly Stable Fluoroantimonate Salts of N_5^+

Ashwani Vij,[†] William W. Wilson,[†] Vandana Vij,[†] Fook S. Tham,[§] Jeffrey A. Sheehy,[†] and Karl O. Christe*,[†,‡]

Contribution from the Propulsion Sciences and Advanced Concepts Division, Air Force Research Laboratory (AFRL/PRS), Edwards AFB, California 93524, Loker Hydrocarbon Research Institute and Department of Chemistry, University of Southern California, Los Angeles, California 90089, and Department of Chemistry, University of California, Riverside, California 92521

Received January 1, 2001. Revised Manuscript Received April 13, 2001

Abstract: The new N_5^+ salt, $N_5^+SbF_6^-$, was prepared from $N_2F^+SbF_6^-$ and HN_3 in anhydrous HF solution. The white solid is surprisingly stable, decomposing only at 70 °C, and is relatively insensitive to impact. Its vibrational spectrum exhibits all nine fundamentals with frequencies that are in excellent agreement with the theoretical calculations for a five-atomic V-shaped ion of C_{2v} symmetry. The $N_5^+Sb_2F_{11}^-$ salt was also prepared, and its crystal structure was determined. The geometry previously predicted for free gaseous N_5^+ from theoretical calculations was confirmed within experimental error. The $Sb_2F_{11}^-$ anions exhibit an unusual geometry with eclipsed SbF_4 groups due to interionic bridging with the N_5^+ cations. The N_5^+ cation is a powerful one-electron oxidizer. It readily oxidizes NO, NO_2, and Br_2 but fails to oxidize Cl_2, Xe, or O_2.

Introduction

The recent discovery of $N_5^+AsF_6^-$ as a marginally stable compound that can be prepared on a macroscopic scale is quite remarkable.[1] The N_5^+ cation represented only the third readily accessible homonuclear polynitrogen species besides N_2 and N_3^- and as such has received much public acclaim.[2] Since N_5AsF_6 is only marginally stable and had given rise to some explosions,[1] it was of great interest to search for more stable N_5^+ salts in order to allow a more thorough characterization of this fascinating cation and to provide a suitable starting material for the pursuit of nitrogen allotropes. In this paper, the synthesis and characterization of surprisingly stable fluoroantimonate salts of N_5^+ and the crystal structure of $N_5^+Sb_2F_{11}^-$ are reported.

Experimental Section

Caution! *HN_3, azides, and polynitrogen compounds are highly endothermic and can decompose explosively. They should be handled only on a small scale with appropriate safety precautions (face shields, leather gloves, and protective clothing). Condensation of neat HN_3 at −196 °C into Teflon ampules containing oxidizers has repeatedly resulted in explosions upon condensation or melting of the HN_3.*

Materials and Apparatus. All reactions were carried out in 0.75-in.-o.d. Teflon-FEP or -PFA ampules that contained Teflon-coated magnetic stirring bars and were closed by stainless steel or Teflon valves. Volatile materials were handled on a stainless steel/Teflon-FEP vacuum line.[3] Nonvolatile solids were handled in the dry nitrogen atmosphere of a glovebox. HN_3 was generated and handled on a Pyrex glass vacuum line equipped with grease-free Kontes glass/Teflon valves. Infrared spectra were recorded on a Mattson Galaxy FT-IR spectrometer using dry powders pressed between AgCl windows in an Econo press (Barnes Engineering Co.). Raman spectra were recorded on a Bruker Equinox 55 FT-RA spectrometer using a Nd−YAG laser at 1064 nm and Pyrex melting point capillaries as sample containers. The thermal stabilities were determined using a DuPont model 910 DSC, crimp-sealed aluminum pans as sample containers, and heating rates of 3 °C/min. The data were recorded and analyzed with a DuPont model 2000 thermal analyst. Impact sensitivities were measured on an Olin Mathieson drop weight tester standardized with RDX (hexahydro-1,3,5-trinitro-1,3,5-triazine, 30 kg·cm, 50%).

The $N_2F^+SbF_6^-$ and $N_2F^+Sb_2F_{11}^-$ starting materials were prepared from *cis*-N_2F_2 and SbF_5 in anhydrous HF solution as previously described.[4−7] The HF (Matheson Co.) was dried by storage over BiF_5 (Ozark Mahoning).[8] The NO and NO_2 (Matheson Co) were purified by fractional condensation prior to their use. The O_2 and Xe (Matheson Co) were used as received. The preparation of HN_3 has previously been described.[1]

Preparation of $N_5^+SbF_6^-$. A Teflon ampule, equipped with a stainless steel valve and containing a Teflon-coated magnetic stirring bar, was passivated with ClF_3. It was attached to the metal vacuum line and treated several times with anhydrous HF until no color was observed upon freezing the HF at −196 °C. It was then loaded with $N_2F^+SbF_6^-$ (4.97 mmol) in the glovebox and attached to the metal vacuum line. The ampule was evacuated and cooled to −196 °C. Anhydrous HF (∼2 mL) was then condensed into the ampule, and the contents were allowed to warm to ambient temperature with occasional stirring. After all the $N_2F^+SbF_6^-$ had dissolved, the ampule was recooled to −196 °C, and some additional neat HF was condensed onto the upper walls of the tube, where the HN_3 was going to be frozen out. The cold ampule was then connected to the glass line, and HN_3 (5.00 mmol)

[†] Air Force Research Laboratory.
[‡] University of Southern California.
[§] University of California, Riverside.

(1) Christe, K. O.; Wilson, W. W.; Sheehy, J. A.; Boatz, J. A. *Angew. Chem., Int. Ed.* **1999**, *38*, 2004.
(2) See, for example: *Chem. Eng. News* **1999**, *77*, Jan 25, 7; **1999**, *77*, Nov 29, 38; **2000**, *78*, Aug 14, 41.
(3) Christe, K. O.; Wilson, W. W.; Schack, C. J.; Wilson, R. D. *Inorg. Synth.* **1986**, *24*, 39.
(4) Ruff, J. K. *Inorg. Chem.* **1966**, *5*, 1971.
(5) Roesky, H. W.; Glemser, O.; Bormann, D. *Chem. Ber.* **1966**, *99*, 1589.
(6) Pankratov, V. A.; Savenkova, N. I. *Zh. Neorg. Khim.* **1968**, *13*, 2610.
(7) Christe, K. O.; Wilson, R. D.; Sawodny, W. *J. Mol. Struct.* **1971**, *8*, 245. Christe, K. O.; Wilson, R. D.; Wilson, W. W.; Bau, R.; Sukumar, S.; Dixon, D. A. *J. Am. Chem. Soc.* **1991**, *113*, 1991.
(8) Christe, K. O.; Wilson, W. W.; Schack, C. J. *J. Fluorine Chem.* **1978**, *11*, 71.

10.1021/ja010141g CCC: $20.00
Published on Web 06/09/2001

was added slowly at −196 °C. The reaction mixture was allowed to warm slowly behind a safety shield to room temperature and kept at this temperature for about 45 min. The volatile materials were removed by pumping for several hours at 20 °C, leaving behind a white powder (1.502 g, weight calculated for 4.97 mmol of N_5SbF_6 = 1.520 g) that was identified by its vibrational spectra as N_5SbF_6.

This reaction was also carried out by first condensing HN_3 at −196 °C into a passivated and preweighed Teflon ampule containing a known amount of HF. The resulting mixture was homogenized at ambient temperature. The ampule was taken into the glovebox, where a stoichiometric amount of $N_2F^+SbF_6^-$ was added at −196 °C. The cold ampule was attached to the metal vacuum line and evacuated. Subsequent slow warming of the reaction mixture to room temperature for about 30 min, followed by removal of all volatile material, resulted in the isolation of $N_5^+SbF_6^-$ in >99% yield.

The safest method of generating HN_3 and reacting it with $N_2F^+SbF_6^-$ involved the use of two Teflon-FEP U-tubes that were interconnected through a porous Teflon filter (Pall Corp) and attached to the metal vacuum line. The first tube contained a weighed amount of NaN_3 and the second one a stoichiometric amount of $N_2F^+SbF_6^-$. Amounts of anhydrous HF, sufficient to dissolve both solids, were condensed at −196 °C into both U-tubes, and the solids were dissolved in the HF at room temperature. The second U-tube, containing the $N_2F^+SbF_6^-$ solution, was cooled to −196 °C, and the HN_3, generated in the first U-tube, together with the excess of HF were co-condensed in a dynamic vacuum into the second U-tube. The resulting mixture was allowed to warm slowly to room temperature. Removal of the HF in a dynamic vacuum resulted in the isolation of very pure $N_5^+SbF_6^-$ in >99% yield. This procedure has been carried out repeatedly on a 5-g scale without incident.

Preparation of $N_5^+Sb_2F_{11}^-$. Freshly distilled SbF_5 (1.449 mmol) was added in the glovebox to a passivated Teflon-FEP ampule, and HF (1.9 mL liquid) was added on the metal vacuum line at −196 °C. The mixture was homogenized at room temperature and taken back into the glovebox. The ampule was cooled inside the glovebox to −196 °C and opened, and $N_5^+SbF_6^-$ (1.444 mmol) was added. The resulting mixture was allowed to warm to room temperature, and all volatile material was pumped off. The white solid residue (758 mg, weight calculated for 1.444 mmol of $N_5^+Sb_2F_{11}^-$ = 755 mg) was shown by vibrational spectroscopy to consist of $N_5^+Sb_2F_{11}^-$.

Reactions of $N_5^+SbF_6^-$ with NO, NO_2, O_2, or Xe. In a typical experiment, a 0.5-in. Teflon-FEP ampule, that was closed by a Teflon valve, was loaded in the drybox with $N_5^+SbF_6^-$ (0.53 mmol). On the vacuum line, NO (4.2 mmol) was added at −196 °C, and the contents of the ampule were allowed to warm slowly with intermittent cooling to room temperature. After the ampule was kept for 2 h at room temperature, it was cooled back to −196 °C, and the volatile gas (1.34 mmol of N_2) was measured and pumped off. The unreacted NO was measured (3.6 mmol) and pumped off at room temperature, leaving behind 0.53 mmol of $NO^+SbF_6^-$ that was identified by vibrational spectroscopy.

In a similar manner, $N_5^+SbF_6^-$ was found to react quantitatively with NO_2 and Br_2, but no reaction was observed with either Cl_2, Xe, or O_2.

Crystal Structure Determination of $N_5^+Sb_2F_{11}^-$. About 1 mL of anhydrous SO_2 was condensed onto 0.200 g of N_5SbF_6 at −196 °C in a 0.5-in.-o.d. sapphire tube (Tyco Corp.) closed by a stainless steel valve. The contents of the tube were warmed to −78 °C, causing all of the N_5SbF_6 to dissolve and form a pale yellowish solution. Anhydrous SO_2ClF (~1.5 mL) was then slowly condensed onto this solution under vacuum. The solvents were then slowly removed under a static vacuum at −64 °C over a period of ~16 h, leaving behind platelike colorless crystals. These crystals were extremely reactive to perfluoropolyether oil and showed an instantaneous evolution of nitrogen gas. The majority of the crystals were very soft and difficult to handle, but a few crystals appeared to exhibit a different habit and better mechanical strength. One of these crystals was immersed in halocarbon grease and mounted on the goniometer head using a precentered Nylon Cryoloop equipped with a magnetic base. The structure of the salt was determined using a Bruker diffractometer equipped with a CCD detector and a low-temperature, LT3, device. The three-circle platform with a fixed *c*-axis was controlled by the SMART[9] software package. The unit cell parameters were determined at −60 °C from three runs of data with 30 frames per run, using a scan speed of 30 s per frame. A complete hemisphere of data was collected, using 1271 frames at 30 s/frame, including 50 frames that were collected at the beginning and end of the data collection to monitor crystal decay. Data were integrated using the SAINT[10] software package, and the raw data were corrected for absorption using the SADABS[11] program. The absence of $h + k$ = odd and $h0l$ reflections (l = odd) showed the presence of a *C*-centered lattice and a *c*-glide plane parallel and perpendicular to the *b*-axis, respectively, indicating *Cc* or *C*2/*c* as the likely space groups. The intensity statistics, $E^2 - 1$ values, indicated a centrosymmetric space group, thereby excluding *Cc* as a possible space group. The space group was thus unambiguously assigned as *C*2/*c*. The structure was solved by the Patterson method using the SHELXS-97[12] program and refined by the least-squares method on F^2 using SHELXL-97.[13] The initial Patterson map revealed the position of the two Sb atoms linked by a fluorine atom. The remaining atoms were located from subsequent difference electron density maps and finally refined anisotropically by the least-squares method on F^2 using the SHELXTL 5.1[14] software for Windows NT. The crystal did not show any significant decomposition during the data collection. The experimental and refinement parameters are listed in Table 1.

Table 1. Crystal Data and Structure Refinement for $N_5^+Sb_2F_{11}^-$

identification code	$N_5^+Sb_2F_{11}^-$
empirical formula	$F_{11}N_5Sb_2$
formula weight	522.55
temperature	213(2) K
wavelength	0.71073 Å
crystal system	monoclinic
space group	*C*2/*c*
unit cell dimensions	a = 10.913(8) Å, α = 90° b = 12.654(8) Å, β = 104.715(18)° c = 16.675(11) Å, γ = 90°
volume	2227(3) Å^3
Z	8
density (calculated)	3.117 Mg/m^3
absorption coefficient	4.995 mm^{-1}
F(000)	1888
crystal size	0.26 × 0.10 × 0.05 mm^3
θ range for data collection	2.51−25.35°
index ranges	$-12 \le h \le 13$ $-15 \le k \le 15$ $-20 \le l \le 17$
reflections collected	9125
independent reflections	2022 [R(int) = 0.0629]
absorption correction	SADABS
max. and min. transmission	0.7883 and 0.3567
refinement method	full-matrix least-squares on F^2
data/restraints/parameters	2022/0/164
goodness-of-fit on F^2	1.122
final R indices [$I > 2\sigma(I)$]	$R1$ = 0.0678, w$R2$ = 0.1913
R indices (all data)	$R1$ = 0.0785, w$R2$ = 0.2019
extinction coefficient	0.00026(18)
largest diff. peak and hole	4.329 and −2.102 e.Å^{-3}

Results and Discussion

Synthesis and Properties of $N_5^+SbF_6^-$. The synthesis of $N_5^+SbF_6^-$ was carried out in the same manner as previously reported[1] for $N_5^+AsF_6^-$ by reacting $N_2F^+SbF_6^-$ with HN_3 in

(9) SMART V 4.045, Software for the CCD Detector System, Bruker AXS, Madison, WI, 1999.

(10) SAINT V 4.035, Software for the CCD Detector System, Bruker AXS, Madison, WI, 1999.

(11) SADABS, Program for absorption correction for area detectors, Version 2.01, Bruker AXS, Madison, WI, 2000.

(12) Sheldrick, G. M. SHELXS-97, Program for the Solution of Crystal Structure, University of Göttingen, Germany, 1997.

(13) Sheldrick, G. M. SHELXL-97, Program for the Refinement of Crystal Structure, University of Göttingen, Germany, 1997.

(14) SHELXTL 5.1 for Windows NT, Program library for Structure Solution and Molecular Graphics, Bruker AXS, Madison, WI, 1997.

anhydrous HF solution at −78 °C, followed by removal of the volatile products at room temperature. The yield of $N_5^+SbF_6^-$

$$N_2F^+SbF_6^- + HN_3 \xrightarrow[-78 \text{ to } 25\ ^\circ\text{C}]{\text{HF}} N_5^+SbF_6^- + HF \quad (1)$$

is essentially quantitative, and the product purity is high. It is essential that the reaction system is completely anhydrous, as water hydrolyzes the N_5^+ salt, generating free SbF_5, which in combination with HF protonates HN_3 under formation of $H_2N_3^+SbF_6^-$.[15]

The $N_5^+SbF_6^-$ salt is a colorless hygroscopic solid that is stable at ambient temperature and, based on the DSC data, starts to decompose at 70 °C. It is surprisingly insensitive to impact. Even at the maximum setting of our apparatus (200 kg·cm), only partial thermal decomposition due to adiabatic heating of the sample was observed, but no explosions. The salt is soluble in and compatible with HF, SO_2, and CHF_3.

The oxidizing properties of $N_5^+SbF_6^-$ were examined in the solid state and in HF solution by treating it with 2 atm of either oxygen or xenon gas between −78 °C and ambient temperature. No oxidations to O_2^+ and Xe_2^+, respectively, were observed under these conditions. Furthermore, solid $N_5^+SbF_6^-$ did not oxidize liquid or gaseous chlorine, but is capable of oxidizing NO (2), NO_2 (3), and Br_2.

$$NO + N_5^+SbF_6^- \xrightarrow[-196 \text{ to } 25\ ^\circ\text{C}]{\text{excess NO}} NO^+SbF_6^- + 2.5N_2 \quad (2)$$

and

$$NO_2 + N_5^+SbF_6^- \xrightarrow[-196 \text{ to } 25\ ^\circ\text{C}]{\text{excess } NO_2} NO_2^+SbF_6^- + 2.5N_2 \quad (3)$$

Since NO, NO_2, Br_2, Cl_2, O_2, and Xe have first ionization potentials of 9.26, 9.75, 10.52, 11.48, 12.07, and 12.13 eV, respectively, these experiments indicate that the N_5^+ cation can oxidize substrates having a first ionization potential of 10.52 eV or less, but cannot oxidize substrates with a first ionization potential of 11.48 eV or more. When solid starting materials or reaction products are involved in these redox reactions, the first ionization potential of the substrate does not equal the electron affinity of the oxidizing agent, as any lattice energy changes must also be taken into account. For the calculation of the electron affinity, the appropriate Born−Haber cycle must be used, as shown in kilocalories per mole for reaction (3).

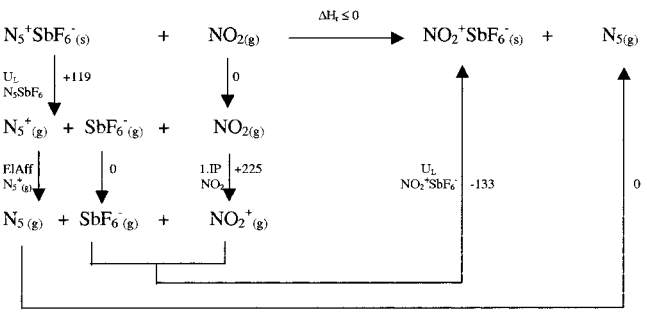

For the redox reaction to proceed, the enthalpy change, or more precisely the free energy change if entropy changes are included, of the reaction must be negative. Assuming ΔH_f to be zero, the electron affinity of $N_5^+{}_{(g)}$ is calculated to have a minimum value of 211 kcal/mol or 9.16 eV, a value significantly lower than the first ionization potential of NO_2 (9.75 eV). The required and experimentally unknown lattice energy values for N_5SbF_6 and NO_2SbF_6 were estimated using the method[16] of Jenkins and Passmore based on Bartlett's volume-based relationship.[17] It should be kept in mind, however, that the structure of $N_{5(g)}$ is unknown and that the final reaction product is 2.5 mol of N_2. The conversion of N_5 to N_2 is also strongly exothermic, as is apparent from the calculated[1] heat of formation of gaseous N_5^+ (351.1 kcal/mol) and the above-derived minimum electron affinity value of N_5^+ (211 kcal/mol).

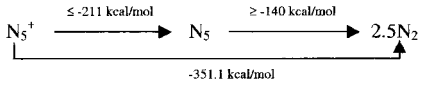

The above results show that N_5^+ is a weaker oxidizer than either PtF_6 that can oxidize O_2 to O_2^+ [18] or O_2^+ that can oxidize Xe to Xe_2^+ under similar conditions.[19,20] Despite the first ionization potential (IP) of N_2 (15.51 eV) being 3.44 eV higher than that of O_2 (12.07 eV), the electron affinity of N_5^+ is substantially lower than that of O_2^+ because in N_5^+ the positive charge is spread over a larger number of atoms, thereby decreasing its oxidizing power. Nevertheless, the fact that N_5^+ can quantitatively oxidize either NO, NO_2, or Br_2 renders it a very strong one-electron oxidizer. Although it is not quite as powerful as PtF_6 or O_2^+ salts, it offers the great advantage of not acting as a fluorinating or oxygenating agent, which can be a very important consideration when dealing with substrates that are easily fluorinated or oxygenated.

Ongoing studies in our laboratory show that the potential hazards of handling neat HN_3 in the synthesis of N_5^+ can be avoided by either replacing HN_3 with the insensitive $(CH_3)_3SiN_3$ or generating the desired HN_3 from a weighed amount of NaN_3 and excess HF in a separate ampule and transferring all volatiles into the reaction vessel containing an HF solution of $N_2F^+SbF_6^-$. The reactions with $(CH_3)_3SiN_3$ are carried out in either HF or SO_2 solution and produce N_5^+ in high yield. When HF is used as the solvent, the first reaction step most certainly involves the formation of $(CH_3)_3SiF$ and HN_3; i.e., HN_3 is generated in situ in the reactor.

Synthesis and Properties of $N_5^+Sb_2F_{11}^-$. To preclude a potential side reaction of $Sb_2F_{11}^-$ with HF and HN_3 to give SbF_6^- and $H_2N_3^+SbF_6^-$, a sample of $N_5^+SbF_6^-$ was reacted with an equimolar amount of SbF_5 in HF solution at room temperature. The resulting $N_5^+Sb_2F_{11}^-$ salt is a colorless solid

$$N_5SbF_6^- + SbF_5 \xrightarrow[25\ ^\circ\text{C}]{\text{HF}} N_5^+Sb_2F_{11}^- \quad (4)$$

that is stable at room temperature and undergoes, according to its DSC data, thermal decomposition at 70 °C; i.e., its thermal stability is comparable to that of $N_5^+SbF_6^-$, but, in contrast to $N_5^+SbF_6^-$, it undergoes a reversible endotherm (melting) at about 30 °C. Consequently, the replacement of SbF_6^- by $Sb_2F_{11}^-$ did not result in increased thermal stability and does not appear to offer any significant advantages for studying the reaction chemistry of N_5^+ salts.

Crystal Structure of $N_5^+Sb_2F_{11}^-$. The structure of $N_5^+Sb_2F_{11}^-$ is shown in Figures 1 and 2, and the important bond lengths

(15) Christe, K. O.; Wilson, W. W.; Dixon, D. A.; Khan, S. I.; Bau, R.; Metzenthin, T.; Lu, R. *J. Am. Chem. Soc.* **1993**, *115*, 1836.

(16) Jenkins, H. D. B.; Roobottom, H. K.; Passmore, J.; Glasser, L. *Inorg. Chem.* **1999**, *38*, 3609.

(17) Mallouk, T. E.; Rosenthal, G. L.; Muller, G.; Busasco, R.; Bartlett, N. *Inorg. Chem.* **1984**, *23*, 3167.

(18) Bartlett, N.; Lohmann, D. H. *Proc. R. Chem. Soc. (London)* **1962**, 277; *J. Chem. Soc.* **1962**, 5253.

(19) Stein, L.; Norris, J. R.; Downs, A. J.; Minihan, A. R. *J. Chem. Soc., Chem. Commun.* **1978**, 502.

(20) Stein, L.; Henderson, W. W. *J. Am. Chem. Soc.* **1980**, *102*, 2856.

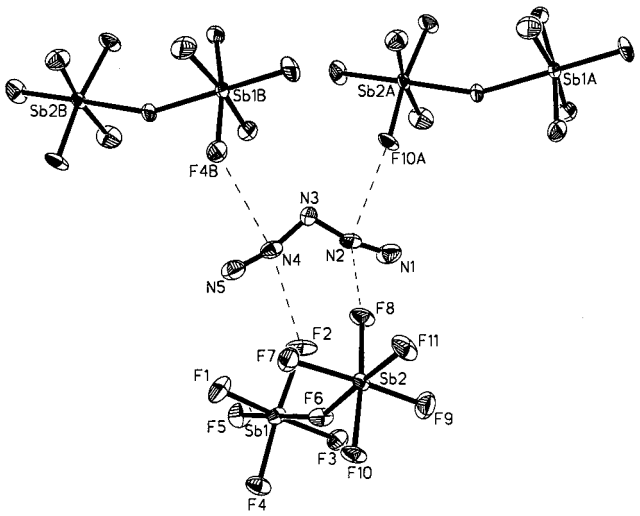

Figure 1. ORTEP diagram of $N_5^+Sb_2F_{11}^-$, showing the thermal ellipsoids at the 30% probability level and the close-range N···F contacts within the crystal lattice.

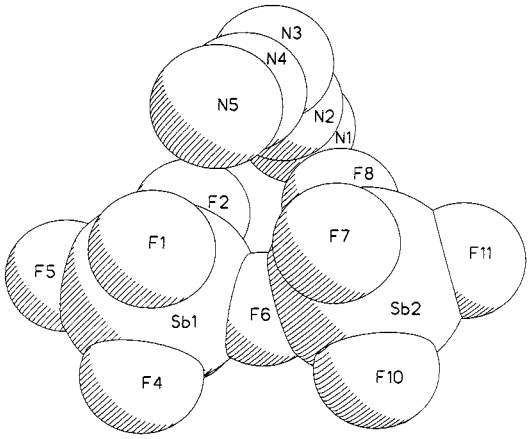

Figure 2. Space-filling representation of $N_5^+Sb_2F_{11}^-$, showing the close packing of the N_5^+ cation within the $Sb_2F_{11}^-$ cavity.

and angles are summarized in Table 2. The observed V-shaped geometry of the N_5^+ cation is in excellent agreement with the theoretical predictions[1] for the free gaseous N_5^+ cation at the B3LYP level of theory, with the calculated terminal and central N−N bond distances of 1.11 and 1.30 Å being close to the observed values of 1.105(19) and 1.299(19) Å, respectively. Furthermore, the terminal N−N distance of 1.105(19) Å in N_5^+ is only slightly longer than that of 1.089(9) Å found for N_2F^+ in $N_2F^+Sb_2F_{11}^-$ [21] and compares well with the N−N bond distances of 1.0976(2) Å in N_2[22] and 1.0927 Å found in HN_2^+,[23,24] indicating that the terminal bonds approximate triple bonds. The central N−N bond length of 1.299(19) Å in N_5^+ is somewhat longer than typical N−N double bonds (1.17−1.25 Å) but is significantly shorter than typical N−N single bonds (1.43−1.75 Å).[25] Additionally, the agreement between calculated [112.3 and 166.7°] and observed [111.2(11) and 167.2(15)°, respectively] bond angles is very good.

(21) Vij, A.; Vij, V.; Tham, F.; Christe, K. O. Unpublished results.
(22) Huber, K. P.; Herzberg, G. *Constants of Diatomic Molecules*; Van Nostrand Reinhold: New York, 1979.
(23) Owrutsky, J. C.; Gudeman, C. S.; Martner, C. C.; Tack, L. M.; Rosenbaum, N. H.; Saykally, R. J. *J. Phys. Chem.* **1986**, *84*, 605.
(24) Botschwina, P. *Chem. Phys. Lett.* **1984**, *107*, 535.
(25) Greenwood, N. N.; Earnshaw, A. *Chemistry of the Elements*, 2nd ed.; Butterworth, Heinemann: Oxford, 1998.

Table 2. Bond Lengths and Angles for $N_5^+Sb_2F_{11}^-$

Bond Lengths (Å)			
Sb(1)−F(5)	1.839(8)	Sb(2)−F(9)	1.849(10)
Sb(1)−F(4)	1.845(8)	Sb(2)−F(8)	1.866(8)
Sb(1)−F(2)	1.851(9)	Sb(2)−F(11)	1.866(8)
Sb(1)−F(3)	1.854(9)	Sb(2)−F(6)	2.007(7)
Sb(1)−F(1)	1.856(10)	N(1)−N(2)	1.102(19)
Sb(1)−F(6)	2.031(7)	N(2)−N(3)	1.303(19)
Sb(2)−F(10)	1.844(7)	N(3)−N(4)	1.295(19)
Sb(2)−F(7)	1.849(9)	N(4)−N(5)	1.107(19)
Bond Angles (deg)			
F(5)−Sb(1)−F(2)	94.8(4)	F(7)−Sb(2)−F(9)	170.7(5)
F(4)−Sb(1)−F(2)	169.9(4)	F(10)−Sb(2)−F(8)	171.3(4)
F(5)−Sb(1)−F(3)	95.4(5)	F(7)−Sb(2)−F(8)	87.9(4)
F(4)−Sb(1)−F(3)	89.7(4)	F(9)−Sb(2)−F(8)	88.8(5)
F(2)−Sb(1)−F(3)	89.3(5)	F(10)−Sb(2)−F(11)	94.8(4)
F(5)−Sb(1)−F(1)	93.6(5)	F(7)−Sb(2)−F(11)	96.7(5)
F(4)−Sb(1)−F(1)	91.0(5)	F(9)−Sb(2)−F(11)	92.2(5)
F(2)−Sb(1)−F(1)	88.4(5)	F(8)−Sb(2)−F(11)	93.9(4)
F(3)−Sb(1)−F(1)	170.8(4)	F(10)−Sb(2)−F(6)	85.0(3)
F(5)−Sb(1)−F(6)	179.9(5)	F(7)−Sb(2)−F(6)	85.9(4)
F(4)−Sb(1)−F(6)	84.7(4)	F(9)−Sb(2)−F(6)	85.3(5)
F(2)−Sb(1)−F(6)	85.1(4)	F(8)−Sb(2)−F(6)	86.3(4)
F(3)−Sb(1)−F(6)	84.5(4)	F(11)−Sb(2)−F(6)	177.5(4)
F(1)−Sb(1)−F(6)	86.4(4)	Sb(2)−F(6)−Sb(1)	155.0(4)
F(10)−Sb(2)−F(7)	91.2(5)	N(1)−N(2)−N(3)	168.1(15)
F(10)−Sb(2)−F(9)	90.8(5)	N(4)−N(3)−N(2)	111.2(11)

The observed geometry supports the previously given rationale[1] that the exceptional stability of N_5^+ is largely due to resonance stabilization, resulting in relatively high bond orders for all the bonds. The bonding in N_5^+ can be described by the following six resonance structures:

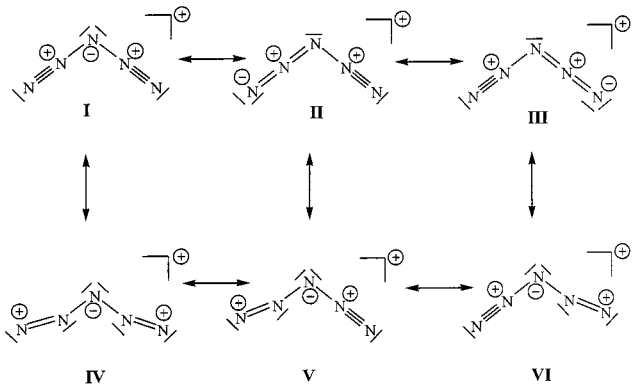

Although structures **IV**−**VI** possess one or two terminal nitrogen atoms with only six valence electrons, it must be kept in mind that conventional Lewis structures are oversimplifications and often do not adequately describe the actual bonding. Inclusion of structures **IV**−**VI** is required to account for the charge distributions calculated at the NBO(B3LYP/aug-cc-pVDZ) level,[26]

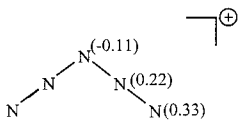

as well as the relative shielding of the N NMR signals (the shielding increases from the terminal nitrogen to the β-nitrogen to the central nitrogen)[1] and the terminal N−N−N bond angles of about 167°.

A least-squares plane analysis for N_5^+ shows that the cation is essentially planar. The N2 atom exhibits a maximum deviation of 0.11 Å from the average mean plane that shows a root-mean-

(26) Fau, S.; Bartlett, R. J. *J. Phys. Chem. A* **2001**, *105*, 4096.

Table 3. Observed Infrared and Raman Spectra of $N_5^+SbF_6^-$, $N_5^+Sb_2F_{11}^-$ and $N_5^+AsF_6^-$ and Their Assignments

observed frequency (cm^{-1}) and relative intensity						assignments (point group)		
$N_5^+SbF_6^-$		$N_5^+Sb_2F_{11}^-$		$N_5^+AsF_6^-$				
IR	Raman	IR	Raman	IR	Raman	N_5^+ (C_{2v})	MF_6^- (O_h)	$Sb_2F_{11}^-$
3357 vw						$(\nu_1+\nu_3+\nu_9)(B_2)=3358$		
3334 vw						$(\nu_1+\nu_8)(B_2)=3323$		
3079 w		3069 w				$(\nu_2+\nu_7)(B_2)=3077$		
2681 vw		2671 vw				$(\nu_1+\nu_9)(B_2)=2682$		
2270 m	2268 (9.4)	2260 m	2261 (9.0)	2270 m	2271 (4.4)	$(\nu_1)(A_1)$		
2205 s	2205 (2.0)	2203 s	2202 (1.9)	2210 s	2211 (0.8)	$(\nu_7)(B_2)$		
1921 vw		1919 vw				$(\nu_3+3\nu_9)(B_2)=1914$		
1891 vw		1883 vw				$(\nu_8+2\nu_9)(B_2)=1883$		
1240 vw		1366 w 1288 vw					comb. bands	comb. bands
1092 ms		1089 s		1088 s		$(\nu_3+\nu_9)(B_2)=1086$[a]		
1064 s		1064 s				$\nu_8(B_2)$		
902 vvw		892 vvw				$(\nu_5+\nu_6)(B_2)=903$		
871 w	872 (0.6)	867 w	866 (0.6)	872 w	871 (0.7)	$\nu_2(A_1)$		
835 vw	837 (0+)	824 vw	824 (0+)			$(2\nu_9)(A_1)=828$[b]		
			692 (5.5)					
		725−650 vs,br	654 (10)					νSbF
			598 (1.4)					
	672 (1)		664 (∼1)	680 sh	669/672 (1.8)	$\nu_3(A_1)$		
655 vs				704 vs			$\nu_3(F_{1u})$	
	652 (10)				686 (10)		$\nu_1(A_{1g})$	
		596 mw 537 mw						νSbF
582 w	571 (0.8)			575 w	579 (1.6)		$\nu_2(E_g)$	
		497 s						νSb−F−Sb
	478 (0+)		470 (0+)			$\nu_5(A_2)$		
447 w		449 w				?		
425 ms		417 ms		420 sh		$\nu_6(B_1)$		
412 mw	416 (0+)	409 sh	417 (0+)			$\nu_9(B_2)$		
			295 (2.1)					
			283 sh					
			272 sh					δSb−F
			231 (2.0)					
284 vs				394 vs			$\nu_4(F_{1u})$	
	282 (2.8)				372 (3.4)		$\nu_5(F_{2g})$	
	204 (5.0)		200 (3.6)		209 (4.4)	$\nu_4(A_1)$		
	107 (5)		135 sh 97 (5.0)		125 (5.5)	lattice vibrations		

[a] In Fermi resonance with $\nu_8(B_2)$. [b] In Fermi resonance with $\nu_2(A_1)$.

square deviation of 0.0058 Å. The N_5^+ mean plane is almost perpendicular (78.1°) to the plane containing the F5−Sb1−F6−Sb2−F11 atoms. The latter is also almost perfectly planar and shows a root-mean-square deviation of 0.014 Å.

The geometry of the $Sb_2F_{11}^-$ anion also deserves special comment. This anion is known to possess little rigidity and can exist in either an eclipsed or a staggered conformation and exhibit a wide range of Sb−F−Sb bridge angles, depending upon the counterion present in the crystal lattice.[27] The eclipsed conformation is rare but has previously also been observed for $BrF_4^+Sb_2F_{11}^-$.[21] In the latter compound, the eclipsed structure results from a packing effect in which one equatorial fluorine ligand of each antimony atom of $Sb_2F_{11}^-$ bridges to a different BrF_4^+ cation. Since the two BrF_4^+ cations and the $Sb_2F_{11}^-$ anion are coplanar, the bridging equatorial fluorine ligands around the antimonies become also coplanar, resulting in the eclipsed configuration. The eclipsed conformation of the $Sb_2F_{11}^-$ anion found for $N_5^+Sb_2F_{11}^-$ is also due to fluorine bridging[28] but

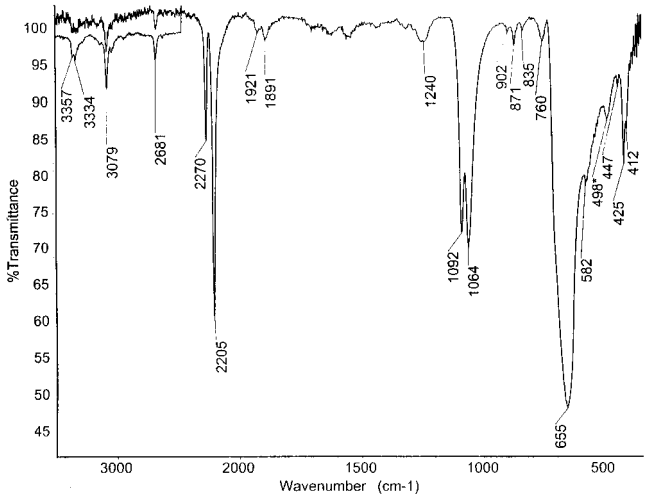

Figure 3. Infrared spectrum of solid $N_5^+SbF_6^-$, recorded as an AgBr pellet at room temperature. The band at 493 cm^{-1}, marked by an asterisk, is due to a small amount of $Sb_2F_{11}^-$.

results from N_5^+ acting as a spacer between the two equatorial SbF_4 units of $Sb_2F_{11}^-$ (Figure 2). In accord with the resonance structures and the calculated charge distributions of N_5^+ (see above), the positively charged nitrogen atoms interact with the

(27) Willner, H.; Bodenbinder, M.; Broechler, R.; Hwang, G.; Rettig, S. J.; Trotter, J.; von Ahsen, B.; Westphal, U.; Jonas, V.; Thiel, W.; Aubke, F. *J. Am. Chem. Soc.* **2001**, *123*, 588.

(28) $N_5^+Sb_2F_{11}^-$ shows numerous N···F contacts shorter than the sum of the van der Waals radii of 3.0 Å. The shortest contacts, 2.723(15) and 2.768(14) Å, arise from N2···F8 and N2···F10[a] ($a = {}^1/_2 + x, {}^1/_2 - y, {}^1/_2 + z$), while the N4···F2 and N4···F4[b] ($b = x, 1 - y, {}^3/_2 - z$) distances, 2.887(15) and 2.813 Å, respectively, are slightly longer.

Table 4. Comparison of Observed and Unscaled Calculated CCSD(T)/6-311+G(2d) Vibrational Frequencies (cm^{-1}) and Intensities (km mol^{-1} and $Å^4$ amu^{-1}) for N_5^+

			abs int			rel int	
	approx mode description in point group C_{2v}	calcd freq	IR	Raman	obsd freq	IR	Raman
A_1	ν_1 in-phase terminal stretches	2229	13	215	2260−2271	m	10.0
	ν_2 sym central stretch	818	0.5	5	866−872	w	0.6
	ν_3 central bending	644	2	1	664−672	obscd	1[a]
	ν_4 in-phase terminal bends	181	0.3	6	200−209	−[b]	4
A_2	ν_5 out-of-phase, out-of-plane bend	475	0	1	470−478	−	0+
B_1	ν_6 in-phase, out-of-plane bend	405	6	0	417−425	ms	0
B_2	ν_7 out-of-phase term stretches	2175	105	42	2203−2211	s	1.9
	ν_8 asym central stretch	1032	138	2	1055−1064	s	not obsd
	ν_9 out-of-phase term bends	399	1	0.5	412−417	mw	0+

[a] Obscured in infrared and interference in Raman by anion bands. [b] Outside of the frequency range of our spectrometer.

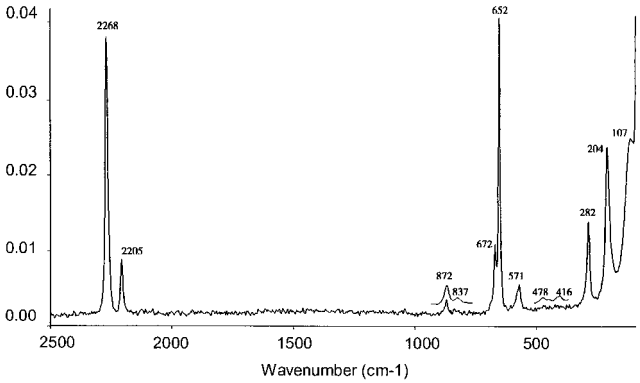

Figure 4. Raman spectrum of solid $N_5^+SbF_6^-$ recorded at room temperature.

negatively charged fluorine ligands (Figure 1). Thus, the β-nitrogens, N2 and N4, bridge to the two eclipsed fluorine atoms, F2 and F8, but since the N_5^+ plane is not perfectly perpendicular to the $F_{ax}-Sb-F-Sb-F_{ax}$ plane, the N2−F8 and N4−F2 distances are somewhat shorter than the N2−F2 and N4−F8 distances.[28] In contrast to $BrF_4^+Sb_2F_{11}^-$, which has an almost linear Sb−F−Sb bridge angle of 175°,[21] that of 155.0(4)° in $N_5^+Sb_2F_{11}^-$ is much closer to those usually found for $Sb_2F_{11}^-$.[27]

Vibrational Spectra of N_5^+. The infrared and Raman spectra of solid $N_5^+SbF_6^-$ are shown in Figures 3 and 4, respectively. The experimentally observed frequencies of $N_5^+SbF_6^-$, $N_5^+Sb_2F_{11}^-$, and $N_5^+AsF_6^-$, together with their assignments, are listed in Table 3. A comparison of the observed and calculated frequencies and intensities of N_5^+ is given in Table 4. As can be seen, the previously missing[1] remaining four fundamental vibrations and numerous combination bands of N_5^+ have been observed and are in excellent agreement with the theoretical predictions for point group C_{2v}. The splittings observed for $\nu_8(B_2)$ and $\nu_2(A_1)$ can be attributed to Fermi resonance. The presence of $Sb_2F_{11}^-$ impurities in the SbF_6^- salt can be readily detected by Raman bands at 692, 598, and 231 cm^{-1} and infrared bands at 708 and 497 cm^{-1} that are characteristic for $Sb_2F_{11}^-$ and do not overlap with the SbF_6^- bands.

Conclusion

The synthesis and thorough characterization of $N_5^+SbF_6^-$ and $N_5^+Sb_2F_{11}^-$ demonstrate that the N_5^+ cation can form exceptionally stable salts with fluoroantimonate anions and that these salts are surprisingly insensitive to impact. The N_5^+ cation is a powerful one-electron oxidizer that can oxidize NO, NO_2, and Br_2 and does not give rise to undesirable fluorination or oxygenation side reactions. The ready availability of a stable polynitrogen cation in addition to the long-known azide anion opens a venue to neutral polynitrogen compounds and may provide the basis for the first synthesis of stable nitrogen allotropes.

Acknowledgment. The authors thank the Defense Advanced Research Project Agency, the U.S. Air Force Office of Scientific Research, and the National Science Foundation for financial support and Drs. T. Schroer, S. Schneider, and M. Gerken from the University of Southern California for experimental support and stimulating discussions.

Supporting Information Available: Tables of structure determination summary, atomic coordinates, bond lengths and angles, and anisotropic displacement parameters of $N_5Sb_2F_{11}$ (PDF). This material is available free of charge via the internet at http://pubs.acs.org.

JA010141G

APPENDIX C

"Crystal Structure of $F_2NO^+AsF_6^-$ and Method for Extracting Meaningful Geometries from Oxygen/Fluorine Disordered Crystal Structures"
Inorg. Chem., 40, 416 (2001)

This Page Intentionally Left Blank

Crystal Structure of $F_2NO^+AsF_6^-$ and Method for Extracting Meaningful Geometries from Oxygen/Fluorine Disordered Crystal Structures

Ashwani Vij,† Xiongzhi Zhang,‡ and Karl O. Christe*,†,‡

Propulsion Sciences and Advanced Concepts Division, Air Force Research Laboratory, Edwards Air Force Base, California 93524-7680, and Loker Hydrocarbon Research Institute, University of Southern California, Los Angeles, California 90089

Received July 11, 2000

Because of their similar space requirements and electronic configurations, oxygen and fluorine ligands in oxofluorides are frequently disordered, particularly when the central atom lies on an intramolecular rotation axis. Depending on the specific occupancy factors, the apparent X−O and X−F bond lengths and bond angles that are obtained from single-crystal X-ray diffraction studies can significantly deviate from the "true" bond lengths and angles. If the degree of disorder is relatively small, these disorder-induced deviations may go unnoticed. If, however, the degree of disorder is significant, the deviations from predicted and, in particular, from the theoretically calculated geometries become so large that they can no longer be ignored. A typical example of such an extreme case of F/O disorder is the SO_2F^- anion for which the observed S−O and S−F bond lengths vary from salt to salt, and all of them deviate from the theoretical predictions.[1]

When encountering and realizing the presence of a significant O/F disorder, crystallographers generally refrain from solving "flawed" data sets. This approach, however, is too conservative. As will be demonstrated in this communication for $F_2NO^+AsF_6^-$, there are many cases where meaningful structures can be derived from disordered data sets.

Our general approach to solving certain disordered structures is outlined for a linear $C_{\infty v}$ triatomic species FXO and a planar C_{2v} tetraatomic species F_2XO. Let us first consider the most simple case, the linear FXO species, whose geometry is fully determined by the two bond lengths R_{O-X} and R_{X-F}. If there is zero disorder, i.e., F occupancies of 100% and 0% for the F and O positions, respectively, R_{O-X} and R_{X-F} have their "true" values (Figure 1a). If there is complete disorder, i.e., 50% occupancy factors, the observed bond lengths become identical and equal to $(^1/_2)(R_{O-X} + R_{X-F})$. Hence, we have an approximately linear relationship between apparent bond lengths and occupancy factors. Although the assumption of a linear relationship might not be strictly valid because oxygen and fluorine differ by one electron, a simulation using weighting factors of 8 and 9, respectively, resulted in corrections of less than 0.5 pm for the extrapolated bond lengths. The midpoint of the plot in Figure 1a can always be obtained for any occupancy factor by dividing the sum of R_1 and R_2 by 2. To obtain the slope of the line, we must know at least one extra bond length and its occupancy factor to be able to extrapolate for 0% and 100% occupancy factors and to obtain the "true" bond distances for R_1 and R_2. This analysis shows that for any disordered triatomic $C_{\infty v}$ species the "true" bond distances R_1 and R_2 can be derived from a disordered data set if the occupancy factors are not 50% and if the actual occupancy can be calculated from the experimental data. Since for the actual occupancy factors the fit between the observed and calculated intensity data must be a maximum, these factors can be obtained by refining the R value as a function of the occupancy factors. The only constraints required for such a refinement are that the sums of the partial O/F occupancies for each position must equal 1.0 and that the total O and the total F occupancies each must also equal 1.0.

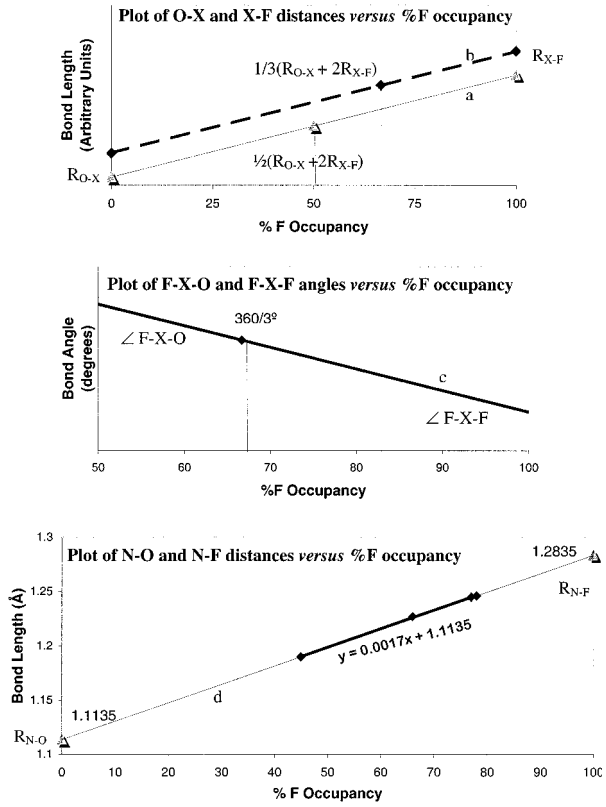

Figure 1. (a) Fluorine occupancy factors (FOF) vs O−X and X−F bond lengths for a linear $C_{\infty v}$ FXO species. (b) FOF vs O−X and X−F bond lengths for a planar C_{2v} F_2XO species. (c) FOF vs F−X−O and F−X−F bond angles for a planar C_{2v} F_2XO species. (d) FOF vs the N−O and N−F bond lengths in F_2NO^+. The data points are "apparent" N−O and N−F bond lengths and the averaged bond length. The "true" N−O and N−F bond lengths of F_2NO^+ are intersections with the 0% and 100% F occupancy lines. (e) FOF vs the F−N−O and F−N−F bond angles in F_2NO^+. The intersections of the line with the fluorine occupancy lines of 50% and 100% gives the true F−N−O and F−N−F bond angles.

The same principal can be applied to the tetraatomic C_{2v} species F_2XO. Here, however, we must determine, in addition to the two bond lengths R_1 and R_2, also one bond angle. Furthermore, the average bond length for equal occupancies is not at the 50/50 position but at the $^2/_3$ F occupancy position because we have two fluorine atoms and only one oxygen atom. The equilibrium bond length becomes $(^1/_3)(2R_{X-F} + R_{O-X})$, as shown in Figure 1b, which becomes the swivel point through which all possible lines must pass. Again, if the observed apparent bond distances are not identical for all three bonds, one can obtain the corresponding occupancy factors by refining the observed diffraction data for a

† Edwards Air Force Base.
‡ University of Southern California, Los Angeles.

(1) Lork, E.; Mews, R.; Viets, D.; Watson, P. G.; Borrmann, T.; Vij, A.; Boatz, J. A.; Christe, K. O. *Inorg. Chem.*, in press.

10.1021/ic0007613 CCC: $20.00
Published on Web 12/21/2000

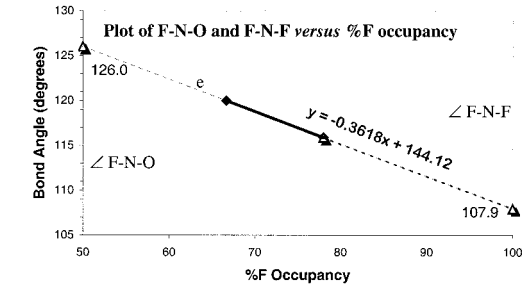

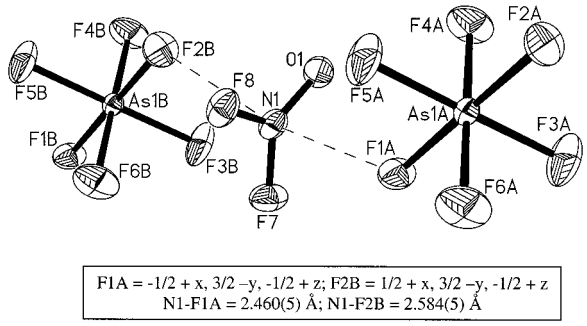

Figure 2. A 30% ORTEP plot of $F_2NO^+AsF_6^-$ showing the fluorine bridging between F_2NO^+ cations and the trans fluorine ligands of AsF_6^-, resulting in an infinite chain structure.

minimum *R* value using the following constraints. The total F occupancies must be 2.0, the total O occupancy must be 1.0, and the total O/F occupancy at each position must be 1.0. The "true" values of R_{O-X} and R_{X-F} are again obtained by extrapolation of the resulting line to F occupancy factors of 0% and 100%, respectively.

The "true" bond angle in C_{2v} F_2XO is obtained in an analogous manner by plotting the F−X−F and F−X−O bond angles versus the F occupancy factors (Figure 1c). For equal occupancies (F occupancy of $^2/_3$), all three bond angles must be equal and be 120°. Again, a plot of the observed bond angles against the occupancy factors, obtained as described above by refinement of the observed data for a minimum *R* value, and extrapolation for 100% F and 50% F occupancies yield the "true" F−X−F and F−X−O bond angles, respectively. The F−X−O and F−X−F bond angles are connected by the relationship ∠F−X−O = ($^1/_2$)(360 − ∠F−X−F).

The merits of our approach are examined for $F_2NO^+AsF_6^-$ (Figure 2). Although the existence of F_2NO^+ salts had been known since 1966 [2] and the cation had been characterized by vibrational[3,4] and NMR[2,4−6] spectroscopy and theoretical calculations,[7,8] the exact geometry of F_2NO^+ was still unknown. We have now prepared a sample of $F_2NO^+AsF_6^-$ according to the literature method[3] and grown single crystals from an anhydrous HF solution by slow cooling. The X-ray diffraction data were collected[9] and refined by standard methods.[10] Although the resulting *R* factor of 3.17% (wR2 = 7.33%) and reasonable thermal parameters indicated a well-determined structure, the apparent N−F (124.6(4) and 125.1(4) pm) and N−O (118.5(4) pm) bond lengths and F−N−F (115.5(3)°) and O−N−F (122.1(3)° and 122.4(3)°) bond angles deviated strongly from the theoretical predictions[7,8] and suggested oxygen/fluorine disorder. This was confirmed by refining the structure with variable occupancy factors as outlined above. A minimum *R* value of 3.03% (wR2 = 6.68%) was obtained for fluorine occupancy factors of 78% and 77% for the two F/O positions and of 45% for the one O/F position. A plot of the apparent N−F and N−O bond lengths as a function of the calculated occupancy factors, together with the equilibrium point ($^1/_3$)(2R_{X-F} + R_{O-X}), is shown in Figure 1d and results in a straight line. Extrapolation of this line to 0% and 100% fluorine occupancy results in the following "true" bond lengths: R_{NO} = 111.4 pm and R_{NF} = 128.4 pm. Application of the outlined method to the bond angles (Figure 1e) results in the following "true" angles ∠F−N−F = 107.9° and ∠O−N−F = 126°. The "true" values, determined in this manner, agree well with those predicted by the density functional B3LYP method[8] (Table 1), particularly if it is kept in mind that the B3LYP method tends to slightly overestimate the bond lengths. While it is easy to estimate the uncertainty in the apparent bond distances and angles, an estimate of the error caused by the occupancy factor analysis is more complex and depends on the shallowness of the minimum of the *R* versus occupancy factor plot and possible slight nonlinearity of the bond distgance−occupancy factor curves.

Table 1. Comparison of the "Apparent" and "True" Experimental Results and the Calculated Geometries of F_2NO^+

	experimental		calculated[a]
	"apparent"	"true"	B3LYP/6-311+G(2d)
R_{N-F} (pm)	124.5(4)	128.4	131.2
	124.6(4)		
R_{N-O} (pm)	119.0(4)	111.4	112.9
∠F−N−F (deg)	115.9(3)	107.9	108.4
∠F−N−O (deg)	122.0(3)	126.0	125.4
	122.1(3)		

[a] Data from ref 8.

In summary, the above analysis demonstrates that the geometry of F_2NO^+, extracted from an oxygen/fluorine disordered structure, is in very good agreement with the theoretical predictions particularly if the inherent differences between solid state and free gaseous species are kept in mind. It also suggests that the proposed approach might be applicable to other disordered structures. It also points out the merits of comparing experimental oxofluoride crystal structures with theoretical calculations. In this manner, the possible presence of O/F disorder may be detected. If the presence of O/F disorder is suspected, it can be substantiated by refinement of the structure with variable occupancy factors and checking for a decrease in the *R* value.

Acknowledgment. The authors thank Professors R. Bau and G. Schrobilgen and Drs. J. Sheehy, W. Wilson, and H. Mercier for helpful discussions. The work was financially supported by the National Science Foundation, the Air Force Office of Scientific Research, and the Defense Advanced Research Project Agency.

Supporting Information Available: An X-ray crystallographic file in CIF format of the disordered $F_2NO^+AsF_6^-$ structure. This material is available free of charge via the Internet at http://pubs.acs.org.

IC0007613

(2) Fox, W. B.; MacKenzie, J. S.; Vanderkooi, N.; Sukornik, B.; Wamser, C. A.; Holmes, J. R.; Eibeck, R. E.; Stewart, B. B. *J. Am. Chem. Soc.* **1966**, *88*, 2604.
(3) Christe, K. O.; Maya, W. *Inorg. Chem.* **1969**, *8*, 1253.
(4) Wamser, C. A.; Fox, W. B.; Sukornik, B.; Holmes, J. R.; Stewart, B. B.; Juurick, R.; Vanderkooi, N.; Gould, D. *Inorg. Chem.* **1969**, *8*, 1249.
(5) Christe, K. O.; Hon, J. F.; Pilipovich, D. *Inorg. Chem.* **1973**, *12*, 84.
(6) Mason, J.; Christe, K. O. *Inorg. Chem.* **1983**, *22*, 1849.
(7) Cacace, F.; Pepi, F. *J. Phys. Chem.* **1994**, *98*, 8009.
(8) Gillespie, R. J.; Robinson, E. A.; Heard, G. L. *Inorg. Chem.* **1998**, *37*, 6884.
(9) X-ray data: $F_2NO^+AsF_6^-$, AsF8NO, fw = 256.93, monoclinic, $P2_1/n$, a = 751.3(2) pm, b = 808.3(2) pm, c = 1031.4(2) pm, β = 107.46(3)°, V = 0.5975(2) nm^3, Z = 4, d_{calcd} = 2.856 Mg/m^3, temperature = 193 K, 1367 independent reflections (R_{int} = 0.0372), R1 = 0.0303, wR2 = 0.0668, S = 1.028.
(10) The occupancies of F and O were refined using free variables. The oxygen/fluorine occupancies at the three positions refined to 55/45%, 23/77%, 22/78%, respectively. The structure was solved using direct methods and refined by least-squares method using SHELXTL 5.10 software suite (Bruker AXS, Madison, WI).

APPENDIX D

"Polynitrogen Chemistry: Preparation and Characterization of $(N_5)_2SnF_6$, N_5SnF_5, and $N_5B(CF_3)_4$"
Chemistry – A European Journal, 9, 2840 (2003)

This Page Intentionally Left Blank

Polynitrogen Chemistry: Preparation and Characterization of $(N_5)_2SnF_6$, N_5SnF_5, and $N_5B(CF_3)_4$

William W. Wilson,*[a] Ashwani Vij,[a] Vandana Vij,[a] Eduard Bernhardt,[c] and Karl O. Christe*[a, b]

Abstract: Metathetical processes were used to convert N_5SbF_6 into $N_5[B(CF_3)_4]$ and $(N_5)_2SnF_6$. The latter salt is especially noteworthy because it contains two N_5^+ ions per anion, thus demonstrating that salts with touching polynitrogen cations can be prepared. This constitutes an important milestone towards our ultimate goal of synthesizing a stable, ionic nitrogen allotrope. The stepwise decomposition of $(N_5)_2SnF_6$ yielded N_5SnF_5. Multinuclear NMR spectra show that in HF the SnF_5^- ion exists as a mixture of $Sn_2F_{10}^{2-}$ and $Sn_4F_{20}^{4-}$ ions. Attempts to isolate FN_5 from the thermolysis of $(N_5)_2SnF_6$ were unsuccessful, yielding only the expected decomposition products, FN_3, N_2, *trans*-N_2F_2, NF_3, and N_2.

Keywords: anions · nitrogen · NMR spectroscopy · polynitrogen · vibrational spectroscopy

Introduction

During the past two decades, polynitrogen chemistry has received increasing attention.[1–16] While at the beginning, most of the efforts were devoted to theoretical studies, the recent syntheses of stable salts of the pentanitrogen(+1) cation (N_5^+)[1, 2] have given a strong impetus to experimental studies in this field. So far, the only method for generating N_5^+ compounds has been their direct synthesis from N_2FAsF_6 or N_2FSbF_6 and HN_3 in HF, according to Equation (1).

$$N_2FMF_6 + HN_3 \xrightarrow{HF} N_5MF_6 + HF \qquad (M = As, Sb) \qquad (1)$$

A major goal of this study was to increase the nitrogen content of the N_5^+ salts by combining N_5^+ with multiply charged anions. This presents a significant challenge, because it results in structures with touching polynitrogen ions that will increase both the endothermicity and sensitivity of these compounds.

The general usefulness of the metathetical method is severely restricted by the small number of N_2F^+ salts available. Except for reports on unstable N_2FBF_4[17] and N_2FPF_6[18] salts, no other N_2F^+ compounds have been described in the literature. Therefore, it was desirable to develop a more general method for the syntheses of N_5^+ salts, such as the exchange of SbF_6^- in N_5SbF_6 for other anions. This situation resembles that previously encountered for the syntheses of NF_4^+ salts.[19, 20] Since SbF_5 is among the strongest known Lewis acids,[21] displacement reactions are rarely feasible, and metathetical approaches are required [Eq. (2)].

$$N_5^+SbF_6^- + M^+Y^- \rightarrow N_5^+Y^- + M^+SbF_6^- \downarrow \qquad (2)$$

For a successful metathetical reaction, each ion must be compatible with the solvent, and both starting materials and one of the products must be highly soluble, while the second reaction product must exhibit low solubility.

Results and Discussion

The choices of counterions capable of forming stable N_5^+ salts are limited. For room temperature stability, the strengths of the conjugate Lewis acids should exceed that of AsF_5, because N_5AsF_6 is only marginally stable at room temperature.[1] The stability of the N_5^+ salt might be further enhanced by the use of a weakly coordinating, bulky anion.

[a] Prof. K. O. Christe, Dr. W. W. Wilson, Dr. A. Vij, V. Vij
ERC, Inc. and Space and Missile Propulsion Division
Air Force Research Laboratory (AFRL/PRSP)
10 East Saturn Boulevard, Bldg 8451
Edwards Air Force Base, CA 93524 (USA)
Fax: (+1) 661-275-5471
E-mail: karl.christe@edwards.af.mil
william.wilson@edwards.af.mil

[b] Prof. K. O. Christe
Loker Research Institute
University of Southern California
Los Angeles, CA 90089-1661 (USA)

[c] Dr. E. Bernhardt
FB 6-Anorganische Chemie
Gerhard-Mercator-Universität Duisburg
Lotharstrasse 1, 47048 Duisburg (Germany)

DOI: 10.1002/chem.200304973

Several solvents were explored for conducting the reaction given in Equation (2). Anhydrous HF was found to be an excellent choice for the SnF_6^{2-} salt, as shown in Equation (3).

$$2\,N_5SbF_6 + Cs_2SnF_6 \xrightarrow[-78\,^\circ C]{HF} (N_5)_2SnF_6 + 2\,CsSbF_6\downarrow \quad (3)$$

The resulting $(N_5)_2SnF_6$ salt was obtained in high yield with a purity of about 94 wt%. The impurities were about 5 wt% of unreacted $N_5^+SbF_6^-$ and 1 wt% of $CsSbF_6$. The $(N_5)_2SnF_6$ salt is a white, friction sensitive (**caution!**) solid, which is marginally stable at room temperature and decomposes at slightly higher temperature or on storage to N_5SnF_5 with the loss of an "FN_5" equivalent, as shown in Equation (4).

$$(N_5)_2SnF_6 \rightarrow N_5SnF_5 + \text{“}FN_5\text{”} \quad (4)$$

Because "FN_5" is unstable with a predicted life time of nanoseconds,[22] only its primary decomposition products, FN_3 and N_2, and secondary decomposition products, *trans*-N_2F_2, NF_3 and N_2, were observed by checking for noncondensible gas at $-196\,^\circ C$ and FT-IR spectroscopy. The relevant decomposition reactions are shown in Equations (5)–(7).

$$\text{“}FN_5\text{”} \rightarrow N_2 + FN_3 \quad (5)$$

$$2\,FN_3 \rightarrow \textit{trans}\text{-}N_2F_2 + 2\,N_2 \quad (6)$$

$$3\,FN_3 \rightarrow NF_3 + 4\,N_2 \quad (7)$$

The N_5SnF_5 salt, formed by the controlled thermal decomposition of $(N_5)_2SnF_6$, is a white solid that starts to decompose at about 50–60 °C. The fact that the thermal stabilities of N_5SbF_6, $N_5[B(CF_3)_4]$ (see below), and N_5SnF_5 are all comparable suggests that the thermal stability of the N_5^+ cation is the limiting factor. The thermal decomposition of N_5SnF_5 was studied by its material balance and vibrational spectroscopy and proceeds smoothly according to Equation (8), yielding SnF_4 as the solid nonvolatile residue.

$$N_5SnF_5 \rightarrow SnF_4 + \text{“}FN_5\text{”} \quad (8)$$

The $(N_5)_2SnF_6$ and N_5SnF_5 salts were characterized by vibrational (Tables 1 and 2, and Figure 1) and multinuclear NMR (Table 3 and Figure 2) spectroscopy. The Raman and infrared spectra are in accord with the expectations for N_5^+ and the fluorostannate anions.[1, 2, 23, 24] One remarkable feature in the vibrational spectra of $(N_5)_2SnF_6$ is the fact that the frequencies of all SnF_6^{2-} modes and of the N_5^+ stretching modes are shifted to significantly higher frequencies relative to $(NF_4)_2SnF_6$[23] and the 1:1 salts of N_5^+.[1, 2] In the absence of a crystal structure, we cannot provide a convincing explanation for this unexpected effect. It should also be noted that in mixtures of $(N_5)_2SnF_6$ and N_5SnF_5, generated by partial decomposition of the former, only one set of bands with intermediate frequencies was observed and not two sets with the frequencies of the 2:1 and 1:1 salts. While the bands for SnF_6^{2-} are sharp and narrow, as expected for a monomeric octahedral anion, the bands due to SnF_5^- are broad and poorly defined. This is in accord with the results from the multinuclear NMR study which show SnF_5^- to be present as both a dimer and a cyclic tetramer.

Table 1. Raman and infrared spectra[a] of solid $(N_5)_2SnF_6$ and their assignments.

Obsd frequencies [cm^{-1}] and relative intensities		Assignments (point group)	
Raman	Infrared	N_5^+ (C_{2v})	SnF_6^{2-} (O_h)
2287 (10.0)	2288 m	$\nu_1(A_1)$	
2274 (1.9)			
2227 (1.9)	2228 s	$\nu_7(B_2)$	
2210 (0+)			
2170 (0.2)			
1112 (0+)	1112 s	$\nu_8(B_2)$	
	1083 m	$(\nu_3 + \nu_9)(B_2) = 1089$	
881 (1.3)	881 w	$\nu_2(A_1)$	
822 (0.1)		$2\nu_9(A_1) = 834$	
672 (2.6)		$\nu_3(A_1)$	
	611 vs		$\nu_3(F_{1u})$
600 (6.1)	602 vw		$\nu_1(A_{1g})$
508 (0.4)			$\nu_2(E_g)$
475 (0.2)		$\nu_5(A_2)$	
	417 ms	$\nu_6(B_1)$	
417 (0.5)		$\nu_9(B_2)$	
266 (1.2)			$\nu_5(F_{2g})$
203 (3.0)		$\nu_4(A_1)$	
195 (4.4)			
159 (1.0)			
126 (9.9)		lattice vibration	
119 (4.0)		lattice vibration	
80 (4.0)		lattice vibration	

[a] The following bands due to the SbF_6^- impurity were also observed. Raman: 654 (1.0), ν_1; 572 (0+), ν_2; 282 (0.3), ν_5.

Table 2. Raman and infrared spectra[a] of solid N_5SnF_5 and their assignments.

Obsd frequencies [cm^{-1}] and relative intensities		Assignments (point group)	
Raman	Infrared	N_5^+ (C_{2v})	SnF_5^-
2269 (10.0)	2270 m	$\nu_1(A_1)$	
2209 (2.0)	2212 s	$\nu_7(B_2)$	
	1230 w		combination band
1090 (0+)	1094 ms	$\nu_8(B_2)$	
	1069 m	$(\nu_3 + \nu_9)(B_2) = 1090$	
	898 w		combination Band
875 (1.0)	878 vw	$\nu_2(A_1)$	
670 (1.8)		$\nu_3(A_1)$	
	670 vs		stretching modes
624 (3.8)	610 s		stretching modes
	590 sh		stretching modes
475 (0.5) vbr	540 sh		stretching modes
	519 m		stretching modes
	421 m	$\nu_6(B_1)$	
420 (0.3)		$\nu_9(B_2)$	
260 sh, br			deformation modes
202 (4.3)		$\nu_4(A_1)$	
120 (4)		lattice vibration	

[a] The following bands due to the SbF_6^- impurity were also observed. Raman: 652 (1.0), ν_1; 575 (0+), ν_2; 280 (0.3), ν_5.

The NMR spectra of N_5SnF_5 in HF were recorded at $-78\,^\circ C$. The ^{14}N spectrum showed a strong resonance at $\delta = -164.7$ ppm and a very broad line at about $\delta = -99.9$ ppm, characteristic for the N_β and the terminal N_α atoms, respectively, of the N_5^+ ion.[1] In addition to the signal due to HF (doublet at $\delta = -189.8$ ppm with $^1J(^1H,^{19}F) = 518.9$ Hz), the

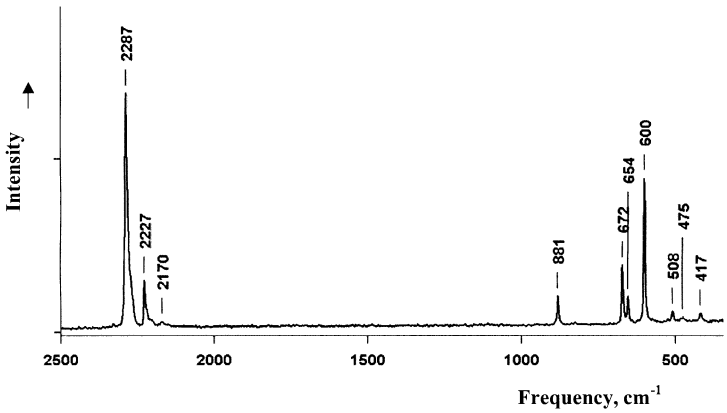

Figure 1. Raman spectrum of solid $(N_5)_2SnF_6$.

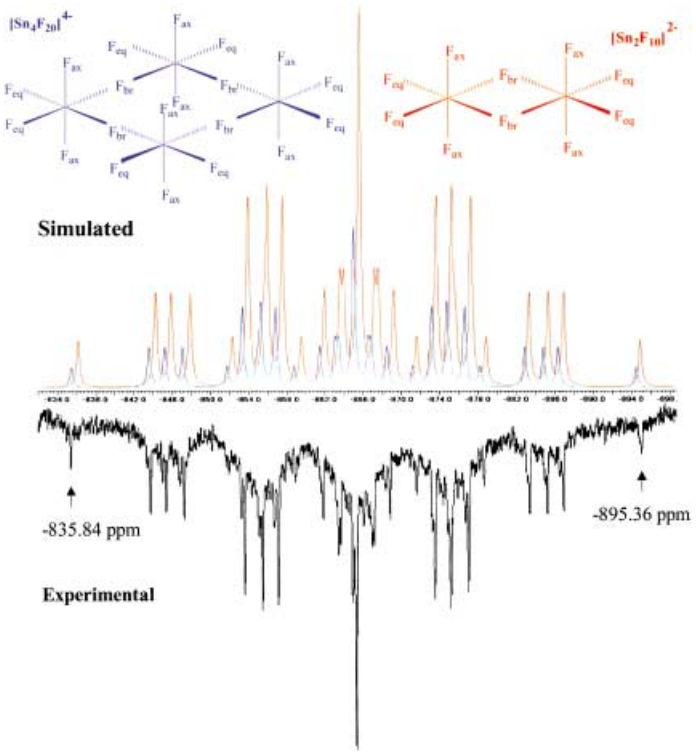

Figure 2. Observed (black trace) and simulated ^{119}Sn NMR spectra of $Sn_2F_{10}^{2-}$ (red trace) and $Sn_4F_{20}^{4-}$ (blue trace) in a 2:1 mole ratio.

^{19}F spectrum showed two very similar sets of signals (Table 3) that varied somewhat in relative intensity from sample to sample and with temperature. The more intense set, with about twice the intensity of the weaker one, is assigned to the dimeric anion, $Sn_2F_{10}^{2-}$. The less intense set has the same area ratios and almost identical shifts and coupling constants and, therefore, must belong to a species with an almost identical molecular structure. The only species that meets these requirements is the cyclic tetramer, $Sn_4F_{20}^{4-}$. Although the ^{19}F NMR spectrum of $Sn_2F_{10}^{2-}$ in SO_2 has been reported previously,[25, 26] its chemical shifts and coupling constants significantly deviate from those recorded in HF. This deviation is probably due to solvent effects, as shown by recording the spectra of Cs_2SnF_6 in HF at -78 and 23 °C (values at this temperature given in parentheses). They showed singlets at $\delta = -160.5$ (-164.5) ppm with $|^1J(^{19}F,^{119}Sn)| = 1416$ (1437) Hz and $|^1J(^{19}F,^{117}Sn)| = 1355$ (1376) Hz, deviating from the values, $\delta = -139$ ppm and $|^1J(^{19}F,^{119}Sn)| = 1604$ Hz,[25] reported for SnF_6^{2-} in SO_2, by about the same amount as found for the $Sn_2F_{10}^{2-}$ signals.[25] The ^{119}Sn spectrum was also recorded and consisted of a complex multiplet (Figure 2). The observed spectrum was successfully simulated assuming first-order triplets of triplets of triplets for both $Sn_2F_{10}^{2-}$ and $Sn_4F_{20}^{4-}$, by using the coupling constants similar to those derived from the tin satellite peaks in the ^{19}F spectra. The ^{119}Sn chemical shifts of $Sn_2F_{10}^{2-}$ and $Sn_4F_{20}^{4-}$ are also almost identical (difference of only 0.4 ppm), thus confirming the close structural relationship of these two anions.

The synthesis of a stable $(N_5)_2SnF_6$ salt is highly significant because it represents the first example of an N_5^+ salt that contains two polynitrogen cations per anion. It demonstrates that salts with touching polynitrogen cations can exist, and that the goal of an ionic nitrogen allotrope might be achievable.

A particularly attractive counterion, $[B(CF_3)_4]^-$, was recently reported by Willner et al.[27] The Lewis acidity of its conjugate parent molecule $B(CF_3)_3CF_2$ (pF^- value of 11.77)[21] exceeds that of SbF_5 (pF^- value of 11.30),[21] and its negative charge is distributed over 12 fluorine atoms, thus rendering it a weakly coordinating anion. For the $[B(CF_3)_4]^-$ salts, HF was a poor solvent choice because the solubility differences between $M[B(CF_3)_4]$ and $MSbF_6$ (M = alkali metal) were found to be too small for an effective metathesis. Although the $M[B(CF_3)_4]$ salts are soluble in water, diethyl ether,

Table 3. Multinuclear NMR spectra[a] of N_5SnF_5 recorded at -78 °C in HF.

Ion	Atom	δ (Multiplicity) (Area ratio)	Coupling constant [Hz]
N_5^+	N_β	−164.7 (s)	
	N_α	−99.9br (s)	
$Sn_2F_{10}^{2-}$	F_{eq}	−173.0 (t) (2)	$^2J(^{19}F_{eq},^{19}F_{ax}) = 37.1$; $\|^1J(^{19}F_{eq},^{117}Sn)\| = 1671$; $\|^1J(^{19}F_{eq},^{119}Sn)\| = 1744$
	F_{ax}	−165.28 (t) (2)	$^2J(^{19}F_{eq},^{19}F_{ax}) = 36.8$; $\|^1J(^{19}F_{ax},^{117}Sn)\| = 1406$; $\|^1J(^{19}F_{ax},^{119}Sn)\| = 1468$
	F_{br}	−147.0 (s) (1)	$\|^1J(^{19}F_{br},^{117/119}Sn)\| = 1196$
	Sn[a]	−865.6 (ttt)	$\|^1J(^{19}F_{eq},^{119}Sn)\| = 1740$; $\|^1J(^{19}F_{ax},^{119}Sn)\| = 1440$; $\|^1J(^{19}F_{br},^{119}Sn)\| = 1200$
$Sn_4F_{20}^{4-}$	F_{eq}	−174.2 (t) (2)	$^2J(^{19}F_{eq},^{19}F_{ax}) = 36.3$; $\|^1J(^{19}F_{eq},^{117}Sn)\| = 1622$; $\|^1J(^{19}F_{eq},^{119}Sn)\| = 1697$
	F_{ax}	−165.33 (t) (2)	$^2J(^{19}F_{eq},^{19}F_{ax}) = 36$; $\|^1J(^{19}F_{ax},^{117/119}Sn)\| = 1440$
	F_{br}	−145.0 (s) (1)	$\|^1J(^{19}F_{br},^{117}Sn)\| = 1178$; $\|^1J(^{19}F_{br},^{119}Sn)\| = 1230$
	Sn[a]	−865.2 (ttt)	$\|^1J(^{19}F_{eq},^{119}Sn)\| = 1760$; $\|^1J(^{19}F_{ax},^{119}Sn)\| = 1468$; $\|^1J(^{19}F_{br},^{119}Sn)\| = 1230$

[a] Coupling constants derived from simulated spectra.

tetrahydrofuran, acetonitrile, and acetone;[27] the incompatibility of N_5SbF_6 with these solvents precluded their use. Therefore, the metathesis was carried out in SO_2, as shown in Equation (9).

$$N_5SbF_6 + K[B(CF_3)_4] \xrightarrow[-64\,^\circ C]{SO_2} N_5[B(CF_3)_4] + KSbF_6\downarrow \quad (9)$$

The precipitate was filtered off and identified by vibrational spectroscopy as $KSbF_6$. The filtrate was taken to dryness, and the residue was characterized by mass balance, and multinuclear NMR and vibrational spectroscopy as 83 wt% $N_5[B(CF_3)_4]$ (Table 4), 14 wt% of $KSbF_6$, and 3 wt% of N_5SbF_6. The impurities are due to the fact that $KSbF_6$ still has an appreciable solubility in SO_2 even at $-64\,^\circ C$, and that a very small excess of N_5SbF_6 was used in the reaction. Since the solubility of $CsSbF_6$ in SO_2 is lower than that of $KSbF_6$, the purity of $N_5[B(CF_3)_4]$ could be further improved by using $Cs[B(CF_3)_4]$ in place of $K[B(CF_3)_4]$ in the above-described metathesis reaction. However, attempts to purify the crude product by recrystallization or to grow single crystals of $N_5[B(CF_3)_4]$ from HF have so far been unsuccessful. They resulted in a reverse metathesis in which the $KSbF_6$ impurity reacted with the $N_5[B(CF_3)_4]$ producing $K[B(CF_3)_4]$ and N_5SbF_6.

Table 4. Raman and infrared spectra[a] of solid $N_5[B(CF_3)_4]$ and their assignments.

Obsd frequencies [cm^{-1}] and relative intensities		Assignments (point group)	
Raman	Infrared	N_5^+ (C_{2v})	$B(CF_3)_4^-$ (T)
	3307 w	$(\nu_1 + \nu_8)(B_2) = 3316$	
	3057 w	$(\nu_2 + \nu_7)(B_2) = 3060$	
	2662 w	$(\nu_1 + \nu_9)(B_2) = 2663$	
	2375 w		$(\nu_9 + \nu_{10})(F) = 2376$
2257 (10.0)	2256 m	$\nu_1(A_1)$	
2200 (2.7)	2197 ms	$\nu_7(B_2)$	
1290 (sh)	1292 sh		$\nu_9(F)$ ^{10}B
1276 (1.6)			$\nu_1(A)$
1270 (sh)	1273 vs		$\nu_9(F)$ ^{11}B
1103 (0.6)(br)	1115 vs, br		$\nu_{10}(F)$
1086 (sh)			$\nu_5(E)$
	1060 sh	$\nu_8(B_2)$	
	929 s		$\nu_{12}(F)$ ^{10}B
	902 vs		$\nu_{12}(F)$ ^{11}B
863 (0.6)		$\nu_2(A_1)$	
728 (6.2)			$\nu_2(A)$
	696 s		$\nu_{13}(F)$
672 (sh)		$\nu_3(A_1)$	
525 (1.8)	521 ms		$\nu_{14}(F)$
525 (1.8)	521 ms		$\nu_{15}(F)$
	489 m	$\nu_5(A_2)$	
	443 w		
	419 m	$\nu_6(B_1)$	
	407 sh	$\nu_9(B_2)$	
319 (2.1)			$\nu_7(E)$
295 (3.3)			$\nu_{16}(F)$
279 (2.7)			$\nu_3(A)$
209 (3.4)		$\nu_4(A_1)$	
110 (0.5)(sh)			$\nu_8(E)$

[a] The following bands due to the SbF_6^- impurity were also observed. Raman: 659 (7.0), ν_1; 574 (0.7), ν_2; 295 (3.3) and 279 (2.7), ν_5; IR: 664 s, br, ν_3.

Multinuclear NMR spectra were recorded for $N_5[B(CF_3)_4]$ in SO_2 at room temperature. In the ^{14}N spectrum, the N_β atom of N_5^+ was observed at $\delta = -163.9$ ppm, in accord with the value of -165.3 ppm reported previously for N_5AsF_6 in HF at $-63\,^\circ C$.[1] In the ^{11}B NMR spectrum, a 13 line resonance was observed at $\delta = -18.0$ ppm with $^2J(^{11}B,^{19}F) = 25.7$ Hz, in close agreement with the values previously reported for $K[B(CF_3)_4]$ ($\delta = -18.9$ ppm, $^2J(^{11}B,^{19}F) = 25.9$ Hz) in CD_3CN.[27] In the ^{13}C NMR spectrum, a quartet of quartets at $\delta = 133.75$ ppm with $^1J(^{13}C,^{19}F) = 301.8$ Hz and $^1J(^{11}B,^{13}C) = 72.1$ Hz are in very good agreement with the previously reported values for $K[B(CF_3)_4]$ ($\delta = 132.9$ ppm, $^1J(^{13}C,^{19}F) = 304.3$ Hz and $^1J(^{11}B,^{13}C) = 73.4$ Hz).[27] There was no evidence for any decomposition products, nor any other unidentified species in the solution of $N_5[B(CF_3)_4]$ in SO_2.

The infrared and Raman spectra of solid $N_5[B(CF_3)_4]$ were recorded and are summarized in Table 4. The observed frequencies and intensities are in good agreement with those previously reported for N_5^+ in N_5SbF_6[2] and N_5AsF_6[1] and for $[B(CF_3)_4]^-$ in its alkali metal salts,[27] and establish that $N_5[B(CF_3)_4]$ is the main product of the metathetical reaction of N_5SbF_6 with $K[B(CF_3)_4]$.

The thermal stability of $N_5[B(CF_3)_4]$ was studied by DSC. In all runs, a moderately sized exothermic effect was always observed with an onset at 50 °C and with a maximum at ~66 °C. Additional exotherms were observed at ~93 °C and ~225 °C, but only the first exotherm is due to the decomposition of the $N_5[B(CF_3)_4]$ salt. When the sample was heated to only 75 °C and then cooled back to room temperature before being reheated to 75 °C, the first exotherm was no longer observed, and the residue left in the Al pan no longer exhibited bands for N_5^+ in the IR spectrum, but still showed bands for $[B(CF_3)_4]^-$. The thermal stability of $N_5[B(CF_3)_4]$ is surprisingly high and approaches that of the N_5SbF_6 salt (70 °C). It appears that the thermal stability of the N_5^+ ion itself might be the limiting factor, and that the thermal decomposition of these salts is triggered by the decay of the N_5^+ ion. The thermal stability of the $[B(CF_3)_4]^-$ ion is high; even after being heated to 250 °C, the infrared bands due to the $[B(CF_3)_4]^-$ ion persisted.

In summary, N_5SbF_6 was successfully converted by metathesis into $N_5[B(CF_3)_4]$ and $(N_5)_2SnF_6$. The latter salt is especially noteworthy because it contains two N_5^+ ions per anion, thus demonstrating that salts with touching polynitrogen cations can be prepared. This constitutes an important milestone towards our ultimate goal of synthesizing a stable, ionic nitrogen allotrope. Although the $(N_5)_2SnF_6$ salt is friction sensitive, its stepwise decomposition can be achieved, yielding N_5SnF_5. Multinuclear NMR spectra show that in HF the SnF_5^- ion exists as a mixture of $Sn_2F_{10}^{2-}$ and $Sn_4F_{20}^{4-}$ ions.

Experimental Section

Caution! *N_5SbF_6 is a highly energetic oxidizer. Contact with potential fuels must be avoided. This material should be handled on a small scale, while using appropriate safety precautions such as face shields, leather gloves, and protective clothing. The $(N_5)_2SnF_6$ salt is friction sensitive and must be handled with special caution.*

N_5SbF_6 was prepared from N_2FSbF_6 and HN_3 in HF, as previously described.[2] $K[B(CF_3)_4]$ was prepared from $K[B(CN)_4]$ and ClF_3 according to the literature method.[27] Cs_2SnF_6 was generated by reaction of a 2:1 mixture of CsF and SnF_2 in 48% aqueous HF with a slight excess of 30% aqueous H_2O_2 at 0 °C. SO_2 (anhydrous, >99.9%) was supplied by Air Products and was used as received. HF was from Matheson and was dried by storage over BiF_5 before use. Infrared spectra were recorded on a Mattson Galaxy 5030 FTIR spectrometer by using neat powders that were sandwiched between two AgCl windows in a Barnes Engineering Co. mini-press. Raman spectra were recorded on a Bruker Equinox 55 FT-RA spectrometer with a Nd-YAG laser at 1064 nm and neat powders in flamed out Pyrex glass capillaries sealed with Halocarbon wax. Multinuclear NMR spectra were recorded on a Bruker Avance 400 FT-NMR spectrometer in SO_2 or HF and 3 mm i.d. Teflon-FEP tubes (Wilmad Glass), heat-sealed and placed in 5 mm o.d. glass NMR tubes (Wilmad Glass). The thermal stabilities were determined on a DuPont Model 910 differential scanning calorimeter by using 0.5–1.8 mg samples in dry hermetically sealed aluminum pans and a heating rate of 10 °C min^{-1}. The data were analyzed with a DuPont Model 2000 Thermal Analyst.

The metathetical synthesis of $N_5[B(CF_3)_4]$ was carried out by using a stainless-steel/Teflon vacuum line[28] and a double Teflon/FEP U-tube apparatus that consisted of a reaction U-tube, a porous Teflon filter assembly, and a receiver U-tube.[23] The double U-tube was equipped with two stainless-steel valves, and two Teflon-coated magnetic stirring bars, one in each of the two U-tubes. N_5SbF_6 (1.053 mmol) was treated with $K[B(CF_3)_4]$ (1.013 mmol) in anhydrous SO_2 (1.8 mL) in the reaction U-Tube at −64 °C. The reaction mixture was stirred at that temperature for 1 h to ensure complete reaction before cooling of the filter assembly to −78 °C with powdered dry ice. The mixture was filtered under 1.5 atm N_2 pressure to remove the precipitated $KSbF_6$ from the solution containing the $N_5[B(CF_3)_4]$. The SO_2 was removed in vacuo at −64 °C leaving behind a white solid in the receiver U-tube. Based upon the observed mass balance and FT-IR and FT-Raman spectroscopy, the filter cake consisted of 0.2185 g $KSbF_6$ (0.2783 g expected for 1.013 mmol) with only traces of $N_5[B(CF_3)_4]$ from the mother liquor. The filtrate residue consisted of 0.4335 g of 83.37 wt% $N_5[B(CF_3)_4]$, 2.81 wt% N_5SbF_6, and 13.82 wt% $KSbF_6$ (0.3615 g expected for 1.013 mmol $N_5[B(CF_3)_4]$, plus 0.0122 g expected for 0.0399 mmol of excess N_5SbF_6, and 0.0598 g expected for 0.2179 mmol $KSbF_6$).

The synthesis of $(N_5)_2SnF_6$ was carried out metathetically by using the same type of double U-Tube as described above. N_5SbF_6 (0.9430 g, 3.084 mmol) and Cs_2SnF_6 (0.7513 g, 1.507 mmol) were added to the reaction U-tube inside the drybox. HF was condensed into the reaction U-tube at −196 °C on the vacuum line. The reaction mixture was warmed to −78 °C and stirred for about 10 min to reduce the possibility of localized heating of the reactants as they were initially solvated. Afterwards, the reaction mixture was allowed to slowly warm to room temperature with constant agitation over ~10 min; this was followed by constant stirring for another 30 min to ensure that the metathesis reaction has gone to completion. The reaction U-tube was then cooled to −196 °C and checked for noncondensibles; none were found, indicating that there was no decomposition of any N_5^+ salt. The reaction mixture was warmed to room temperature and stirred again for 15 min before the mixture was cooled to −78 °C for 15 min in preparation for the low-temperature filtration procedure. At that point the filter assembly was cooled briefly to −78 °C with powdered dry ice, and the mixture was filtered under 1.5 atm N_2 pressure to remove the precipitated $CsSbF_6$ from the $(N_5)_2SnF_6$/HF filtrate, which was collected in the receiver U-tube at −78 °C. The gaseous N_2 was evacuated from the double U-tube, and the receiver U-tube was warmed to −64 °C. The HF was removed in vacuo at −64 °C over several hours until only some clear colorless droplets were seen in the receiver U-tube. The −64 °C bath was removed, and pumping on the reaction products was continued as they gradually warmed to room temperature. Finally, the white solid $(N_5)_2SnF_6$ product appeared in the receiver U-tube after about 5 minutes; pumping was continued for one additional hour at room temperature to ensure the complete removal of the HF solvent. Based upon mass measurements, and FT-IR and FT-Raman spectroscopy, the filter cake consisted of 1.2267 g of 90.1 wt% $CsSbF_6$, and 9.9 wt% $(N_5)_2SnF_6$ (1.1047 g expected for 2.997 mmol $CsSbF_6$ and 0.1220 g expected for 0.327 mmol $(N_5)_2SnF_6$). Using the same methods of investigation, the reaction products were found to consist of 0.4676 g of 94.0 wt% $(N_5)_2SnF_6$, 4.6 wt% N_5SbF_6, and 1.4 wt% $CsSbF_6$ (0.4398 g expected for 1.180 mmol $(N_5)_2SnF_6$, plus 0.0213 g expected for 0.0697 mmol of excess N_5SbF_6, and 0.0065 g expected for 0.0176 mmol $CsSbF_6$).

Acknowledgement

This work was funded by the Defense Advanced Research Projects Agency, with additional support from the Air Force Office of Scientific Research and the National Science Foundation. We thank Drs. R. Corley, A. Morrish, D. Woodbury, M. Berman, Prof. H. Willner, and M. Finze for their steady support, and Drs. R. Wagner, S. Schneider, T. Schroer, M. Gerken, and R. Haiges for their collaboration and stimulating discussions.

References

[1] K. O. Christe, W. W. Wilson, J. A. Sheehy, J. A. Boatz, *Angew. Chem.* **1999**, *111*, 2112; *Angew. Chem. Int. Ed.* **1999**, *38*, 2004.
[2] A. Vij, W. W. Wilson, V. Vij, F. S. Tham, J. A. Sheehy, K. O. Christe, *J. Am. Chem. Soc.* **2001**, *123*, 6308.
[3] G. A. Olah, G. K. S. Prakash, G. Rasul, *J. Am. Chem. Soc.* **2001**, *123*, 3308.
[4] M. T. Nguyen, T. K. Ha, *Chem. Phys. Lett.* **2001**, *335*, 311.
[5] S. Fau, R. J. Bartlett, *J. Phys. Chem. A.* **2001**, *105*, 4096.
[6] R. J. Bartlett, *Chem. Ind.* **2000**, 140, and references therein; a compilation of data for N_2 to N_{10} can be found at http://www.qtb.u-fl.edu/~bartlett/polynitrogen.pdf.
[7] G. Chung, M. W. Schmidt, M. S. Gordon, *J. Phys. Chem. A.* **2000**, *104*, 5647, and references therein.
[8] M. N. Glukhovtsev, H. Jiao, P. von R. Schleyer, *Inorg. Chem.* **1996**, *35*, 7124 and references therein.
[9] H. H. Michels, J. A. Montgomery, Jr., K. O. Christe, D. A. Dixon, *J. Phys. Chem.* **1995**, *99*, 187.
[10] G. Schatte, H. Willner, *Z. Naturforsch. Teil. B* **1991**, *46*, 483.
[11] G. Rasul, G. K. S. Prakash, G. A. Olah, *J. Am. Chem. Soc.* **1994**, *116*, 8985.
[12] W. E. Thompson, M. E. Jacox, *J. Chem. Phys.* **1990**, *93*, 3856.
[13] J. P. Zheng, J. Waluk, J. Spanget-Larsen, D. M. Blake, J. G. Radziszewski, *Chem. Phys. Lett.* **2000**, *328*, 227.
[14] T. Ruchti, T. Speck, J. P. Connelly, E. J. Bieske, H. Linnartz, J. P. Maier, *J. Chem. Phys.* **1996**, *105*, 2591.
[15] F. Cacace, G. de Petris, A. Troiani, *Science* **2002**, *295*, 480.
[16] M. I. Eremets, R. J. Hemley, H. Mao, E. Gregoryanz, *Nature* **2001**, *411*, 170.
[17] A. V. Pankratov, N. I. Savenkova, *Russ. J. Inorg. Chem.* **1968**, *13*, 1345.
[18] K. O. Christe, R. D. Wilson, W. W. Wilson, R. Bau, S. Sukumar, D. A. Dixon, *J. Am. Chem. Soc.* **1991**, *113*, 3795.
[19] a) K. O. Christe, J. P. Guertin, A. E. Pavlath, *Inorg. Nucl. Chem. Lett.* **1966**, *2*, 83; b) W. W. Wilson, K. O. Christe, *J. Fluorine Chem.* **1980**, *15*, 83; c) K. O. Christe, W. W. Wilson, R. D. Wilson, *Inorg. Chem.* **1980**, *19*, 1494; d) K. O. Christe, W. W. Wilson, R. D. Wilson, *Inorg. Chem.* **1980**, *19*, 3254; e) W. W. Wilson, K. O. Christe, *J. Fluorine Chem.* **1982**, *19*, 253.
[20] I. V. Nikikitin, V. Ya. Rosolovskii, *Russ. Chem. Rev.* **1985**, *54*, 426.
[21] K. O. Christe, D. A. Dixon, D. McLemore, W. W. Wilson J. A. Sheehy, J. A. Boatz, *J. Fluorine Chem.* **2000**, *101*, 151; K. O. Christe, D. A. Dixon, *Paper 53*, *presented at the 16th ACS Winter Fluorine Conference*, St. Pete Beach, FL, **2003**.
[22] H. M. Netzloff, M. S. Gordon, K. O. Christe, W. W. Wilson, A. Vij, V. Vij, J. A. Boatz, *J. Chem. Phys.*, **2003**, in press.
[23] K. O. Christe, C. J. Schack, R. D. Wilson, *Inorg.Chem.***1977**, *16*, 849.
[24] K. O. Christe, C. J. Schack, *Inorg.Chem.***1978**, *17*, 2749.
[25] P. A. W. Dean, *Can. J. Chem.* **1973**, *51*, 4024.
[26] P. A. W. Dean, D. F. Evans, *J. Chem. Soc. A* **1967**, 698.
[27] E. Bernhardt, G. Henkel, H. Willner, G. Pawelke, H. Burger, *Chem. Eur. J.* **2001**, *7*, 4696.
[28] K. O. Christe, R. D. Wilson, C. J. Schack, *Inorg. Synth.***1986**, *24*, 3.

Received: April 4, 2003 [F4973]

This Page Intentionally Left Blank

APPENDIX E

"On the Existence of FN_5, a Theoretical and Experimental Study"
J. Phys. Chem. A, 107, 6638 (2003)

This Page Intentionally Left Blank

On the Existence of FN_5, a Theoretical and Experimental Study

Heather M. Netzloff and Mark S. Gordon*

Department of Chemistry, Iowa State University, Ames, Iowa 50011

Karl Christe,* William W. Wilson, Ashwani Vij, Vandana Vij, and Jerry A. Boatz

Air Force Research Laboratory, Edwards AFB, California 93524, and Loker Research Institute, University of Southern California, Los Angeles, California 90089

Received: January 31, 2003; In Final Form: June 2, 2003

The possible existence of FN_5 was studied by ab initio electronic structure theory. Calculations were carried out at the MP2/6-31+G(d) and CCSD(T)/aug-cc-pVDZ levels of theory for the $N_5^+AsF_6^-$ ion pair and its decomposition to FN_5 and AsF_5. Six different vibrationally stable isomers of FN_5 were identified. Intrinsic reaction coordinate (IRC) and dynamic reaction path (DRP) calculations were used to study the isomerization of FN_5 and its decomposition to FN_3 and N_2. A Rice−Ramsperger−Kassel−Marcus (RRKM) analysis was performed, indicating upper limits to the lifetimes of the FN_5 isomers in the nanosecond range. These theoretical predictions were confirmed by an experimental study of the thermolyses of N_5AsF_6 and $[N_5]_2SnF_6$ and the displacement of FN_5 from N_5SbF_6 with CsF, using FT-IR spectroscopy. In accord with the theoretical predictions, the primary reaction product FN_5 could not be observed, but its decomposition products FN_3, F_2N_2, and NF_3 were identified.

Introduction

Polynitrogen compounds are of great interest as high-energy density materials (HEDM).[1−5] Although theoretical studies have predicted numerous kinetically stable polynitrogen compounds,[4] almost all attempts to synthesize them have failed due to their very high endothermicities, low energy barriers toward decomposition, and a lack of suitable synthetic methods. The high-energy content of polynitrogen compounds arises from an unusual property of nitrogen that sets it apart from most other chemical elements. Its single and double bond energies are considerably less than one-third and two-thirds, respectively, of its triple bond energy. Therefore, the decomposition of polynitrogen species to N_2 is accompanied by a large release of energy.[1]

Recently, the N_5^+ cation has been synthesized and characterized.[1,2] It represents only the second known homonuclear polynitrogen species after N_3^-,[6] which is stable and can be prepared on a macroscopic scale. Its bent structure of C_{2v} symmetry (Figure 1) was established by a crystal structure determination of $N_5^+Sb_2F_{11}^-$ and vibrational and NMR spectroscopy, and is in accord with ab initio and density functional theory (DFT) calculations.[1,2,7] The bent structure avoids the unfavorable neighboring positive charges that would result from a linear structure.[1]

Most salts consisting of an X^+ cation and a complex fluoro anion, MF_6^-, are prepared by the transfer of an F^- anion from the parent FX molecule to the strong Lewis acid MF_5 (eq 1).

$$FX + MF_5 \leftrightarrow X^+MF_6^- \qquad (1)$$

Usually, this reaction is reversible and the FX molecule can be regenerated by either thermolysis of $X^+MF_6^-$ or a displacement reaction between $X^+MF_6^-$ and a stronger Lewis base, such as CsF (eq 2). Only a few $X^+MF_6^-$ salts are known for which FX

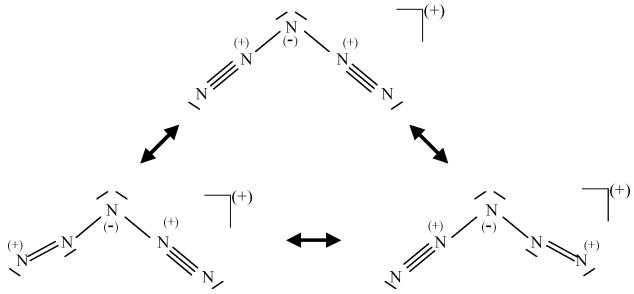

Figure 1. N_5^+ resonance structures.

$$X^+MF_6^- + CsF \rightarrow FX + CsMF_6 \qquad (2)$$

cannot be generated in this manner. Typical examples are the NF_4^+,[8] ClF_6^+,[9] and BrF_6^+ [10] salts where the corresponding FX parent compounds cannot exist because the maximum coordination number of the central atom would be exceeded.[11] The reverse case, where an amphoteric FX molecule exists but the corresponding X^+ cation does not, is also known but rare. A typical example is FN_3, which does not form a stable N_3^+ salt with strong Lewis acids.[12]

The availability of several marginally stable N_5^+ salts, such as $N_5^+AsF_6^-$,[1] $N_5^+SbF_6^-$,[2] and $[N_5]^+_2[SnF_6]^{2-}$ [13] that can be readily subjected to thermolysis or displacement reactions, offered an ideal opportunity to probe the possible existence of the unknown FN_5 molecule. While carrying out the theoretical study, we have also investigated the potential energy surfaces of the $N_5^+AsF_6^-$ ion pair and its FN_5 decomposition product to better understand the likely structure and stability of this new polynitrogen species.

10.1021/jp030157o CCC: $25.00
Published on Web 08/02/2003

Experimental Section

Caution! *Reactions of N_5^+ salts can be violent and can result in explosions,[1,2] particularly when highly shock sensitive FN_3[12,14] is formed as a decomposition product. Therefore, these materials should be handled only on a small scale with appropriate safety precautions (face shield, leather gloves, and protective clothing).*

Materials and Apparatus. All reactions were carried out in a demountable Teflon-PFA condensing sidearm of a 5 cm path length, Teflon-FEP infrared cell equipped with AgCl windows. Nonvolatile solids were loaded in the dry nitrogen atmosphere of a glovebox into the sidearm of the IR cell. The cell was then evacuated and placed into the FT-IR spectrometer. The decomposition or displacement reactions were initiated by gentle warming, and the volatile decomposition products were continuously monitored by infrared spectroscopy using a Mattson Galaxy FT-IR spectrometer. Volatile materials were handled on a stainless steel/Teflon-FEP vacuum line.[15]

The $N_5^+AsF_6^-$,[1] $N_5^+SbF_6^-$,[2] and $[N_5]^+_2[SnF_6]^{2-}$ [13] starting materials were prepared by literature methods. The CsF (KBI) was fused in a platinum crucible, transferred while hot into the drybox, and finely powdered.

Computational Methods

Initial optimizations of all structures were performed using second-order perturbation theory (MP2)[16] and the 6-31+G(d) basis set.[17] Hessians (energy second derivatives) were calculated for the final equilibrium structures to determine if they are minima (positive definite Hessian) or transition states (one negative eigenvalue). At the final MP2/6-31+G(d) geometries, improved relative energies were obtained using singles and doubles coupled cluster theory with triples included perturbatively (CCSD(T))[18] and the aug-cc-pVDZ basis set.[19] The MP2 calculations were performed using the electronic structure code GAMESS,[20] and the CCSD(T) calculations were carried out using ACES II.[21]

Intrinsic reaction coordinate (IRC) pathways[22] were employed in the study of the FN_5 species to connect isomer minima, transition states, and decomposition products. The IRC is the minimum energy path (MEP) in mass weighted Cartesian coordinates. IRC calculations were performed with GAMESS using the second-order method developed by Gonzalez and Schlegel[23] with a step size of 0.1 $(amu)^{1/2}$ bohr.

A simple Rice−Ramsperger−Kassel−Marcus (RRKM) analysis was performed on the isomers included in the potential energy surfaces obtained with the IRC calculations. The RRKM theory of reaction dynamics can be used to give an upper limit to the lifetime of the minima.[24] It assumes a microcanonical equilibrium and a locally separable reaction coordinate. The microscopic rate constant is proportional to the sum of states of the ith reaction channel ($W_N^i(E - E_0^i)$) divided by the reaction density of states (ρ_N):

$$k \propto W_N^i(E - E_0^i)/\rho_N(E) \tag{3}$$

$$k = \frac{\prod_{i=1}^{3N-6} \nu_i}{\prod_{i=1}^{3N-7} \nu_i^{TS}} \left(\frac{E - E_0^{barrier}}{E}\right)^{3N-7} \tag{4}$$

where k is the rate constant, ν_i is the ith frequency of the minima, ν_i^{TS} is the ith frequency of the transition state, E is the applied energy, and $E_0^{barrier}$ is the barrier energy. Note that the lifetime $\tau = 1/k$.

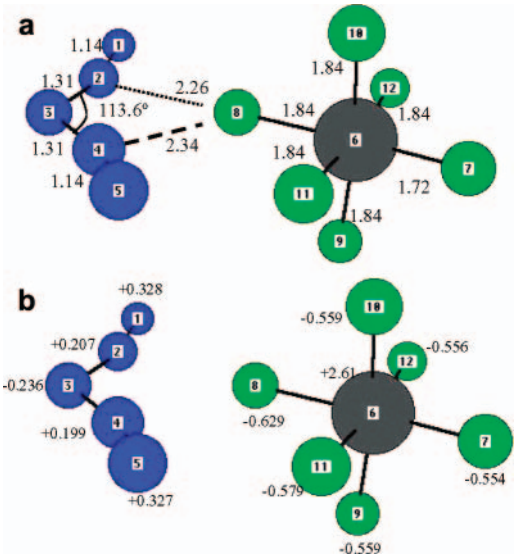

Figure 2. Optimized ion pair, $[N_5]^+[AsF_6]^-$: (a) bond distances (Å) and angles; (b) Mulliken charges.

Finally, to further study the decomposition and stability of several FN_5 isomers, the dynamic reaction path (DRP) method was used to add photons (kinetic energy (KE)) to one or more FN_5 vibrational normal modes.[25] The DRP method, a classical trajectory approach, is based on a quantum chemical potential energy surface (PES) that need not be known ahead of time. Unlike the IRC, energy is strictly conserved along the dynamic reaction path. Thus, larger step sizes can be used. In this way a classical trajectory is developed "on-the-fly" without prior knowledge of the PES. GAMESS can use normal modes as the initial dynamic reaction coordinates. An initial KE and velocity direction is supplied to one or more modes (in units of quanta).[26] The strategy is to provide energy to those modes that appear to lead to desired reaction products. Because there is often significant mode−mode mixing, the applied energy is usually in excess of the reaction/decomposition barrier. This is a direct dynamics method in that the ab initio (in the present case, MP2) gradients/forces are calculated at each step and are then used to solve Newton's equations of motion and propagate the system. Step sizes ranged from 0.1 to 0.2 fs, depending on how well energy conservation criteria were satisfied.

Results and Discussion

$N_5^+AsF_6^-$ Ion Pair. The starting points for the calculations were the AsF_6^- and N_5^+ ions separated by a distance of ~10.0 Å, in C_1 symmetry, followed by a complete geometry optimization. The resulting ion pair is shown in Figure 2a. At the MP2/6-31+G(d) level of theory, the ion pair is 98.8 kcal/mol lower in energy than the separated ions (Table 1).

MP2 Mulliken charges on the N_5^+ and AsF_6^- units within the ion pair show that the charge separation is ±0.825; thus, there is relatively little charge transfer between the ions. In comparison with the separated ions (Figures 2b and 3b), the N_5^+ unit in the ion pair has a less negative charge on the central N by approximately 0.3, whereas the terminal N atoms are about 0.2 less positive than in the isolated N_5^+ ion. In the case of AsF_6^- in the ion pair, all As−F bonds except for the bond opposite to the N_5^+ unit have been elongated by about 0.085 Å (Table 2). This effect can be explained by the partial removal

TABLE 1: Energies (hartrees), Zero Point Energy (ZPE) Corrections, and Relative Energies (kcal/mol) for Ion Pair, Separated Ions, and Separated Neutrals (reference = ion pair)

molecule	*E*(MP2/6-31+G(d))	ZPE (kcal/mol)	relative energy[a]
$N_5^+AsF_6^-$	−3102.913474	23.3	0
N_5^+	−272.602102	12.4	
AsF_6^-	−2830.15549	9.9	
$N_5^+ + AsF_6^-$	−3102.757592	22.3	98.8
FN_5 (bifurcated)	−372.481754	14.0	
AsF_5	−2730.358788	8.6	
$FN_5 + AsF_5$	−3102.840542	22.6	46.5

[a] Includes ZPE correction.

TABLE 2: Bond Distances and Angles for Ion Complex and Separated Ions (Refer to Figures 2a and 3a)

distances (Å)		angles (deg)	
		Ion Complex	
N1−N2	1.144	N2−N3−N4	113.56
N2−N3	1.305	F10−As6−F8	86.88
N3−N4	1.312		
N4−N5	1.144		
As6−F7	1.722		
As6−F8	1.843		
As6−F9	1.843		
As6−F10	1.843		
As6−F11	1.843		
As6−F12	1.843		
N1−F8	2.720		
N2−F8	2.258		
N3−F8	2.737		
N4−F8	2.338		
N5−F8	2.879		
		N_5^+	
N1−N2	1.143	N2−N3−N4	110.17
N2−N3	1.313	N1−N2−N3	167.15
N3−N4	1.313		
N4−N5	1.143		
		AsF_6^-	
As−F	1.758	F−As−F	90.0

of an electron from bonding orbitals. It is interesting to note that the bond distances in N_5^+ do not exhibit a similar effect and are essentially unchanged.

In isolated N_5^+, the central N has a large negative charge (Figure 3b). This charge is reduced by a factor of 2 in the ion pair. All other N atoms are positive, with the terminal N atoms being most positive. This type of charge distribution can be rationalized by the valence bond structures[1,2,27] given in Figure 1. It must be kept in mind, however, that the magnitude of the charges varies strongly with the calculation method, although their signs and relative order remain the same. Thus, at the NBO (B3LYP/aug-cc-pVDZ) level of theory, the charges on N1, N2, and N3 are significantly smaller and amount to +0.33, +0.22, and −0.11, respectively.[28]

As can be seen from Figure 2a, the closest N−F distances in the ion pair are N2−F8 = 2.26 Å and N4−F8 = 2.34 Å. They are much longer than a typical N−F bond (∼1.3 Å),[29] but significantly shorter than the sum of their van der Waals radii (3.0 Å)[30] and the shortest N···F contacts observed in the crystal structure of $N_5^+Sb_2F_{11}^-$ (2.72 and 2.78 Å).[2]

Because there is still a large charge separation between the components of the ion pair, it is of interest to consider how much energy would be required to transfer F^- from AsF_6^- to N_5^+ to make gaseous AsF_5 and FN_5. At the MP2/6-31+G(d) level of theory, the ion pair is 46.5 kcal/mol lower in energy than the separated AsF_5 and *bifurcated(bif)*-FN_5 molecules,

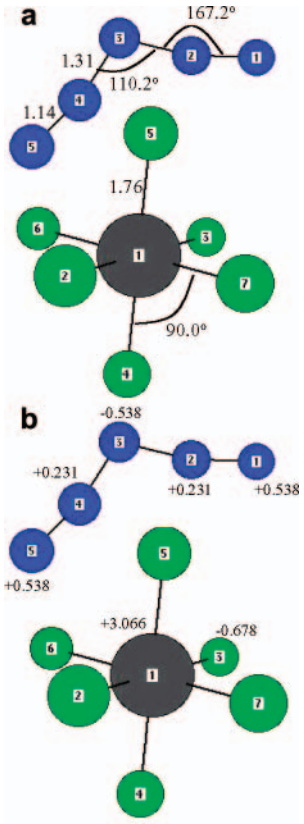

Figure 3. Separated Ions, N_5^+ and AsF_6^-: (a) bond distances (Å) and angles; (b) Mulliken charges.

indicating that it takes at least this much energy to transfer F^- from AsF_6^- to N_5^+ to make *bif*-FN_5 and AsF_5 (Figure 4). Thus, the ion pair is reasonably stable to dissociation to gaseous AsF_5 and *bif*-FN_5. Because an ion pair is only a poor approximation to a crystalline solid, the 25.5 kcal/mol difference between the lattice energy of $N_5^+AsF_6^-$ (124 ± 4 kcal/mol)[31] and the ion pair energy (98.8 kcal/mol) must be added to the above minimum decomposition energy barrier of 46.5 kcal/mol when the thermal stability of solid N_5AsF_6 is considered. The resulting minimum decomposition energy barrier of 72.0 kcal/mol for crystalline N_5AsF_6 is in accord with the experimental observation that this salt is marginally stable at room temperature.[1] The experimentally observed irreversible decomposition of N_5AsF_6 at higher temperatures[1] is due to the subsequent rapid, highly exothermic, and irreversible decompositions of FN_5 and FN_3 (see below).

In addition to the $[AsF_6]^-[N_5]^+$ structure discussed above, a geometry search revealed a second, lower energy isomer. This C_{2v} structure is obtained from the structure shown in Figure 2a by rotating the $[AsF_6]^-$ anion so that the As_6, F_7, and F_8 atoms are coplanar with $[N_5]^+$. The C_2 rotation axis then passes through atoms N_3 and As_6. The second symmetry plane contains N_3, As_6, and F_9-F_{12} with F_9 and F_{11} pointing toward the $[N_5]^+$ cation and F_{10} and F_{12} pointed away from it. Some of the distinguishing features of this C_{2v} geometry are the As−F distances ($As-F_{7,8}$ = 1.75 Å; $As-F_{9,11}$ = 1.81 Å; $As-F_{10,12}$ = 1.72 Å); the N_1-F_8 (N_5-F_7) distance is 2.80 Å. The F_9-N_2, F_9-N_4, $F_{11}-N_2$, and $F_{11}-N_4$ distances are each 2.47 Å. The geometry of the $[N_5]^+$ cation is virtually identical to that in Figure 2a. This second bifurcated isomer is ∼10 kcal/mol lower in energy than the structure shown in Figure 2a, most likely because of the electrostatic interactions between four F atoms with N. However, the higher energy structure is more likely to

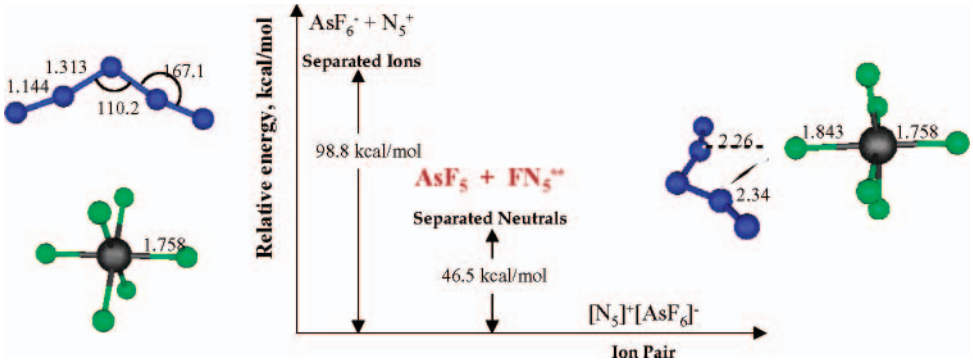

Figure 4. Relative energy diagram (kcal/mol): ion pair, separated ions, and separated neutrals (reference = ion pair). Energies: MP2/6-31+G(d). FN_5 = bifurcated FN_5 isomer.

TABLE 3: Energies (hartrees), ZPE Corrections (kcal/mol), and Energies Relative to the cis (2) Isomer (kcal/mol) for FN_5 Isomers, Transition States, and Decomposition Products, $FN_3 + N_2$

molecule	E(MP2/G)[a]	ZPE	E(CCSD(T))[b]	ΔE(MP2/G)[d]	ΔE(CCSD(T))[d]	ΔE(MP2/aug)[c,d]
bifurcated (1)	−372.48175	14.0	−372.62048	−1.1	10.5	−1.4
cis (2)	−372.47998	14.0	−372.63717	0	0	0
trans (3)	−372.47509	14.0	−372.63252	3.1	2.9	3.3
harp (4)	−372.47275	13.5	−372.62892	4.0	4.7	3.7
wag (5)	−372.47104	13.7	−372.62794	5.3	5.5	4.8
cyclic (6)	−372.48349	15.7	−372.64098	−0.5	−0.7	−4.2
TS2p[e]	−372.44101	11.3	−372.61175	21.8	13.2	21.6
TS14[e]	−372.45042	13.1	−372.6048	17.6	19.4	16.7
TS42[e]	−372.46467	13.8	−372.62343	9.4	8.4	9.2
TS4p[e]	−372.45809	11.8	−372.62459	11.5	5.7	10.6
FN_3	−263.29092	8.3	−263.40485			
N_2	−109.26193	3.1	−109.3007			
$FN_3 + N_2$	−372.55285	11.4	−372.70555	−48.3	−45.5	−46.0

[a] Basis set = 6-31+G(d). [b] Basis set = aug-cc-pVDZ. [c] Basis set = aug-cc-pVDZ. [d] Includes ZPE correction. [e] TS notation: TS2p = cis(2) → $FN_3 + N_2$. TS14 = bifurcated(1) → harp(4). TS42 = harp(4) → cis(2). TS4p = harp(4) → $FN_3 + N_2$.

TABLE 4: Distances, Angles, and Dihedral Angles for FN_5 Isomers-MP2/6-31+G(d) (Refer to Figure 5)

	distances (Å)							
isomer	N1−N2	N2−N3	N3−N4	N4−N5	F−N1	F−N2	F−N3	F−N4
bifurcated	1.166	1.339	1.308	1.147		1.837	2.459	2.179
cis	1.239	1.396	1.279	1.152	1.452			
trans	1.251	1.404	1.275	1.152	1.416			
harp	1.233	1.362	1.293	1.157	1.495			
wag	1.253	1.393	1.285	1.156	1.412			
cyclic	1.318	1.337	1.351	1.337	1.345			

	angles (deg)			
isomer	F−N1−N2	N1−N2−N3	N2−N3−N4	N3−N4−N5
bifurcated		137.78	109.38	160.37
cis	112.16	117.42	107.54	169.77
trans	107.39	107.33	170.27	104.98
harp	129.23	119.27	162.54	112.42
wag	106.25	112.88	114.85	169.22
cyclic	121.29	101.59	109.70	109.70

	dihedral angles (deg)		
isomer	F−N1−N2−N3	N1−N2−N3−N4	N2−N3−N4−N5
bifurcated	180	180	180
cis	0	180	180
trans	180	180	180
harp	0	0	180
wag	180	0	180
cyclic	180	0	0

TABLE 5: Distances, Angles, and Dihedral Angles for FN_5 Transition States-MP2/6-31+G(d) (Refer to Figure 6)

	distances (Å)							
molecule	N1−N2	N2−N3	N3−N4	N4−N5	F−N1	F−N2	F−N3	F−N4
TS14	1.144	1.315	1.356	1.16	2.022	2.351	2.716	2.049
TS2p	1.248	1.27	1.675	1.138	1.489			
TS42	1.230	1.448	1.264	1.155	1.495			
TS4p	1.242	1.264	1.563	1.142	1.509			

	angles (deg)			
molecule	F−N1−N2	N1−N2−N3	N2−N3−N4	N3−N4−N5
TS14	91.62	150.36	107.04	145.03
TS2p	107.44	125.92	106.07	150.15
TS42	113.49	118.76	109.55	171.99
TS4p	108.68	138.9	113.77	152.47

	dihedral angles (deg)		
molecule	F−N1−N2−N3	N1−N2−N3−N4	N2−N3−N4−N5
TS14	0	0	180
TS2p	0	180	180
TS42	7.33	−92.57	−172.06
TS4p	0	0	180

yield the neutral species $AsF_5 + FN_5$. In either case, the ion complex is clearly much lower in energy than the separated neutrals.

FN_5 Isomers. Because the F^- ion can attach itself in different ways to the three different nitrogen atoms of N_5^+, it is necessary to explore the different possible isomers of FN_5 and their relative energies and stabilities. An exhaustive study was performed, and six stable isomers were found. Their relevant energies and geometries are listed in Tables 3 and 4, respectively. Optimized structures were obtained for each isomer and Hessians confirmed that these structures are minima on the potential energy surface. The relevant geometrical features are summarized in Figure 5 and Table 4. The N−F and N−N bond lengths are similar for all isomers except for the bifurcated isomer (1) and the cyclic structure (6). All isomers are planar molecules. Both MP2 and CCSD(T) calculations predict the cis and cyclic isomers to be among the lowest energy species. Indeed, except for the bifurcated isomer, the two levels of theory predict similar

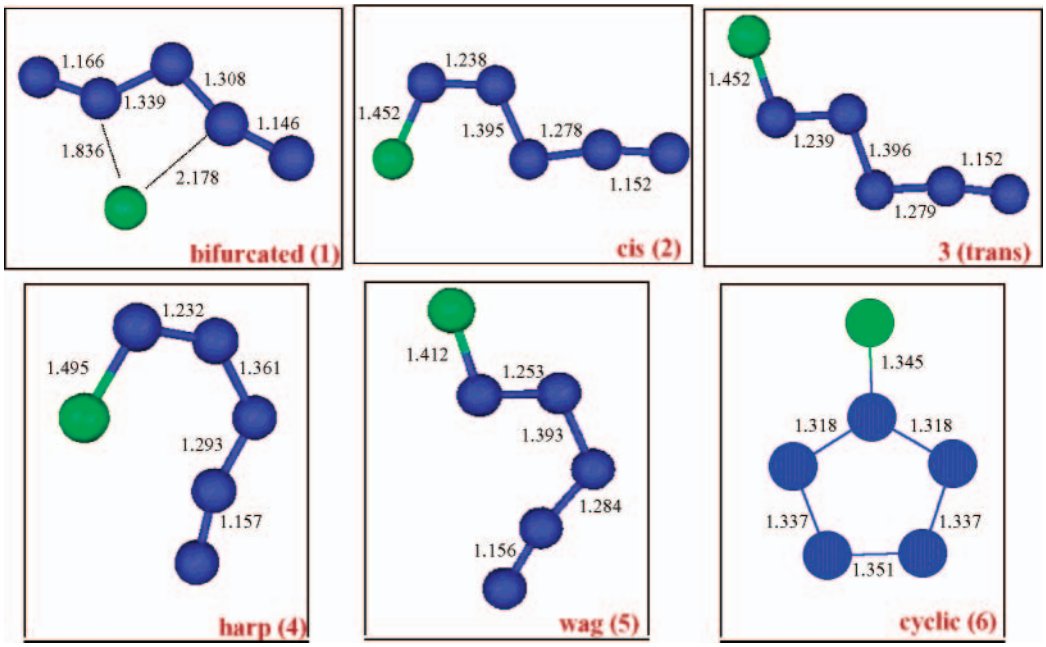

Figure 5. FN_5 isomers (MP2/6-31+G(d) geometries). Bond distances in ångstroms.

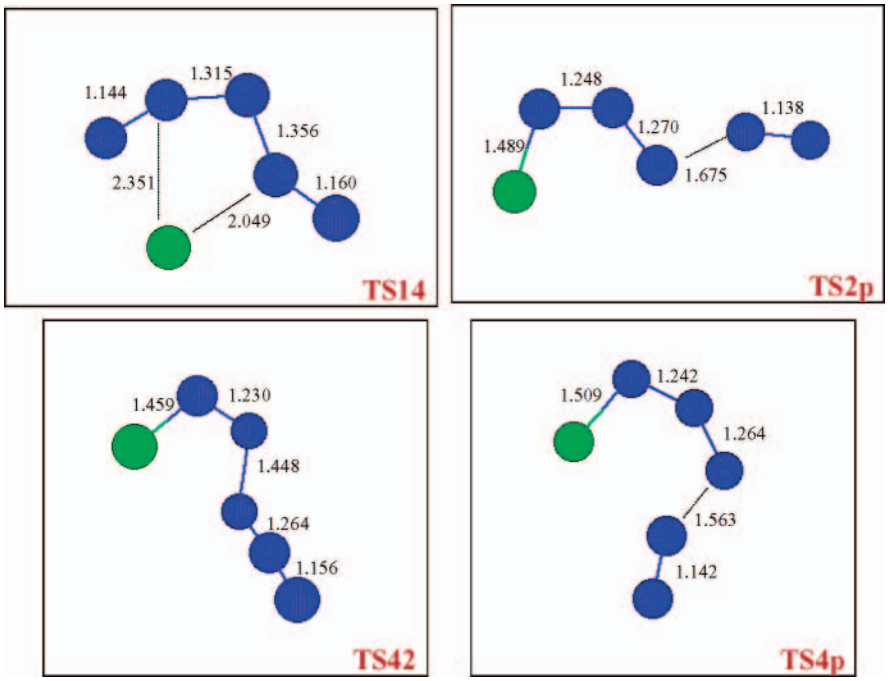

Figure 6. FN_5 transition states (MP2/6-31+G(d) geometries). Bond distances in ångstroms.

relative energies (Table 3). Note that the MP2 results are not very basis set dependent. The cis, trans, wag, and harp isomers are all within a few kcal/mol of each other and can be easily interconverted by simple rotations around the N3−N4 and N4−N5 bonds. The more accurate and reliable CCSD(T) method places the bifurcated isomer 3−11 kcal/mol above the other isomers. Because the two N−F distances in this "bifurcated" isomer differ by 0.342 Å, this isomer might reasonably be described as an N_β-bonded isomer with a weak secondary interaction to the other N_β atom, whereas the other four noncyclic isomers are all N_α-bonded. The cyclic isomer (6) is less likely to form in the experiments because it would probably involve a fluoride attacking N_5^+ from the backside at its central N_γ atom. Such an approach is not likely because both reacting atoms apparently carry partial negative charges that should repel each other. Furthermore, *cyclic*-FN_5 has been predicted to have a low barrier to decomposition of 6.7 kcal/mol at the CCSD(T) level of theory.[32]

Because N_2 is so stable, the dissociation of FN_5 to FN_3 and N_2 is 45.5 kcal/mol exothermic at the CCSD(T) level of theory (Table 3) and is irreversible. Therefore, it is important to explore the possible decomposition pathways for the preferred FN_5 isomers and to determine their energy barriers toward decomposition.

To explore both the isomerization and decomposition pathways, IRC studies were performed at the MP2 level of theory to connect minima with the corresponding transition states (TS). Transition states are illustrated in Figure 6, and FN_3 is depicted in Figure 7; detailed geometries are given in Table 5. The first IRC was started from the "bifurcated" isomer, which most

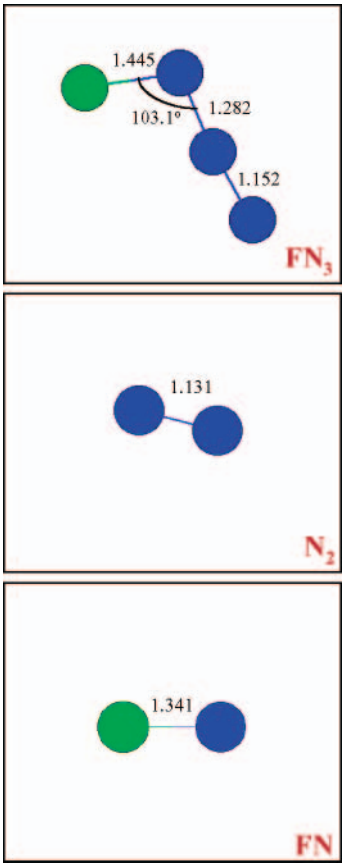

Figure 7. Optimized FN_3, N_2, and FN (MP2/6-31+G(d) geometries). Bond distances in ångstroms.

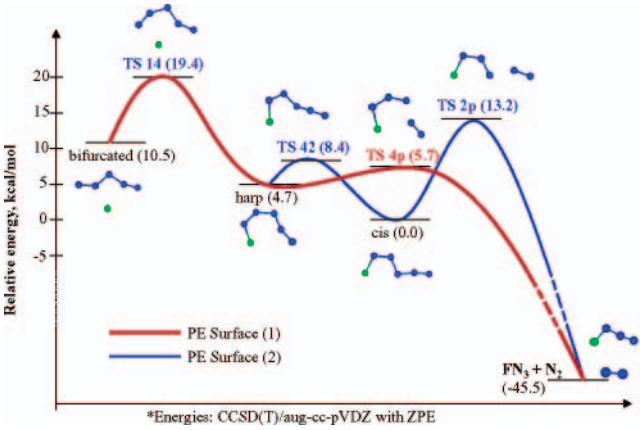

Figure 8. Relative isomerization/decomposition PESs with FN_5 isomers (reference = cis isomer). Energies: CCSD(T)/aug-cc-pVDZ with ZPE.

closely resembles the original ion pair. Structurally, the isomer that most naturally connects with the bifurcated isomer is the harp isomer, because this simply requires F to move to a neighboring nitrogen atom of the N_5 moiety via TS14. Starting from harp, two PESs have been identified (Figure 8) that the harp isomer can take to reach decomposition products: a "direct" decomposition route (through TS4p) or an isomerization via the cis isomer (through TS42). The cis isomer decomposes directly to $FN_3 + N_2$ (through TS2p). As shown in Figure 8 and Table 6, the bottleneck for both reaction paths is the initial barrier towards isomerization from bifurcated to harp (through TS 14), predicted to be 8.9 kcal/mol. The subsequent activation energies are much smaller, so once the harp isomer is reached, the decomposition to $FN_3 + N_2$ should proceed even more easily.

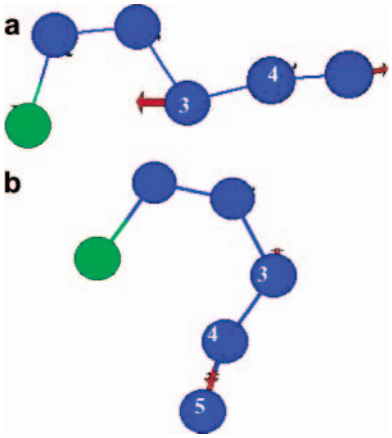

Figure 9. FN_5 vibrational modes selected for DRP analysis: (a) cis, mode 10; (b) harp, mode 12. The molecular structures were distorted along the negative of the vibrational displacements; these displacements are shown in the picture.

TABLE 6: Activation Energies (kcal/mol) for Isomerization and Decomposition Reactions

barriers	ΔE(MP2/G)[a,d]	ΔE(CCSD(T))[b,d]	ΔE(MP2/aug)[c,d]
TS14	18.8	8.9	18.1
TS42	5.4	3.7	5.5
TS2p	21.8	13.2	21.6
TS4p	7.5	1.0	6.9

[a] Basis set = 6-31+G(d). [b] Basis set = aug-cc-pVDZ. [c] Basis set = aug-cc-pVDZ. [d] Includes ZPE correction.

The two PESs are qualitatively similar at the MP2/6-31+G-(d) and CCSD(T)/aug-cc-pVDZ levels of theory. The MP2 activation energies are larger than those from CCSD(T), and all transition states and minima, excluding the initial bifurcated species, are higher in energy than the reference cis isomer. CCSD(T) predicts that all minima and TSs are higher in energy than the reference cis isomer (Table 3).

The results of a *qualitative* RRKM analysis (using the vibrational frequencies in Table 7) for the two isomerization reactions, and two decomposition reactions are shown in Tables 8 and 9. Several values were chosen for E, the applied energy, in eq 4 for each minimum. Because the CCSD(T) and MP2 activation energies are different (Table 6), a given value of E corresponds to different excess energies above the barrier. So, in Tables 8 and 9, a given amount of energy above a barrier corresponds to different values of E. Because the CCSD(T) energies were obtained as single energy calculations at the MP2 geometries, the frequencies used in both sets of RRKM calculations are those obtained from MP2. Thus, the CCSD(T) results are only qualitative, but these frequencies are not expected to be very different. Because the CCSD(T) barriers are much lower in energy than those based on MP2, the corresponding lifetimes will be smaller. Of course, the shorter the predicted lifetime, the more likely it is that the isomerization or dissociation will occur. At the CCSD(T) level of theory, the predicted lifetimes for the two isomerization reactions, bifurcated (1) → harp (4) and harp (4) → cis (2), are on the order of a few nanoseconds even in the case where an energy that is only 5 kcal/mol above the barrier is added. When this excess energy rises to 40 kcal/mol, these lifetimes decrease to 1−2 ps. The lifetimes for the decomposition reactions, from harp and cis to FN_3 and N_2, are even shorter.

DRP Calculations. To further study the decomposition and stability of the *harp*- and *cis*-FN_5 isomers, the dynamic reaction

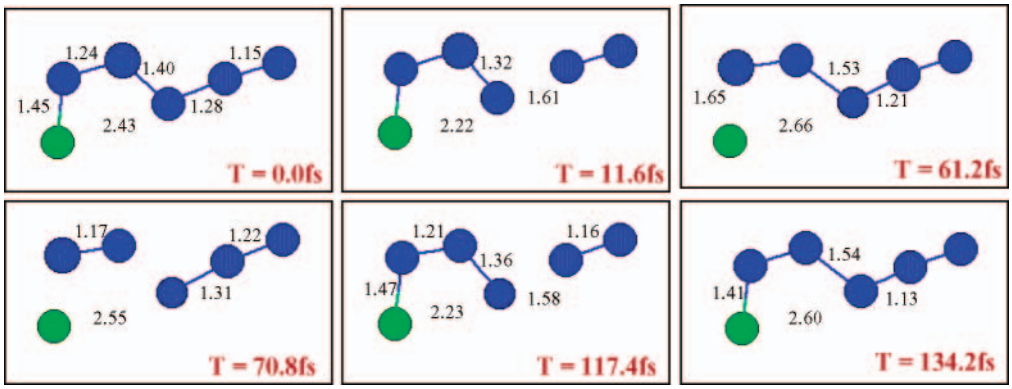

Figure 10. Stages along the trajectory for adding an initial KE of 34.9 kcal/mol to mode 10, cis isomer. Distances in ångstroms (initial bond lengths shown at $T = 0.0$ fs; if bond lengths have changed by >0.40 Å, new values are reported in next pane).

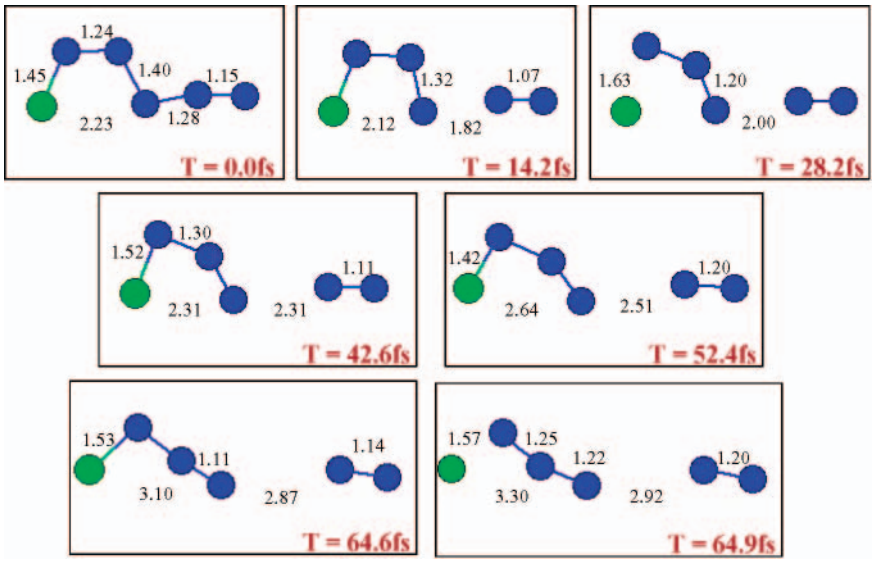

Figure 11. Stages along the trajectory for adding an initial KE of 51.3 kcal/mol to mode 10, cis isomer.

TABLE 7: Vibrational Frequencies and Corresponding IR Intensities for FN_5 Isomers and Transition States in the Isomerization/Decomposition PES Surfaces (MP2/6-31+G(d))

molecule	frequencies, cm^{-1} [IR intensities, $debye^2/(amu\ Å^2)$]
bifurcated (1)	130 (0.032), 232 (0.415), 316 (0.479), 418 (0.048), 460 (0.084), 541 (1.693), 565 (0.308), 669 (0.984), 1007 (2.234), 1212 (2.616), 1965 (5.003), 2269 (2.992)
cis (2)	113 (0), 178 (0.044), 300 (0.190), 485 (0.064), 554 (0.001), 638 (0.122), 691 (3.290), 822 (2.306), 999 (1.784), 1196 (3.807), 1532 (1.153), 2321 (9.337)
trans (3)	122 (0.001), 164 (0.044), 340 (0.075), 399 (0.226), 460 (0.047), 521 (0.185), 716 (0.321), 947 (4.070), 1050 (0.308), 1220 (4.531), 1481 (0.069), 2356 (8.660)
harp (4)	49 (0.016), 221 (0.006), 315 (0.533), 452 (0.091), 518 (1.043), 546 (0.001), 721 (1.974), 860 (0.785), 916 (0.790), 1139 (2.967), 1546 (2.382), 2175 (6.153)
wag (5)	146 (0.005), 148 (0.010), 361 (0.023), 395 (0.396), 472 (0.092), 517 (0.012), 766 (2.388), 988 (0.448), 1024 (2.399), 1123 (4.000), 1443 (0.102), 2252 (5.988)
cyclic (6)	272 (0.052), 435 (0.045), 614 (0.002), 701 (0.143), 727 (0), 1022 (0.018), 1034 (0.198), 1090 (0.088), 1132 (0.024), 1211 (0.175), 1378 (0.134), 1387 (1.832)
TS14	493 i, 115, 307, 391, 423, 456, 516, 701, 898, 1120, 1901, 2311
TS4p	823 i, 115, 159, 328, 335, 442, 591, 699, 807, 1206, 1550, 1993
TS42	109 i, 204, 310, 446, 500, 611, 724, 806, 864, 1230, 1538, 2409
TS2p	728 i, 86, 125, 242, 265, 444, 581, 706, 823, 1111, 1505, 2046

path (DRP) method[25,26] was used to provide kinetic energy to one or more vibrational normal modes.

For the cis isomer, mode 10 (Figure 9a) is a good candidate for breaking the N3−N4 bond because ν_{10} is the symmetric N3−N4−N5 stretching mode. At the MP2/6-31+G(d) level, the barrier for the decomposition, *cis*-$FN_5 \rightarrow FN_3 + N_2$, is approximately 22 kcal/mol. With the addition of approximately 35 kcal/mol to this mode, the N3−N4 bond undergoes only oscillations, and at least 51 kcal/mol of KE must be applied to this mode to break the N3−N4 bond (the bond breaks after 5.6 fs into such a trajectory run). Figures 10 and 11 show various structures along the trajectories with the addition of 35 and 51 kcal/mol of KE, respectively. Further illustration of this phenomenon is shown in Figure 12 where the coordinate changes in terms of the normal modes of the equilibrium structure for both $E = 35$ and $E = 51$ kcal/mol are plotted. With the addition of 35 kcal/mol, the KE is quickly redistributed to other modes. This dissipates the applied energy, so bond oscillations due to the activation of other modes result. For $E = 51$ kcal/mol, the energy remains localized in mode 10; the

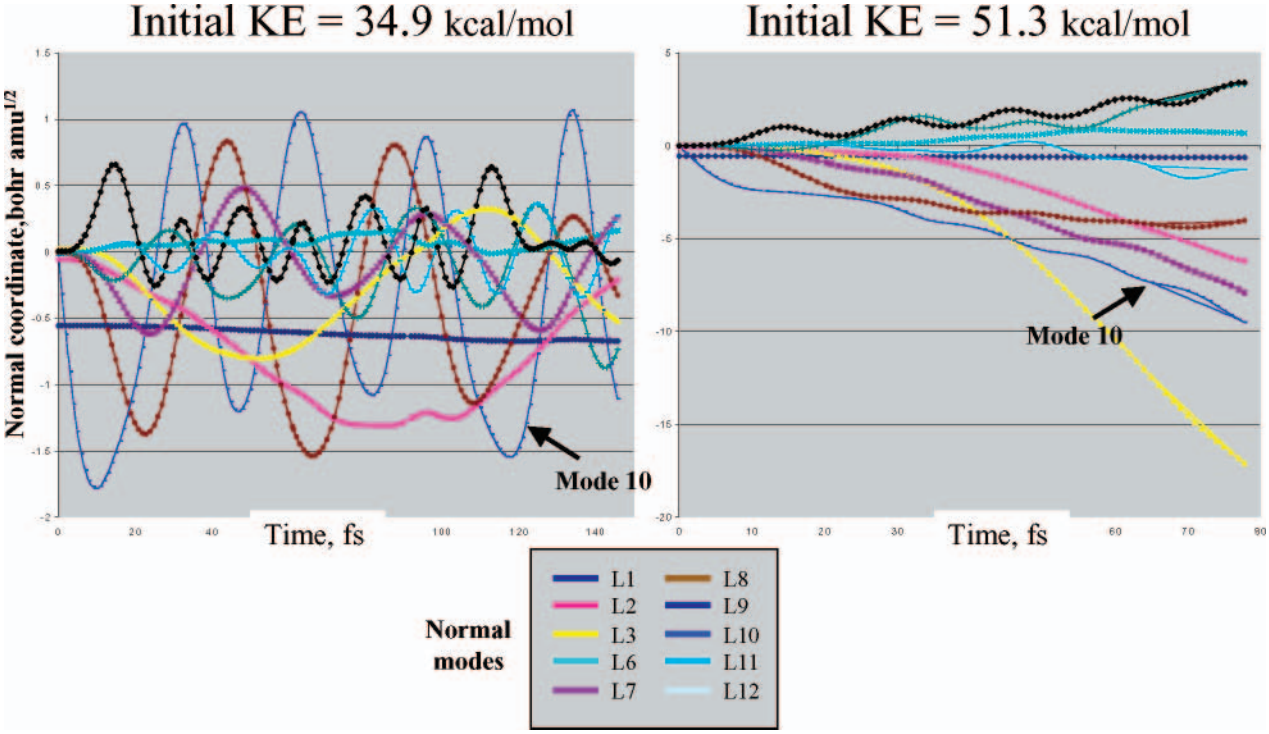

Figure 12. Normal coordinate change for cis isomer: addition of KE to mode 10.

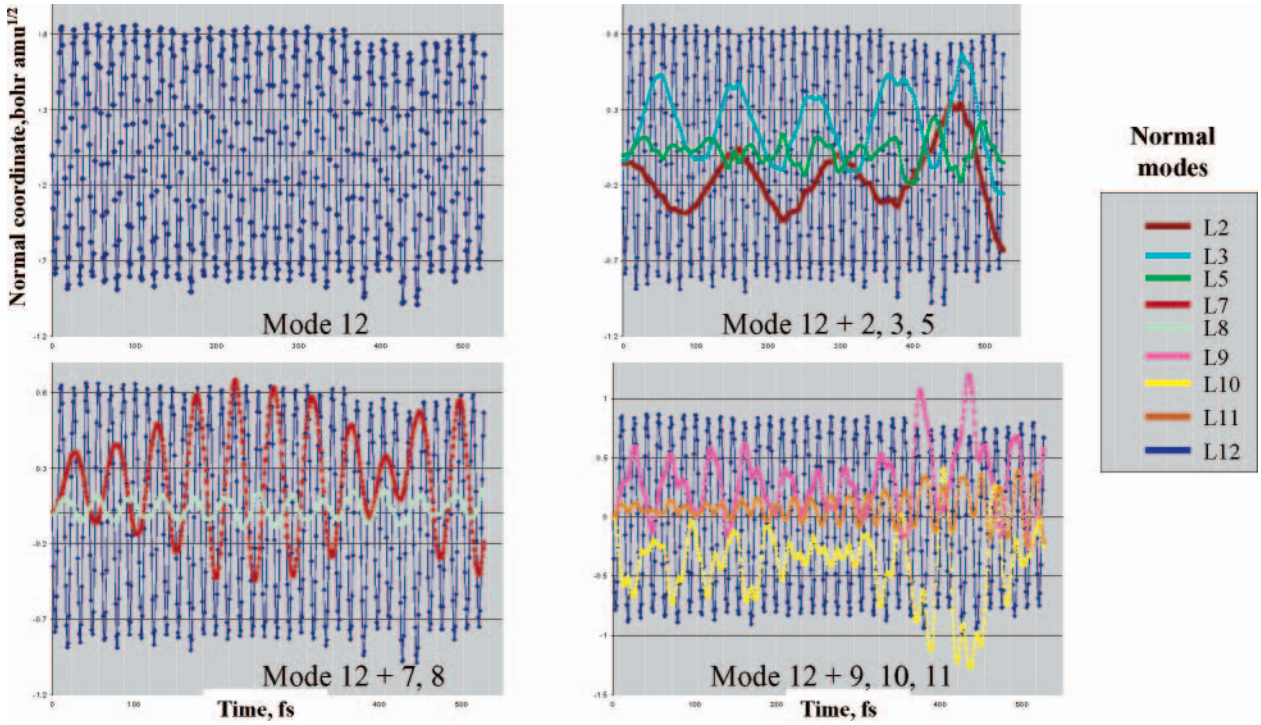

Figure 13. Normal coordinate change for harp isomer: addition of KE to mode 12.

modes become well separated and do not undergo wild oscillations. There is enough energy available to "push" the N_2 fragment away so it is not recaptured during oscillations.

As noted earlier, the harp isomer can decompose in a direct or stepwise manner. The MP2/6-31+G(d) barrier to direct decomposition is 7.5 kcal/mol, whereas the barrier for the isomerization, harp → cis, is 5.4 kcal/mol. In the analysis of this structure, ν_{12} (Figure 9b) appears to be a good candidate for N3−N4 bond breaking because ν_{12} is the N4−N5 stretching mode. After the addition of 44 kcal/mol, the N3−N4 bond breaks, but it then re-forms and oscillates. As in the case for the cis isomer, this can be seen in the graphs of normal mode coordinate change versus time. Figure 13 shows that the energy applied to ν_{12} dissipates to other modes even more rapidly than in the case of the cis isomer. Of course, these DRP calculations are only suggestive about possible dynamic processes. One would need to explore many more trajectories to obtain quantitatively meaningful kinetics data.

The MP2 and CCSD(T) RRKM analyses for the addition of energy, corresponding to this DRP for both the cis and harp isomers, are given in Table 9. The examples discussed above are in boldface in Table 9. Consider the decomposition of the

TABLE 8: RRKM Analysis for Isomerization and Decomposition Reactions as a Function of Excess Energy

excess energy (kcal/mol)	E[CCSD(T)][b,c] (kcal/mol)	E[MP2/G][a,c] (kcal/mol)	CCSD(T) lifetime	MP2/G lifetime
	Bifurcated−TS14−Harp			
5	13.9	23.8	5.5 ns	1.9 μs
10	18.9	28.8	78.3 ps	7.6 ns
20	28.9	38.8	4.0 ps	100.9 ps
30	38.9	48.8	1.2 ps	14.6 ps
40	48.9	58.8	0.6 ps	4.8 ps
	Harp−TS42- -Cis			
5	8.7	10.4	0.3 ns	2.1 ns
10	13.7	15.4	23.1 ps	78.7 ps
20	23.7	25.4	4.6 ps	9.5 ps
30	33.7	35.4	2.5 ps	4.3 ps
40	43.7	45.4	1.9 ps	2.8 ps
	Harp−TS4p- -$FN_3 + N_2$			
5	6.0	12.5	0.3 ps	0.9 ns
10	11.0	17.5	0.1 ps	18.3 ps
20	21.0	27.5	67.0 fs	1.3 ps
30	31.0	37.5	56.0 fs	451.4 fs
40	41.0	47.5	51.2 fs	256.8 fs
	Cis−TS2p−$FN_3 + N_2$			
5	18.2	26.8	7.2 ns	480.2 ns
10	23.2	31.8	50.1 ps	1.5 ns
20	33.2	41.8	1.3 ps	15.3 ps
30	43.2	51.8	0.3 ps	1.9 ps
40	53.2	61.8	0.1 ps	0.6 ps

[a] Basis set = 6-31+G(d). [b] Basis set = aug-cc-pVDZ. [c] Includes ZPE correction.

cis isomer, using ν_{10}. At least seven (four) vibrational quanta are required to surmount the barrier in this mode for MP2 (CCSD(T)), corresponding to lifetimes of 0.2 and 855 ms, respectively. For an E value of 35 kcal/mol, corresponding to 10 vibrational quanta, the lifetimes are 216 and 0.9 ps, respectively. The trajectory with $E = 35$ kcal/mol was only run for ~0.15 ps, and only bond oscillations were observed. For $E = 52$ kcal/mol (15 quanta), the predicted lifetimes are 116 fs and 1.7 ps for CCSD(T) and MP2, respectively. The $E = 52$ kcal/mol trajectory shows complete bond dissociation after ~6 fs (0.006 ps). For the harp isomer, the addition of $E = 44$ kcal/mol to mode 12 (7 quanta) shows no dissociation after ~600 fs (0.6 ps). Upper limit lifetimes for this isomer, depending on whether one is considering the isomerization or decomposition channel, are ~3 and 0.3 ps, respectively, at the MP2 level and 1.9 ps and 50.4 fs, respectively, at the CCSD(T) level. It is important to reiterate here the following point: the reason that the amount of energy required to cause dissociation in the DRP trajectories exceeds the calculated barrier heights is that the energy provided to a specific vibrational mode does not localize in the bond that breaks in the reaction.

Experimental Results. The vacuum thermolyses of $N_5^+AsF_6^-$ (eq 5) and $[N_5]^+_2[SnF_6]^{2-}$ (eq 6), and the displacement reaction between CsF and $N_5^+SbF_6^-$ (eq 7) were studied experimentally by fast, in situ FT-IR spectroscopy of the gaseous reaction products.

$$N_5^+AsF_6^- \rightarrow [FN_5] + AsF_5 \quad (5)$$

$$(N_5)^+_2SnF_6^{2-} \rightarrow [FN_5] + N_5^+SnF_5^- \quad (6)$$

$$N_5^+SbF_6^- + CsF \rightarrow [FN_5] + CsSbF_6 \quad (7)$$

In excellent agreement with the above theoretical lifetime predictions for FN_5, this molecule could not be observed directly; however, its expected decomposition products (eq 8−11) were observed.

TABLE 9: RRKM Analysis for Isomerization and Decomposition Reactions as a Function of Vibrational Quanta

applied energy (quanta)	E (kcal/mol)	CCSD(T)[b] lifetime	MP2/G[a] lifetime
	Harp−TS42−Cis		
	Mode 12 (Harp)		
1	6.21	18.2 ns	2.5 ms
2	12.42	36.2 ps	353.0 ps
3	18.63	8.2 ps	29.3 ps
4	24.84	4.2 ps	10.1 ps
5	31.05	2.9 ps	5.6 ps
6	37.26	2.2 ps	3.9 ps
7	**43.47**	**1.9 ps**	**3.0 ps**
8	49.68	1.6 ps	2.4 ps
9	55.89	1.5 ps	2.1 ps
10	62.1	1.4 ps	1.9 ps
11	68.31	1.3 ps	1.7 ps
12	74.52	1.2 ps	1.6 ps
13	80.73	1.2 ps	1.5 ps
14	86.94	1.1 ps	1.4 ps
15	93.15	1.1 ps	1.3 ps
	Harp−TS4p−$FN_3 + N_2$		
	Mode 12 (Harp)		
1	6.21	0.3 ps	
2	12.42	99.5 fs	1.0 ns
3	18.63	72.0 fs	11.2 ps
4	24.84	61.5 fs	2.0 ps
5	31.05	56.0 fs	811.5 fs
6	37.26	52.6 fs	459.4 fs
7	**43.47**	**50.4 fs**	**311.4 fs**
8	49.68	48.7 fs	234.6 fs
9	55.89	47.5 fs	189.2 fs
10	62.1	46.5 fs	159.8 fs
11	68.31	45.8 fs	139.4 fs
12	74.52	45.1 fs	124.6 fs
13	80.73	44.6 fs	113.3 fs
14	86.94	44.2 fs	104.6 fs
15	93.15	43.8 fs	97.6 fs
	Cis−TS2p−$FN_3 + N_2$		
	Mode 10 (Cis)		
1	3.49		
2	6.98		
3	10.47		
4	13.96	855.1 ms	
5	17.45	30.0 ns	
6	20.94	0.3 ns	
7	24.43	25.4 ps	0.2 ms
8	27.92	5.5 ps	77.1 ns
9	31.41	1.9 ps	2.0 ns
10	**34.9**	**891.3 fs**	**215.8 ps**
11	38.39	491.2 fs	46.2 ps
12	41.88	306.0 fs	14.8 ps
13	45.37	208.2 fs	6.1 ps
14	48.86	151.3 fs	3.0 ps
15	**52.35**	**115.5 fs**	**1.7 ps**

[a] Basis set = 6-31+G(d). [b] Basis set = aug-cc-pVDZ.

$$[FN_5] \rightarrow FN_3 + N_2 \quad (8)$$

$$FN_3 \rightarrow [FN] + N_2 \quad (9)$$

$$2[FN] \rightarrow F_2N_2 \quad (10)$$

$$3F_2N_2 \rightarrow 2NF_3 + 2N_2 \quad (11)$$

Because reactions 8−11 are all strongly exothermic, the thermodynamically most stable products, NF_3 and N_2,[33] were obtained as the major final products. However, the formation of smaller amounts of FN_3 and F_2N_2[34] was also observed, thus confirming the above sequence of reactions.

Conclusions

In contrast to FN_3 that can be isolated at room temperature but does not form stable N_3^+ salts with strong Lewis acids,[12]

N_5^+ salts are stable but their FN_5 parent molecule has very limited kinetic stability. Because of the general difficulty of correctly modeling infinite crystal lattices,[35] the ion pair $N_5^+AsF_6^-$ and its dissociation products were studied. It is shown that at the MP2/6-31+G(d) level the ion pair and crystalline $N_5^+AsF_6^-$ are more stable than the free FN_5 and AsF_5 molecules by 46.5 and 72.0 kcal/mol, respectively. These values represent minimum dissociation energy barriers; the latter value is in accord with the observed marginal stability of crystalline $N_5^+AsF_6^-$ at room temperature. The FN_5 molecule can exist as at least six different, vibrationally stable isomers (one cyclic,[32] one bifurcated, and four chainlike structures) that differ in energy by only 6.4, 9.0, and 11.2 kcal/mol at the MP2/6-31+G(d), MP2/aug-cc-pVDZ, and CCSD(T)/aug-cc-pVDZ levels, respectively. Decomposition studies of FN_5 reveal two distinct pathways to $FN_3 + N_2$. The energy change from the initial bifurcated FN_5 isomer to $FN_3 + N_2$ is predicted to be -56.0 kcal/mol at the CCSD(T) level of theory.

IRC, DRP, and RRKM calculations suggest that the energy barriers for these decomposition pathways are very low, resulting in predicted lifetimes for FN_5 at room temperature on the order of nanoseconds. These predictions of an extremely short-lived FN_5 are confirmed by our experimental FT-IR studies on the thermolyses of $N_5^+AsF_6^-$ and $[N_5]^+_2[SnF_6]^2$, and the displacement reaction between CsF and $N_5^+SbF_6^-$, which showed only the expected decomposition products FN_3, F_2N_2, and NF_3, but no evidence for the intermediate FN_5.

Acknowledgment. This work was supported by a grant (to M.S.G.) from the Air Force Office of Scientific Research (AFOSR) and by a Grand Challenge grant of computer time from the High Performance Computing Modernization Program (to M.S.G. and J.A.B.) at the High Energy Maui High Performance Computation Center. We also thank Dr. Galina Chaban and Prof. William Hase for insightful discussions about the DRP calculations. H.M.N. was supported by a Department of Energy Computational Science Graduate Fellowship and a Miller Fellowship from the Iowa State University Department of Chemistry. The work at the Air Force Research Laboratory was supported by the Defense Advanced Research Projects Agency (DARPA) and AFOSR, and that at USC was supported by DARPA, AFOSR, and the National Science Foundation. We thank Prof. Jenkins for the lattice energy estimate for N_5AsF_6 and Drs. R. Corley, M. Berman, and D. Woodbury for their steady support. The calculations described here were performed on both local Iowa State University/DOE Ames Laboratory workstations, as well as computers at the Maui High Performance Computation Center.

References and Notes

(1) Christe, K. O.; Wilson, W. W.; Sheehy, J. A.; Boatz, J. A. *Angew. Chem., Int. Ed. Engl.* **1999**, *38*, 2004.

(2) Vij, A.; Wilson, W. W.; Vij, V.; Tham, F. S.; Sheehy, J. A.; Christe, K. O. *J. Am. Chem. Soc.* **2001**, *123*, 6308.

(3) Lauderdale, W. J.; Stanton, J. F.; Bartlett, R. J. *J. Phys. Chem.* **1992**, *96*, 1173.

(4) Glukhovtsev, M. N.; Jiao, H.; Schleyer, P. v. R. *Inorg. Chem.* **1996**, *35*, 7124.

(5) Bartlett, R. J. *Chem. Ind.-London* **2000**, *4*, 140.

(6) Curtius, T. *Ber. Dtsch. Chem. Ges.* **1890**, *23*, 3023.

(7) Pyyko, P.; Runeberg, N. *J. Mol. Struct. (THEOCHEM.)* **1991**, *234*, 279.

(8) (a) Christe, K. O.; Guertin, J. P.; Pavlath, A. E. *Inorg. Nucl. Chem. Lett.* **1966**, *2*, 83. (b) Guertin, J. P.; Christe, K. O.; Pavlath, A. E. *Inorg. Chem.* **1966**, *5*, 1921. (c) Tolberg, W. E.; Rewick, R. T.; Stringham, R. S. *Inorg. Chem.* **1967**, *6*, 1156.

(9) (a) Christe, K. O. *Inorg. Nucl. Chem. Lett.* **1972**, *8*, 741. (b) Robero, F. Q. *Inorg. Nucl. Chem. Lett.* **1972**, *8*, 737. (c) Christe, K. O. *Inorg. Chem.* **1973**, *12*, 1580.

(10) (a) Gillespie, R. J.; Schrobilgen, G. J. *J. Chem. Soc., Chem. Commun.* **1974**, 90. (b) Gillespie, R. J.; Schrobilgen, G. J. *Inorg. Chem.* **1974**, *13*, 1230. Christe, K. O.; Wilson, R. D. *Inorg. Chem.* **1975**, *14*, 694.

(11) (a) Christe, K. O.; Wilson, W. W.; Schrobilgen, G. J.; Chiracal, R. V. *Inorg. Chem.* **1988**, *27*, 789. (b) Christe, K. O.; Wilson, W. W. *J. Am. Chem. Soc.* **1992**, *114*, 9934.

(12) Schatte, G.; Willner, H. *Z. Naturforsch.* **1991**, *46b*, 483.

(13) Wilson, W. W.; Vij, A.; Vij, V.; Bernhardt, E.; Christe, K. O. *Chem. Eur. J.*, in press.

(14) Gholivand, K.; Schatte, G.; Willner, H. *Z. Inorg. Chem.* **1987**, *26*, 2137.

(15) Christe, K. O.; Wilson, W. W.; Schack, C. J.; Wilson, R. D. *Inorg. Synth.* **1986**, *24*, 39.

(16) Moller, C.; Plesset, M. S. *Phys. Rev.* **1934,** *46*, 618.

(17) Hehre, W. J.; Ditchfield, R.; Pople, J. A. *J. Chem. Phys.* **1972,** *56*, 2237.

(18) Raghavachari, K.; Trucks, G. W.; Pople, J. A.; Head-Gordon, M. *Chem. Phys. Lett.* **1989**, *157*, 479.

(19) Dunning, T. H. *J. Chem. Phys.* **1989**, *90*, 1007.

(20) Schmidt, M. W.; Baldridge, K. K.; Boatz, J. A.; Elbert, S. T.; Gordon, M. S.; Jensen, J. H.; Koseki, S.; Matsunaga, N.; Nguyen, K. A.; Su, S.; Windus, T. L. *J. Comput. Chem.* **1993**, *14*, 1347.

(21) ACES II is a program product of the Quantum Theory Project, University of Florida. Authors: Stanton, J. F.; Gauss, J.; Watts, J. D.; Nooijen, M.; Oliphant, N.; Perera, S. A.; Szalay, P. G.; Lauderdale, W. J.; Kucharski, S. A.; Gwaltney, S. R.; Beck, S.; Balková, A.; Bernholdt, D. E.; Baeck, K. K.; Rozyczko, P.; Sekino, H.; Hober, C.; Bartlett, R. J. Integral packages included are VMOL (Almlöf, J.; Taylor, P. R.); VPROPS (Taylor, P. R.) ABACUS (Helgaker, T.; Jensen, H. J. Aa.; Jørgensen, P.; Olsen, J.; Taylor, P. R.).

(22) Garrett, B. C.; Redmon, M.; Steckler, R.; Truhlar, D. G.; Baldridge, K. K.; Bartol, D.; Schmidt, M. W.; Gordon, M. S. *J. Phys. Chem.* **1988**, *92*, 1476.

(23) Gonzales, C.; Schlegel, H. B. *J. Chem. Phys.* **1989**, *90*, 2154.

(24) (a) Robinson, P. J.; Holbrook, K. A. Unimolecular Reactions; Wiley-Interscience: New York, 1972. (b) Forst, W. *Theory of Unimolecular Reactions*; Academic Press: New York, 1973. (c) Schranz, H. W.; Nordholm, S.; Freasier, B. C. *Chem. Phys.* **1986**, *108*, 69.

(25) (a) Stewart, J. J. P.; Davis, L. P.; Burggraf, L. W. *J. Comput. Chem.* **1987**, *8*, 1117. (b) Maluendes, S. A.; Dupuis, M. *J. Chem. Phys.* **1990**, *93*, 5902.

(26) (a) Taketsugu, T.; Gordon, M. S. *J. Phys. Chem.* **1995**, *99*, 8462. (b) Gordon, M. S.; Chaban, G.; Taketsugu, T. *J. Phys. Chem.* **1996,** *100*, 11512.

(27) Harcourt, R. D.; Klapoetke, T. M. *Z. Naturforsch.* **2002**, *57b*, 983.

(28) Fau, S.; Bartlett, R. J. *J. Phys. Chem. A* **2001**, *105*, 4096.

(29) (a) Christe, K. O.; Lind, M. D.; Thorup, N.; Russell, D. R.; Fawcett. J. *Inorg. Chem.* **1988**, *27*, 2450. (b) Vij, A.; Zhang, X.; Christe, K. O. *Inorg. Chem.* **2001**, *40*, 416 and references therein.

(30) Bondi, A. *J. Phys. Chem.* **1964**, *68*, 441.

(31) Jenkins, H. D. B. Private communication.

(32) (a) Hammerl, A.; Klapoetke, T. M.; Schwerdtfeger, P. Private communication. (b) Inagaki, S.; Goto, N. *J. Am. Chem. Soc.* **1987**, *109*, 3234.

(33) Gmelin Handbook, F Suppl. Vol. 4, pp 385, 1986.

(34) (a) Haller, J. F. Ph.D. Thesis, Cornell University, Ithaca, NY, 1942. (b) Bohn, R. K.; Bauer, S. H. *Inorg. Chem.* **1967**, *6*, 309. (c) Kuczkowski, R.; Wilson, E. B. *J. Chem. Phys.* **1963**, *39*, 1030. (d) King, S.-T.; Overend, J. *Spectrochim. Acta* **1966**, *22*, 689.

(35) Christe, K. O.; Zhang, X.; Sheehy, J. A.; Bau, R. *J. Am. Chem. Soc.* **2001**, *123*, 6338.

APPENDIX F

"Synthesis and Characterization of the $SO_2N_3^-$, $(SO_2)_2N_3^-$, and $SO_3N_3^-$ Anions"
Inorg. Chem., 41, 4275 (2002)

This Page Intentionally Left Blank

Inorg. Chem. **2002**, *41*, 4275–4285

Synthesis and Characterization of the $SO_2N_3^-$, $(SO_2)_2N_3^-$, and $SO_3N_3^-$ Anions†

Karl O. Christe,*,‡,§ Jerry A. Boatz,‡ Michael Gerken,§ Ralf Haiges,§ Stefan Schneider,§ Thorsten Schroer,§ Fook S. Tham,|| Ashwani Vij,‡ Vandana Vij,‡ Ross I. Wagner,§ and William W. Wilson‡

Propulsion Sciences and Advanced Concepts Division, Air Force Research Laboratory (AFRL/PRS), Edwards AFB, California 93524, Loker Hydrocarbon Research Institute and Department of Chemistry, University of Southern California, Los Angeles, California 90089, and University of California, Riverside, California 92521

Received March 7, 2002

SO_2 solutions of azide anions are bright yellow, and their Raman spectra indicate the presence of covalently bound azide. Removal of the solvent at −64 °C from CsN_3 or $N(CH_3)_4N_3$ solutions produces yellow $(SO_2)_2N_3^-$ salts. Above −64 °C, these salts lose 1 mol of SO_2, resulting in white $SO_2N_3^-$ salts that are marginally stable at room temperature and thermally decompose to the corresponding azides and SO_2. These anions were characterized by vibrational and ^{14}N NMR spectroscopy and theoretical calculations. Slow loss of the solvent by diffusion through the walls of a sealed Teflon tube containing a sample of $CsSO_2N_3$ in SO_2 resulted in white and yellowish single crystals that were identified by X-ray diffraction as $CsSO_2N_3 \cdot CsSO_3N_3$ with $a = 9.542(2)$ Å, $b = 6.2189(14)$ Å, $c = 10.342(2)$ Å, and $\beta = 114.958(4)°$ in the monoclinic space group $P2_1/m$, $Z = 2$, and $Cs_2S_2O_5 \cdot Cs_2S_2O_7 \cdot SO_2$, respectively. Pure $CsSO_3N_3$ was also prepared and characterized by vibrational spectroscopy. The S–N bond in $SO_2N_3^-$ is much weaker than that in $SO_3N_3^-$, resulting in decreased thermal stability, an increase in the S–N bond distance by 0.23 Å, and an increased tendency to undergo rotational disorder. This marked difference is due to SO_3 being a much stronger Lewis acid (pF^- value of 7.83) than SO_2 (pF^- value of 3.99), thus forming a stronger S–N bond with the Lewis base N_3^-. The geometry of the free gaseous $SO_2N_3^-$ anion was calculated at the RHF, MP2, B3LYP, and CCSD(T) levels. The results show that only the correlated methods correctly reproduce the experimentally observed orientation of the SO_2 group.

Introduction

Sulfur dioxide is a very interesting molecule. It not only serves as a very useful inorganic solvent but also exhibits a rich reaction chemistry. In addition to being a ligand with at least 9 different bonding modes,[1] it is also amphoteric and can act either as an electron donor (Lewis base) or acceptor (Lewis acid) molecule. As a donor, it can coordinate through its free valence electron pairs on either sulfur or oxygen. A typical example for the latter case is the oxygen-bridged adduct between SbF_5 and SO_2.[2] As an acceptor, SO_2 likes to expand its coordination number around sulfur from three to four. Typical examples for compounds in which SO_2 acts as an acceptor are the SO_2X^- anions, where X^- stands for a halide or pseudo-halide ion.[3]

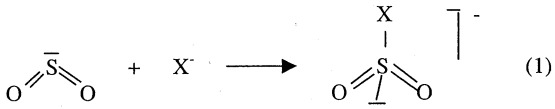

(1)

During reactions, aimed at the metathetical synthesis of $N_5^+N_3^-$, the yellow color of the solutions of colorless N_3^- in colorless SO_2 raised our curiosity. This is in marked

* To whom correspondence should be addressed. E-mail: karl.christe@edwards.af.mil.

† This paper is dedicated to Professor Dieter Naumann on the occasion of his 60th birthday.

‡ Air Force Research Laboratory.
§ University of Southern California.
|| UC Riverside.

(1) Greenwood, N. N.; Earnshaw, A. *Chemistry of the Elements*, 2nd ed.; Butterworth-Heinemann: Oxford, 1998; pp 721−746.
(2) Bacon, J.; Dean, P. A. W.; Gillespie, R. J. *Can. J. Chem.* **1969**, *47*, 1655.
(3) Kornath, A.; Blecher, O.; Ludwig, R. *J. Am. Chem. Soc.* **1999**, *121*, 4019 and references therein.

10.1021/ic020183l CCC: $22.00
Published on Web 07/18/2002

contrast to solutions of N_3^- in other polar solvents, such as water, that are colorless. Therefore, the SO_2/N_3^- system was studied in more detail. The results from this study were presented at the 13th European Symposium on Fluorine Chemistry,[4] and a full account of this work is given in this paper. Our original report[4] provided the first evidence for the existence of the azidosulfite anion and was recently confirmed by an independent crystal structure determination of $[N(CH_3)_4]^+[SO_2N_3]^-$.[5] Despite many known sulfur−nitrogen compounds,[1] including sulfuryl diazide[6] and azidosulfates,[7−12] no other reports on azidosulfites were found in the literature.

The $SO_3N_3^-$ anion has previously been prepared by (a) the direct reaction between SO_3 and NaN_3;[8] (b) the reaction of H_2NNHSO_3H and KNO_2;[7] (c) the reaction of [Na]-[SO_3Cl] and N_3^-;[9,12] and (d) the reaction of $S_2O_6N_3^-$ with KOH/NaOH.[10] Despite this diversity of available synthetic routes, the $SO_3N_3^-$ anion had been characterized only by elemental analyses and infrared spectroscopy.

Experimental Section

Caution! Azides are highly endothermic and often can decompose explosively. They should be handled on a small scale with appropriate safety precautions.

Materials and Apparatus. Reactions were carried out in either flamed-out Pyrex glass tubes or Teflon-FEP or -PFA ampules that contained Teflon coated magnetic stirring bars and were closed by stainless steel or Teflon valves. Volatile materials were handled either on a stainless steel/Teflon-FEP vacuum line[13] or a Pyrex glass vacuum line equipped with grease-free Kontes glass-Teflon valves. Nonvolatile solids were handled in the dry nitrogen atmosphere of a glovebox. Infrared spectra were recorded on either a Mattson Galaxy 5030 or Midac M Series FT-IR spectrometer using dry powders pressed between AgCl windows in an Econo press (Barnes Engineering Co.). Raman spectra were recorded on either a Bruker Equinox 55 FT-RA spectrometer using a Nd:YAG laser at 1064 nm and Pyrex melting point capillaries, glass NMR tubes, or 9 mm Teflon-FEP tubes as sample containers or a Cary Model 83 spectrometer using the 488 nm exciting line of an Ar ion laser. NMR spectra were recorded on a Bruker Avance 400 FT-NMR spectrometer.

The $N(CH_3)_4^+N_3^-$,[14] CsN_3,[15] and $CsSO_3Cl$[16] starting materials were prepared by literature methods. The SO_2 (Air Products, anhydrous grade, 99.9%) was dried over CaH_2. Trimethylsilyl azide (Aldrich, 95%) was condensed from a storage vessel at −35 °C into the reaction vessel at −196 °C.

Preparation of $M^+SO_2N_3^-$ [M = Cs or $N(CH_3)_4$]. In a typical experiment, a 5 mm Pyrex glass NMR tube, closed by a concentric, grease-free Teflon valve (Wilmad Glass Co.), was loaded with CsN_3 (1.335 mmol) in the glovebox. The tube was attached to the Pyrex vacuum line and evacuated; then, anhydrous SO_2 (0.765 mL) was condensed into the tube at −196 °C. The mixture was warmed to room temperature, and the CsN_3 dissolved giving a yellow solution. In the presence of traces of moisture, a small amount of a white precipitate formed that was identified by its infrared and Raman spectra as $Cs_2S_2O_5$.[17] The tube and its contents were cooled to −22 °C, and the SO_2 solvent was pumped off in a dynamic vacuum, leaving behind a white solid (322.0 mg, weight calculated for 1.335 mmol of $CsSO_2N_3$ = 319.1 mg).

Preparation of $M^+(SO_2)_2N_3^-$ [M = Cs or $N(CH_3)_4$]. In a manner similar to that used for the preparation of $CsSO_2N_3$, CsN_3 (1.346 mmol) was loaded into a Pyrex NMR tube equipped with a glass-Teflon valve, and anhydrous SO_2 (0.769 mL) was added in vacuo to the tube at −196 °C. After warming to room temperature to dissolve all the CsN_3, the tube was cooled to −64 °C, and the SO_2 was removed slowly in a dynamic vacuum for 4 h. The nonvolatile residue consisted of a yellow solid (406 mg, weight calculated for 1.346 mmol of $Cs(SO_2)_2N_3$ = 407.9 mg).

Preparation of $CsSO_3N_3$. Inside a drybox, a glass vessel, equipped with a Kontes glass-Teflon valve and a Teflon-coated stirring bar, was loaded with $CsSO_3Cl$ (2.383 mmol). On a glass vacuum line, $(CH_3)_3SiN_3$ (8.940 mmol) was distilled onto the solid at −196 °C and allowed to warm to room temperature. After stirring the suspension for 2 days, volatiles were removed at room temperature yielding a white solid. Raman spectroscopic characterization of the solid revealed the presence of $CsSO_3Cl$ and $CsSO_3N_3$. Four additional cycles of adding fresh $(CH_3)_3SiN_3$, followed by removal of all volatiles at room temperature while monitoring the progress of the reaction by Raman spectroscopy, resulted in a quantitative yield of pure $CsSO_3N_3$.

Crystal Structure Determination of $CsSO_2N_3 \cdot CsSO_3N_3$. About 0.5 mL of SO_2 was condensed onto anhydrous CsN_3 in a 4 mm FEP NMR tube that was then evacuated at −196 °C and heat-sealed. The yellowish solution was allowed to stand for several weeks during which time SO_2 diffused slowly through the walls of the tube, and a mixture of diffraction-quality, prismatic, clear, colorless (compound **1**, $CsSO_2N_3 \cdot CsSO_3N_3$), and pale yellow (compound **2**, $Cs_2S_2O_5 \cdot Cs_2S_2O_7 \cdot SO_2$) crystals was formed. The FEP tube was then cut open under a stream of cold N_2 gas at approximately −80 °C, and the crystalline contents were dropped into the lip of a low temperature crystal-mounting apparatus. A Nylon Cryoloop, attached to a magnetic base, was used to trap a crystal having the dimensions 0.10 × 0.27 × 0.52 mm^3, using PFPE (perfluoropolyether) oil, and to mount it on the magnetic goniometer. The single-crystal diffraction data were collected on a Bruker 3-circle platform diffractometer, equipped with a SMART[18] CCD (charge coupled device) detector with the χ-axis fixed at 54.74°, and using Mo Kα radiation (λ = 0.71073 Å) from a fine-focus tube. This diffractometer was equipped with an LT-3 apparatus for low temperature data collection using controlled liquid nitrogen boil off. Cell constants were determined from 90 30-s frames at

(4) Vij, A.; Wilson, W.; Sheehy, J.; Boatz, J.; Gerken, M.; Schneider, S.; Schroer, T.; Haiges, R.; Wagner, R.; Tham, F.; Christe, K. Presented at the 13th European Symposium on Fluorine Chemistry, Bordeaux, France, July 15−20, 2001; Paper B7.
(5) Kornath, A.; Blecher, O.; Ludwig, R. *Z. Anorg. Allg. Chem.* **2002**, *628*, 183.
(6) Curtius, T.; Schmidt, F. *Ber. Dtsch. Chem. Ges.* **1922**, *55*, 1571.
(7) Traube, W.; Vockerodt, A. *Ber. Dtsch. Chem. Ges.* **1914**, *47*, 943.
(8) Beck, G. *J. Prakt. Chem. (Leipzig)* **1940**, *156*, 227.
(9) Elsner, H.; Ratz, H. German Patent 886,298, 1953.
(10) Lehmann, H. A.; Holznagel, W. *Z. Anorg. Allg. Chem.* **1958**, *293*, 314.
(11) Ruff, J. K. *Inorg. Chem.* **1965**, *4*, 567.
(12) Shozda, R. J.; Vernon, J. A. *J. Org. Chem.* **1967**, *32*, 2876.
(13) Christe, K. O.; Wilson, W. W.; Schack, C. J.; Wilson, R. D. *Inorg. Synth.* **1986**, *24*, 39.
(14) Christe, K. O.; Wilson, W. W.; Bau, R.; Bunte, S. W. *J. Am. Chem. Soc.* **1992**, *114*, 3411.
(15) Gerken, M.; Schneider, S.; Schroer, T.; Christe, K. O. *Z. Anorg. Allg. Chem.*, in press.
(16) Ciruna, J. A.; Robinson, E. A. *Can. J. Chem.* **1968**, *46*, 1715.
(17) Siebert, H. *Anwendungen der Schwingungsspectroskopie in der Anorganischen Chemie, Anorganische und Allgemeine Chemie in Einzeldarstellungen, VII*; Springer-Verlag: Berlin, 1966; p 102. Herlinger, A. W.; Long, T. V. *Inorg. Chem.* **1969**, *8*, 2661.
(18) *SMART V 4.045, Software for the CCD Detector System*; Bruker AXS: Madison, WI, 1999.

Table 1. ^{14}N NMR Spectra of Aqueous and SO_2 Solutions of MN_3 (M = Na, Cs, or $N(CH_3)_4$) and of MSO_2N_3 (M = Cs or $N(CH_3)_4$) in CH_3NO_2, CH_3CN, or CHF_3 Solution

	chem shift, ppm (line width, Hz)		
compound (solvent)	central nitrogen	terminal nitrogen	area ratio
NaN_3 (H_2O, 20 °C)	−133.5 (18)	−282.2 (60)	1:2
NaN_3[b] (SO_2, 20 °C)	−135.8 weak	not obsd	
CsN_3 (SO_2, 20 °C)	−133.9 (15)	−201.7 (76)	1:2
(SO_2, −25 °C)	−134.3 (19)	−200.1 (150)	1:2
(SO_2, −65 °C)	−134.7 (51)	−198.9 (235)	1:2
$CsSO_2N_3$ (CH_3NO_2, −22 °C)	−132.5 (16)	−209.9 (155)	1:2
$N(CH_3)_4N_3$[d] (H_2O, 22 °C)	−133.4 (18)	−281.0 (58)	1:2
$N(CH_3)_4N_3$[d] (SO_2, −65 °C)	−135.0 (35)	−199.8 (200)	1:2
$N(CH_3)_4SO_2N_3$[a,e] (CH_3CN, −40 °C)	−132.7[f]	−205.3 (140)	*f*
$N(CH_3)_4SO_2N_3$ (CHF_3, −90 °C)[b]	−136.4 weak	not obsd	
$N(CH_3)_4(SO_2)_2N_3 \cdot nSO_2$ (CH_3CN, −40 °C)[c,e]	−133.1[f]	−203.7 (192)	*f*

[a] Clear colorless solution with faint yellow solid. [b] Low solubility. [c] Pale yellow solution with yellow solid. [d] The sharp resonances due to $N(CH_3)_4^+$ were observed at −139.3 (H_2O) and −336.9 ppm (SO_2). [e] Resonances due to CH_3CN and $N(CH_3)_4^+$ were observed at −137.7 (~300 Hz) and −338 ppm, respectively. [f] Not determined because of overlap with solvent resonance.

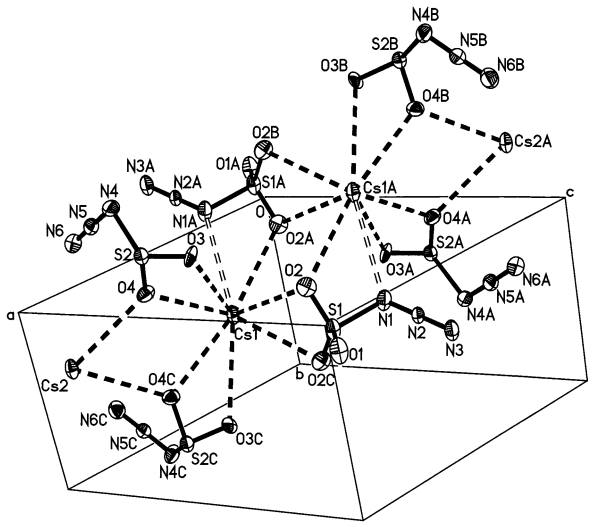

Figure 1. Crystal structure of $CsSO_2N_3 \cdot CsSO_3N_3$.

Table 2. Crystal Data for $CsSO_2N_3 \cdot CsSO_3N_3$ (**1**)

chemical formula	$Cs_2N_6O_5S_2$
fw	494.00
T, °C	−100 (2)
space group	$P2_1/m$ (No.11)
a, Å	9.542(2)
b, Å	6.2189(14)
c, Å	10.342(2)
β, deg	114.958(4)
V, Å^3	556.4(2)
Z	2
ρ_{calcd}, g cm^{-3}	2.949
μ, mm^{-1}	6.939
λ, Å	0.71073
R1,[a] wR2[b] [$I > 2\sigma(I)$]	0.0398, 0.1068
R1,[a] wR2[b] (all data)	0.0416, 0.1085

[a] $R1 = (\sum(F_o - F_c)/F_o)$. [b] $wR2 = [\sum(w(F_o - F_c)^2)/wF_o^2)]^{1/2}$.

−100 °C (**1**) or at −70 °C (**2**). A complete hemisphere of data was collected, using 1271 frames at 30 s/frame at a detector resolution of 512 × 512 pixels, including 50 frames that were collected at the beginning and end of the data collection to monitor crystal decay. The frames were then processed on a PC running on Windows NT software by using the SAINT software[19] to give the *hkl* file corrected for Lp/decay. The absorption correction was performed using the SADABS[20] program. The structures were solved by the direct method, using the SHELX-97 program,[21] and refined by the least-squares method on F^2, SHELXL-97,[22] incorporated in SHELXTL Suite 5.10 for Windows NT.[23] All atoms were refined anisotropically. For the anisotropic displacement parameters, the *U*(eq) is defined as one-third of the trace of the orthogonalized U_{ij} tensor.

Table 3. Atomic Coordinates ($\times 10^4$) and Equivalent Isotropic Displacement Parameters (Å^2 × 10^3) for $CsSO_2N_3 \cdot CsSO_3N_3$

	x	*y*	*z*	*U*(eq)[a]
Cs(1)	6199(1)	2500	3672(1)	38(1)
Cs(2)	10539(1)	2500	1983(1)	39(1)
S(1)	6914(2)	2500	7536(2)	42(1)
S(2)	9094(3)	−2500	3854(2)	40(1)
O(1)	8336(7)	2500	8827(6)	59(2)
O(2)	6625(5)	562(8)	6701(5)	49(1)
O(3)	8278(16)	−3010(20)	4683(12)	47(5)
O(4)	8677(11)	−276(12)	3266(9)	45(2)
O(5)[b]	10543(17)	−3070(30)	3910(30)	45(7)
N(1)	5404(10)	1975(19)	8035(10)	49(4)
N(2)	5694(7)	2500	9245(6)	31(1)
N(3)	5843(12)	3101(19)	10317(11)	51(4)
N(4)	7990(17)	−4208(17)	2097(14)	55(3)
N(5)	7791(13)	−3134(14)	1059(12)	40(2)
N(6)	7645(14)	−2130(30)	100(13)	52(5)

[a] *U*(eq) is defined as one-third of the trace of the orthogonalized U_{ij} tensor. [b] O(5) is the minor component of the rotationally disordered $SO_2N_3^-$ anion (see Results and Discussion section) and is not shown in Figure 1.

Theoretical Calculations. Theoretical calculations were carried out on IBM RS/6000 work stations using the GAMESS,[24] Gaussian 98,[25] and ACES II[26] program systems and the restricted Hartree−Fock (RHF),[27] the density functional B3LYP,[28] and the correlated

(19) *SAINT V 4.035*, *Software for the CCD Detector System*; Bruker AXS: Madison, WI, 1999.
(20) *SADABS*, *Program for absorption correction for area detectors*, version 2.01; Bruker AXS: Madison, WI, 2000.
(21) Sheldrick, G. M. *SHELXS-97*, *Program for the Solution of Crystal Structure*; University of Göttingen: Göttingen, Germany, 1997.
(22) Sheldrick, G. M. *SHELXL-97*, *Program for the Refinement of Crystal Structure*; University of Göttingen: Göttingen, Germany, 1997.
(23) *SHELXTL 5.10 for Windows NT*, *Program library for Structure Solution and Molecular Graphics*; Bruker AXS: Madison, WI, 1997.
(24) Schmidt, M. W.; Baldridge, K. K.; Boatz, J. A.; Elbert, S. T.; Gordon, M. S.; Jensen, J. H.; Koseki, S.; Matsunaga, N.; Nguyen, K. A.; Su, S. J.; Windus, T. L.; Dupuis, M.; Montgomery, J. A. *J. Comput. Chem.* **1993**, *14*, 1347−1363.
(25) Frisch, M. J.; Trucks, G. W.; Schlegel, H. B.; Scuseria, G. E.; Robb, M. A.; Cheeseman, J. R.; Zakrzewski, V. G.; Montgomery, J. A., Jr.; Stratmann, R. E.; Burant, J. C.; Dapprich, S.; Millam, J. M.; Daniels, A. D.; Kudin, K. N.; Strain, M. C.; Farkas, O.; Tomasi, J.; Barone, V.; Cossi, M.; Cammi, R.; Mennucci, B.; Pomelli, C.; Adamo, C.; Clifford, S.; Ochterski, J.; Petersson, G. A.; Ayala, P. Y.; Cui, Q.; Morokuma, K.; Malick, D. K.; Rabuck, A. D.; Raghavachari, K.; Foresman, J. B.; Cioslowski, J.; Ortiz, J. V.; Stefanov, B. B.; Liu, G.; Liashenko, A.; Piskorz, P.; Komaromi, I.; Gomperts, R.; Martin, R. L.; Fox, D. J.; Keith, T.; Al-Laham, M. A.; Peng, C. Y.; Nanayakkara, A.; Gonzalez, C.; Challacombe, M.; Gill, P. M. W.; Johnson, B. G.; Chen, W.; Wong, M. W.; Andres, J. L.; Head-Gordon, M.; Replogle, E. S.; Pople, J. A. *Gaussian 98*, revision A.6; Gaussian, Inc.: Pittsburgh, PA, 1998.
(26) Stanton, J. F.; Gauss, J.; Watts, J. D.; Nooijen, M.; Oliphant, N.; Perera, S. A.; Szalay, P. G.; Lauderdale, W. J.; Gwaltney, S. R.; Beck, S.; Balkova, A.; Bernholdt, D. E.; Baeck, K. K.; Rozyczko, P.; Sekino, H.; Hober, C.; Bartlett, R. J. *ACES II*, *Quantum Theory Project*; University of Florida: Gainesville, FL. Integral packages included are VMOL (Almlof, J.; Taylor, P. R.), BPROPS (Taylor, P. R.), and ABACUS (Helgaker, T.; Jensen, H. J. A.; Jorgensen, P.; Olsen, J.; Taylor, P. R.).

Table 4. Most Important Bond Lengths [Å] and Angles [deg] of the $SO_2N_3^-$ Anion in Its Cs^+ Salt Compared to Those in $[N(CH_3)_4]^+SO_2N_3^-$ and the Calculated[a] Values

	calcd				obsd	
	RHF	B3LYP	MP2	CCSD(T)	$Cs^+SO_2N_3^-$	$[N(CH_3)_4]^+SO_2N_3^-$ [b]
			Bond Distances (Å)			
S−N	1.907	2.226	2.356	2.198	1.981(12)	2.005(2)
S−O[c]	1.464	1.492	1.492	1.494	1.410(10)[e]	1.453(2)
S−O[d]	1.462	1.490	1.491	1.493	1.495(8)	1.457(2)
$N_\alpha-N_\beta$	1.205	1.207	1.223	1.222	1.209(16)	1.214(2)
$N_\beta-N_\gamma$	1.113	1.169	1.205	1.182	1.130(16)	1.144(2)
			Bond Angles (deg)			
O−S−N[d]	101.46	99.21	99.94	99.01	100.1(5)	96.82(8)
O−S−N[c]	102.09	102.42	102.24	101.46	102.7(11)[f]	100.87(9)
S− $N_\alpha-N_\beta$	112.0	110.29	106.81	108.67	110.0(8)	110.22(14)
$N_\alpha-N_\beta-N_\gamma$	178.9	179.16	179.32	179.37	178.2(15)	178.6(2)
O−S−O	112.6	114.58	115.58	114.90	111.1(9)[e]	112.72(10)

[a] A 6-31+G(d) basis set was used for all calculations. [b] Data from ref 2. [c] Oxygen atom that is approximately perpendicular to the plane of the N_3S fragment. [d] Oxygen atom that is approximately in plane with the N_3S fragment. [e] Average value from disordered positions. [f] Taken from the major component of the disordered oxygen position.

MP2[29] and single- and double-excitation coupled cluster methods,[30] including a noniterative treatment of connected triple excitations.[31]

Results and Discussion

SO_2/N_3^- System. In common solvents, such as water, the N_3^- anion dissolves without color and retains its centrosymmetric, linear $D_{\infty h}$ structure, as shown by its spectroscopic properties. For example, an aqueous NaN_3 solution exhibits in the Raman spectrum only the symmetric N_3^- stretching mode at 1340 cm^{-1} and in the ^{14}N NMR spectrum two resonances at −282.2 and −133.5 ppm, respectively, with an area ratio of 2:1. By contrast, a solution of CsN_3 in liquid SO_2 is intense yellow and exhibits a strong Raman band at 2016 cm^{-1}, and its ^{14}N resonance for the two terminal nitrogen atoms is deshielded by 80 ppm relative to that of the free ion (Table 1). The ^{14}N NMR spectrum of a 1:1 mixture of CsN_3 and SO_2 in CH_3NO_2 solution exhibits also two resonances at $\delta = -209.9$ and −132.5 ppm, respectively, with an area ratio of 2:1. These chemical shifts are similar to those of −201.7 and −133.9 ppm observed for the SO_2 solution. The observation of a single resonance for the terminal nitrogen atoms, even for solutions of the 1:1 and 1:2 adducts in CH_3CN at low temperatures, and the weak temperature dependence of the chemical shifts indicate that the SO_2 groups in azidosulfites undergo rapid exchange on the NMR time scale.

These observations are strong indications that SO_2 forms adducts with the azide anion. The combining ratios of N_3^- with SO_2 were studied both experimentally and by theoretical calculations. It was found that at −64 °C SO_2 forms with $Cs^+N_3^-$ yellow 2:1 adducts that at about −30 °C lose 1 mol of SO_2 and yield white 1:1 adducts. The 1:1 adducts are marginally stable at room temperature and, when heated to about 60 °C, decompose to pure N_3^- and SO_2. The corresponding $N(CH_3)_4^+$ salts are thermally somewhat less stable. The underlying chemistry can be used for the conversion of insoluble halides, such as fluoride, into azide. For example, CsF is insoluble in most organic solvents and reacts only incompletely with reagents such as trimethylsilyl azide. It reacts, however, with SO_2 forming soluble SO_2F^-. The fluoride in SO_2F^- can then readily be exchanged for azide using trimethylsilyl azide, resulting in the formation of $SO_2N_3^-$. The latter is then thermally decomposed to give pure azide and SO_2.[15] During the pyrolysis of $SO_2N_3^-$, no evidence was obtained for any N_2 elimination before the loss of all the SO_2 which might have offered a potential synthesis for NSO_2^- salts.[32−34] In the presence of small amounts of moisture, colorless cesium salts of $S_2O_5^{2-}$ and $S_2O_7^{2-}$ can be formed as insoluble byproducts.[35]

$$H_2O + SO_2 \rightarrow H_2SO_3 \quad (2)$$

$$SO_2 + H_2SO_3 + 2CsN_3 \rightarrow Cs_2S_2O_5\downarrow + 2HN_3 \quad (3)$$

As SO_2 has very little vapor pressure below −64 °C, the isolation of well-defined adducts containing more than two SO_2 molecules per N_3^- could not be studied experimentally.

In agreement with the experimental observations, the theoretical calculations show that SO_2 can form stable 1:1 and 2:1 adducts with N_3^-. In the 1:1 adduct, the SO_2

(27) Levine, I. N. *Quantum Chemistry*, 3rd ed.; Allyn and Bacon: Boston, 1983, p 373.
(28) The B3LYP functional uses a three-parameter exchange functional of Becke (B3) [Becke, A. D. *J. Chem. Phys.* **1993**, *98*, 5648. Stephens, P. J.; Devlin, C. F.; Chabalowski, C. F.; Frisch, M. J. *J. Phys. Chem.* **1994**, *98*, 11623.] and the Lee, Yang, and Parr (LYP) correlation gradient-corrected functional [Lee, C.; Yang, W.; Parr, R. G. *Phys. Rev. B* **1988**, *37*, 785.].
(29) (a) Pople, J. A.; Binkley, J. S.; Seeger, R. *Int. Quantum Chem.* **1976**, *10*, 1. (b) Bartlett, R. J.; Silver, D. M. *Int. Quantum Chem.* **1975**, *9*, 183. (c) Dupuis, M.; Chin, S.; Marquez, A. In *Relativistic and Electron Correlation Effects in Molecules*; Malli, G., Ed.; Plenum: New York, 1994. (d) Frisch, M. J.; Head-Gordon, M.; Pople, J. A. *Chem. Phys. Lett.* **1990**, *166*, 275. (e) Bartlett, R. J.; Stanton, J. F. J. Applications of post-Hartree−Fock methods: A Tutorial. In *Reviews of Computational Chemistry*; Lipkowitz, K. B., Boyd, D. B., Eds.; VCH Publishers: New York, 1994, Vol. V.
(30) Purvis, G. D., III; Bartlett, R. J. *J. Chem. Phys.* **1982**, *76*, 1910.
(31) Raghavachari, K.; Trucks, G. W.; Pople, J. A.; Head-Gordon, M. *Chem. Phys. Lett.* **1989**, *157*, 479.
(32) Roesky, H. W.; Schmieder, W.; Isenberg, W.; Boehler, D.; Sheldrick, G. M. *Angew. Chem., Int. Ed. Engl.* **1982**, *21*, 153. Roesky, H. W.; Panday, K. P.; Krebs, B.; Dartmann, M. *J. Chem. Soc., Dalton Trans.* **1984**, 2271.
(33) Chivers, T.; Schmidt, K. J.; McIntyre, D. D.; Vogel, H. J. *Can. J. Chem.* **1989**, *67*, 1788.
(34) Morgon, N. H.; Linnert, H. V.; Riveros, J. M. *J. Phys. Chem.* **1995**, *99*, 11667.
(35) Seel, F.; Mueller, E. *Chem. Ber.* **1955**, *88*, 1747.

molecule is attached to one of the terminal nitrogens of the azide anion. This is in accord with the negative charges in N_3^- residing mainly on the terminal nitrogen atoms, thus making them the better donors. The N−S bond of the

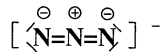

resulting adducts is relatively long, varies strongly with the computational level, and ranges for the 1:1 adduct from 1.91 Å at the RHF level to 2.36 Å at the MP2 level.

For the 2:1 adducts, the two SO_2 groups could reside on either the same or both terminal nitrogen atoms. The energy differences between the 1,1-adduct (rN−S = 2.47 Å at MP2) and the 1,3-adduct (rN−S = 2.56 Å) are predicted to be small, that is, less than 1 kcal/mol at the MP2 and less than 4 kcal/mol at the B3LYP level of theory in favor of the 1,1-adduct.

On the basis of our calculations, the addition of a third SO_2 molecule to the 1,1 adduct lengthens the two original 1,1 N−S bonds to 2.52 Å, but the third N−S bond to the other terminal nitrogen is much weaker at 2.87 Å. Similarly, the addition of a fourth SO_2 molecule affects the three original N−S bonds relatively little; the two geminal N−S bonds at 2.54 Å become slightly longer, and the third N−S bond at 2.80 Å becomes slightly shorter. However, the fourth N−S bond at 3.19 Å becomes much longer. These calculations at the MP2 level confirm that in the presence of excess SO_2 the N−S bonds become very weak, thus accounting for the observed facile N−S bond breakage on an NMR time scale. A more detailed discussion of the calculated structures will be given in a following section.

The $SO_2N_3^-$ anion can be described as either a donor−acceptor adduct between the Lewis acid SO_2 and the Lewis base N_3^- or, by analogy with many known SO_2X^- (X = halogen or pseudohalogen) anions, as an azidosulfite anion. Whereas either description is acceptable, the description of the higher $(SO_2)_nN_3^-$ adducts as azidopolysulfites is inappropriate because there is no significant interaction between the SO_2 ligands. For the analogous $(SO_3)_nN_3^-$ adducts, azidopolysulfate structures have previously been suggested;[10] however, it appears likely that these SO_3 analogues also contain discrete SO_3 units and not polysulfate anions.

The white crystals (compound **1**), obtained from a sample of $CsSO_2N_3$ in SO_2 solution that was kept in a Teflon NMR tube at room temperature for several weeks, had the composition $CsSO_2N_3 \cdot CsSO_3N_3$. These crystals were stable only at low temperature or under an atmosphere of SO_2 at room temperature. The asymmetric unit in the crystal lattice of **1** shows two cesium, two sulfur, and five oxygen atoms besides six nitrogen atoms forming two azide groups (Figure 1 and Tables 2−4). The cesium and sulfur atoms, and O1 and N2, lie on special positions. The large thermal ellipsoids observed for the N1, N3, N4, N5, and N6 atoms indicate a disorder across the crystallographic mirror plane. These atoms were then moved off the mirror plane and refined which resulted in two disordered azide conformations on the sulfur groups. In $SO_2N_3^-$, the sulfur atom S2 is connected to three oxygen positions with a total occupancy of 2 and,

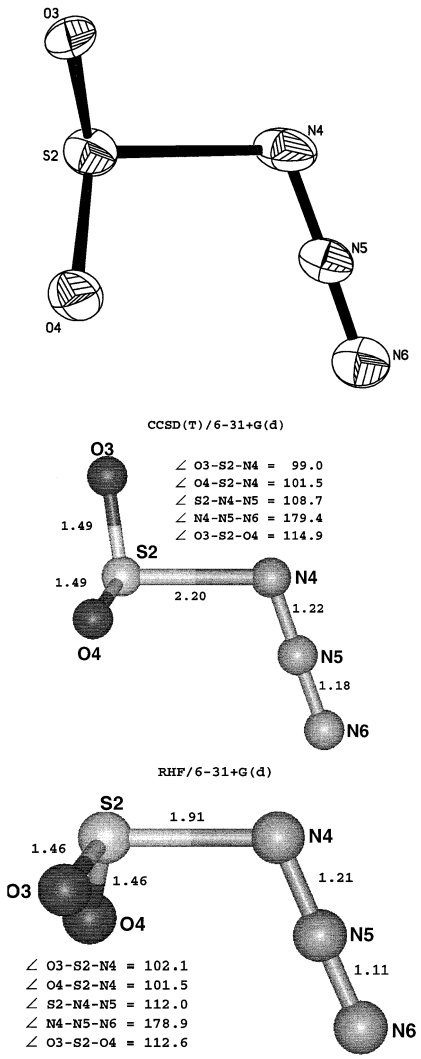

Figure 2. ORTEP plot (30%) of the experimental $SO_2N_3^-$ structure and the structures calculated at the CCSD(T)/6-31+G(d) and RHF/6-31+G(d) levels of theory.

therefore, is attributed to an SO_2 group. The oxygen atoms on S2 exhibit rotational disorder and have refined occupancies for O3 and O5 of 64% and 36%, respectively. A comparison of the geometry found in this study for $SO_2N_3^-$ in its cesium salt (see Figure 2) with that in the ordered $N(CH_3)_4^+$ salt[5] and the theoretical predictions at the correlated level (see Figure 2 and Table 4) shows good agreement and demonstrates that the counterion does not strongly influence the structure of $SO_2N_3^-$.

The $SO_3N_3^-$ anion is also slightly disordered. The N1 and N3 atoms are disordered across the crystallographic symmetry plane through S1, O1, and N2. Figure 3 depicts one of the two disordered components. Furthermore, the rotation of the SO_3 group with respect to the N_3 group deviates from the predictions at the MP2 and B3LYP levels of theory (see Table 5 and Figure 3). In the free gaseous anion, the O1, S1, N1, N2, and N3 atoms are all predicted to be coplanar, with O1 being trans to the azide group, while in the experimental solid-state structure it is cis. Because the calculated energy difference between the cis and trans rotamers is very small because of the weak S−N bond and

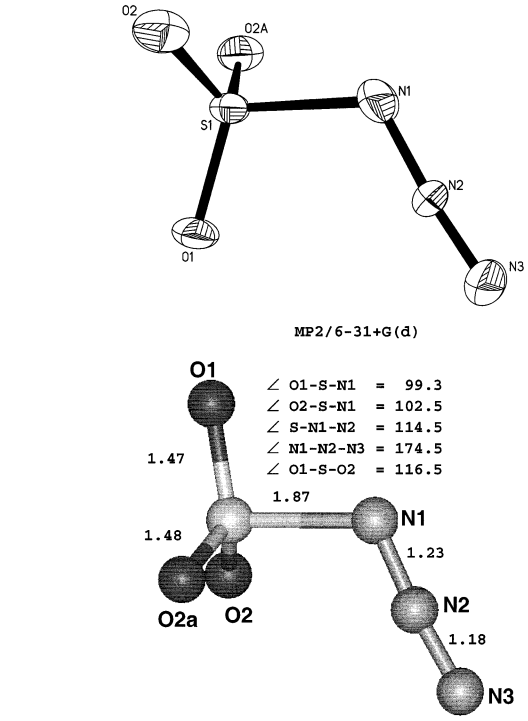

Figure 3. ORTEP plot (30%) of the experimental $SO_3N_3^-$ structure and the structure calculated at the MP2/6-31+G(d) level of theory.

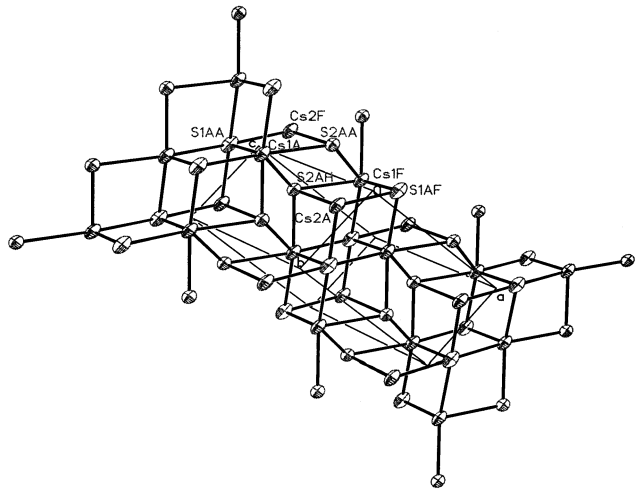

Figure 4. Packing diagram of $CsSO_2N_3 \cdot CsSO_3N_3$ showing the cesium−sulfur network.

its low frequency (33 cm^{-1}) torsion mode, the orientation of the SO_3 group is easily affected by the strong oxygen−cesium interactions in the lattice (see later).

A comparison of the experimental structures of $SO_2N_3^-$ and $SO_3N_3^-$ shows a remarkable difference of 0.23 Å for the S−N distances, that is, 1.981(12) Å for $SO_2N_3^-$ and 1.754(10) Å for $SO_3N_3^-$. The observed difference agrees well with that of 0.32 Å predicted at the B3LYP level and can be rationalized by the large difference in the Lewis acidities of SO_2 and SO_3. On the basis of the Christe/Dixon pF^- scale,[36] SO_2 and SO_3 have pF^- values of 3.99 and 7.83, respectively. If one views the $SO_2N_3^-$ and $SO_3N_3^-$ anions as Lewis acid/Lewis base adducts (see a previous section), it is not surprising that the stronger Lewis acid SO_3 forms the more stable adduct with the azide anion. Because of its longer S−N bond, the $SO_2N_3^-$ anion should undergo SO_n group rotation even more easily than $SO_3N_3^-$. Therefore, one can expect the orientations of the SO_n groups in the $SO_nN_3^-$ anions to vary significantly from one salt to another. The $N_\beta-N_\gamma$ distances at ∼1.13 Å are significantly shorter than the $N_\alpha-N_\beta$ distances at ∼1.21 Å and are characteristic for covalent azides with significant triple and double bond character, respectively. With increasing S−N bond length and a weakening of the $SO_2-N_3^-$ interaction, the $N_\alpha-N_\beta$ and $N_\beta-N_\gamma$ bonds become, as expected, more similar, and their values approach those of the free N_3^- anion.

Table 5. Most Important Bond Lengths [Å] and Angles [deg] of the $SO_3N_3^-$ Anion in Its Cs^+ Salt Compared to the Calculated Values

	calcd		
	B3LYP/6-31+G(d)	MP2/6-31+G(d)	obsd
	Bond Distances (Å)		
S−N	1.876	1.871	1.754(10)
S−O′	1.473	1.472	1.440(5)
$S-O_2$	1.479	1.478	1.447(6)
$N_\alpha-N_\beta$	1.223	1.233	1.207(11)
$N_\beta-N_\gamma$	1.151	1.175	1.120(11)
	Bond Angles (deg)		
O′−S−N	99.59	99.31	92.7(4)
O_2-S-N	102.94	102.47	107.2(4)
$S-N_\alpha-N_\beta$	114.21	114.52	110.0(8)
$N_\alpha-N_\beta-N_\gamma$	175.39	174.48	173.5(10)
$O'-S-O_2$	116.18	116.45	114.9(2)
S−N−N−N	180.00	180.00	180.0
O′−S−N−N	180.00	180.00	180.0

The $CsSO_2N_3 \cdot CsSO_3N_3$ structure exhibits many short contacts indicative of strong interionic interactions. Thus, all the Cs···O distances fall within the range 3.047(6) (Cs2···O1)−3.40(2) (Cs2···O5) Å and are considerably shorter than the sum of their van der Waals radii of about 4.5 Å.[37] The Cs···N contacts of 3.219(13) and 3.305(11) Å, involving the $SO_2N_3^-$ and the $SO_3N_3^-$ groups, respectively, are also significantly shorter than the sum of their van der Waals radii of about 4.54 Å. The S1···Cs2 contact of 3.848-(2) Å is also considerably shorter than the average distance of ∼4.43 Å for the remaining Cs···S contacts.

The short Cs···O contacts mentioned here result in a three-dimensional network of four-membered Cs_2O_2 rings involving alternating SO_3N_3 and SO_2N_3 units (Figure 1). A mean least-squares plane analysis of these two four-membered rings shows that they are twisted by 93.4° with respect to each other. The cesium−sulfur network (Figure 4) forms the basic crystal lattice that is built up of face- and edge-sharing cuboids stacked in a stair-like fashion.

The yellow impurity (**2**) was identified as a double salt of $Cs_2S_2O_5$ and $Cs_2S_2O_7$ with a molecule of SO_2 present as a solvate. The crystal structures of the separate anions have previously been reported,[38−41] and the structure of this ternary compound will be discussed in a forthcoming paper.

Vibrational Spectra and Theoretical Calculations. The vibrational spectra of $CsSO_2N_3$, $N(CH_3)_4SO_2N_3$, $Cs(SO_2)_2N_3$,

(36) Christe, K. O.; Dixon, D. A.; McLemore, D.; Wilson, W. W.; Sheehy, J. A.; Boatz, J. A. *J. Fluorine Chem.* **2000**, *101*, 151.

(37) Bondi, A. *J. Phys. Chem.* **1964**, *68*, 441.

(38) Lindqvist, I. *Acta Crystallogr.* **1957**, *10*, 406.

Table 6. Vibrational Spectra of Solid $[N(CH_3)_4][SO_2N_3]$ and $Cs[SO_2N_3]$ and Assignment of the $SO_2N_3^-$ Anion Bands Based on the Unscaled Frequencies and Intensities Calculated at the RHF, MP2, B3LYP, and CCSD(T) Levels of Theory[a]

vibrational frequencies, cm^{-1}									
calcd for free $SO_2N_3^-$				exptl				assignments	
				$N(CH_3)_4^+$	Cs^+				
RHF	MP2	B3LYP	CCSD(T)	Raman, −65 °C	IR, 22 °C	Raman, 22 °C	Raman, −100 °C	$SO_2N_3^-$	$N(CH_3)_4^+$
				3039(45)					
				3035(40)sh					
				2995(11)sh					
				2981(13)sh					
				2958(36)					
				2923(11)					
				2915(10)					ν(CH) modes
				2883(4)					
				2859(4)					
				2824(2)sh					
				2817(5)					
				2797(3)					
				2019(19)	2036vs	2036(20)	2042(16)	(1333 + 428 + 269)	
2375(1456)[146]	2143(889)[107]	2106(1182)[120]	2043	2014(27)		2013(25)	2018(30)	$\nu_{as}(N_3)$	
				1488(2)					$\nu_2(A_1)$, $\delta_s(CH_3)$
				1469(13)					$\nu_6(E)$, $\delta_{as}(CH_3)$
				1463(15)					
				1417(2)					$\nu_{16}(F_2)$, $\delta_s(CH_3)$
				1404(2)					
				1332(2)	1329m	1330(5)	1333(5)	(2 × 663)	
				1294(2)					$\nu_{17}(F_2)$, CH_3 rock
1411(434)[10]	1239(3)[34]	1350(42)[17]	1291	1272(7)	1272m	1274(13)	1274(14)	$\nu_s(N_3)$	
1289(431)[7.3]	1244(249)[56]	1198(297)[25]	1202	1197(5)	1196s	1190(9)	1188(9)	$\nu_{as}(SO_2)$	
				1188(7)					$\nu_7(E)$, CH_3 rock
				1179(2)					
				1143(2)			1145(1)		
1164(207)[20]	1087(199)[203]	1065(266)[65]	1056	1083(47)	1073s	1077(100)	1078(61)	$\nu_s(SO_2)$	
				1076(20)sh					
				952(12)					$\nu_{18}(F_2)$, $\nu_{as}(CN_4)$
				758(9)					$\nu_3(A_2)$, $\nu_s(CN_4)$
793(10)[10]	586(1)[4]	646(6)[1]	598	665(0+)	662mw	660(3)	663(2)	$\delta(N_3)$ in SN_3 plane	
700(18)[0.1]	550(1)[1]	608(6)[0.3]	549					$\delta(N_3)$ out of SN_3 plane	
607(116)[1.4]	497(33)[4]	504(27)[4]	505	544(4)	547m	540(7)	543(5)	δ_{sciss} (SO_2)	
				460(5)					$\nu_{19}(F_2)$, $\delta(CN_4)$
499(263)[6.4]	329(133)[10]	369(122)[8]	368	405(12)	414ms	420(15)	428(17)	$\delta_s SO_2N$	
				377(2)					$\nu_{12}(F_1)$, $\tau(CH_3)$
352(13)[2.9]	181(11)[12]	220(1)[6]	223	295(10)		309(30)	317(45)	$\tau(SO_2)$	
310(189)[29]	167(38)[17]	181(50)[20]	177	224(100)		258(84)	269(100)	ν(SN)	
150(4.0)[11]	69(4)[11]	106(9)[14]	96	154(28)		169(20)	175(24)	δ_{sciss} (SNN)	
							125sh		
				100(24)		96(100)	103(56)	lattice vibrations	
				86(17)sh		86sh			
				78(31)			78(27)		
17(0.9)[8.4]	30(1)[10]	22(1)[7]	25					$\tau(O_2S-N_3)$	

[a] Bands arising from the FEP sample tube were observed at 735(2) cm^{-1} in the spectrum of the $N(CH_3)_4^+$ salt.

$N(CH_3)_4(SO_2)_2N_3$, and $CsSO_3N_3$ are summarized in Tables 6−8 and Figures 5−7. The assignments were made by comparison with the calculated spectra and are supported by normal coordinate analyses. The correctness of the given mode descriptions was established by the calculated potential energy distributions. All the listed calculations were carried out with a 6-311+G(d) basis set. The calculations at the B3LYP level were also done with 6-311+G(2d) and aug-cc-pvtz basis sets and showed that the choice of the basis set had little influence on the results. For the ease of presentation, the spectra are discussed in the following order: $SO_2N_3^-$, $(SO_2)_2N_3^-$, N_3^- in SO_2 solution, and $SO_3N_3^-$.

$SO_2N_3^-$. The structure of the $SO_2N_3^-$ anion is well established by the crystal structures of its $N(CH_3)_4^+$ [5] and Cs^+ (Figure 2) salts and the results from the theoretical calculations (Figure 2 and Table 4). It must be emphasized that only the calculations at a correlated level duplicate the experimentally observed orientation of the SO_2 group. At the RHF level, the SO_2 group points in the same direction as the azido group. However, the energy difference between the two calculated structures is only about 1 kcal/mol because of the rotational barrier along the N−S bond in $SO_2N_3^-$ (ν = 22 cm^{-1} at the B3LYP level) being even lower than that in $SO_3N_3^-$ (ν = 33 cm^{-1}). The agreement between the observed and the calculated spectra (see Table 6) is satisfac-

(39) Baggio, S. *Acta Crystallogr.* **1971**, *27*, 517.
(40) Wang, Y.; Chen, I.-C. *Acta Crystallogr., Sect. C* **1984**, *40*, 1780.
(41) Hvoslef, J.; Tracy, M. L.; Nash, C. P. *Acta Crystallogr., Sect. C* **1986**, *42*, 353.

Table 7. Vibrational Spectra of $[N(CH_3)_4][(SO_2)_2N_3]$ and $[Cs][(SO_2)_2N_3]$ and Assignments for $(SO_2)_2N_3^-$ Based on the Frequencies and Intensities Calculated at the MP2 and B3LYP Levels of Theory[a,b]

vibrational frequencies, cm^{-1}							
calcd for free $O_2SNNNSO_2^-$		calcd for free $(O_2S)_2NNN^-$		exptl		assignments	
MP2	B3LYP	B3LYP	MP2	$N(CH_3)_4^+$ Raman, −80 °C[a]	Cs^+ Raman, −100 °C	$(O_2S)_2N_3^-$	$N(CH_3)_4^+$
				3052(8)sh			
				3043(12)			
				3037(8)sh			
				2992(13)}			
				2976(5)			$\nu(CH_3)$ modes
				2960(6)			
				2930(10)			
				2903(1)			
				2826(4)			
2096(10)[93]	2076(35)[11]	2125(21)[137]	2102(12)[206]	2028(1)	2028(27)	$\nu_{as}(N_3)$	
				1981(13)	2019(17)		
				1492(1)			$\nu_2(A_1)$, $\delta_s(CH_3)$
				1471(1)			$\nu_6(E)$, $\delta_{as}(CH_3)$
				1455(6)			
				1422(1)			$\nu_{16}(F_2)$, $\delta_s(CH_3)$
				1383(1)			
				1333(13)			
1241(0)[46]	1379(0)[22]	1339(2)[11]	1252(4)[58]	1316(2)	1308(3.6)	$\nu_s(N_3)$	
				1299(5)			$\nu_{17}(F_2)$, CH_3 rock
1236(1)[67]	1243(11)[29]	1235(5)[24]	1242(5)[38]		1273(5)		
1228(8)[13]	1241(0)[17]	1224(5)[24]	1217(0.1)[32]	1250(1)	1246(2)	$\nu_{as}(SO_2)$	
					1223(3)		
				1177(1)			$\nu_7(E)$, CH_3 rock
				1140(100)	1120(100)		
1052(1)[457]	1094(4)[307]	1088(2)[176]	1080(4)[287]	1136(98)	1113(6)	$\nu_s(SO_2)$	
1052(5)[143]	1077(7)[112]	1078(6)[51]	1067(2)[219]	1128(30)	1099(41)		
				1082(1)	1096sh		
				1074(1)			
				956(4)			$\nu_{18}(F_2)$, $\nu_{as}(CN_4)$
				756(6)			$\nu_3(A_2)$, $\nu_s(CN_4)$
563(0)[2]	640(0)[4]	638(0)[2]	563(0.1)[0.6]		644(2)		
546(0)[1]	620(0)[1]	606(0)[2]	502(0.3)[1.4]		617(1.6)		
					546(0.4)		
488(1)[0]	501(1)[11]	504(1)[2]	491(0.1)[5]	536(4)	535(5)	$\delta_{sciss}(SO_2)$	
487(0)[5]	498(0)[0]	503(0)[5]	487(1)[5]				
				458(2)			$\nu_{19}(F_2)$, $\delta(CN_4)$
				384(1)			$\nu_{12}(F_1)$, $\tau(CH_3)$
				370(1)	352(2)		
276(2)[8]	306(0)[15]	323(2)[6]	312(2)[5]	292(1)	310(5)		
261(1)[5]	281(5)[1]	308(4)[4]	276(3)[15]	231(7)	254(4)		
201(0)[10]	209(0)[16]	247(1)[3]	221(1)[9]		206(5)		
201(0)[15]	172(0)[3]	181(0)[8]	162(0.4)[2]	172(7)	183(4)		
140(0)[5]	131(0)[10]	146(1)[4]	139(0.4)[7]		161(14)		
135(1)[0]	130(2)[1]	112(0)[15]	109(0.1)[7]	128(10)	139(12)		
109(0)[1]	71(0)[4]	78(0)[4]	79(0.03)[9]		117(5)		
97(0)[2]	52(0)[3]	73(0)[6]	68(0.08)[6]	105(9)	105(11)		
71(0)[5]	20(0)[10]	34(0)[2]	45(0.01)[3]		89(5)		
47(0)[1]	19(0)[1]	30(0)[3]	26(0.05)[2]		78(5)		
					69(4)		
34(0)[0]	1(0)[1]	22(0)[0]	23(0.03)[2]		54(4)		

[a] Bands arising from the FEP sample tube were observed at 734(3) cm^{-1} for the $N(CH_3)_4(O_2S)_2N_3$ sample. [b] Raman spectra of $Cs(O_2S)_2N_3$ recorded at −130 °C on the Cary instead of the Bruker Equinox showed significant changes in the relative intensities of some of the bands.

tory if one keeps in mind that the skeletal modes involving the very long N−S bonds are strongly correlation dependent. Thus, the uncorrelated RHF method underestimates the bond length of the S−N bond resulting in high-frequency values for the modes involving the N−S bond. On the other hand, all the correlated methods significantly overestimate the S−N bond length (see Tables 4 and 5) resulting in low-frequency values for these modes. If one assumes that the actual bond lengths and frequencies fall between the uncorrelated and the correlated values, the fit between calculated and observed data becomes satisfactory. These results, together with our previous study of the SO_2F^- anion,[42] demonstrate the difficulties associated with the accurate calculation of highly ionic, long bonds. In view of the significant discrepancies between the observed and calculated frequencies, the calculated force fields have not been included in this paper.

$(SO_2)_2N_3^-$. Whereas the structure of the $SO_2N_3^-$ anion is firmly supported by its crystal structures, only Raman data are available for the $(SO_2)_2N_3^-$ ion. Because the negative charges in N_3^- are located on the two terminal nitrogen atoms

(42) Lork, E.; Mews, R.; Viets, D.; Watson, P. G.; Borrmann, T.; Vij, A.; Boatz, J. A.; Christe, K. O. *Inorg. Chem.* **2001**, *40*, 1303.

Table 8. Vibrational Spectra of [Cs][SO_3N_3]

vibrational frequencies, cm^{-1}				
exptl		calcd		assignments
IR, 22 °C	Raman, 22 °C	MP2	B3LYP	$SO_3N_3^-$ (C_s)
3337m				2134 + 1247 ($\nu_1 + \nu_{11}$)
2469m				1269 + 1247 ($\nu_3 + \nu_{11}$)
2450m				2 × 1247 (2 × ν_{11})
2283w				1247 + 1045 ($\nu_4 + \nu_{11}$)
2134vs	2138(23)	2272(19)[81]	2192(827)[89]	ν_1(A′), $\nu_{as}(N_3)$
	2118(15)			
1483w				2 × 744 (2 × ν_5)
	1278(8)	1285(1)[1]	1323(136)[8]	ν_2(A′), $\nu_s(N_3)$
1269vs		1283(9)[16]	1241(318)[14]	ν_3(A′), $\nu_{as}(SO_3)$
1247vs	1250(9)	1261(9)[7]	1218(336)[9]	ν_{11}(A″), $\nu_{as}(SO_3)$
1114w	1089(5)			
1045vs	1052(100)	1022(4)[44]	987(158)[40]	ν_4(A′), $\nu_s(SO_3)$
1028w				562 + 464 ($\nu_{13} + \nu_9$)
744s	746(18)	706(0.5)[5]	700(18)[5]	ν_5(A′), $\delta(N_3)$ in plane
640sh	644(10)	558(0.1)[0.1]	593(8)[0.1]	ν_{12}(A″), $\delta(N_3)$ out of plane
626vs		563(9)[7]	572(349)[6]	ν_6(A′), $\delta(SO_3)$ umbrella
618m				2 × 313 (2 × ν_4)
579w				
562s	558(13)	519(1)[4]	510(28)[4]	ν_{13}(A″), $\delta_{as}(SO_3)$
556s				
547s	550sh	518(0.5)[3]	509(18)[3]	ν_7(A′), $\delta_{sciss}(SO_2)$
464m	464(54)	363(2)[29]	369(34)[24]	ν_9(A′), ν(S−N)
	370(28)	314(1)[11]	314(11)[9]	ν_8(A′), $\delta_{rock}(SO_3)$
	364sh			
	313(8)	322(0)[1]	318(0)[1]	ν_{14}(A″), $\delta_{wag}(SO_3)$
	185(23)	123(0)[7]	139(1)[6]	ν_{10}(A′), δ_{sciss}(S−N−N)
	112sh			
		49(0)[6]	33(0)[6]	ν_{15}(A″), τ(S−N)

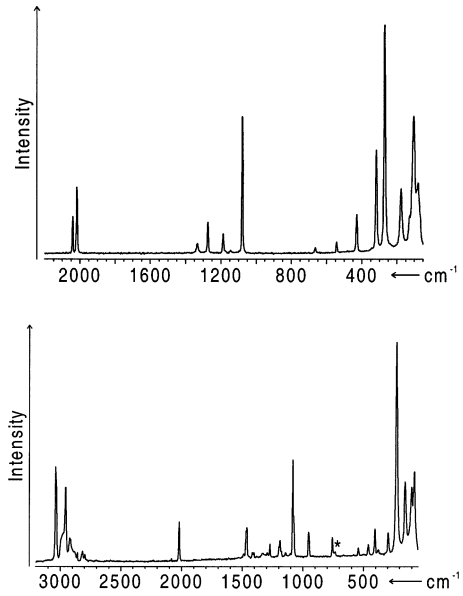

Figure 5. Raman spectra of $CsSO_2N_3$ (upper trace) and of $N(CH_3)_4SO_2N_3$ (lower trace). The band marked by an asterisk is due to the FEP sample tube.

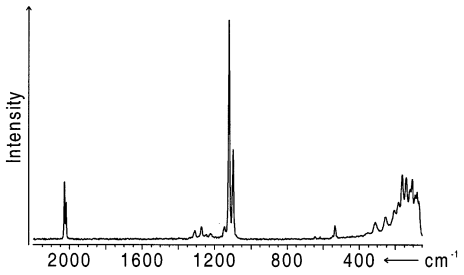

Figure 6. Raman spectrum of $Cs(SO_2)_2N_3$.

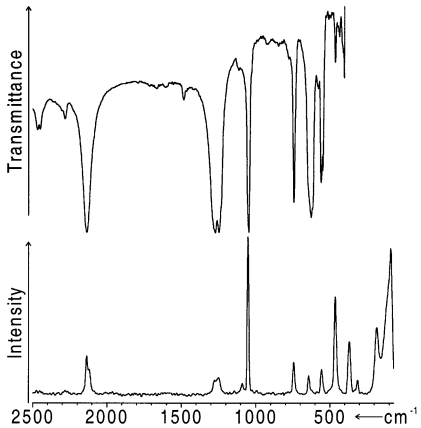

Figure 7. Infrared (upper trace) and Raman (lower trace) spectra of $CsSO_3N_3$.

(see previous discussion), the SO_2 groups must be attached to these. However, the two SO_2 groups could be attached to the same or to different nitrogen atoms. Theoretical calculations at the B3LYP and MP2 levels of theory (Figures 8 and 9) favor the geminal 1,1-$(SO_2)_2N_3^-$ over the terminal 1,3-$O_2SNNNSO_2^-$ adduct by 3.5 and 0.4 kcal/mol, respectively. Figure 8 also shows that the B3LYP and MP2 calculations result in very different minimum energy structures for the 1,3-adduct. At the MP2 level, there is, in addition to the N_α—S bond with 2.56 Å, also significant $\pi-\pi$ interaction between the N═N and S═O double bonds resulting in an N_β—O interaction of 2.84 Å, while at the B3YLP level the interaction occurs mainly through N−S bonds. Calculations were also carried out using the MP2 structure as the starting point for the B3LYP calculation and vice versa, but in each case, the calculations reverted

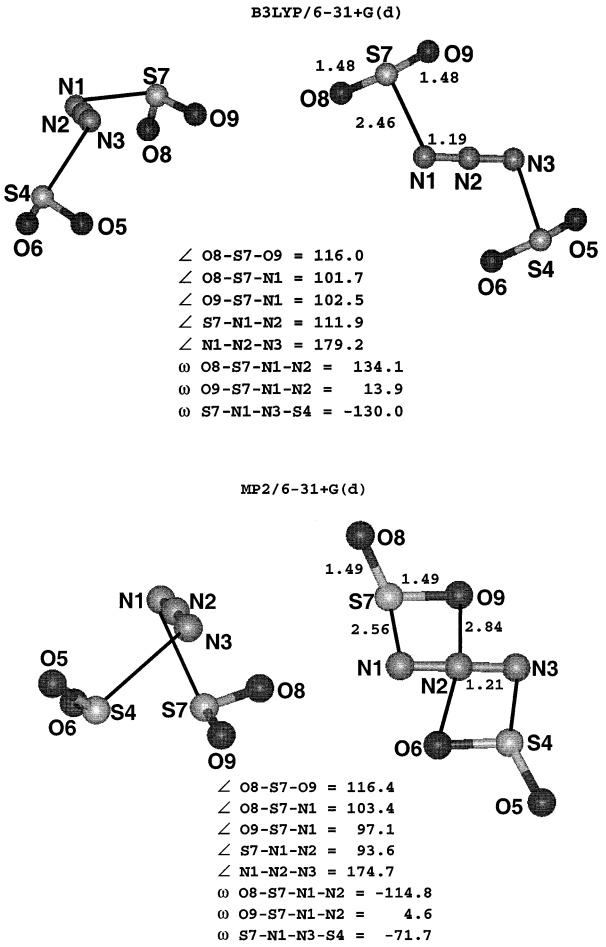

Figure 8. Structures of the 1,3-$(SO_2)_2N_3^-$ anion calculated at the B3LYP/6-31+G(d) and MP2/6-31+G(d) levels.

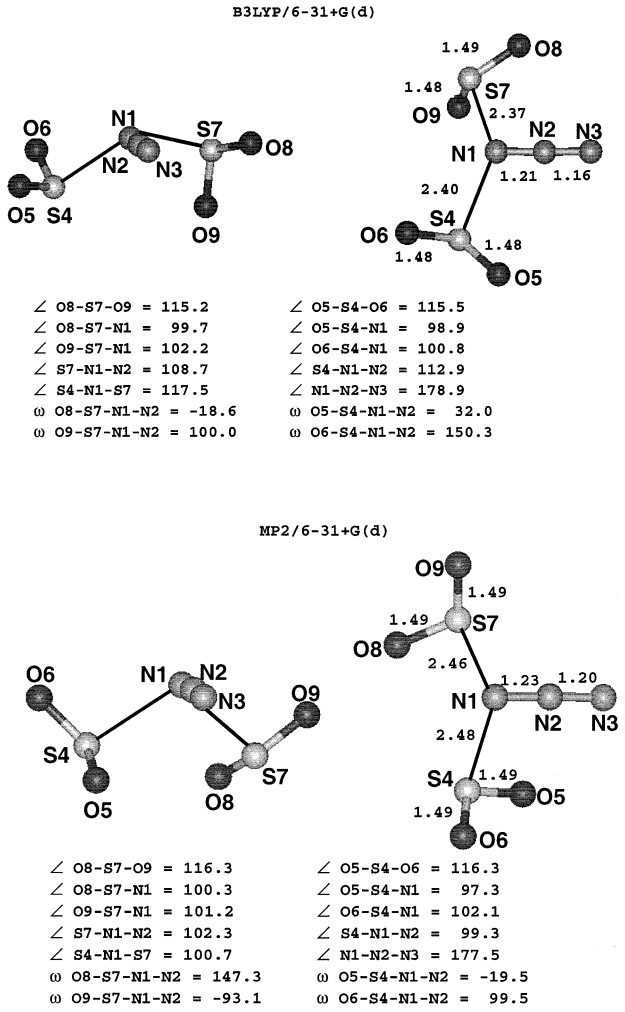

Figure 9. Structures of the 1,1-$(SO_2)_2N_3^-$ anion calculated at the B3LYP/6-31+G(d) and MP2/6-31+G(d) levels.

back to the structures shown in Figure 8, establishing that they are the true minima for each method. For the 1,1-adducts, the MP2 and B3LYP structures are more similar (Figure 9).

Distinction between the 1,1- and the 1,3-structures is possible from the observed Raman intensities (see Table 7). In the 1,3-structures, the relative intensities of the antisymmetric and the symmetric azide stretching modes are comparable, while in the 1,1-adducts, the antisymmetric stretching mode is much more intense than the symmetric one. Furthermore, in the 1,3-adduct, many of the low frequency skeletal modes are of low Raman intensity, while in the 1,1-adduct they are more intense and of comparable intensity. The observed spectra (see Table 7 and Figure 6) clearly favor the energetically preferred 1,1-structure.

SO_2 Solutions of N_3^-. The Raman spectra of the yellow solutions of N_3^- in liquid SO_2 show bands at about 2016(s) ($\nu_{as}N_3$), 1274(w) ($\nu_{as}SO_2$), 1120(vs) ($\nu_{sym}SO_2$), 646(mw) (δN_3), 400(br), and 230(br) cm^{-1} that are in accord with the spectra observed for the yellow, solid 1,1-$(SO_2)_2N_3^-$ adduct. In view of the similar spectra and the fact that the theoretical calculations indicate that the bonding of a third and fourth SO_2 ligand to $(SO_2)_2N_3^-$ becomes increasingly weaker (see previous discussion), the yellow species present in the N_3^-/SO_2 solutions is attributed to the 1,1-$(SO_2)_2N_3^-$ anion.

$SO_3N_3^-$. The structure of this anion is firmly established by the X-ray diffraction results (Figure 3). The theoretical calculations at the MP2 and B3LYP levels (see Tables 5 and 8 and Figure 3) result in almost identical geometries; however, compared to the experimental structure, the SO_3 group is rotated by 60° about the S−N axis. As for $SO_2N_3^-$, both methods significantly overestimate the N−S bond length, in this case by 0.12 Å. This bond distance overestimate results in an underestimate of those vibrational frequencies involving the S−N bond (see Table 8), but otherwise, the agreement between observed and calculated spectra is satisfactory. The fact that the S−N bond in $SO_3N_3^-$ is significantly shorter than that in $SO_2N_3^-$ has already been explained here by the increased Lewis acidity of SO_3. This increased withdrawal of electron density and negative charge from the azide anion in $SO_3N_3^-$ also causes a marked decrease in the N−N bond lengths, an increase in the average N_3 streching and bending frequencies, and an increased bond length difference between the $N_\alpha-N_\beta$ and $N_\beta-N_\gamma$ bonds.

Conclusions

The N_3^- anion acts as a pseudohalide and dissolves in liquid SO_2 forming yellow donor−acceptor adducts contain-

ing at least two SO_2 molecules per N_3^-. At low temperature, yellow $(SO_2)_2N_3^-$ salts can be isolated in which both SO_2 molecules are probably attached to the same terminal nitrogen atom. At about −30 °C, 1 mol of SO_2 can be pumped off, resulting in marginally stable, colorless $SO_2N_3^-$ salts that can be converted at about 50 °C into pure azides. The azidosulfites are analogous to the previously known azidosulfates but possess a significantly weaker S−N bond resulting in lowered thermal stability.

Acknowledgment. The authors thank Dr. Robert Corley for his steady encouragement and the National Science Foundation, the Defense Advanced Projects Agency, and the Air Force Office of Scientific Research for financial support. S.S. thanks the Alexander von Humboldt Foundation for a Feodor-Lynen fellowship, and M.G., the Natural Sciences and Engineering Research Council of Canada for a postdoctoral fellowship. This work was also supported in part by a grant of IBM SP time from the Aeronautical Systems Center at Wright-Patterson Air Force Base, a Department of Defense High Performance Computing Major Shared Resource Center.

Supporting Information Available: Tables of structure determination summary, atomic coordinates, bond lengths and angles, and anisotropic displacement parameters of $CsSO_2N_3 \cdot CsSO_3N_3$ in CIF format. This material is available free of charge via the Internet at http://pubs.acs.org.

IC020183L

This Page Intentionally Left Blank

APPENDIX G

"The $(SO_2)_2N_3^-$ Anion"
Inorg. Chem., 42, 419 (2003)

This Page Intentionally Left Blank

Inorg. Chem. **2003**, *42*, 416–419

The $(SO_2)_2N_3^-$ Anion

Karl O. Christe,*,†,‡ Michael Gerken,†,§ Ralf Haiges,† Stefan Schneider,† Thorsten Schroer,† Irena Tsyba,† and Robert Bau†

Loker Hydrocarbon Research Institute and Department of Chemistry, University of Southern California, Los Angeles, California 90089, and Propulsion Sciences and Advanced Concepts Division, Air Force Research Laboratory, Edwards AFB, California 93524

Received July 26, 2002

The recently proposed $(SO_2)_2N_3^-$ anion was structurally characterized by single-crystal X-ray diffraction of the [Cs][$(SO_2)_2N_3$] salt ($P2_1/c$, $a = 8.945(2)$ Å, $b = 10.454(2)$ Å, $c = 8.152(2)$ Å, $\beta = 109.166(3)°$, $Z = 4$, and $R_1 = 0.0329$ at 130 K). In the $(SO_2)_2N_3^-$ anion, both SO_2 ligands are coordinated to one terminal nitrogen atom of the N_3^- anion.

Introduction

Sulfur dioxide has been extensively used as a nonaqueous inorganic solvent,[1−3] and many SO_2 solvates of metal cations have been structurally well characterized by X-ray crystallography.[4] Halide and pseudo-halide anions, such as F^-,[5,6] Cl^-,[6,7] Br^-,[6] I^-,[6,8] CN^-,[9] SCN^-,[10] OCN^-,[11] and recently N_3^-,[11,12] were also found to form adducts with SO_2 in a 1:1 ratio. These adducts can be viewed as halosulfites and pseudo-halosulfites. The strength of the bond between these anions and SO_2 was found to decrease with increasing anion size.[6,11,13] In the SO_2F^- anion, for example, the S−F bond is basically a single bond, while the S-anion bonds in SO_2I^- and SO_2SCN^- are best described as contacts or secondary bonds.[5]

In a recent paper in this journal, we reported the syntheses and characterization of the [M][SO_2N_3] and [M][$(SO_2)_2N_3$] salts, where M was $N(CH_3)_4$ and Cs.[12] These salts are of significant interest for polynitrogen chemistry because SO_2 is an excellent solvent for carrying out metathetical reactions involving azide ions. Because the reactions of the azide ions with the SO_2 solvent can complicate the desired metathetical reactions, a better understanding of the nature of these $(SO_2)_nN_3^-$ adducts is very important. Whereas the [M][SO_2N_3] salts were well characterized by single-crystal X-ray diffraction, the [M][$(SO_2)_2N_3$] salts were characterized only by vibrational spectroscopy. Although the vibrational spectra favored a structure in which both SO_2 molecules are attached to the same terminal nitrogen atom of the azide ion, a more definite proof for the proposed structure was highly desirable. There were two previous reports on adducts with an SO_2 to anion ratio of larger than 1, but none provided any structural evidence. Thus, in 1938, Jander and Mesech have studied the interaction of SO_2 with the halide and SCN^- anions by vapor pressure measurements. They found evidence for the existence of 1:2, 2:1, 3:1, and 4:1 adducts, depending on the nature of the anion and countercation.[14] Similarly, a UV and infrared spectroscopic study of halides and halosulfites

* To whom correspondence should be sent. E-mail: karl.christe@edwards.af.mil.

† University of Southern California.

‡ Air Force Research Laboratory.

§ Present address: Department of Chemistry and Biochemistry, The University of Lethbridge, Alberta, T1K 3M4, Canada.

(1) Waddington, T. C. In *Nonaqueous Solvent Systems*; Waddington, T. C., Ed.; Academic Press: London, 1965; p 253.
(2) Karcher, W.; Hechts, H. In *Chemistry in Nonaqueous Ionizing Solvent*; Jander, G., Spandou, J., Addison, C. C., Eds.; Pergamon: Oxford, 1967; Vol. 3, p 79.
(3) Burow, D. F. In *Nonaqueous Solvents*; Lagowski, J. J., Ed.; Academic Press: New York, 1970; p 138.
(4) Mews, R.; Lork, E.; Watson, P. G.; Görtler, B. *Coord. Chem. Rev.* **2000**, *197*, 277.
(5) (a) Kornath, A.; Neumann, F.; Ludwig, R. *Inorg. Chem.* **1997**, *36*, 5570. (b) Lork, E.; Mews, R.; Viets, D.; Watson, P. G.; Borrmann, T.; Vij, A.; Boatz, J.; Christe, K. O. *Inorg. Chem.* **2001**, *40*, 1303. (c) Kessler, U.; van Wüllen, L.; Jansen, M. *Inorg. Chem.* **2001**, *40*, 7040.
(6) Burow, D. F. *Inorg. Chem.* **1972**, *11*, 573.
(7) Kuhn, N.; Bohnen, H.; Bläser, D.; Boese, R.; Maulitz, A. H. *J. Chem. Soc., Chem. Commun.* **1994**, 2283.
(8) (a) Snow, M. R.; Ibers, J. A. *Inorg. Chem.* **1973**, *12*, 224. (b) Ellers, P. G.; Kubas, G. J. *Inorg. Chem.* **1978**, *17*, 894.
(9) Kornath, A.; Blecher, O.; Ludwig, R. *J. Am. Chem. Soc.* **1999**, *121*, 4019.
(10) Kornath, A.; Blecher, O.; Ludwig, R. *Z. Anorg. Allg. Chem.* **2000**, *626*, 731.
(11) Kornath, A.; Blecher, O.; Ludwig, R. *Z. Anorg. Allg. Chem.* **2002,** *628*, 183.
(12) Christe, K. O.; Boatz, J. A.; Gerken, M.; Haiges, R.; Schneider, S.; Schroer, S.; Tham, F. S.; Vij, A.; Vij, V.; Wagner, R. I.; Wilson W. W. *Inorg. Chem.* **2002**, *41*, 4275−4285..
(13) Maulitz, A. H.; Boese, R.; Kuhn, N. *J. Mol. Struct.* **1995**, *333*, 227.
(14) Jander, G.; Mesech, H. *Z. Phys. Chem., Abt. A*, **1938**, *183*, 121.

10.1021/ic0259078 CCC: $25.00
Published on Web 12/05/2002

in SO_2 solution provided evidence for the presence of 2:1 adducts; however, questionable structures were proposed for these $(SO_2)_2X^-$ anions that involved an O_2S-SO_2 moiety, coordinated to the halides through only one sulfur atom.[6]

In the present paper, we report the X-ray crystal structure of $[Cs][(SO_2)_2N_3]$, thereby establishing the structure of the $(SO_2)_2N_3^-$ anion beyond doubt.

Experimental Section

Caution! *Azides are highly endothermic and often can decompose explosively. Although no explosion has occurred while conducting these experiments, the materials should be handled on a small scale with appropriate safety precautions.*

Materials and Apparatus. Reactions were carried out in Teflon-FEP ampules that were closed by stainless steel valves. Volatile materials were handled on a Pyrex glass vacuum line equipped with grease-free Kontes glass−Teflon valves. Nonvolatile solids were handled in the dry argon atmosphere of a glovebox. The CsN_3 was prepared by literature methods.[15] The SO_2 (Air Products, anhydrous grade, 99.9%) was dried over CaH_2.

Crystal Growth of $[Cs][(SO_2)_2N_3]$. Inside the drybox, approximately 0.02 g of CsN_3 (0.07 mmol) was loaded into a 9-mm FEP tube, which was sealed on one side and fused to a piece of 3/8 in. FEP tubing equipped with a Whitey SS−IRF2 valve on the other side. Anhydrous SO_2 (0.5 mL) was added in vacuo to the solid at −196 °C. After warming to room temperature to dissolve all the CsN_3, the tube was cooled to −64 °C, and the SO_2 solvent was removed slowly under a dynamic vacuum at −64 °C, yielding a pale yellow crystalline solid. The ampule was cut open at −78 °C under a dry nitrogen stream, and the crystals were immediately transferred into an aluminum trough, kept at −100 °C by a stream of cold dry nitrogen. A crystal selected in the cold stream was mounted on a glass fiber by rapidly bringing it into contact with a droplet of Fomblin oil (Z-25) adhering to the tip of the fiber. The mounted crystal was rapidly transferred into the cold nitrogen stream of the goniometer head. The crystal used in this study had the dimensions $0.80 \times 0.34 \times 0.313$ mm^3.

Crystal Structure Determination of $[Cs][(SO_2)_2N_3]$. (a) Collection and Reduction of X-ray Data. X-ray diffraction data were collected using a Bruker 3-circle platform diffractometer, equipped with a SMART APEX CCD (charge coupled device) detector with the χ-axis fixed at 54.74° (using the program SMART[16]), and using Mo Kα radiation ($\lambda = 0.71073$ Å) from a fine-focus tube. The diffractometer was equipped with a cryo-cooler from CRYO Industries for low-temperature data collection using controlled liquid nitrogen boil off. Cell constants were determined from 60 10-s frames at 130 K. A complete hemisphere of data was collected up to a resolution of 0.75 Å. Processing was carried out by using the program SAINT,[17] which applied Lorentz and polarization correction to three-dimensionally integrated diffraction spots. The program SADABS[18] was used for the scaling of diffraction data, the application of a decay correction, and an empirical absorption correction based on redundant reflections.

(b) Solution and Refinement of the Structure. All data were processed using the SHELXTL package (version 5.1)[19] for structure determination, refinement, and molecular graphics. The XPREP program was used to confirm the unit cell dimensions and the crystal lattices. The structure was solved by the direct method. Successive difference Fourier synthesis revealed all atoms. The structure was refined by the least-squares method on F^2. All atoms were refined anisotropically. For the anisotropic displacement parameters, the U(eq) is defined as one-third of the trace of the orthogonalized U_{ij} tensor.

Table 1. Crystal Data for $[Cs][(SO_2)_2N_3^-$

chemical formula	Cs N3 O4 S2
fw	303.06
T, K	130(2)
space group	$P2_1/c$ (No. 14)
a, Å	8.945(2)
b, Å	10.454(2)
c, Å	8.152(2)
β, deg	109.166(3)
V, Å^3	720.0(2)
Z	4
ρ_{calcd}, g cm^{-3}	2.796
μ, mm^{-1}	5.685
R1,[a] wR2[b] [$I > 2\sigma(I)$]	0.0329, 0.0822
R1,[a] wR2[b] (all data)	0.0333, 0.0826

[a] $R1 = (\sum(F_o - F_c)/F_o)$. [b] $wR2 = [\sum(w(F_o - F_c)^2)w/F_o^2)]^{1/2}$.

Results and Discussion

Preparation and Crystal Growth of $[Cs][(SO_2)_2N_3]$. Yellow 2:1 adducts of SO_2 and either CsN_3 or $[N(CH_3)_4][N_3]$ precipitate from their SO_2 solutions at low temperature.[12] While the $[N(CH_3)_4][(SO_2)_2N_3]$ salt is only marginally stable in a dynamic vacuum at −64 °C, that is, close to the freezing point of the SO_2 solvent, the corresponding Cs^+ salt is stable in a dynamic vacuum up to −30 °C.

Crystal Structure of $[Cs][(SO_2)_2N_3]$. Details of the crystal data for $[Cs][(SO_2)_2N_3]$ are provided in Table 1; the observed bond lengths, angles, and contacts are listed in Table 2, together with the geometric parameters previously calculated[12] for the $(SO_2)_2N_3^-$ anion. The atomic coordinates and equivalent isotropic displacement parameters are listed in Table 3.

The $[Cs][(SO_2)_2N_3]$ salt crystallizes in the monoclinic space group $P2_1/c$ and contains the $(SO_2)_2N_3^-$ anion (Figure 1). The $(SO_2)_2N_3^-$ anions form double-layered sheets in the bc-plane, with half of the SO_2 groups in the center and the azide groups on the perimeters of the sheets (Figure 2). The Cs^+ cations are located within the sheets close to the perimeters and form contacts to the terminal azide nitrogen of the adjacent double-layers.

In the $(SO_2)_2N_3^-$ anion, the two SO_2 groups are bound to the same terminal nitrogen atom of N_3^-. The azide group is essentially linear with a significant difference in the N−N bond lengths (1.141(6) and 1.219(6) Å), which are very similar to those found in $[N(CH_3)_4][SO_2N_3]$ (1.144(2) and 1.214(2) Å).[11] In the $(SO_2)_2N_3^-$ anion, one S−N bond (2.201(5) Å) is significantly shorter than the second one (2.427(4) Å). However, both S−N bonds are longer than that found for the $SO_2N_3^-$ anion in $[N(CH_3)_4][SO_2N_3]$ (2.005(2) Å).[11] The marked difference between the S−N bond lengths

(15) Gerken, M.; Schneider, S.; Schroer, T.; Haiges, R.; Christe, K. O. *Z. Anorg. Allg. Chem.* **2002**, *628*, 909.
(16) *SMART V 5.625, Software for the CCD Detector System*; Bruker AXS: Madison, WI, 2001.
(17) *SAINT V 6.22, Software for the CCD Detector System*; Bruker AXS: Madison, WI, 2001.
(18) *SADABS, Program for absorption correction for area detectors, Version 2.03*; Bruker AXS: Madison, WI, 2001.
(19) *SHELXTL 6.10 for Windows NT, Program library for Structure Solution and Molecular Graphics*; Bruker AXS: Madison, WI, 2000.

Table 2. Experimental Bond Lengths [Å], Angles [deg], and Contacts [Å] for [Cs][$(SO_2)_2N_3$] and Calculated[12] Bond Lengths and Angles for the $(SO_2)_2N_3^-$ Anion

		calculated	
	observed	B3LYP/6-31+G(d)	MP2/6-31+G(d)
N(2)−N(3)	1.141(6)	1.16	1.20
N(1)−N(2)	1.219(6)	1.21	1.23
S(1)−N(1)	2.201(5)	2.37	2.46
S(2)−N(1)	2.427(4)	2.40	2.48
S(1)−O(2)	1.449(4)	1.49	1.49
S(1)−O(1)	1.460(3)	1.48	1.49
S(2)−O(3)	1.433(4)	1.48	1.49
S(2)−O(4)	1.439(4)	1.48	1.49
N(1)−N(2)−N(3)	177.6(5)	178.9	177.5
S(1)−N(1)−S(2)	109.8(2)	117.5	100.7
N(2)−N(1)−S(1)	108.5(3)	108.7	102.3
N(2)−N(1)−S(2)	102.6(3)	112.9	99.3
O(2)−S(1)−O(1)	114.1(2)	115.2	116.3
O(3)−S(2)−O(4)	115.9(2)	115.5	116.3
O(2)−S(1)−N(1)	99.9(2)		
O(1)−S(1)−N(1)	97.1(2)		
O(3)−S(2)−N(1)	96.5(2)		
O(4)−S(2)−N(1)	96.3(2)		
Observed Contacts			
N(3)···Cs(1A)	3.377(4)	N(3)···Cs(1B)	3.434(4)
N(3)···Cs(1C)	3.548(4)	N(1)···Cs(1F)	3.351(4)
O(1)···Cs(1)	3.807(4)	O(1)···Cs(1D)	3.114(3)
O(2)···Cs(1)	3.287(3)	O(2)···Cs(1B)	3.139(3)
O(3)···Cs(1C)	3.176(3)	O(3)···Cs(1E)	3.430(3)
O(4)···Cs(1F)	3.243(4)	O(4)···Cs(1G)	3.329(3)

Table 3. Atomic Coordinates ($\times 10^4$) and Equivalent Isotropic Displacement Parameters (Å^2 $\times$ 10^3) for [Cs][$(SO_2)_2N_3^-$]

	x	*y*	*z*	*U*(eq)[a]
Cs(1)	2061(1)	768(1)	8967(1)	18(1)
S(1)	5507(1)	2332(1)	7631(2)	17(1)
S(2)	7207(1)	5091(1)	10692(2)	18(1)
O(3)	8352(4)	4630(3)	12259(4)	24(1)
O(4)	7694(5)	6163(3)	9883(5)	28(1)
O(1)	4375(4)	3355(3)	7554(5)	25(1)
O(2)	5671(4)	1419(3)	9016(5)	24(1)
N(3)	9574(5)	2165(4)	10774(6)	26(1)
N(2)	8664(5)	2788(3)	9789(5)	20(1)
N(1)	7672(5)	3467(4)	8786(6)	25(1)

[a] U(eq) is defined as one-third of the trace of the orthogonalized U^{ij} tensor.

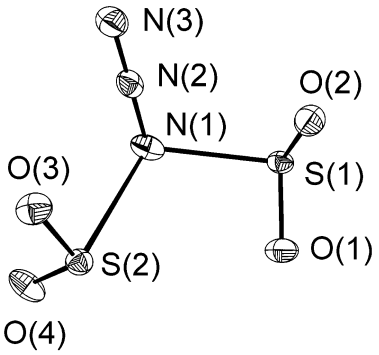

Figure 1. Structure of the $(SO_2)_2N_3^-$ ion in [Cs][$(SO_2)_2N_3$]. Thermal ellipsoids are shown at the 50% probability level.

observed for the two SO_2 ligands in $(SO_2)_2N_3^-$ is in contrast to the calculated structure of the free gaseous anion, in which both SO_2 ligands exhibit similar S−N distances. The differences between the observed solid state and the calculated gas-phase structures are likely due to packing effects

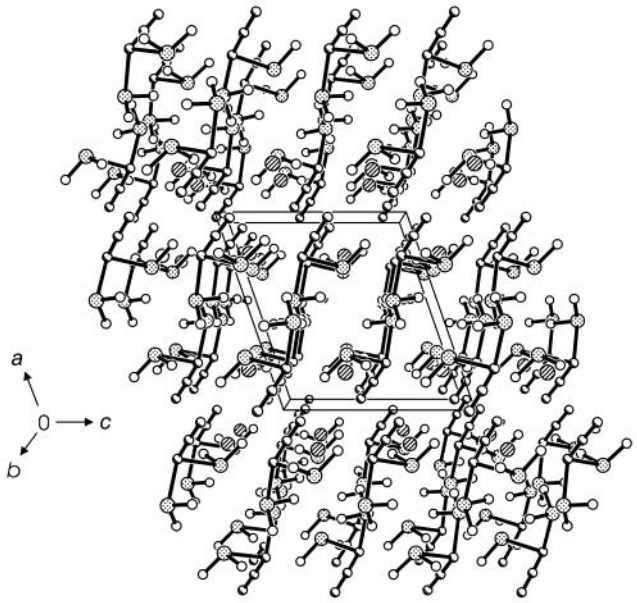

Figure 2. View of the packing of [Cs][$(SO_2)_2N_3$] along the *b*-axis.

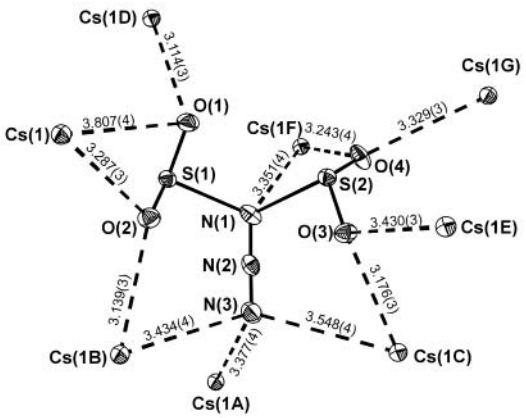

Figure 3. Closest interionic contacts (Å) in [Cs][$(SO_2)_2N_3$]. Thermal ellipsoids are shown at the 50% probability level.

and anion−cation interactions in the solid state. The Cs^+ cation forms strong interionic contacts to N(1), N(3), and the oxygen atoms of the anion which are as short as 3.114-(3) Å (Figure 3). Because of the weakness of the N−S bonds, the orientation of the SO_2 groups in the $(SO_2)_2N_3^-$ anion is largely governed by the contacts to the Cs^+ cations. The agreement between the calculated and observed structures of the $(SO_2)_2N_3^-$ anion is quite good considering the weak S−N bonds and the strong anion−cation interactions.

The observed structure of the 1,1-$(SO_2)_2N_3^-$ anion is in agreement with the previous predictions[12] which were based on the experimental vibrational spectra of the Cs^+ and $N(CH_3)_4^+$ salts. The 1,1-isomer has been calculated to be more stable than the 1,3-$(SO_2)_2N_3^-$ anion by 3.5 (0.4) kcal/mol at the B3LYP (MP2) level of theory.[12] Preferential 1,1-coordination has also been observed for the $H_2N_3^+$ cation[20] and dinuclear metal azide complexes.[21]

(20) Christe, K. O.; Wilson, W. W.; Dixon, D. A.; Khan, S. I.; Bau, R.; Metzenthin, T.; Lu, R. *J. Am. Chem. Soc.* **1993**, *115*, 1836.
(21) Kornath, A. *Angew. Chem.* **2001**, *113*, 3231; *Angew. Chem., Int. Ed.* **2001**, *40*, 3135.

Conclusions. At low temperature, yellow $[Cs][(SO_2)_2N_3]$ crystallizes from a solution of CsN_3 in liquid SO_2. The crystal structure of $[Cs][(SO_2)_2N_3]$ contains the $(SO_2)_2N_3^-$ anion in which both SO_2 ligands are coordinated to the same terminal nitrogen. This study provides the first crystal structure of a halide or pseudohalide anion bound to more than one SO_2 ligand.

Acknowledgment. The authors thank the National Science Foundation, the Defense Advanced Projects Agency, and the Air Force Office of Scientific Research for financial support. M.G. thanks the Natural Sciences and Engineering Research Council of Canada for a postdoctoral fellowship, and R. H. thanks the Deutsche Forschungsgemeinschaft for a postdoctoral fellowship.

Supporting Information Available: Additional tables in PDF format. Tables of structure determination summary, atomic coordinates, bond lengths and angles and anisotropic displacement parameters of $[Cs][(SO_2)_2N_3]$ in CIF format. This material is available free of charge via the Internet at http://pubs.acs.org.

IC0259078

APPENDIX H

"Experimental Detection of the Pentaazacyclopentadienide (Pentazolate) Anion, *cyclo*-N_5^-"
Angew. Chem. Int. Ed., 41, 3051 (2002)

This Page Intentionally Left Blank

Experimental Detection of the Pentaazacyclopentadienide (Pentazolate) Anion, *cyclo*-N_5^-**

Ashwani Vij,* James G. Pavlovich, William W. Wilson, Vandana Vij, and Karl O. Christe*

Dedicated to Professor George Olah on the occasion of his 75th birthday

Nitrogen and oxygen are unique among the chemical elements. In contrast to the other elements, their homonuclear single-bond energies are significantly less than one third of their triple- or one half of their double-bond energies. Consequently, homonuclear polynitrogen and polyoxygen species are thermodynamically highly unstable and the number of known compounds is very limited. Owing to the highly endothermic heats of formation, their syntheses and handling present great challenges. It is, therefore, no surprise that for oxygen only one metastable allotrope, that is, ozone, is known and for nitrogen none are known that can be isolated in bulk, while most other elements can exist in the form of many stable allotropes.

Polynitrogen compounds have been studied extensively for the last two decades. In view of the great experimental difficulties, most of the efforts have been limited to theoretical studies.[1–9] The first major breakthrough in the synthesis area was achieved in 1999 with the synthesis of the N_5^+ ion in the form of a marginally stable AsF_6^- salt.[10] Subsequently, the thermally more stable $N_5^+SbF_6^-$ was synthesized, and the crystal structure of $N_5^+Sb_2F_{11}^-$ was determined.[11]

Based on Born–Haber cycle considerations, the stability of an ionic salt is governed by three factors: the lattice energy, the electron affinity of the cation, and the first ionization potential of the anion. Furthermore, each ion must possess a sufficiently high activation energy barrier toward decomposition. For the successful combination of N_5^+ with a polynitrogen anion in the form of a stable salt, an anion with a high first ionization potential is required. Theoretical calculations from our and other[1,5,8,12–18] research groups predict that the unknown pentazolate anion (see Figure 1) has a first ionization potential and activation energy barrier toward decomposition that might be high enough for the formation of stable $N_5^+N_5^-$. As a result, the synthesis of the N_5^- ion is hotly pursued in numerous laboratories.

Although the existence and stability of substituted pentazole ring compounds have been demonstrated successfully more than 40 years ago by Huisgen and Ugi[19–22] and substituted pentazoles have been well characterized,[23–28] all attempts to prepare either the parent HN_5 molecule[29,30] or its anion, N_5^-, have so far been unsuccessful. Herein, we report the first experimental detection of this important anion.

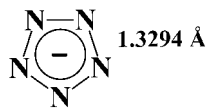

Figure 1. Minimum energy structure of the planar D_{5h} pentazolate anion from ref. [1], calculated at the CCSD(T)/aug-cc-pVTZ level of theory.

In our pursuit of the N_5^- ion, the following strategy was employed: a) the use of Ugi–Huisgen-type, substituted phenylpentazoles as starting materials; b) the transfer of maximum negative charge to the pentazole ring by the use of highly electron-donating substituents on the phenyl ring in *para*-position to the pentazolyl substituent to increase the aromaticity and stability of the pentazole ring, while at the same time weakening the connecting C–N bond; c) the selective cleavage of the C–N bond, while keeping the N–N bonds of the pentazole ring intact; and d) the use of an analytical method that is ideally suited for the generation and detection of anions. Similar approaches have been described, but attempts to cleave the C–N bond by ozonolysis were unsuccessful.[22,31] The reasons, outlined above, prompted us to choose *para*-hydroxy-[31] and *para*-dimethylamino-substituted phenylpentazoles[21] as starting materials and negative-ion electrospray ionization mass spectrometry (ESI-MS)[32–34] as the analytical tool.

The arylpentazoles and the corresponding diazonium salt precursors were prepared and characterized by multinuclear NMR spectroscopy.[24–28] For the cleavage experiments, these pentazoles were dissolved in strongly polar solvents, such as CH_3CN or a mixture of CH_3OH and CH_2Cl_2, and infused into the spectrometer's ion source at 10 μL min^{-1} with a syringe pump.[35] In tandem mass spectrometry (MS-MS) experiments, the desired negative-ion peaks are mass-selected and subjected to product ion mass analysis following collision-induced dissociation (CID) at variable collision voltages using N_2 or Ar as the collision gas.

The most interesting results were obtained with *para*-hydroxyphenylpentazole in CH_3CN. An intense [parent–H]$^-$ base peak was observed at *m*/*z* 162 and mass-selected for subsequent MS-MS studies (Figure 2). It was found advantageous to add a base, such as pyridine, to the CH_3CN solutions to increase significantly the concentration of this *para*-pentazolylphenolate anion. Using a low collision voltage of −10 V, the *m*/*z* 162 ion $[OC_6H_4N_5]^-$ underwent stepwise N_2, N_2, and CO loss (see Scheme 1), giving rise to intense peaks with *m*/*z* values of 134 $[OC_6H_4N_3]^-$, 106 $[OC_6H_4N]^-$, and 78 $[C_5H_4N]^-$, respectively. The loss of the first N_2 molecule is due

[*] Dr. A. Vij, Dr. K. O. Christe, Dr. W. W. Wilson, V. Vij
ERC, Inc. and Propulsion Sciences and Advanced Concepts Division
Air Force Research Laboratory (AFRL/PRSP)
Edwards Air Force Base, CA 93524 (USA)
Fax: (+1) 661-275-5471
E-mail: ashwani.vij@edwards.af.mil
karl.christe@edwards.af.mil
and
Loker Hydrocarbon Research Institute
University of Southern California
Los Angeles, CA 90089-1661 (USA)
Dr. J. G. Pavlovich
Department of Chemistry
University of California, Santa Barbara, CA 93106 (USA)

[**] This work was funded predominantly by the Defense Advanced Research Projects Agency, with additional support from the Air Force Office of Scientific Research and the National Science Foundation. The mass spectrometer instrumentation at UCSB was supported under the Army Research Office Award no. DAAD19-00-1-0026. We thank Dr. Robert Corley, Dr. Arthur Morrish, Dr. Don Woodbury, Dr. Michael Berman, and Prof. W. Kaska for their support, and Dr. Michael Gerken, Dr. Thorsten Schroer, Dr. Stefan Schneider, Dr. Ralf Haiges, Dr. Ross Wagner, and Dr. Suresh Suri for their collaboration and stimulating discussions.

  0044-8249/02/4116-3051 $ 20.00+.50/0

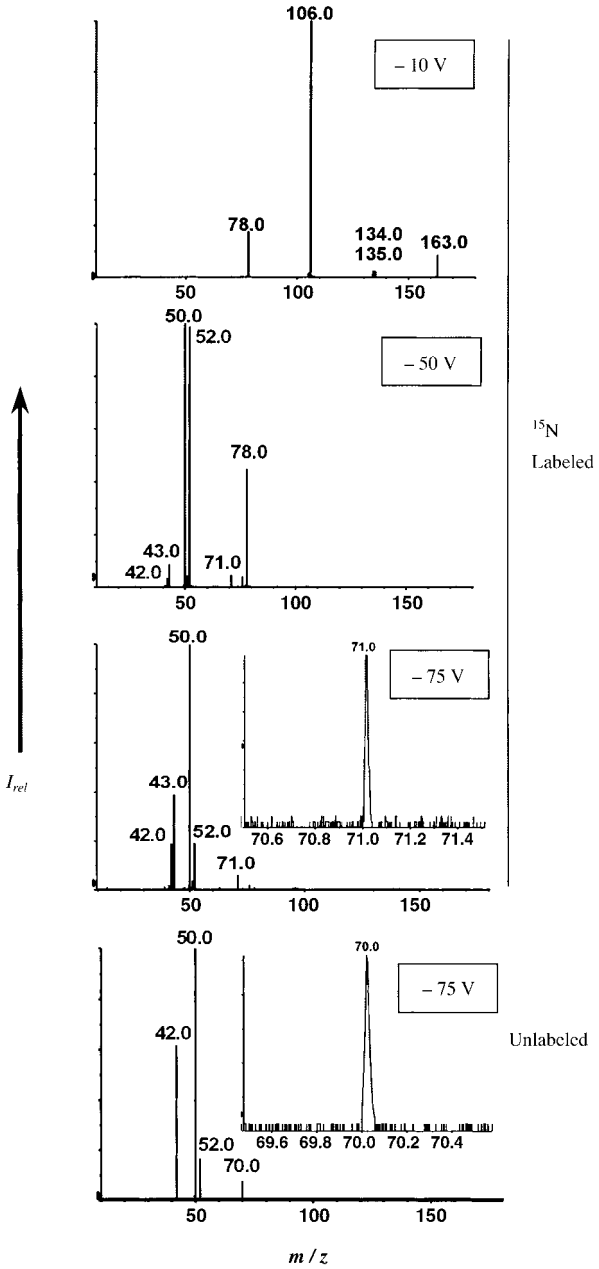

Figure 2. Negative ion, full-range CID mass spectra of the mass selected, ^{15}N labeled (*m/z* 163) and unlabeled (*m/z* 162) peaks due to $[OC_6H_4N_5]^-$ recorded at collision voltages of −75, −50, and −10 V. All spectra are multichannel spectra and the typical mass resolution and noise level are shown for the *m/z* 70 and 71 peaks in the inserts.

to the opening of the pentazole ring and produces the 4-azidophenolate ion. The second N_2 loss occurs from the azido group and generates the deprotonated quinone–imide, $[N{=}C_6H_4{=}O]^-$. This ion then undergoes CO extrusion giving a $[C_5H_4N]^-$ ion. Secondary fragmentation of the *m/z* 134 ion at a collision voltage of −30 V gave rise to intense peaks at *m/z* 78 $[C_5H_4N]^-$, 52 $[C_3H_2N]^-$, and 50 $[C_3N]^-$. The product ion spectra of the *m/z* 106 and 78 ions at collision voltages of −75 V gave only a very intense *m/z* peak at 50 $[C_3N]^-$.

Using high collision voltages of about −75 V for the CID of the *m/z* 162 ion, however, gave a very different fragmentation pattern. The only peaks observed were *m/z* 70, 52, 50, and 42. The *m/z* 70 peak can only be due to N_5^-, and the *m/z* 52 and 50

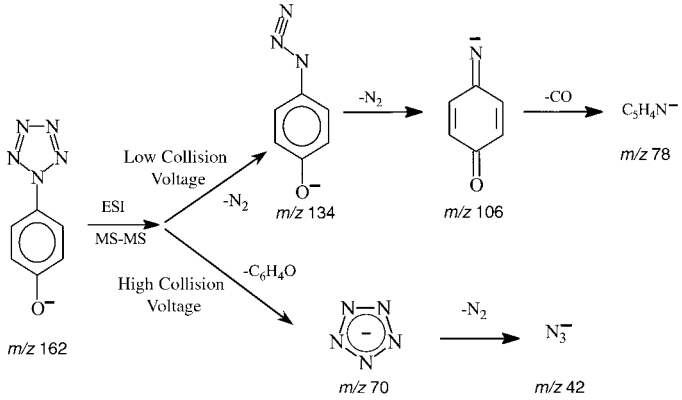

Scheme 1. ESI-MS-MS fragmentation of the mass-selected unlabeled 4-pentazolylphenolate anion at low and high collision voltages.

peaks are due to $[C_3H_2N]^-$ and $[C_3N]^-$, respectively, and, as shown above, result from the fragmentation of the $[C_5H_4N]^-$ ion. The *m/z* 42 peak is attributed to the azide anion, N_3^-. Since the 4-azidophenolate ion does not eliminate N_3^- but only N_2 (see above results for the MS-MS of the *m/z* 134 peak), the N_3^- ion can only come from the decomposition of an N_5^- ion. These results clearly demonstrate that at high collision voltages the pentazolate anion is formed. The fragmentation of the *m/z* 70 ion to N_3^- by loss of dinitrogen is in accord with the theoretically predicted decomposition pathway of N_5^-[8] and further supports its identification as N_5^-.

Additional evidence for the formation of the pentazolate anion was obtained by studies using ^{15}N labeled 4-hydroxyphenylpentazole. In these experiments, the 4-hydroxyphenyldiazonium salt was reacted with azide that was ^{15}N labeled in one terminal position. This resulted in a pentazole ring containing one ^{15}N label either in the N2, N3, N4, or N5 positions. Its ESI-MS spectrum (see Figure 2 and Scheme 2) at high collision voltages gave the *m/z* 71 peak expected for a singly labeled pentazolate anion. Furthermore, the observation of both an *m/z* 135 peak and an *m/z* 134 peak for the ^{15}N-labeled and unlabeled $[OC_6H_4N_3]^-$ ions, respectively, and of single *m/z* 106 and 78 peaks provides proof that the first two steps of the low collision voltage decomposition must involve

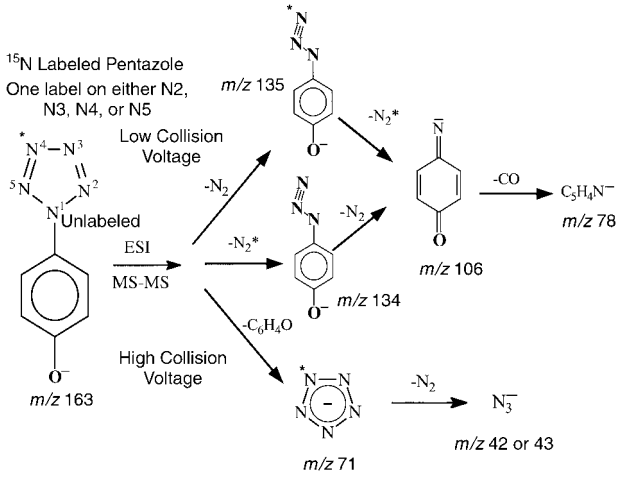

Scheme 2. ESI-MS-MS fragmentation observed for the mass-selected ^{15}N singly labeled 4-pentazolylphenolate anion at low and high collision voltages.

  0044-8249/02/4116-3052 $ 20.00+.50/0

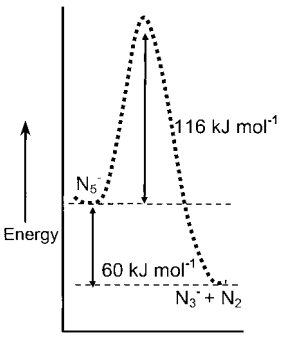

Figure 3. Activation energy barrier and decomposition enthalpy of the pentazolate anion calculated at the CCSD(T)/aug-cc-pVTZ level of theory.[8]

N_2 elimination, while the third step is the CO extrusion from the $[N{=}C_6H_4{=}O]^-$ ion.

The N_3^- and N_2 fragments have been calculated at the CCSD(T)/aug-cc-pVTZ level of theory to be 60 kJ mol^{-1} lower in energy than N_5^-, with an energy barrier of 116 kJ mol^{-1} to the cycloreversion (Figure 3).[8] These values indicate that bulk N_5^- salts should be manageable on a preparative scale. Furthermore, the formation of the N_5^- ion from a starting material containing a pentazole ring and the vibrational instability of open-chain N_5^-[8] establish beyond doubt that the observed N_5^- species must be the long-sought pentazolate anion.

In summary, our results constitute the first experimental detection of the pentazolate anion and demonstrate that in suitably substituted phenylpentazoles the C–N bond can be cleaved while leaving the pentazole ring intact. Since the substituted phenylpentazoles are easily accessible, this approach holds great promise for the bulk synthesis of N_5^- salts, and experiments in this direction are in progress in our laboratories. The pentazolate anion is the polynitrogen counterpart to the cyclopentadienide anion. It, therefore, has great potential as a pentahapto ligand for transition metals[13,36] and could lay the foundation for a field of purely inorganic metallocene-type chemistry. Our results on N_5^+[10,11] and N_5^-, together with the recent observations of the N_4 molecule as a metastable species with a lifetime exceeding one microsecond,[37] the observation of a new but ill-characterized polynitrogen species from a discharge generated nitrogen plasma,[38] and exciting progress in high nitrogen compounds,[28,39] indicate a bright future for experimental polynitrogen chemistry.

Experimental Section

Caution! Although no explosions were encountered in the course of this work, pentazoles can spontaneously lose nitrogen and should be handled by using appropriate safety precautions (small scale, face shield, leather gloves, protective clothing, and blast shields) until reliable safety data for these compounds become available.

The NMR spectra were recorded at 400.13 MHz (^{1}H), 100.62 MHz (^{13}C), 29.91 MHz (^{14}N), and 40.56 MHz (^{15}N) on a Bruker Avance 400 NMR spectrometer using solutions in a standard glass precision 5 mm tube at -10 ± 1 °C. The pentazoles are more stable in 1:1 mixtures of CD_2Cl_2 and CD_3CN than in other solvent mixtures that contain some CD_3OD. The following external references were used: ^{1}H, TMS (0 ppm), ^{13}C (CD_2Cl_2) 54.00 ppm or (CD_3CN) 1.39 ppm referenced to $(CH_3)_4Si$ (0 ppm); $^{14/15}$N, 1:1 mixture of 50 % ^{15}N labeled CD_3NO_2 and CH_3NO_2 (0 ppm).

The following arylpentazoles were prepared from the corresponding aryldiazonium salts and sodium azide in water at ice/salt-bath temperatures: *para*-R-C_6H_4-*cyclo*-N_5 (R = OH, O^- (for the counterions see below), OCH_3, OC_6H_5, $N(CH_3)_2$, O-C_6H_4-*cyclo*-N_5). For the preparation of ^{15}N-labeled pentazoles, singly labeled $Na^+[^{15}N{=}N{=}N]^-$ was used. In a typical preparation, 4-hydroxyaniline hydrochloride (2.4 mmol) was dissolved in water (≈ 15 mL) in a 50 mL beaker, cooled in an ice-salt bath, and slightly acidified with 1N aqueous HCl. A cold solution of sodium nitrite (2.6 mmol) in water (~ 10 mL) was slowly added with vigorous stirring, resulting in the instant formation of 4-hydroxyphenyldiazonium chloride. A cold aqueous solution of sodium azide (2.5 mmol) was slowly added with stirring, resulting in spontaneous effervescence and the formation of a brownish solid. This solid was filtered off at 0 °C, washed with ice-cold water and then with cold methanol (−25 °C) twice, and finally dried in vacuo. 4-Hydroxyphenylpentazole was obtained in 20–35 % yield, contaminated with ≈ 10 % of 4-hydroxyphenylazide, and characterized by multinuclear NMR studies. For the preparation of the cesium or tetramethylammonium (TMA) salts, equivalent amounts of $N(CH_3)_4OH$ or $CsOCH_3$ in methanol, respectively, were added to the 4-hydroxyphenylpentazole solutions at −40 °C and these solutions were then allowed to warm slowly to −10 °C. Alternatively, the 4-pentazolylphenolate anion could be generated by adding pyridine to a solution of 4-hydroxyphenylpentazole in CH_3CN at −25 °C.

For the following ^{1}H NMR spectra, H_a and H_b correspond to the hydrogen atoms at the *ortho* and *meta* positions, respectively, relative to the pentazole-bearing carbon atom (C_{ipso}), and for the ^{13}C NMR spectra, the carbon in the *para* position, bearing the electron-releasing group, that is -OH or -O^-, is labeled as (C_p). In the case of the $^{14/15}$N NMR spectra, N1 is the nitrogen atom in the pentazole ring that is bonded to the aryl group, N2/N5 are bonded directly to N1, and N3 and N4 are bonded to N2 and N5, respectively. In the corresponding azides, N1 refers to the nitrogen atom attached to the phenyl group and N3 is the terminal nitrogen atom. The ^{15}N-labeled azides were obtained by the thermal decomposition of the corresponding pentazoles at 25 °C, resulting in the 2 and 3 positions being labeled. Evolved N_2 gas can be observed at $\delta = -72$ ppm (literature value $\delta = -73$ ppm[25]). Spectral data, obtained for the compounds in either a 1:1 mixture of CD_2Cl_2 and CD_3CN or a mixture of other solvents are:

4-Hydroxyphenylpentazole: ^{1}H: $\delta = 7.02$ (H_b AB, 2H, $^3J_{H,H} = 9.2$ Hz), 7.95 ppm (H_a AB, 2H, $^3J_{H,H} = 9.2$ Hz); ^{13}C: $\delta = 126.4$ (s, C_i), 123.2 (s, C_o), 117.0 (s, C_m), 161.2 ppm (s, C_p); ^{14}N: $\delta = -81.6$ ppm (br, N1); ^{15}N: $\delta = 4.2$ (s, N2/N5), −27.6 ppm (s, N3/N4). Literature values[31]: ^{1}H: $\delta = 7.04$ (d, H_b, $J = 6.4$ Hz), 8.01 ppm (d, 2H, $J = 6.5$ Hz). The previously reported coupling constant of about 6.4 Hz appears to be incorrect.

4-Hydroxyphenylazide: ^{1}H: $\delta = 6.75$ (H_b AB, 2H, $^3J_{H,H} = 8.8$ Hz), 6.83 ppm (H_a AB, 2H, $^3J_{H,H} = 8.8$ Hz); ^{13}C: $\delta = 131.5$ (s, C_i), 120.4 (s, C_o), 116.9 (s, C_m), 155.3 ppm (s, C_p), ^{15}N: $\delta = -136.6$ (s, N2), −149.1 ppm (s, N3); ^{15}N: $\delta = -141.2$ (s, N2), −152.5 ppm (s, N3). Literature values [40]: ^{1}H: $\delta = 6.83$ (H_b d, 2H, $J = 9$ Hz), 6.92 ppm (H_a d, 2H, $J = 9$ Hz).

Cesium/TMA 4-pentazolylphenolate: ^{1}H: $\delta = 6.66$ (H_b AB, 2H, $^3J_{H,H} = 7.2$ Hz), 6.74 ppm (H_a AB, 2H, $^3J_{H,H} = 7.2$ Hz); ^{13}C: $\delta = 122.8$ (s, C_i), 120.7 (s, C_o), 119.9 (s, C_m), 172.1 ppm (s, C_p); ^{14}N: $\delta = -81.1$ ppm (br, N1); ^{15}N: $\delta = 1.9$ (s, N2/N5), −29.7 ppm (s, N3/N4).

Cesium/TMA 4-azidophenolate: ^{1}H: $\delta = 6.61$ (H_b AB, 2H, $^3J_{H,H} = 6.8$ Hz), 7.95 ppm (H_a AB, 2H, $^3J_{H,H} = 6.8$ Hz); ^{13}C: $\delta = 125.1$ (s, C_i), 120.2 (s, C_o), 120.1 (s, C_m), 165.4 ppm (s, C_p); ^{15}N: $\delta = -135.7$ (s, N2), −150.9 ppm (s, N3). Literature values [31]: CD_3OD (CD_2Cl_2): ^{1}H: $\delta = 6.59$ (6.47) (d, 2H, $J = 9.0$ (8.8) Hz), 6.69 ppm (6.65) (d, 2H, $J = 9.0$ (8.8) Hz); ^{15}N (CD_2Cl_2): $\delta = -131.7$ (s, 1N), −148.4 ppm (s, 1N). In the literature data,[31] no assignments to the individual nitrogen atoms were given, and due to the nuclear Overhauser effect, the ^{15}N signals cannot be integrated.

Received: April 30, 2002
Revised: July 3, 2002 [Z19192]

[1] R. J. Bartlett, *Chem. Ind.* **2000**, 140, and references therein; a compilation of data for N_2 to N_{10} can be found at http://www.qtp.ufl.edu/~bartlett/polynitrogen.pdf.
[2] S. Fau, R. J. Bartlett, *J. Phys. Chem. A* **2001**, *105*, 4096.
[3] M. Tobita, R. J. Bartlett, *J. Phys. Chem. A* **2001**, *105*, 4107.
[4] T. M. Klapötke, *Angew. Chem.* **1999**, *111*, 2694; *Angew. Chem. Int. Ed.* **1999**, *38*, 2536, and references therein.
[5] M. N. Glukhovtsev, H. Jiao, P. von R. Schleyer, *Inorg. Chem.* **1996**, *35*, 7124.
[6] H. H. Michels, J. A. Montgomery, Jr., K. O. Christe, D. A. Dixon, *J. Phys. Chem.* **1995**, *99*, 187.
[7] M. W. Schmidt, M. S. Gordon, J. A. Boatz, *Int. J. Quantum Chem.* **2000**, *76*, 434; G. Chung, M. W. Schmidt, M. S. Gordon, *J. Phys. Chem. A* **2000**, *104*, 5647.
[8] M. T. Nguyen, T. K. Ha, *Chem. Phys. Lett.* **2001**, *335*, 311.

  0044-8249/02/4116-3053 $ 20.00+.50/0

[9] X. Wang, H. R. Hu, A. Tian, N. B. Wong, S. H. Chien, W. K. Li, *Chem. Phys. Lett.* **2000**, *329*, 483.
[10] K. O. Christe, W. W. Wilson, J. A. Sheehy, J. A. Boatz, *Angew. Chem.* **1999**, *111*, 2112; *Angew. Chem. Int. Ed.* **1999**, *38*, 2004.
[11] A. Vij, W. W. Wilson, V. Vij, F. S. Tham, J. A. Sheehy, K. O. Christe, *J. Am. Chem. Soc.* **2001**, *123*, 6308.
[12] L. Gagliardi, G. Orlandi, S. Evangelisti, B. O. Roos, *J. Chem. Phys.* **2001**, *114*, 10733.
[13] M. Lein, J. Frunzke, A. Timoshkin, G. Frenking, *Chem. Eur. J.* **2001**, *7*, 4155.
[14] S. Fau, K. J. Wilson, R. J. Bartlett, *J. Phys. Chem. A* **2002**, *106*, 4639.
[15] M. T. Nguyen, M. Sana, G. Leroy, J. Elguero, *Can. J. Chem.* **1983**, *61*, 1435.
[16] M. T. Nguyen, M. A. McGinn, A. F. Hegarty, J. Elguero, *Polyhedron* **1985**, *4*, 1721.
[17] V. A. Ostrovskii, G. B. Erusalimskii, M. B. Shcherbinin, *Russ. J. Org. Chem.* **1995**, *31*, 1284.
[18] M. N. Glukhovtsev, P. von R. Schleyer, C. Maerker, *J. Phys. Chem.* **1993**, *97*, 8200.
[19] R. Huisgen, I. Ugi, *Angew. Chem.* **1956**, *68*, 705; R. Huisgen, I. Ugi, *Chem. Ber.* **1957**, *90*, 2914.
[20] I. Ugi, R. Huisgen, *Chem. Ber.* **1958**, *91*, 531.
[21] I. Ugi, H. Perlinger, L. Behringer, *Chem. Ber.* **1958**, *91*, 2324.
[22] I. Ugi, *Angew. Chem.* **1961**, *73*, 172.
[23] J. D. Wallis, J. D. Dunitz, *J. Chem. Soc. Chem. Commun.* **1983**, 910.
[24] M. Witanowski, L. Stefaniak, H. Januszewski, K. Bahadur, G. A. Webb, *J. Cryst. Mol. Struct.* **1975**, *5*, 137.
[25] R. Müller, J. D. Wallis, W. v. Philipsborn, *Angew. Chem.* **1985**, *97*, 515; *Angew. Chem. Int. Ed. Engl.* **1985**, *24*, 513.
[26] R. N. Butler, S. Collier, A. F. M. Fleming, *J. Chem. Soc. Perkin Trans. 2* **1996**, 801.
[27] a) R. N. Butler, A. Fox, S. Collier, L. A. Burke, *J. Chem. Soc. Perkin Trans. 2* **1998**, 2243; b) L. A. Burke, R. N. Butler, J. C. Stephens, *J. Chem. Soc. Perkin Trans. 2* **2001**, 1679.
[28] A. Hammerl, T. M. Klapötke, *Inorg. Chem.* **2002**, *41*, 906.
[29] R. Janoschek, *Angew. Chem.* **1993**, *105*, 242; *Angew. Chem. Int. Ed. Engl.* **1993**, *32*, 230.
[30] K. F. Ferris, R. J. Bartlett, *J. Am. Chem. Soc.* **1992**, *114*, 8302.
[31] V. Benin, P. Kaszynski, J. G. Radziszewski, *J. Org. Chem.* **2002**, *67*, 1354.
[32] M. Yamashita, J. B. Fenn, *J. Chem. Phys.* **1984**, *88*, 4451; C. M. Whitehouse, R. N. Dreyer, M. Yamashita, J. B. Fenn, *Anal. Chem.* **1985**, *57*, 675.
[33] *Electrospray Ionization Mas Spectrometry* (Ed.: R. B. Cole), Wiley-Interscience, New York, **1997**.
[34] B. H. Lipshutz, K. L. Stevens, B. James, J. G. Pavlovich, J. P. Snyder, *J. Am. Chem. Soc.* **1996**, *118*, 6796.
[35] The MS and MS-MS experiments were carried out on a PE Sciex Qstar Pulsar quadrupole/time-of-flight tandem mass spectrometer (Applied Biosystems, Foster City, California) operated with a room temperature turbo-ionspray source and using Analyst QS data acquisition software. The samples were dissolved in a 1:10 mixture of pyridine and acetonitrile, and infused via a syringe pump at 5 μL min^{-1}. The instrument was run in the negative ion mode with the capillary voltage at −4500 V and the dissociation potential (source CID) at −20 V. The TOF Pulser frequency was set for 5 kHz with a 1 s accumulation time per spectrum. Data were aquired over the mass range of 10–600 *m*/*z* for MS acquisition. In the MS-MS mode, the quadrupole mass analyzer was set to pass the parent ion at unit mass resolution. N_2 or Ar was used as the collision gas. The gas settings were as follows: source nebulizer gas = 30, desolvation gas = 0, curtain gas = 25, collision gas = 5.
[36] L. Gagliardi, P. Pyykkö, *J. Phys. Chem.* **2002**, in press.
[37] F. Cacace, G. de Petris, A. Troiani, *Science* **2002**, *295*, 480.
[38] J. P. Zheng, J. Waluk, J. Spanget-Larsen, D. M. Blake, J. G. Radziszewski, *Chem. Phys. Lett.* **2000**, *328*, 227.
[39] D. E. Chavez, M. A. Hiskey, R. D. Gilardi, *Angew. Chem.* **2000**, *112*, 1681; *Angew. Chem. Int. Ed.* **2000**, *39*, 1791.
[40] I. R. Dunkin, A. A. El-Ayeb, S. L. Gallivan, M. A. Lynch, *J. Chem. Soc. Perkin Trans. 2* **1997**, 1419.

First Synthesis of Optically Pure Propargylic *N*-Hydroxylamines by Direct, Highly Diastereoselective Addition of Terminal Alkynes to Nitrones**

Roger Fässler, Doug E. Frantz, Jürg Oetiker, and Erick M. Carreira*

Dedicated to Professor Andrea Vasella

Optically active propargylic alcohols serve as versatile building blocks for asymmetric synthesis.[1] The corresponding propargylic amines or *N*-hydroxylamines could also serve in a similar capacity were it not for the fact that general, useful methods that provide access to such compounds are not available.[2] The latter are not only synthetic equivalents of the former, but also are amenable to further elaborations, such as cyclization to afford isoxazolines.[3] Herein, we document the first general method for the preparation of optically active propargylic *N*-hydroxylamines [Eq. (1), Tf = trifluoromethanesulfonyl]. The method prescribes the use of nitrones which are conveniently prepared through condensation of the corresponding aldehydes and a mannose-derived glycosidic *N*-hydroxylamine.[4] Reaction of the nitrones with a broad range of terminal acetylenes in the presence of Zn^{II} ions, 2-dimethylaminoethanol, and NEt_3 gives adducts in high diastereoselectivity and yield. Following its addition, the auxiliary is easily removed by treatment of the products with *N*-hydroxylamine hydrochloride; a process which allows for re-isolation and reuse of the auxiliary. The method we document should find use in medicinal chemistry to provide access to a new class of useful building blocks for the asymmetric synthesis of pharmacologically important compounds.

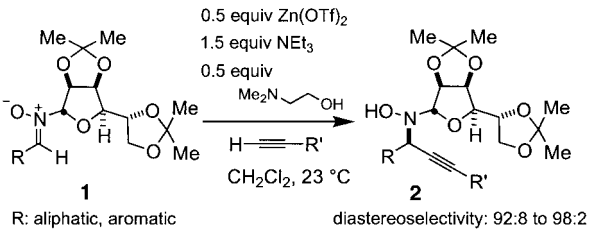

(1)

There are scant, scattered reports that document diastereoselective additions to chiral nitrones. These typically involve additions of Grignard or organolithium compounds

[*] Prof. Dr. E. M. Carreira, R. Fässler, J. Oetiker
Laboratorium für Organische Chemie
ETH Hönggerberg
Wolfgang-Pauli-Strasse 10, 8093 Zürich (Switzerland)
Fax: (+41) 1-632-1328
E-mail: carreira@org.chem.ethz.ch
Dr. D. E. Frantz
Merck & Co., Inc, WYN-3
466 Devon Park Drive
Wayne, PA 19087 (USA)

[**] We thank the ETH, Roche Research Foundation, the Swiss National Science Foundation, Merck, and Aventis for their generous support.

Supporting information for this article is available on the WWW under http://www.angewandte.org or from the author.

  0044-8249/02/4116-3054 $ 20.00+.50/0

APPENDIX I

"Enthalpies of Formation of Gas Phase N_3, N_3^-, N_5^+, and N_5^- from *Ab Initio* Molecular Orbital Theory, Stability Predictions for $N_5^+N_3^-$ and $N_5^+N_5^-$, and Experimental Evidence for the Instability of $N_5^+N_3^-$"
J. Am. Chem. Soc., 126, 834 (2004)

This Page Intentionally Left Blank

J|A|C|S
ARTICLES
Published on Web 12/24/2003

Enthalpies of Formation of Gas-Phase N_3, N_3^-, N_5^+, and N_5^- from Ab Initio Molecular Orbital Theory, Stability Predictions for $N_5^+N_3^-$ and $N_5^+N_5^-$, and Experimental Evidence for the Instability of $N_5^+N_3^-$

David A. Dixon,*,† David Feller,† Karl O. Christe,*,‡,§ William W. Wilson,‡ Ashwani Vij,‡ Vandana Vij,‡ H. Donald Brooke Jenkins,|| Ryan M. Olson,⊥ and Mark S. Gordon⊥

Contribution from the Chemical Sciences Division and Fundamental Sciences Directorate, Pacific Northwest National Laboratory, P.O. Box 999, Richland, Washington 99352, Air Force Research Laboratory, Edwards Air Force Base, California 93524, Loker Hydro-carbon Research Institute, University of Southern California, Los Angeles, California 90089, Department of Chemistry, University of Warwick, Coventry CV4 7AL, West Midlands, U.K., and Department of Chemistry, Spedding Hall, Iowa State University, Ames, Iowa 50011

Received May 27, 2003; E-mail: david.dixon@pnl.gov; kchriste@usc.edu

Abstract: Ab initio molecular orbital theory has been used to calculate accurate enthalpies of formation and adiabatic electron affinities or ionization potentials for N_3, N_3^-, N_5^+, and N_5^- from total atomization energies. The calculated heats of formation of the gas-phase molecules/ions at 0 K are $\Delta H_f(N_3(^2\Pi)) = 109.2$, $\Delta H_f(N_3^-(^1\Sigma^+)) = 47.4$, $\Delta H_f(N_5^-(^1A_1')) = 62.3$, and $\Delta H_f(N_5^+(^1A_1)) = 353.3$ kcal/mol with an estimated error bar of ± 1 kcal/mol. For comparison purposes, the error in the calculated bond energy for N_2 is 0.72 kcal/mol. Born−Haber cycle calculations, using estimated lattice energies and the adiabatic ionization potentials of the anions and electron affinities of the cations, enable reliable stability predictions for the hypothetical $N_5^+N_3^-$ and $N_5^+N_5^-$ salts. The calculations show that neither salt can be stabilized and that both should decompose spontaneously into N_3 radicals and N_2. This conclusion was experimentally confirmed for the $N_5^+N_3^-$ salt by low-temperature metathetical reactions between N_5SbF_6 and alkali metal azides in different solvents, resulting in violent reactions with spontaneous nitrogen evolution. It is emphasized that one needs to use adiabatic ionization potentials and electron affinities instead of vertical potentials and affinities for salt stability predictions when the formed radicals are not vibrationally stable. This is the case for the N_5 radicals where the energy difference between vertical and adiabatic potentials amounts to about 100 kcal/mol per N_5.

Introduction

The discovery of stable N_5^+ salts,[1,2] the long-known existence of stable N_3^- salts,[3] and the recent experimental detection of the N_5^- anion[4] have stimulated research in polynitrogen chemistry and a search for nitrogen allotropes. The high endothermicity of polynitrogen compounds renders their preparation and handling very difficult, and reliable stability predictions are important for the selection of suitable target compounds. The enthalpies of formation of crucial species, such as N_3, N_3^-, N_5, N_5^+, and N_5^-, are not accurately known from experiment, because of the difficulty in handling these compounds and ions. There have been a number of theoretical studies on allotropes of nitrogen using ab initio molecular orbital theory without the use of empirical parameters, but these studies have not reliably established the energetics of these compounds. In particular, we note the extensive work of the Bartlett group on these species,[5,6] the work of Nguyen and Ha on decomposition mechanisms for N_5^x, $x = -1, 0, +1$,[7] and that of Martin and co-workers on N_3.[8] Several theoretical studies on the stability of $N_5^+N_3^-$ and $N_5^+N_5^-$ have been published.[5,6,9] In the most recent work, Fau, Wilson, and Bartlett performed ab initio MP2 and CCSD(T) molecular orbital theory and B3LYP density functional theory calculations on $N_5^+N_5^-$ and $N_5^+N_3^-$ and their individual ions as well as on quasi-periodic clusters of $N_5^+N_5^-$. This work suggested that on a closed shell singlet surface the $N_5^+N_5^-$ ion pair is stable to dissociation into the

† PNNL.
‡ AFRL.
§ USC.
|| University of Warwick.
⊥ Iowa State University.

(1) Christe, K. O.; Wilson, W. W.; Sheehy, J. A.; Boatz, J. A. *Angew. Chem., Int. Ed.* **1999**, *38*, 2004.
(2) Vij, A.; Wilson, W. W.; Vij, V.; Tham, F. S.; Sheehy, J. A.; Christe, K. O. *J. Am. Chem. Soc.* **2001**, *123*, 6308.
(3) Curtius, T. *Ber. Dtsch. Chem. Ges.* **1890**, *23*, 3023.
(4) Vij, A.; Pavlovich, J. G.; Wilson, W. W.; Christe, K. O. *Angew. Chem., Int. Ed.* **2002**, *41*, 3051.
(5) Fau, S.; Bartlett, R. J. *J. Phys. Chem. A* **2001**, *105*, 4096.
(6) Fau, S.; Wilson, K. J.; Bartlett, R. J. *J. Phys. Chem. A* **2002**, *106*, 4639.
(7) Nguyen, M. T.; Ha, T.-K. *Chem. Phys. Lett.* **2001**, *335*, 311. Nguyen, M. T.; Ha, T.-K. *Chem. Phys. Lett.* **2000**, *317*, 135.
(8) Martin, J. M. L.; Francois, J. P.; Gijbels, R. *J. Chem. Phys.* **1990**, *93*, 4485.
(9) Gagliardi, L.; Orlandi, G.; Evangelsti, S.; Roos, B. O. *J. Chem. Phys.* **2001**, *114*, 10733.

10.1021/ja0303182 CCC: $27.50

cation and anion by 114 kcal/mol but is still ~300 kcal/mol above $5N_2$ molecules. Thus, the singlet coupled ion pair represents a metastable structure on the potential energy surface. Approximate transition state searches suggested that the singlet coupled ion pair is stable by 15−25 kcal/mol to dissociation for the channel producing N_3 and N_2. These authors also suggested that $N_5^+N_3^-$ is unlikely to be stable. The authors noted that this is consistent with their calculated vertical electron affinity and ionization potential calculations, suggesting that the $N_5^+N_3^-$ ion pair is less ionic than the $N_5^+N_5^-$ ion pair because the high ionization potential of N_5^-, relative to that of N_3^-, causes in $N_5^+N_5^-$ effective resistance to charge transfer from the anion to the cation.[6]

This interesting concept and our own interests in such compounds led us to perform a different set of calculations on the stability of these compounds. We have also used high level ab initio molecular orbital theory to address the important question of whether the combination of a stable polynitrogen cation, such as N_5^+, with a stable polynitrogen anion, such as N_3^-, can lead to a stable ionic nitrogen allotrope, such as $N_5^+N_3^-$. The stability predictions were made using Born−Haber cycles, a well-established and widely used method[10] for evaluating the stability of ionic salts, if reliable values for the lattice energies of the salts, the first ionization potential of the anion, and the electron affinity of the cation are available. This approach also requires an excellent knowledge of the nature and stability of the most likely decomposition products.

A critical prerequisite for such stability calculations is the use of accurate heats of formation and electron affinities and ionization potentials. We have developed an approach[11] to the reliable calculation of molecular thermodynamic properties, notably enthalpies of formation, based on ab initio molecular orbital theory without using empirical parameters. Our approach involves an accurate calculation of the total atomization energy of a molecule and combines this value with known enthalpies of formation of the atoms to calculate the molecular enthalpy of formation at 0 K. This method starts with coupled cluster theory, including a perturbative triples correction (CCSD(T)),[12−14] combined with the correlation-consistent basis sets[15,16] extrapolated to the complete basis set (CBS) limit to treat the correlation energy of the valence electrons. This step is followed by a number of smaller corrections that are presumed to be additive, including core−valence interactions and relativistic effects, both scalar and spin−orbit. Finally, one must include the zero-point energy obtained from experiment, theory, or some combination. The standard enthalpies of formation of compounds at 298 K can then be calculated from the 0 K value and other calculated properties by using standard thermodynamic and statistical mechanics expressions.[17]

This paper provides a conclusive answer to the question of whether the lattice energies of these salts are sufficient to stabilize them as solids, thus preventing spontaneous electron transfer from the anion to the cation and spontaneous decomposition. Furthermore, for $N_5^+N_3^-$, experimental data are provided in support of our theoretical predictions.

Experimental Section

Caution! Reactions of N_5^+ salts with azide ions are violent and can result in explosions. Therefore, these materials should be handled only on a small scale with appropriate safety precautions (face shield, leather gloves, and protective clothing).

Materials and Apparatus. All reactions were carried out in a Teflon-PFA double U-tube apparatus that consisted of a reaction U-tube, a porous Teflon filter assembly, and a receiver U-tube. Volatile materials were handled on a stainless steel/Teflon-FEP vacuum line.[18] Nonvolatile solids were handled in the dry nitrogen atmosphere of a glovebox. Infrared spectra were recorded on a Mattson Galaxy FT-IR spectrometer using dry powders pressed between AgCl windows in an Econo press (Barnes Engineering Co.). Raman spectra were recorded on a Bruker Equinox 55 FT-RA spectrometer using a Nd:YAG laser at 1064 nm and Pyrex melting point capillaries as sample containers.

The N_5SbF_6 was prepared using our previously reported procedure.[2] The CsN_3 (Aldrich Chemical Co.) was pretreated with an excess of $(CH_3)_3SiN_3$ to remove any traces of moisture. The SO_2 (Air Products) was used as received.

Reactions of N_5SbF_6 with CsN_3. In a typical experiment, N_5SbF_6 (2.285 mmol) and CsN_3 (2.267 mmol) were loaded in the drybox into a Teflon-PFA reaction vessel that was closed by a Teflon valve. On the vacuum line, anhydrous SO_2 (5.0 mL, liquid) was added at −196 °C. The reaction mixture was warmed to the melting point of SO_2 (−64 °C). After the SO_2 had partially melted and the slurry of reactants was gently agitated, a violent reaction took place producing a bright yellow flame. The reactor was quickly quenched with liquid nitrogen. A check for noncondensable gases at −196 °C revealed 9.05 mmol of N_2 as expected for the complete decomposition of 2.267 mmol of N_5N_3 to N_2. Pumping off all volatiles at −64 °C produced 0.8890 g of a white solid residue (weight expected for 2.267 mmol of $CsSbF_6$ = 0.836 g). The extra weight was due to some residual SO_2. Raman and infrared spectra of the white solid, after pumping at room temperature, showed it to be pure $CsSbF_6$.

This reaction can be moderated by the separate dissolution of the starting materials in SO_2 and the combination of the resulting clear solutions at −64 °C. Under these conditions, the decomposition reaction proceeded rapidly but without violence and gave the same results as described above.

Reactions of N_5SbF_6 with NaN_3. To equimolar amounts of NaN_3 and N_5SbF_6 was added CHF_3 as a solvent at −196 °C, and the resulting mixture was warmed to −95 °C and then to −64 °C. No N_2 evolution was observed under these conditions. The CHF_3 was pumped off at −95 °C, and SO_2 was added as a solvent at −196 °C. The mixture was warmed to −64 °C, but again no N_2 evolution was observed. Pumping off the SO_2 at −64 °C resulted in a white solid residue that, based on its room-temperature Raman spectrum, consisted of a mixture of unreacted NaN_3 and N_5SbF_6, indicating that no reactions had occurred due to the very low solubility of NaN_3 in these solvents.

(10) Greenwood, N. N.; Earnshaw, A. *Chemistry of the Elements*, 2nd ed.; Butterworth-Heinemann: Oxford, 1998; p 82.
(11) Peterson, K. A.; Xantheas, S. S.; Dixon, D. A.; Dunning, T. H., Jr. *J. Phys. Chem. A* **1998**, *102*, 2449. Feller, D.; Peterson, K. A. *J. Chem. Phys.* **1998**, *108*, 154. Dixon, D. A.; Feller, D. *J. Phys. Chem. A* **1998**, *102*, 8209. Feller, D.; Peterson, K. A. *J. Chem. Phys.* **1999**, *110*, 8384. Feller, D.; Dixon, D. A. *J. Phys. Chem. A* **1999**, *103*, 6413. Feller, D. *J. Chem. Phys.* **1999**, *111*, 4373. Feller, D.; Dixon, D. A. *J. Phys. Chem. A* **2000**, *104*, 3048. Feller, D.; Sordo, J. A. *J. Chem. Phys.* **2000**, *113*, 485. Feller, D.; Dixon, D. A. *J. Chem. Phys.* **2001**, *115*, 3484. Dixon, D. A.; Feller, D.; Sandrone, G. *J. Phys. Chem. A* **1999**, *103*, 4744. Ruscic, B.; Feller, D.; Dixon, D. A.; Peterson, K. A.; Harding, L. B.; Asher, R. L.; Wagner, A. F. *J. Phys. Chem. A* **2001**, *105*, 1. Ruscic, B.; Wagner, A. F.; Harding, L. B.; Asher, R. L.; Feller, D.; Dixon, D. A.; Peterson, K. A.; Song, Y.; Qian, X.; Ng, C.; Liu, J.; Chen, W.; Schwenke, D. W. *J. Phys. Chem. A* **2002**, *106*, 2727.
(12) Purvis, G. D., III; Bartlett, R. J. *J. Chem. Phys.* **1982**, *76*, 1910.
(13) Raghavachari, K.; Trucks, G. W.; Pople, J. A.; Head-Gordon, M. *Chem. Phys. Lett.* **1989**, *157*, 479.
(14) Watts, J. D.; Gauss, J.; Bartlett, R. J. *J. Chem. Phys.* **1993**, *98*, 8718.
(15) Dunning, T. H., Jr. *J. Chem. Phys.* **1989**, *90*, 1007.
(16) Kendall, R. A.; Dunning, T. H., Jr.; Harrison, R. J. *J. Chem. Phys.* **1992**, *96*, 6796.
(17) Curtiss, L. A.; Raghavachari, K.; Redfern, P. C.; Pople, J. A. *J. Chem. Phys.* **1997**, *103*, 1063.
(18) Christe, K. O.; Wilson, W. W.; Schack, C. J.; Wilson, R. D. *Inorg. Synth.* **1986**, *24*, 39.

Computational Approaches

Enthalpies of Formation. The augmented correlation consistent basis set aug-cc-pVnZ (n = D, T, Q)[19] was used for nitrogen. Only the spherical components (5-*d*, 7-*f*, 9-*g* and 11-*h*) of the Cartesian basis functions were used. This family of basis sets contains an additional shell (e.g., spd for DZ) of diffuse functions that are necessary for an accurate description of anions. Calculations were performed using the MOLPRO,[20] Gaussian,[21] and GAMESS[22] suites of programs. The open shell CCSD(T) calculations were carried out at the R/UCCSD(T) level. In this approach, a restricted open shell Hartree−Fock (ROHF) calculation was initially performed to generate the set of molecular orbitals and the spin constraint was relaxed in the coupled cluster calculation.[23−25] The CCSD(T) total energies were extrapolated to the CBS limit by using a mixed exponential/Gaussian function of the form:

$$E(n) = E_{\mathrm{CBS}} + A\exp[-(n-1)] + B\exp[-(n-1)^2] \qquad (1)$$

with $n = 2$ (aug-cc-pVDZ), 3 (aug-cc-pVTZ), etc., as first proposed by Peterson et al.[26] This extrapolation method has been shown to yield atomization energies in the closest agreement with experiment by a small measure as compared to other extrapolation approaches up through $n = 4$.[8]

Most geometries were optimized at the frozen core CCSD(T) level with various augmented correlation-consistent basis sets. With the exception of the N_5 radical, all geometries were optimized with the aug-cc-pVTZ or aug-cc-pVQZ basis sets. If the CCSD(T)/aug-cc-pVQZ geometry was not available, the CCSD(T)/aug-cc-pVTZ geometry was used for the CCSD(T)/aug-cc-pVQZ calculation. Geometries for the N_5 radicals were obtained from ZAPT2/6-311+G(2df) and CCSD(T)/aug-cc-pVDZ calculations. Vibrational frequencies were calculated at the CCSD(T) and MP2 levels with the aug-cc-pVDZ basis set. Calculations were performed on SGI, IBM, and Apple G4 computers.

Core−valence corrections, ΔE_{CV}, were obtained at the CCSD(T)/cc-pCVTZ level of theory.[27] Scalar relativistic corrections (ΔE_{SR}), which account for changes in the relativistic contributions to the total energies of the molecule and the constituent atoms, were included at the CI-SD (configuration interaction singles and doubles) level of theory using the cc-pVTZ basis set. ΔE_{SR} is taken as the sum of the mass−velocity and 1-electron Darwin (MVD) terms in the Breit−Pauli Hamiltonian.[28] Because N has a ^{4}S ground state, there are no atomic spin−orbit corrections to the total atomization energies. The spin−orbit coupling constant for N_3 is 71.3 cm^{-1} based on experiment,[29] leading to a spin−orbit correction of 0.10 kcal/mol.

By combining our computed $\sum D_0$ values with the known enthalpies of formation[30] at 0 K for N of $\Delta H_f^0(\mathrm{N}) = 112.53 \pm 0.02$ kcal mol^{-1}, we can derive ΔH_f^0 values for the molecules under study in the gas phase. We obtain enthalpies of formation at 298 K by following the procedures outlined by Curtiss and co-workers[16] and by using the stationary electron convention; that is, we do not assume a change in the enthalpy of formation of the electron as a function of temperature.

Lattice Energies. For this study, eq 2[31]

$$U_{\mathrm{L}} = 2I[\alpha V_{\mathrm{m}}^{-1/3} + \beta] \qquad (2)$$

was used to estimate the lattice energy, U_L, of the salts $N_5^+N_5^-$ and $N_5^+N_3^-$ from estimated ion volumes. I is the ionic strength (=1), V_m is the molecular (formula unit) volume of the lattices involved which is equal to the sum of the individual ion volumes of the cation, V_+, and anion, V_-, and α and β take the values 28.0 kcal mol^{-1} nm and 12.4 kcal mol^{-1}, respectively, for 1:1 salts. The individual ion volumes can be estimated from an ion volume database,[31] inferred in some cases from established crystal structure data, or calculated. To calculate the volumes of the ions, we chose to use the volumes that we have used in free energy of solvation calculations.[32] The electron densities were calculated at the B3LYP/6-31+G* level,[33] and the volume was taken to be that inside the 0.001 au contour of the electron density.

Results and Discussion

Calculated Geometries. The calculated geometries for the molecules, N_2, N_3, N_3^-, N_5^-, and N_5^+ are summarized in Table 1.

N_2. As expected, the geometry for N_2 at the CCSD(T)/aug-cc-pVQZ level is in excellent agreement with the experimental value.[34] Theory overestimates experiment by 0.0028 Å. For comparative purposes, we also optimized the N−N bond length with the larger aug-cc-pV5Z basis set. This produced a small 0.0010 Å decrease in the bond length, indicating that the aug-cc-pVQZ bond lengths should be within approximately 0.001 Å of the basis set limit for the other molecules that could be treated at this level of theory. If the frozen core approximation is removed via calculations with the core/valence (CV) cc-pCVQZ basis set, another 0.0020 Å shortening of the bond length is observed. The final CCSD(T)/aug-cc-pV5Z + CV bond length of 1.0975 Å is almost identical to the experimental value of 1.0977 Å.

N_3. The geometry for N_3 ($D_{\infty h}$) is in excellent agreement with the experimental value.[35] The calculations predict a value for the NN bond that is slightly shorter than the experimental value. This result is in contrast to N_2 where the calculations predict a longer bond at the CCSD(T)/aug-cc-pVQZ level.

(19) Woon, D. E.; Dunning, T. H., Jr. *J. Chem. Phys.* **1993**, *98*, 1358.
(20) MOLPRO is a package of ab initio programs. Werner, H. J.; Knowles, P. J.; Almlof, J.; Amos, R. D.; Berning, A.; Cooper, D. L.; Deegan, M. J. O.; Dobbyn, A. J.; Eckert, F.; Elbert, S. T.; Hampel, C.; Lindh, R.; Lloyd, A. W.; Meyer, W.; Nicklass, A.; Peterson, K. A.; Pitzer, R. M.; Stone, A. J.; Taylor, P. R.; Mura, M. E.; Pulay, P.; Schütz, M.; Stoll, H.; Thorsteinsson, T. *MOLPRO*; Universität Stuttgart and University of Birmingham: Stuttgart, Germany and Birmingham, England, 2000.
(21) Frisch, M. J.; Trucks, G. W.; Schlegel, H. B.; Scuseria, G. E.; Robb, M. A.; Cheeseman, J. R.; Zakrzewski, V. G.; Montgomery, J. A.; Stratmann, R. E.; Burant, J. C.; Dapprich, S.; Millam, J. M.; Daniels, A. D.; Kudin, K. N.; Strain, M. C.; Farkas, O.; Tomasi, J.; Barone, V.; Cossi, M.; Cammi, R.; Mennucci, B.; Pomelli, C.; Adamo, C.; Clifford, S.; Ochterski, J.; Petersson, G. A.; Ayala, P. Y.; Cui, Q.; Morokuma, K.; Malick, D. K.; Rabuck, A. D.; Raghavachari, K.; Foresman, J. B.; Cioslowski, J.; Ortiz, J. V.; Stefanov, B. B.; Liu, G.; Liashenko, A.; Piskorz, P.; Komaromi, I.; Gomperts, R.; Martin, R. L.; Fox, D. J.; Keith, T.; Al-Laham, M. A.; Peng, C. Y.; Nanayakkara, A.; Gonzalez, C.; Challacombe, M.; Gill, P. M. W.; Johnson, B.; Chen, W.; Wong, M. W.; Andres, J. L.; Gonzalez, A. C.; Head-Gordon, M.; Replogle, E. S.; Pople, J. A. *Gaussian 98*, revision A.6; Gaussian, Inc.: Pittsburgh, PA, 1998.
(22) Schmidt, M. W.; Baldridge, K. K.; Boatz, J. A.; Elbert, S. T.; Gordon, M. S.; Jensen, J. H.; Koseki, S.; Matsunaga, N.; Nguyen, K. A.; Su, S.; Windus, T. L.; Dupuis, M.; Montgomery, J. A. *J. Comput. Chem.* **1993**, *14*, 1347.
(23) Rittby, M.; Bartlett, R. J. *J. Phys. Chem.* **1988**, *92*, 3033.
(24) Knowles, P. J.; Hampel, C.; Werner, H.-J. *J. Chem. Phys*. **1994**, *99*, 5219.
(25) Deegan, M. J. O.; Knowles, P. J. *Chem. Phys. Lett*. **1994**, *227*, 321.
(26) Peterson, K. A.; Woon, D. E.; Dunning, T. H., Jr. *J. Chem. Phys*. **1994**, *100*, 7410.
(27) Peterson, K. A.; Dunning, T. H., Jr. Private communication.
(28) Davidson, E. R.; Ishikawa, Y.; Malli, G. L. *Chem. Phys. Lett*. **1981**, *84*, 226.
(29) Douglas, A. E.; Jones, W. J. *Can. J. Phys.* **1965**, *43*, 2216.
(30) Chase, M. W., Jr. NIST-JANAF Tables, 4th ed. *J. Phys. Chem. Ref. Data*, Mono. 9, **1998**, Suppl. 1.
(31) Jenkins, H. D. B.; Roobottom, H. K.; Passmore, J.; Glasser, L. *Inorg. Chem*. **1999**, *38*, 3609. Jenkins, H. D. B.; Tudela, D.; Glasser, L. *Inorg. Chem*. **2002**, *41*, 2364.
(32) Zhan, C.-G.; Dixon, D. A. *J. Phys. Chem. A* **2001**, *105*, 11534. Zhan, C.-G.; Dixon, D. A. *J. Phys. Chem. A* **2002**, *106*, 9737. Zhan, C.-G.; Bentley, J.; Chipman, D. M. *J. Chem. Phys.* **1998**, *108*, 177. Zhan, C.-G.; Chipman, D. M. *J. Chem. Phys.* **1998**, *109*, 10543.
(33) Becke, A. D. *J. Chem. Phys.* **1993**, *98*, 5648. Lee, C.; Yang, W.; Parr, R. G. *Phys. Rev. B* **1988**, *37*, 785. Stephens, P. J.; Devlin, F. J.; Chabalowski, C. F.; Frisch, M. J. *J. Phys. Chem.* **1994**, *98*, 11623.
(34) Huber, K. P.; Herzberg, G. *Molecular Spectra and Molecular Structure: Constants of Diatomic Molecules*; Van Nostrand Reinhold Col, Inc.: New York, 1979; Vol. 4.
(35) Brazier, C. R.; Bernath, F. P.; Burkholder, J. B.; Howard, C. J. *J. Chem. Phys*. **1988**, *89*, 1762.

Table 1. Calculated Valence Correlated Geometries N_m^x [a]

species	basis	*r* (NN)	*θ* (NNN)
$N_2(\tilde{X}^1A)$	CCSD(T)/aug-cc-pVDZ	1.1209	
	CCSD(T)/aug-cc-pVTZ	1.1040	
	CCSD(T)/aug-cc-pVQZ	1.1005	
	CCSD(T)/aug-cc-pV5Z	1.0995[b]	
	expt[34]	1.0977	
$N_3(\tilde{X}^2\Pi_g)$	CCSD(T)/aug-cc-pVDZ	1.1997	180.0[c]
	CCSD(T)/aug-cc-pVTZ	1.1840	
	CCSD(T)/aug-cc-pVQZ	1.1802	
	expt[35]	1.18115	
$N_3^-(\tilde{X}^1\Sigma_g^+)$	CCSD(T)/aug-cc-pVDZ	1.2072	180.0[c]
	CCSD(T)/aug-cc-pVTZ	1.1912	
	CCSD(T)/aug-cc-pVQZ	1.1876	
	expt[36]	1.1884	
$N_5^-(\tilde{X}^1A_1')$	CCSD(T)/aug-cc-pVDZ	1.3429	108.0[c]
	CCSD(T)/aug-cc-pVTZ	1.3309	
$N_5^+(\tilde{X}^1A_1)$	CCSD(T)/aug-cc-pVDZ	1.1319	165.87
		1.3413	107.90
	CCSD(T)/aug-cc-pVTZ	1.1159	167.08
		1.3238	108.48
	expt[2]	1.10	168.1
		1.30	111.2
$N_5(^2A_1)$[d]	ZAPT2/6-311+G(2df)	1.292	121.0
		1.343	100.1
		1.355	109.5
	CCSD(T)/aug-cc-pVDZ	1.422	102.3
		1.165	137.7
		2.576	81.1
N_5^-−TS[e]	MP2/aug-cc-pVDZ	1.270	125.5
		1.702	99.4
		1.215	107.8
	CCSD(T)/6-311+G(d)[7]	1.252	128.9
		1.764	
		1.191	

[a] Bond distances in angstroms and bond angles in degrees. [b] Core/valence correlation at the CCSD(T)/cc-pCVQZ level shortens the bond length by 0.0020 Å, resulting in an estimated CCSD(T)/aug-cc-pV5Z+CV value of 1.0975 Å. [c] Constrained by symmetry to these angles. Linear for N_3 and N_3^- and D_{5h} for N_5^-. [d] The radical is cyclic with the symmetry unique atom N1 at the apex. N1 is bonded to N2 and N5, and N2 is bonded to N3, and N3 is bonded to N4. The bond distances are in the order: *r*(N1−N2) and *r*(N1−N5); *r*(N2−N3) and *r*(N4−N5); and *r*(N3−N4). The bond angles are in the order ∠N2N1N5; ∠N1N2N3 and ∠N1N5N4; and ∠N2N3N4 and ∠N5N4N3. [e] The transition state for the anion decomposition is cyclic with the symmetry unique atom N1 at the apex. N1 is bonded to N2 and N5, and N2 is bonded to N3, and N3 is bonded to N4. The bond distances are in the order *r*(N1−N2) and *r*(N1−N5); *r*(N2−N3) and *r*(N4−N5); and *r*(N3−N4). The bond angles are in the order ∠N2N1N5; ∠N1N2N3 and ∠N1N5N4; and ∠N2N3N4 and ∠N5N4N3.

N_3^-. The calculated geometry for N_3^- is also in very good agreement with experiment, with the calculated NN bond length again being slightly shorter than experiment.[36]

N_5^+. The geometry for N_5^+ has been measured in the crystal by X-ray diffraction techniques.[2] The calculated values are in good agreement with the crystal structure values considering the uncertainty in the experimental values and the different environment. The calculated geometrical parameters for N_5^+ are the same as those reported by Fau and Bartlett at the CCSD(T)/aug-cc-pVTZ level,[5] whereas the geometries calculated for N_3^- at the same level differ slightly.

N_5^-. The value of 1.334 Å calculated for the NN bond length in N_5^- at the CCSD(T)/6-311+(G(d,p) level[7] lies between our values calculated at the CCSD(T) level with the aug-cc-pVDZ and aug-cc-pVTZ basis sets, respectively.

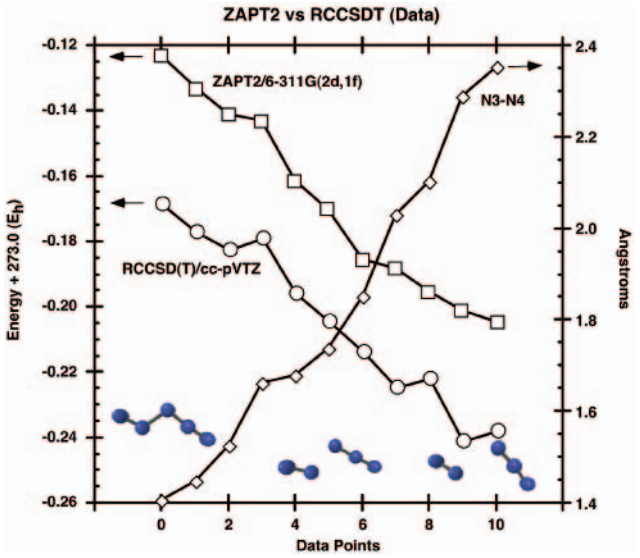

Figure 1. Schematic showing the decomposition of the N_5 radical formed by electron attachment to N_5^+ at the ZAPT2/6-311G(2d,f) and CCSD(T)/cc-pVTZ levels. The radical smoothly dissociates to products. The *x* axis corresponds to the calculation number describing the dissociation, and the *y* axis corresponds to the energy or to the N3−N4 (numbered starting from the right) interaction distance representing the separation between the N_2 and N_3 molecules. The large squares correspond to the ZAPT/6-311G(2d,-1f) potential energy surface, and the circles correspond to the CCSD(T)/cc-pVTZ potential energy surface. The small squares represent the N3−N4 distance which increases.

N_5 (Open Isomer). ZAPT2[37] calculations with the 6-311+G-(2df) basis set followed by CCSD(T)/cc-pVTZ single-point calculations confirm previous conclusions[7] that the N_5 radical starting from this geometry is vibrationally unstable. Starting from the optimized N_5^+ structure, the neutral species dissociates without a barrier to $N_3 + N_2$ as shown in Figure 1.

N_5 (Cyclic Isomer). The N_5 radical cyclic isomer would be generated by detaching an electron from cyclic N_5^-. The HOMO of N_5^- is a degenerate in-plane orbital involving essentially lone pair interactions. Production of the N_5 radical leads to $(e)^3$ occupancy which Jahn−Teller distorts to a C_{2v} structure. Two states can be derived from the $(e)^3$ occupancy, a $^2A_1$ state and a $^2B_1$ state (a $^2B_2$ state would be a π radical). The geometry for the cyclic N_5 (C_{2v}) $^2A_1$ radical was found to be a stationary point on the ZAPT2/6-311+G(2df) potential energy surface. The cyclic N_5 radical at the ZAPT2/6-311+G(2df) geometry is 66.8 kcal/mol above the $N_3 + N_2$ asymptote at the CCSD(T)/cc-pVTZ level. The longest NN ZAPT/6-311+G(2df) bond distance is that in the base of the pentagon, 1.354 Å. The shortest NN bonds are those connected to the apex, 1.292 Å. We took this geometry and initiated an optimization at the R/UCCSD-(T)/aug-cc-pVDZ level for both the $^2A_1$ and the $^2B_1$ states under the constraint of C_{2v} symmetry. The $^2B_1$ state smoothly dissociated to the $N_3 + N_2$ asymptote, showing that on the CCSD(T)/aug-cc-pVDZ surface, this state is not a minimum. The N_3 distance converges faster than the N_2 distance. The $^2A_1$ state is difficult to optimize but finally optimizes to a structure with two elongated N_2 molecules complexed weakly to an N atom (see Table 1), as it cannot go to the products $N_2 + N_3$. At the CCSD(T)/aug-cc-pVTZ level using the optimized CCSD-

(36) Polak, M.; Gruebele, M.; Saykally, R. J. *J. Am. Chem. Soc.* **1987**, *109*, 2884.

(37) Fletcher, G. D.; Gordon, M. S.; Bell, R. S. *Theor. Chem. Acc.* **2002**, *107*, 57.

(T)/aug-cc-pVDZ geometry, the $^2A_1$ state is 60.2 kcal/mol above the $N_2 + N_3$ asymptote. These calculations strongly suggest that, on electron detachment from N_5^-, the resulting radical has a path on the $^2B_1$ surface that leads directly to the $N_3 + N_2$ asymptote and that there is no stable cyclic N_5 radical structure, as has already been noted previously.[7] As part of a study of $Fe(\eta^5\text{-}N_5)_2$, Frenking and co-workers reported a structure for the $^2A_1$ state of the N_5 radical at the B3LYP/6-31G(d) level which could be a minimum, although the structure was not discussed.[38] Our result is also consistent with the prediction[7] of Nguyen and Ha that cyclic N_5 is not stable with respect to dissociation.

Calculated Frequencies. The calculated vibrational frequencies for N_2, N_3, N_3^-, N_5^-, N_5 (cyclic), and N_5^+ are summarized in Table 2.

N_2. The harmonic frequency at the frozen core CCSD(T)/aug-cc-pVQZ level is within 5 cm^{-1} of the experimental value.[34] Even at the CCSD(T)/aug-cc-pVTZ level, the N_2 frequency is within 20 cm^{-1}, and, at the CCSD(T)/aug-cc-pVDZ level, it is within 40 cm^{-1}. This level of agreement is in part fortuitous. Whereas the aug-cc-pV5Z basis set frequency is identical to the experimental value, introduction of core/valence correlation increases ω_e by 9.2 cm^{-1}. Thus, the final CCSD(T)/aug-cc-pV5Z + CV value is 9 cm^{-1} larger than experiment.

N_3. For N_3, the frequencies calculated at the MP2/aug-cc-pVDZ level are in qualitative agreement with the experimental values[39] for the π bend and the symmetric stretch and in good agreement for the antisymmetric stretch. In this case, we have used the experimental frequencies to calculate the zero-point energy.

N_3^-. For N_3^-, the calculated antisymmetric harmonic stretch is in excellent agreement with the gas-phase experimental value.[35,40] The value for the ν_2 bending frequency for this ion has been measured in the solid state, and a free space estimate for ν_1 has been obtained based on the spectrum measured for the solid.[41,42] For this ion, we used the experimental frequencies for the zero-point energy determination. Use of the theoretical frequencies introduces a difference of 0.19 kcal/mol because the calculated bend and antisymmetric stretch are ~50 cm^{-1} lower than the experimental values. The frequencies calculated by us for ν_1 and ν_3 are in reasonable agreement with those previously calculated at the CASPT2 level[17] and at the CEPA level.[42]

N_5^-. For this ion, we used the frequencies calculated at the CCSD(T)/aug-cc-pVDZ level for the zero-point energy calculation as there are no experimental values available. Quite good agreement is found for the frequencies of N_5^- calculated at the MP2/aug-cc-pVDZ level and at the CCSD(T)/aug-cc-pVDZ level. The CASPT2 frequencies[17] are similar to our values.

N_5 (Cyclic Isomer). Frequencies were calculated at the ZAPT2/6-311+G(2df)level of theory for the $^2A_1$ state. No experimental values are available for this species. As noted above, the $^2B_1$ structure is not a minimum for the cyclic radical at the R/UCCSD(T)/aug-cc-pVDZ level.

Table 2. Calculated Valence Correlated Harmonic Vibrational Frequencies (cm^{-1})

method	mode number	mode symmetry	mode description	ω	expt
		N_2			
CCSD(T)/aug-cc-pVDZ	1	σ_g	N_2 str	2319	2331[a] (2358.6)
CCSD(T)/aug-cc-pVTZ	1	σ_g	N_2 str	2340	
CCSD(T)/aug-cc-pVQZ	1	σ_g	N_2 str	2354	
CCSD(T)/aug-cc-pV5Z	1	σ_g	N_2 str	2359[b]	
		N_3			
MP2/cc-pVTZ	1	π	bend[h]	594	457[c]
	2	σ_g	symmetric str	1434	1320[c]
	3	σ_u	asymmetric str	1620	1645[c]
		N_3^-			
CCSD(T)/aug-cc-pVDZ	1	π	bend	578	626[d]
	2	σ_g	symmetric str	1281	1335[e]
	3	σ_u	asymmetric str	1999	1986[f]
		N_5^-			
CCSD(T)/aug-cc-pVDZ	1	e_1'	NN str	1202	
	2	a_1'	NN str	1141	
	3	e_2'	NN str	1078	
	4	e_2'	bend	1001	
	5	e_2''	bend	739	
MP2/aug-cc-pVDZ	1	e_1'	NN str	1143	
	2	e_2'	NN str	1123	
	3	a_1'	NN str	1094	
	4	e_2'	bend	1039	
	5	e_2''	bend	740	
		N_5^+			
MP2/aug-cc-pVDZ	1	b_2	NN str	2260	2267[g]
	2	a_1	NN str	2179	2206[g]
	3	b_2	NN str	1199	1064[g]
	4	a_1	NN str	881	870[g]
	5	a_1	bend	669	671[g]
	6	b_2	bend	431	414[g]
	7	a_2	out-of-plane bend	426	474[g]
	8	b_1	bend	374	421[g]
	9	a_1	bend	179	204[g]
		N_5^-−TS			
MP2/aug-cc-pVDZ	1	b_2	NN str	1649	
	2	a_1	NN str	1572	
	3	a_1	NN str	1244	
	4	a_1	NN str	905	
	5	b_2	bend	848	
	6	b_1	bend	684	
	7	a_2	out-of-plane bend	591	
	8	b_2	bend	182	
	9	a_1	NN str	862i	
		N_5 (cyclic) $^2A_1$			
ZAPT2/6-311+G(2df)	1	b_2	NN str	1221	
	2	a_1	NN str	1147	
	3	a_1	NN str	1064	
	4	b_2	NN str	1033	
	5	a_1	NN str	1002	
	6	a_1	bend	843	
	7	b_2	bend	798	
	8	a_2	out-of-plane bend	729	
	9	b_1	bend	363	

[a] Reference 34. Value in parentheses is the harmonic value. [b] Core/valence correlation at the CCSD(T)/cc-pCVQZ level of theory increases the harmonic frequency by 9.2 cm^{-1}, resulting in an estimated CCSD(T)/aug-cc-pV5Z+CV value of 2368 cm^{-1}. [c] Reference 39. [d] Lamoureux, R. T.; Dows, D. A. *Spectrochim. Acta, Part A* **1975**, *31*, 1945. From N_3^- in a KI lattice. [e] References 41 and 42. [f] Reference 36. [g] Reference 2. [h] Average of 565 and 622 cm^{-1}.

N_5^+. For N_5^+, there is reasonable agreement between the frequencies calculated at the MP2/aug-cc-pVDZ level and the average of the frequencies taken from measurements in the solid state.[2] The largest discrepancy is found for the highest frequency b_2 mode with a difference of ~140 cm^{-1}. The calculated a_2 and b_1 modes deviate by ~50 cm^{-1} from the experimental values. The fact that the differences cancel out leads to

(38) Lein, M.; Frunzke, J.; Timoshkin, A.; Frenking, G. *Chem.-Eur. J.* **2001**, *7*, 4155.
(39) Jacox, M. E. *J. Phys. Chem. Ref. Data* **1994**, Monograph No. 3.
(40) Polak, M.; Gruebele, M.; Saykally, R. J. *J. Chem. Phys.* **1988**, *89*, 110.
(41) Sherman, W. F.; Wilkinson, G. R. In *Vibrational Spectroscopy of Trapped Species*; Hallam, H. E., Ed.; Wiley: London, 1973.
(42) See for a quoted value for ν_1: Botschwina, P. *J. Chem. Phys.* **1986**, *85*, 4591.

Table 3. Contributions to the Total Energy for N_x^m and Relative Energies

contribution[a]	N (^{4}S)	N_2 ($^1\Sigma^+$)	N_3 ($^2\Pi$)	N_3^- ($^1\Sigma^+$)	N_5^- ($^1A_1'$)	N_5^+ ($^1A_1$)	N_5–TS ($^1A_1$) MP2	N_5–TS ($^1A_1$) ref 7 geom
aug-cc-pVDZ[b]	−54.486849	−109.295320	−163.770896	−163.863661	−273.142269	−272.683885	−273.101846	−273.099657
aug-cc-pVTZ[b]	−54.516714	−109.380845	−163.900633	−163.997758	−273.360072	−272.900359	−273.317071	−273.315909
aug-cc-pVQZ[b]	−54.525300	−109.407243	−163.939895	−164.038815	−273.428772	−272.965446	−273.383465	−273.382442
Est. CBS eq 1[c]	−54.530069	−109.422126	−163.961942	−164.061926	−273.467671	−273.001946	−273.420892	−273.419928
ΔE_{elec} CBS eq 1[d]		227.15	233.26	296.00	512.87	220.63	483.52	482.91
ΔE_{CV} [e]		0.65	1.03	1.22	1.66	1.80		
ΔE_{SR} [f]		−0.11	−0.51	−0.51	−1.04	−0.85		
ΔE_{ZPE} [g]		−3.35	−5.54	−6.53	−13.12	−12.27	−10.96	−10.0
$\sum D_0$ [h]		224.34	228.34[k]	290.18	500.37	209.31		
ΔH_f(0 K)[i]	112.53	0.72	109.25	47.41	62.28	353.34		
ΔH_f(0 K) expt		0.0[30]	99.7 ± 5[30]	48 ± 2				
			112 ± 5[43,44]					
ΔH_f(298 K)[j]		0.76	108.6	47.4	59.6	351.6		

[a] Total energies in hartrees and energy differences in kcal/mol. [b] Valence electron only CCSD(T) total energy with the given basis set. Open shell systems were treated with the R/UCCSD(T) method. [c] Estimated frozen core, complete basis set energy obtained from eq 1 using the CCSD(T)/aug-cc-pVxZ (x = D, T, Q) energies. For the sake of comparison, the CBS dissociation energy of N_2 with the aug-cc-pVTZ through aug-cc-pV5Z basis sets is 226.63 kcal/mol. [d] Valence electron atomization energy from extrapolated total energies obtained with eq 1. [e] Core/valence correction obtained from R/UCCSD(T)/cc-pCVTZ calculations. [f] Scalar relativistic correction obtained from CISD/cc-pVTZ calculations. [g] Zero-point vibrational energy contribution. [h] $\sum D_0 = \Delta E_{elec} + \Delta E_{CV} + \Delta E_{SR} + \Delta E_{SO} + \Delta E_{ZPE}$. [i] Enthalpy of formation at 0 K. [j] Enthalpy of formation at 298 K. [k] Spin−orbit correction of +0.10 kcal/mol for N_3.

calculated and experimental zero-point energies that are essentially identical. We used the average experimental values in our zero-point energy calculations. Our calculated frequencies are in qualitative agreement with those calculated at the CCSD(T)/6-311+G(2d) and B3LYP/6-311+G(2d) levels.[1,2] The CCSD(T) values are in general lower than our MP2 values except for the a_2 and b_1 modes which are higher. The CASPT2 frequencies differ from ours more than might be expected, especially for the two highest modes.[17]

Calculated Enthalpies of Formation. The total atomization energies are given in Table 3. The ΔH_f^0 values were converted to 298 K following the procedure of Curtiss and co-workers.[16]

N_2. As shown in Table 3, the error in the atomization energy of N_2 is 0.76 kcal mol^{-1} when compared to experiment.[30] This leads to an error in the calculated enthalpy of formation at 0 K of 0.76 kcal mol^{-1}. We can thus estimate that the error bars in our heats of formation are likely to be on the order of ±1 kcal/mol.

N_3. The enthalpy of formation of N_3 has been reported by a number of authors. The NIST value[30] of 100 ± 5 kcal mol^{-1} at 0 K is almost 10 kcal mol^{-1} below our calculated value. Our calculated value of 109.2 kcal mol^{-1} is in much better agreement with the value of 112 ± 5 based on the experimental measurement of the acidity of HN_3 and the measurement of the electron affinity of N_3^-.[43,44] Our value of 109.25 kcal mol^{-1} is in excellent agreement with the scaled value of 109.25 kcal mol^{-1} given by Martin et al.[8] The calculated atomization energies show that reaction 3

$$N_3(^2\Pi)\,(g) \rightarrow N(^4S)\,(g) + N_2(^1\Sigma^+)\,(g) \qquad (3)$$

is only 4 kcal mol^{-1} endothermic at 0 K.

N_3^-. The enthalpy of formation of N_3^- has been determined from gas-phase acidity measurements and the enthalpy of formation of HN_3 to be 48 ± 2 kcal mol^{-1}.[43] This value is in excellent agreement with our calculated value of 47.2 kcal mol^{-1}. Fau and Bartlett calculated the enthalpy of formation of N_3^- by a variety of methods.[5] Their best estimated enthalpy of formation of 47.8 kcal mol^{-1} is in good agreement with our value. The electron affinity of N_3 has been measured to be 2.68 ± 0.01 eV.[44] Our calculated adiabatic electron affinity of 2.69 eV is in excellent agreement with this result. With an ANO (4s3p2d1f) basis set, the CASPT2 electron affinity was predicted to be 2.64 eV.[17]

N_5^+. The enthalpy of formation of N_5^+, calculated by us, is 353.4 kcal mol^{-1}. This result is in reasonable agreement with the value of 347.1 kcal mol^{-1}, calculated by Fau and Bartlett.[5] Christe and co-workers[1,2] predicted the enthalpy of formation of N_5^+ to be 351.1 kcal mol^{-1} at the CCSD(T) level with a polarized double-ζ basis set. Nguyen and Ha predict a heat of formation of 351.3 ± 3.6 kcal/mol based on CCSD(T)/6-311+G(3df) calculations and the experimental energy of N_3.[7]

The adiabatic electron affinity of N_5^+ is given by the energy difference between its enthalpy of formation and those of the first metastable neutral reaction or decomposition products. Because the intermediate, open-chain N_5 radical, formed by the addition of an electron to N_5^+, is unstable and spontaneously dissociates to N_3 (g) + N_2 (g), the energy of reaction 4 provides the adiabatic electron affinity of N_5^+.

$$N_5^+\,(g) + e^- \rightarrow N_3\,(g) + N_2\,(g) \qquad (4)$$

The N_3 radical and N_2 only form a weakly bound van der Waals complex with a binding energy on the order of less than 1 kcal mol^{-1}. Our calculated value of 243.3 kcal mol^{-1} (10.55 eV) for reaction 4 is much higher than either the vertical electron affinity of 6.04 eV reported by Fau et al.[5] or the adiabatic ionization energy of 7.4 ± 0.2 eV reported by Nguyen and Ha,[7] but is in excellent agreement with our experimental bracketing study[2] that showed the electron affinity of N_5^+ to fall between 10.52 and 11.48 eV.

N_5^-. The enthalpy of formation of N_5^- is calculated to be 62.2 kcal mol^{-1}, in excellent agreement with the value of 62.1 ± 3.6 kcal/mol given by Nguyen and Ha.[7] This value can be used to calculate the adiabatic ionization potential of N_5^- in the same manner as discussed above for N_5^+. As noted above, loss of an electron from the degenerate HOMO of N_5^- leads to

(43) Pellerite, M. J.; Jackson, R. L.; Brauman, J. I. *J. Phys. Chem.* **1981**, *85*, 1624.
(44) Illenberger, E.; Comita, P. B.; Brauman, J. I.; Fenzlaff, H. P.; Heni, M.; Heinrich, N.; Koch, W.; Frenking, G. *Ber. Bunsen-Ges. Phys. Chem.* **1985**, *89*, 1026. Jackson, R. L.; Pellerite, M. J.; Brauman, J. I. *J. Am. Chem. Soc.* **1981**, *103*, 1802.

either a $^2B_1$ or a $^2A_1$ radical. We have shown that formation of the $^2B_1$ radical provides a pathway leading to $N_3 + N_2$, so the following channel (reaction) represents the adiabatic ionization process:

$$N_5^-(g) \rightarrow N_3(g) + N_2(g) + e^- \quad [47.9 \text{ kcal mol}^{-1} (2.08 \text{ eV})] \quad (5)$$

Use of this channel gives an adiabatic ionization potential of 2.08 eV for N_5^-. Because of the dissociative nature of the cyclic N_5 radical, this is the most appropriate value to use in the Born−Haber cycles discussed below.

The important dissociation channel for N_5^- is the formation of $N_3^- + N_2$. We predict this channel to be exothermic by 14.2 kcal mol^{-1} at 0 K. This value is in good agreement with the value of 14.3 kcal mol^{-1} reported by Nguyen and Ha at the CCSD(T)/aug-cc-pVTZ level.[7] It is important to know if there is a barrier separating N_5^- from the asymptotic products N_3^- and N_2. Nguyen and Ha calculated the energy barrier to dissociation as 27.7 kcal mol^{-1} at the CCSD(T)/aug-cc-pVTZ level including zero-point corrections based on a geometry calculated at the CCSD(T)/6-311+G(d) level.[7] We have calculated the energy of the transition state at the CCSD(T)/CBS level with Nguyen and Ha's geometry and with the geometry optimized by us at the MP2/aug-cc-pVDZ level. We calculated the geometry at the latter level to get a value of the zero-point energy as well as the value of the imaginary frequency characterizing the transition state. The results are given in Tables 1−3. Our calculated energy barrier using the MP2 geometry is 29.4 kcal mol^{-1}, and when the zero-point energy difference is included, the barrier is 27.2 kcal mol^{-1}. The energy barrier using the Nguyen and Ha geometry is 0.61 kcal mol^{-1} higher in energy than our value based on the MP2 geometry, showing that the two geometries give essentially identical barrier heights. The barrier calculated[7] by Nguyen and Ha is very similar to our CCSD(T)/CBS value using their geometry. At the CASPT2/ANO(4s3p2d) level, the barrier is predicted to be 26 kcal mol^{-1}, and the dissociation energy to N_3^- and N_2 is predicted to be exothermic by 9 kcal mol^{-1},[17] 5 kcal mol^{-1} lower than our value. A calculation of the imaginary frequency for the transition state of the N_5^- decomposition shows a large value of 862i cm^{-1}, suggesting that the ion might be able to tunnel through the barrier to reach the products. We can make a crude estimate of the tunneling effect by using the Wigner expression.[45] This leads to an enhancement of the dissociation rate by 1.7 at 298 K. This suggests that tunneling should be considered when predicting the stability of N_5^-. For lower temperatures, a larger tunneling effect would be expected.

The origin of the difference between the vertical and the adiabatic potentials, of course, is the dissociation energy of neutral N_5 to N_3 and N_2. Vertical electron affinities or ionization potentials for the ionic systems under study correspond to removal or addition of an electron to the ion to form a radical at the geometry of the ion. Only when the neutral radicals are vibrationally stable species with geometries similar to those of the starting materials will their vertical EA or IP values approximate the adiabatic values. If this is not the case, the radicals generated by the neutralization process spontaneously undergo further decomposition. If these decompositions to the first well-defined, vibrationally stable products do not involve any significant activation energy barriers and if they occur on a fast time scale, it is appropriate to add their energies to the vertical potentials.

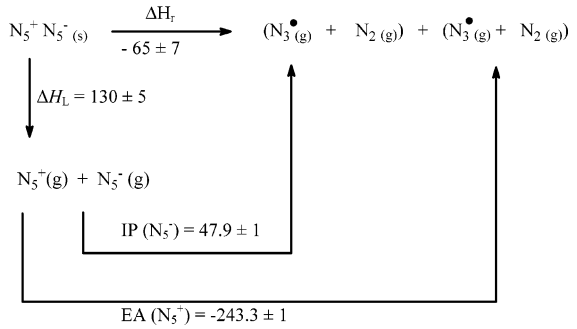

Figure 2. Born−Haber cycle in kcal mol^{-1} for the decomposition reaction of solid $N_5^+N_5^-$. The large negative value for ΔH_r demonstrates the unlikelihood of this salt to exist.

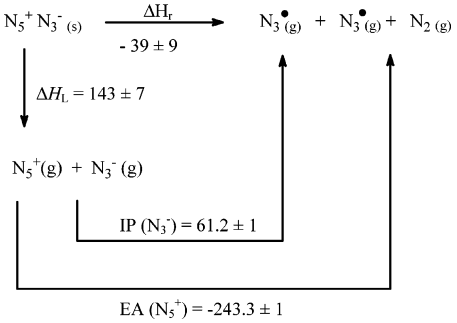

Figure 3. Born−Haber cycle in kcal mol^{-1} for the decomposition reaction of solid $N_5^+N_3^-$. The large negative value for ΔH_r demonstrates that this salt is also unlikely to exist.

Lattice Energy Calculations. Prediction of lattice energies, U_L, based on eq 2 requires an estimate of the relevant ion volumes and gives the following results:

$N_5^+N_3^-$. $V(N_5^+)$ is estimated to be 0.051 (±0.020) nm^3 based on the reported[2] crystal structure volume for $N_5^+Sb_2F_{11}^-$ by subtraction of $V(Sb_2F_{11}^-)$ (Table 6, ref 31). $V(N_3^-)$ is equal to 0.058 (±0.014) nm^3 (Table 5, ref 31), and thus $V(N_5^+N_3^-)$ = 0.109 (±0.024) nm^3, leading to an estimate for $U_L(N_5^+N_3^-)$ = 142 (±7) kcal mol^{-1}.

$N_5^+N_5^-$. An upper limit for $V(N_5^-)$ can be estimated from consideration of $V(N_2)$ and $V(N_3^-)$. The volume of solid dinitrogen, $V(N_2)$, which is dimorphous,[46] can be obtained from crystal structure data for the α-cubic and the hexagonal forms and averages to $V(N_2)$ = 0.046 (±0.001) nm^3, leading to $V(N_5^+N_5^-)$ = 0.155 (±0.014) nm^3, giving a value for $U_L(N_5^+N_5^-)$ = 129 (±5) kcal mol^{-1}. Alternatively, we can estimate the volume of the ions at the B3LYP/6-31+G* level as described above: $V(N_5^+)$ = 0.068 nm^3; $V(N_5^-)$ = 0.088 nm^3, $V(N_3^-)$ = 0.065 nm^3. These estimated volumes yield $U_L(N_5^+N_5^-)$ = 129 kcal mol^{-1} and $U_L(N_5^+N_3^-)$ = 135 kcal mol^{-1}, well within the above error limits. The corresponding lattice enthalpies, ΔH_L, appropriate for use in the cycles of Figures 2 and 3 are $U_L(N_5^+N_5^-) + 2RT$ and $U_L(N_5^+N_3^-) + {}^3/_2RT$, respectively.

Stability Predictions Based on Born−Haber Cycles. For a chemical reaction to be thermodynamically favorable, its free

(45) Johnston, H. S. *Gas-Phase Reaction Rate Theory*; Ronald Press: New York, 1966. Steinfeld, J. I.; Francisco, J. S.; Hase, W. L. *Chemical Kinetics and Dynamics*; Prentice-Hall: Englewood Cliffs, NJ, 1989.

(46) Landolt, B. *Crystal Structure Data for Inorganic Compounds*; Springer-Verlag: Berlin, 1993.

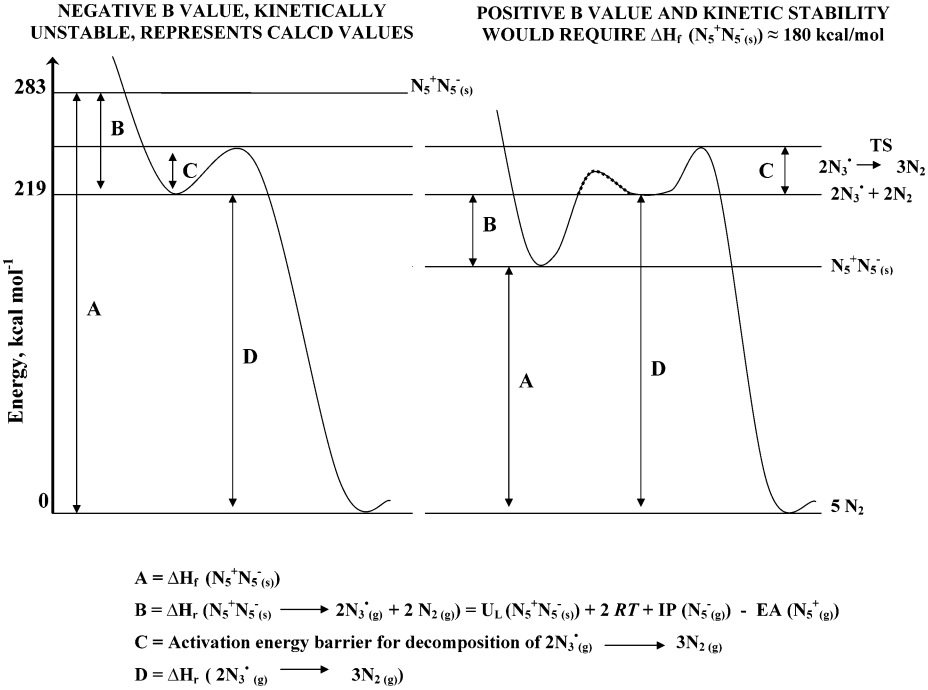

Figure 4. Potential energy curves in kcal mol^{-1} for the decomposition reaction of solid $N_5^+N_5^-$ to dinitrogen. The left curve is based on the calculated values from this study and shows that a hypothetical $N_5^+N_5^-$ would spontaneously decompose to $2N_3$ (g) + $2N_2$ (g). The right curve shows that for $N_5^+N_5^-$ to be stable, its enthalpy of formation would have to be significantly lower than those of the gaseous species ($2N_3$ + $2N_2$). The broken line indicates that the barrier might possibly exceed the *B* value.

energy change must be zero or negative. If the reaction involves a barrier, a sufficient amount of activation energy must be supplied to overcome this barrier. If the reaction does not have an activation energy barrier, a spontaneous reaction occurs when its free energy change becomes negative. An example of such a reaction is the dissociation of an ionic solid into two radicals (reaction 6), assuming that the electron transfer from the cation to the anion proceeds without a barrier.

$$A^+B^-(s) \rightarrow A(g) + B(g) \qquad (6)$$

If A (g) and B (g) are kinetically stable species possessing an activation energy barrier toward further decomposition, the stability of solid A^+B^- is determined solely by the sum of the adiabatic electron affinity of A^+, the adiabatic first ionization potential of B^-, and the lattice energy of solid A^+B^-. If, however, the radicals A and B are vibrationally unstable and undergo further spontaneous decomposition without a barrier, then the energies of the first vibrationally stable decomposition products must be used in place of those of A (g) and B (g). This is the case for $N_5^+N_5^-$, where both the open and the cyclic N_5 radicals are vibrationally unstable. Therefore, the decomposition of $N_5^+N_5^-$ (s) is given by reaction 7, and the corresponding Born−Haber cycle is shown in Figure 2.

$$N_5^+N_5^-(s) \rightarrow 2N_3(g) + 2N_2(g) \qquad (7)$$

Those for $N_5^+N_3^-$ (s) are given by eq 8 and Figure 3.

$$N_5^+N_3^-(s) \rightarrow 2N_3(g) + N_2(g) \qquad (8)$$

The values shown in the Born−Haber cycles of Figures 2 and 3 are enthalpies. Because the stabilities of the compounds depend on the free energy changes and not the enthalpy changes, the entropy contributions from the $T\Delta S$ term to the free energy must also be included. For the reactions considered in this paper, these contributions are always negative. We can estimate the entropy changes for reactions 7 and 8 as follows. The entropy for the solid is not known, but we can use the entropies of $NH_4^+NO_3^-$ and $NH_4^+N_3^-$, which are 36 and 27 cal/mol K,[47] respectively, to estimate the value for the N_5^+ salts. Given the well-established entropies of N_2 and N_3 of 45.8 and 54.1 cal/mol K, respectively, we obtain at 298 K for reaction 7 $-T\Delta S = -49$ kcal/mol, if the entropy of $NH_4^+NO_3^-$ is used to estimate that of the solid, and $-T\Delta S = -51$ kcal/mol, if the entropy of $NH_4^+N_3^-$ is used. For reaction 8, the respective values are $-T\Delta S = -35$ and -38 kcal/mol at 298 K. Thus, significantly positive reaction enthalpy values would be required for the compensation of the large negative entropy contributions and the stabilization of $N_5^+N_5^-$ and $N_5^+N_3^-$. A positive ΔG_r value represents the minimum dissociation energy barrier, but one should keep in mind that the actual barrier can well be higher. If, however, the ΔG_r change is negative, spontaneous decomposition occurs in the absence of a significant reaction barrier. The potential energy curves for both scenarios are depicted in Figure 4 for $N_5^+N_5^-$.

The left curve of Figure 4 represents the case of the enthalpy of reaction 7 being negative and having no significant activation energy barrier. It results in spontaneous decomposition of the solid to the first vibrationally stable intermediates, that is, N_3 radicals and N_2. The right curve of Figure 4 represents the scenario of a positive reaction enthalpy, the only condition under which solid $N_5^+N_5^-$ might exist. This, however, is a hypothetical case, requiring the enthalpy of formation of $N_5^+N_5^-$ to be about 100 kcal mol^{-1} more negative than the calculated value. Because the values for the IP of N_5^- and the EA of N_5^+ are fixed, the lattice energy of $N_5^+N_5^-$ would have to be about 100 kcal/mol

(47) Wagman, D. D.; Evans, W. H.; Parker, V. B.; Schumm, R. H.; Halow, I.; Bailey, S. M.; Churney, K. L.; Nutall, R. L. *J. Phys. Chem. Ref. Data* **1982**, *11*, Supplement No. 2.

higher than our calculated value, which is impossible based on the molar volumes of the ions involved. The relatively small uncertainties in our ΔH_r values, -65 ± 7 kcal mol^{-1} for $N_5^+N_5^-$ and -39 ± 9 kcal mol^{-1} for $N_5^+N_3^-$, together with the large $-T\Delta S$ terms, allow us to predict with confidence that both compounds cannot be stabilized in the form of ionic solids.

The potential energy surface for N_5^+/N_5^- is quite complicated. The asymptotic energy of $N_5^+ + N_5^-$ is 416 kcal/mol above that of $5N_2$ molecules at 0 K. Our approach to the ion pair energy provides an estimate of 297 kcal/mol above $5N_2$, in good agreement with the Fau et al.[6] value of 296 kcal/mol. The highly endoergic heat of formation means that the complex is metastable as are all polynitrogen compounds. Thus, there may be a number of decomposition paths.[48] Neither the N_5 radical derived from N_5^+ at the cation geometry nor the N_5 radical derived from N_5^- at the anion geometry are stable species as shown above. These two N_5 species are doublets, and hence there can be both a triplet coupling and a singlet coupling of the two unpaired electrons after the electron transfer process. The singlet coupling, if the geometries remain similar to the parent ion geometries, should generally be considered as an open shell singlet, not necessarily restricted to a closed shell description.[6] Enforcing singlet closed shell (i.e., RHF) pairing in the ground-state wave function prevents the two N_5 species from coming apart as N_5 radicals (or their dissociative products N_2 and N_3) even though the product formation of $2N_3 + 2N_2$ is more than 80 kcal/mol exothermic. On the other hand, the triplet surface could lead to direct dissociation. Including the open shell-singlet paired configuration in a more general multiconfigurational wave function may have the same result. To further study the N_5^+/N_5^- ion pair potential surface, we optimized the lowest $^3A'$ and $^3A''$ states at the ROHF/6-31+G(d) (restricted open shell Hartree−Fock) level, and the lowest $^1A'$ and $^1A''$ states using TCSCF (two-configuration self-consistent field) wave functions and the same 6-31+G(d) basis set. For both spin states, the lower energy state is A′. Geometry optimization of the $^3A'$ state (lowest energy triplet at this level of theory) leads to a large separation of the anion and cation, with a concomitant decrease in the charges on the two species to nearly zero. So, the lowest energy triplet is clearly on its way to dissociation to two radicals, and subsequently to N_2 and N_3. The other three states (two singlets and one triplet) do not appear to dissociate at these levels of theory. The $^3A'$ state is about 40 kcal/mol above the $^1A'$ state but is still ∼80 kcal/mol below the separated ion pair dissociation asymptote, showing that there is an electron transfer step leading to dissociation that occurs significantly below the energy of the separated ions. Higher levels of theory may alter these results, and we did not further explore the barriers to dissociation. These results and those of other workers do show that the potential energy surface is very complicated and that there are many potential highly exothermic paths leading to formation of N_3 and/or N_2. In addition, we note that all of these comparisons are at 0 K and that at higher temperatures, there is a significant entropic effect favoring formation of N_2 and N_3. These results are all consistent with our conclusion that formation of a stable N_5^+/N_5^- ion pair is unlikely, so it cannot be isolated.

Experimental Results and their Comparison with the Predictions. All of our attempts to prepare solid $N_5^+N_3^-$ by the metathesis reaction 9 failed.

$$N_5^+SbF_6^-(s) + M^+N_3^-(s) \rightarrow MSbF_6(s)\downarrow + N_5^+N_3^-(s) \quad (9)$$

In liquid SO_2, the $N_5^+SbF_6^-$ salt is highly soluble. Using very soluble (solubility at -64 °C $= 3.14 \times 10^{-3}$ mol mL^{-1}) CsN_3, violent reactions occurred resulting in quantitative formation of poorly soluble (solubility at -64 °C $= 6.56 \times 10^{-6}$ mol mL^{-1}) $CsSbF_6$ and $4N_2$. Using poorly soluble (solubility at -64 °C $= 9.23 \times 10^{-5}$ mol mL^{-1}) NaN_3, the metathesis did not proceed to any measurable extent, and unreacted NaN_3 and N_5SbF_6 were recovered. It was also shown that solid NaN_3 and N_5SbF_6 can be mixed as dry powders at room temperature and the Raman spectrum of the mixture can be recorded without evidence of reaction provided that the laser power is kept at a low level. Attempts to carry out the metathesis in CHF_3 solution were also unsuccessful because of the low solubility of the starting materials in this solvent. These experiments show that, in all cases where metathesis took place, only spontaneous decomposition was observed and, thus, confirm the above given theoretical predictions.

These results are consistent with the predictions by us and by Fau and Bartlett[5] that $N_5^+N_3^-$ will not be stable. Fau and Bartlett[5] noted that the reaction of N_5^+ and N_3^- does not lead to ion pair formation and that N_5N_3 is a weak complex even on the closed shell singlet energy surface. This structure is located at -149 kcal/mol on the way toward the $2N_3 + N_2$ final products at -182 kcal/mol (energies with respect to the separated ions). Their results suggest that on the triplet coupled surface, and possibly on the multiconfigurational singlet surface, this species will fully dissociate.

Assessment of the Performance of Solid $N_5^+N_5^-$ as a Monopropellant. It was recently suggested[6,52] that $N_5^+N_5^-$, if it "could be stabilized, would be an ideal monopropellant because its density is nearly twice that of hydrazine while the energy densities (heat of reaction per gram) are comparable." Indeed, the previous energy density estimate of 2.11 kcal/g for $N_5^+N_5^-$ is close to our estimate of 1.98 kcal/g. However, our energy density estimate for hydrazine is significantly lower. If one assumes its decomposition to proceed according to eq 10,

$$3N_2H_4 \rightarrow 4NH_3 + N_2 \quad (10)$$

the maximum energy density of N_2H_4 would be only 1.17 kcal/g.[30] The actual value, however, is even lower because there is always some decomposition of NH_3 to N_2 and H_2.[53] Hence, we conclude that the energy densities of $N_5^+N_5^-$ and N_2H_4 differ

(48) The energy of the $N_7 + N_3$ channel is 324 kcal/mol above $5N_2$ molecules using the G3 heat of formation of N_7, and thus $N_7 + N_3$ is 27 kcal/mol above the $N_5^+N_5^-$ ion pair.[49] The barrier[6] to form $N_7 + N_3$ from N_5^+/N_5^- is very similar to the endothermicity of the reaction, and this process again involves two open shell molecules. A closed shell asymptote of geometry similar to that of the end-on addition of N_5^+ to N_5^- is $N_8 + N_2$, which is 230 kcal/mol above $5N_2$ at the CCSD(T)/6-311G*//MP2/6-31G* level[50] and, thus, substantially downhill from the ion pair by ∼67 kcal/mol. The N_8 molecule that is formed, azidopentazole, has a barrier to formation of 4 N_2 of only 13−14 kcal/mol at the CCSD(T)/6-311G* level[49] and 19 kcal/mol at the CASPT2/ANO-4s3p2d1f level.[51]

(49) Wang, X.; Tian, A.; Wong, N. B.; Law, H.-K.; Li, W.-K. *Chem. Phys. Lett.* **2001**, *338*, 367.
(50) Chung, G.; Schmidt, M. W.; Gordon, M. S. *J. Phys. Chem. A* **2000**, *104*, 5647.
(51) Gagliardi, L.; Evangelisti, S.; Bernhardsson, A.; Lindh, R.; Roos, B. O. *Int. J. Quantum Chem.* **2000**, *77*, 311.
(52) *Nature*, Science Update, May 15, 2002. *Scientific American*, News, May 15, 2002. *Die Welt*, May 15, 2002.
(53) Schmidt, E. W. *Hydrazine and its Derivatives Preparation, Properties, Applications*; John Wiley & Sons: New York, 1984.

by a factor of 2. Based on our molar volume estimates, the density of $N_5^+N_5^-$ is expected to be 1.50 g/cm^3. Even so, we agree with the conclusion[6] that a hypothetical polynitrogen compound, such as $N_5^+N_5^-$, would be an excellent monopropellant for rocket propulsion or explosives, if it could be synthesized in a stable form.

Conclusions

The following conclusions can be drawn from our studies:

(i) Our results quantitatively examine the stability of $N_5^+N_5^-$ and $N_5^+N_3^-$ and show that both compounds are unstable in the solid state.

(ii) Our results show that for Born−Haber cycle based stability estimates for species, such as N_5^+ and N_5^-, which decompose to vibrationally unstable species upon neutralization, it is important to use adiabatic ionization potentials and electron affinities.

(iii) In view of the instability of the N_5 radicals and their strongly exothermic spontaneous decompositions to N_3 radicals and N_2, both N_5^+ and N_5^- are not good choices for preparing a stable ionic nitrogen allotrope.

(iv) Our results suggest that $N_5^+N_5^-$ would be even more unstable than $N_5^+N_3^-$, because the former would contain two unstable N_5 species after transfer of the electron.

(v) Stability calculations for individual ions or ion pairs may not provide sufficient information for stability predictions. Rigorous Born−Haber cycles, including realistic lattice energy estimates, and an evaluation of the stability of the decomposition products are required to make meaningful predictions.

(vi) Our theoretical predictions concerning the instability of $N_5^+N_3^-$ and the use of the adiabatic electron affinities and ionization potentials are confirmed by extensive experimental studies involving the low-temperature metatheses of $N_5^+SbF_6^-$ with different alkali metal azides in various solvents and the determinations of electron affinities by bracketing methods, respectively.

Acknowledgment. The authors thank Dr. Jerry Boatz for many helpful discussions and Dr. Chang-guo Zhan for help with the volume calculations. The work at Pacific Northwest National Laboratory (PNNL) was supported in part by the U.S. Department of Energy, Offices of Basic Energy Sciences, Division of Chemical Sciences, and Biological and Environmental Research, under Contract No. DE-AC06-76RLO 1830 for PNNL. Part of this research was performed in the William R. Wiley Environmental Molecular Sciences Laboratory (EMSL) at the PNNL using the Molecular Sciences Computing Facility. The EMSL is a national user facility funded by the Office of Biological and Environmental Research in the U.S. Department of Energy. PNNL is a multiprogram national laboratory operated by Battelle Memorial Institute for the U.S. Department of Energy. The work at the Air Force Research Laboratory was supported by the Defense Advanced Projects Agency (DARPA) and the Air Force Office of Scientific Research (AFOSR). The work at the University of Southern California was funded by DARPA, AFOSR, and the National Science Foundation. The work at Iowa State University was funded by an AFOSR high energy density matter (HEDM) grant.

JA0303182

APPENDIX J

"First Structural Characterization of Binary As(III) and Sb(III) Azides"
Chemistry – A European Journal, 10, 508 (2004)

This Page Intentionally Left Blank

First Structural Characterization of Binary As^{III} and Sb^{III} Azides

Ralf Haiges,*[a] Ashwani Vij,*[b] Jerry A. Boatz,[b] Stefan Schneider,[a] Thorsten Schroer,[a] Michael Gerken,[a] and Karl O. Christe*[a, b]

Abstract: The highly explosive molecules $As(N_3)_3$ and $Sb(N_3)_3$ were obtained in pure form by the reactions of the corresponding fluorides with $(CH_3)_3SiN_3$ in SO_2 and purification by sublimation. The crystal structures and ^{14}N NMR, infrared, and Raman spectra were determined, and the results compared to ab initio second-order perturbation theory calculations. Whereas $Sb(N_3)_3$ possesses a propeller-shaped, pyramidal structure with perfect C_3 symmetry, the $As(N_3)_3$ molecule is significantly distorted from C_3 symmetry due to crystal packing effects.

Keywords: ab initio calculations · antimony · arsenic · azides · structure elucidation · vibrational spectroscopy

Introduction

The syntheses of the highly explosive binary triazides of arsenic and antimony have recently been reported.[1–4] However, the structures of these interesting compounds could not be determined because they were difficult to crystallize or obtained only as oils. We have now been able to prepare $M(N_3)_3$ (M = As, Sb) as very pure solids and obtained their single crystals by slow and careful sublimation of the solids.

Results and Discussion

Syntheses and properties: The reaction of AsF_3 or SbF_3 in SO_2 with excess $(CH_3)_3SiN_3$ at room temperature results in complete azide–fluoride exchange yielding a clear solution of $As(N_3)_3$ or precipitation of $Sb(N_3)_3$, respectively, according to Equation (1) (M = As, Sb).

$$MF_3 + 3\,(CH_3)_3SiN_3 \xrightarrow{SO_2} M(N_3)_3 + 3\,(CH_3)_3SiF \qquad (1)$$

Removal of the volatile compounds, SO_2, $(CH_3)_3SiF$, and excess $(CH_3)_3SiN_3$, at ambient temperature results in pure triazides.

$As(N_3)_3$, which had previously been prepared by the reaction of $AsCl_3$ with NaN_3 and been reported to be a yellowish liquid,[1] was obtained as a white solid. Single crystals of arsenic triazide were obtained by slow and careful sublimation in a dynamic vacuum. The crystalline product melts at 37 °C. The molten $As(N_3)_3$ decomposes at 62 °C, resulting in a milky liquid that explodes at about 160 °C.

Crude $Sb(N_3)_3$ was isolated as a white solid with a decomposition point of 130 °C. Despite previous reports of explosive decomposition upon attempted sublimation,[2] we were able to obtain colorless crystals by sublimation of the crude product in a static vacuum at 100–110 °C. It should be emphasized that $As(N_3)_3$ and $Sb(N_3)_3$ are sensitive to mechanical shock and can explode violently.

Crystal structure of $As(N_3)_3$: Clear colorless $As(N_3)_3$ crystallizes in the monoclinic system (Table 1). The crystal structure of $As(N_3)_3$ is shown in Figure 1, and the atomic coordinates and bond lengths are listed in Tables 2 and 3. The three azido groups are arranged in a pyramidal, propeller-type fashion, which is in contrast to the $[C(N_3)_3]^+$ ion, which exhibits a trigonal planar arrangement for the central carbon atom and the three α-nitrogen atoms.[5] This difference in the structures of $M(N_3)_3$ (M = As, Sb) and $[C(N_3)_3]^+$ is due to the presence of a sterically active lone valence electron pair on As and Sb (see Figure 2).

The presence of a sterically active, free valence-electron pair on As was verified both experimentally and theoretically. Experimentally, a difference electron-density contouring of the X-ray diffraction data clearly shows the presence of the free pair (see Figure 3a). Theoretically, the RHF/6–

[a] Dr. R. Haiges, Dr. S. Schneider, Dr. T. Schroer, Dr. M. Gerken, Prof. K. O. Christe
Loker Research Institute
University of Southern California
Los Angeles, CA 90089–1661 (USA)
Fax: (+1) 213-740-6679
E-mail: kchriste@usc.edu

[b] Dr. A. Vij, Dr. J. A. Boatz, Prof. K. O. Christe
ERC, Inc. and Space and Missile Propulsion Division
Air Force Research Laboratory (AFRL/PRSP)
10 East Saturn Boulevard, Bldg 8451
Edwards Air Force Base, CA 93524 (USA)
E-mail: kchriste@usc.edu

DOI: 10.1002/chem.200305482

Table 1. Crystal data and structure refinement for $As(N_3)_3$ and $Sb(N_3)_3$.

	$As(N_3)_3$	$Sb(N_3)_3$
formula	AsN9	N9Sb
M_r	201.01	247.84
T [K]	213(2)	223(2)
space group	$P2_1/c$	$R\bar{3}$
a [Å]	7.3263(7)	7.6998(9)
b [Å]	11.716(1)	
c [Å]	6.9865(7)	
α [°]	90	55.79(2)
β [°]	107.219(2)	
V [Å^3]	572.8(1)	291.26(6)
Z	4	2
ρ_{calcd} [g cm^{-3}]	2.331	2.826
μ [mm^{-1}]	5.863	4.667
crystal size [mm]	$0.34\times0.25\times0.14$	$0.12\times0.10\times0.08$
λ [Å]	0.71073	0.71073
R_{int}	0.0272	0.0422
transmission factors	0.4941, 0.2404	0.7065, 0.6043
goodness-of-fit on F	1.098	1.132
$R1$, $wR2$ $[I>2\sigma(I)]$	0.0240 0.0641	0.0320, 0.0849
$R1$, $wR2$ (all data)	0.0254, 0.0650	0.0328, 0.0856

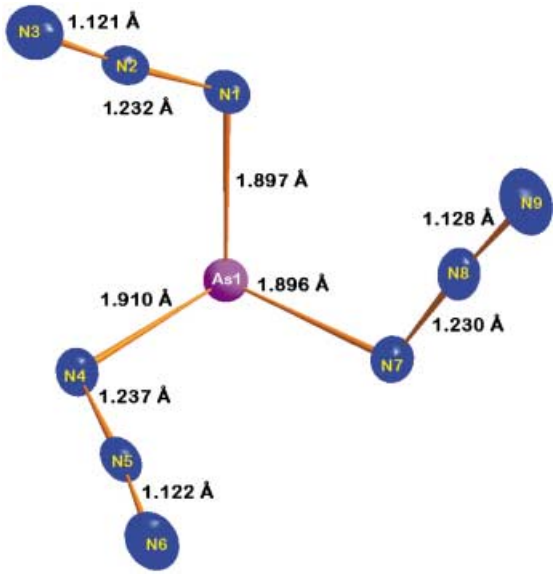

Figure 1. An ORTEP plot of $As(N_3)_3$ with displacement ellipsoids at the 40% probability level.

Table 2. Atomic coordinates ($\times10^4$) and equivalent isotropic displacement parameters [Å$^2\times10^3$] for $As(N_3)_3$. U_{eq} is defined as one third of the trace of the orthogonalized U_{ij} tensor.

	x	y	z	U_{eq}
As1	2858(1)	4451(1)	6183(1)	21(1)
N1	1116(3)	4819(2)	3655(3)	27(1)
N2	1725(3)	4783(2)	2190(3)	22(1)
N3	2190(3)	4790(2)	799(3)	35(1)
N4	4850(3)	3837(2)	5241(3)	25(1)
N5	4994(2)	2785(2)	5223(3)	23(1)
N6	5226(3)	1840(2)	5180(4)	37(1)
N7	1743(3)	3030(2)	6499(3)	26(1)
N8	250(3)	2776(2)	5209(3)	27(1)
N9	-1129(3)	2495(2)	4091(4)	41(1)

Table 3. Bond lengths [Å], bond angles [°], and torsion angles for $As(N_3)_3$ and $Sb(N_3)_3$.

	$As(N_3)_3$	$Sb(N_3)_3$
M–N1	1.897(2)	2.119(4)
M–N4	1.910(2)	2.119(4)[a]
M–N7	1.896(2)	2.119(4)[b]
N1–N2	1.232(3)	1.233(6)
N2–N3	1.121(3)	1.131(6)
N4–N5	1.237(3)	1.233(6)[a]
N5–N6	1.122(3)	1.131(6)[a]
N7–N8	1.231(3)	1.233(6)[b]
N8–N9	1.128(3)	1.131(6)[b]
N1-M-N4	97.87(9)	90.1(2)
N1-M-N7	96.51(9)	90.1(2)[a]
N7-M-N4	96.22(8)	90.1(2)[b]
N2-N1-M	117.1(2)	115.8(3)
N5-N4-M	117.1(2)	115.8(3)[a]
N8-N7-M	116.6(2)	115.8(3)[b]
N3-N2-N1	175.9(2)	178.3(5)
N6-N5-N4	175.8(2)	178.3(5)[a]
N9-N8-N7	176.3(2)	178.3(5)[b]
M-N1-N2-N3	161(4)	148(17)
M-N4-N5-N6	171(4)	
M-N7-N8-N9	171(4)	
N1-M-N4-N5	102.5(2)	
N1-M-N7-N8	5.1(2)	
N4-M-N1-N2	11.9(2)	9.9(3)
N4-M-N7-N8	103.8(2)	
N7-M-N1-N2	109.1(2)	100.1(3)
N7-M-N4-N5	5.0(2)	

[a] Transformation = z, x, y. [b] Transformation = y, z, x.

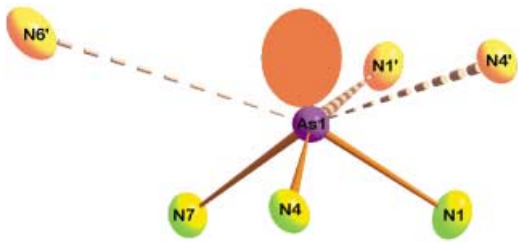

Figure 2. An ORTEP plot of $As(N_3)_3$ at the 40% probability level showing the sterically active free valence-electron pair of arsenic and the three closest nitrogen contacts that give the arsenic atom a coordination number of seven.

31G(d) Boys localized orbitals[6] of the C_3(anti) local minimum geometry were computed, and a two-dimensional contour plot of the sterically active lone pair on the arsenic atom is shown in Figure 3b. Similarly, the MP2/6–31G(d) total electron density was analyzed by using Bader's Atoms in Molecules (AIM) method.[7] A two-dimensional contour plot of the laplacian of the total electron density (i.e., $\nabla^2\rho$) is shown in Figure 3c. The localized negative region of the laplacian on the arsenic atom along the direction of the C_3 symmetry axis is consistent with the presence of a sterically active lone pair.

In $As(N_3)_3$, the three azido groups point away from the arsenic lone pair. The torsion angles (Table 3) clearly show that the $As(N_3)_3$ structure lacks perfect C_3 symmetry. The values for the N7-As1-N4-N5 and N1-As1-N7-N8 angles are similar with 5.0(2) and 5.1(2)°, respectively, but different

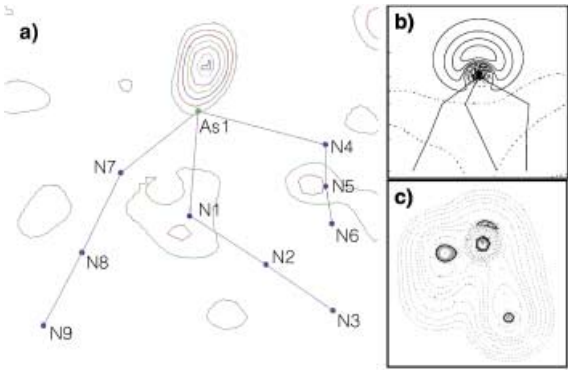

Figure 3. Experimental and theoretical evidence for the presence of a sterically active free valence-electron pair in $As(N_3)_3$: a) Difference electron density contour from the X-ray diffraction data. b) Contour plot of the RHF/6–31G(d) Boys localized sterically active lone pair orbital on As, in a plane containing the C_3 symmetry axis of the C_3(*anti*) structure; solid and dashed contours correspond to positive and negative values, respectively; the spacing between contour lines is 0.05 $bohr^{3/2}$. c) Contour plot of the MP2/6–31G(d) laplacian of the total electron density of the C_3(*anti*) geometry, in a plane containing the C_3 symmetry axis; solid and dashed lines correspond to negative and positive values, respectively.

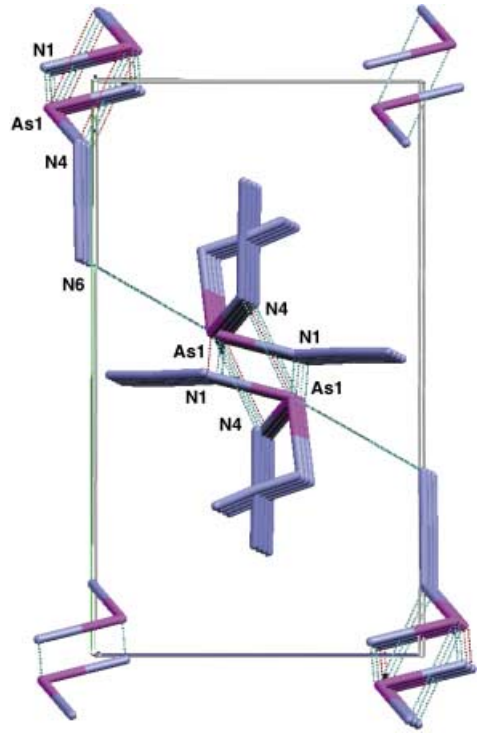

Figure 5. Crystal packing of $As(N_3)_3$, viewed along the chains and the *a* axis, showing the stacking of the arsenic–nitrogen parallelograms around the inversion centers along the origin and cell edges. The individual chains are linked to each other through diagonal As1–N6 contacts that penetrate the *ab* plane.

from the N4-As1-N1-N2 angle of 11.9(2)°, indicating the presence of nonequivalent azido groups. A mean least-squares planes analysis of the azido groups relative to the plane formed by the three α-nitrogen atoms further substantiates the nonequivalence of these groups. The twists of the azido groups N1-N2-N3, N4-N5-N6, and N7-N8-N9 relative to the mean plane formed by N1, N4, and N7 are 46.9(2), 43.0(2) and 57.9(3)°, respectively.

Packing diagrams for $As(N_3)_3$ are shown in Figures 4 and 5. It is well known that arsenic atoms can accommodate at least six closely packed fluoride ligands, as in AsF_6^-. It is, therefore, not surprising that arsenic seeks a coordination number higher than four in $As(N_3)_3$. For $SbCl(N_3)_2$, it has previously been shown[8] that the antimony atom can expand its coordination number by the formation of nitrogen bridges involving the α-nitrogen atoms of the azido ligands. This bridging mode results in four-membered rings containing two antimony and two N_α atoms. These rings are interconnected through the antimony atoms, thus forming infinite zigzag chains. The same bridging principle is observed for $As(N_3)_3$, in which two of its azido groups, N1-N2-N3 and N4-N5-N6, participate in the formation of the infinite chain structure through the formation of fused As_2N1_2 and As_2N4_2 dimeric parallelograms (see Figure 4). These chains run along the *a* axis with the two parallelograms twisted at ~74° with respect to each other. The bridge bond lengths are 2.970 Å for the rings involving the N4 atoms and 3.069 Å for the rings involving the N1 atoms. The nonequivalence of the two rings is caused by N6 forming an additional bridge of 3.198 Å to an arsenic atom of a neighboring chain, perpendicular to the *ab* plane, thus interconnecting the

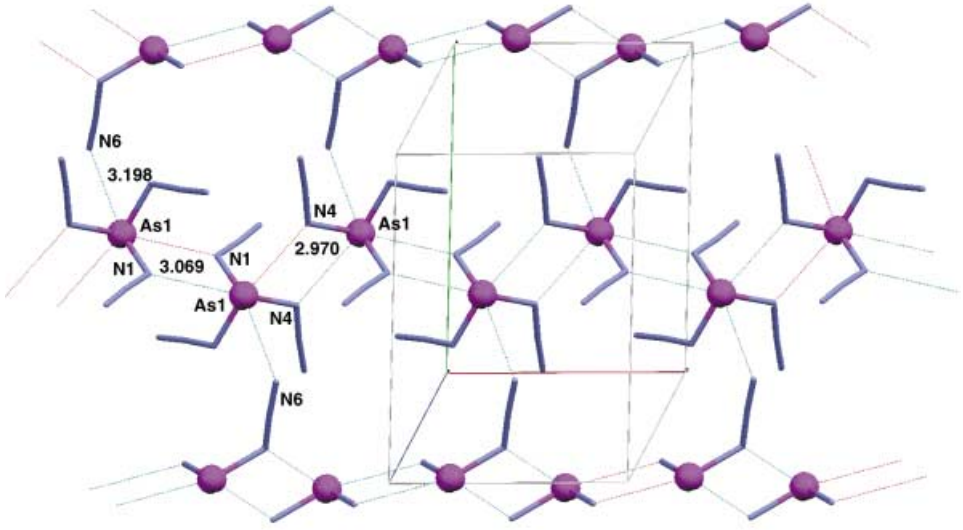

Figure 4. Crystal packing of $As(N_3)_3$ along the *b* axis showing the zig-zag arrangement of alternating $As1_2N1_2$ and $As1_2N4_2$ parallelograms. These chains run along the *a* axis and are linked to adjacent chains by As1–N6 bonds. The N7-N8-N9 azido groups do not participate in the bridging.

individual chains to form a three dimensional network (see Figure 5). Like the chlorine ligand in $SbCl(N_3)_2$, the third azido ligand, N7-N8-N9, does not participate in the bridging. This packing arrangement accounts for the nonequivalence of the three azido ligands in $As(N_3)_3$ and provides the arsenic atoms with a coordination number of seven with three azido ligands, three nitrogen bridges, and one free valence-electron pair. The arrangement is that of a distorted monocapped octahedron, with the free valence-electron pair occupying the monocap position. The angle, formed by the bridge bonds, is significantly larger than that between the azido ligands (Figure 2). The relative ease with which crystal packing effects can deform the $As(N_3)_3$ structure from the ideal C_3 symmetry is also supported by the theoretical calculations (see below). It was found that the four stable isomers, which exhibit different orientations of the azido groups, differ in energy by a mere 3 kcal mol^{-1} or less.

Crystal structure of of $Sb(N_3)_3$: This molecule (Figure 6 and Tables 3 and 4) represents a "text-book" example of perfect C_3 symmetry. The asymmetric SbN_3 unit has an azido group

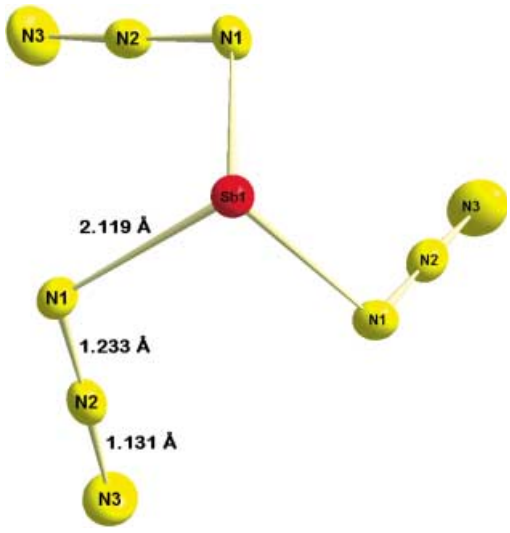

Figure 6. An ORTEP plot of $Sb(N_3)_3$ with displacement ellipsoids at the 40% probability level.

Table 4. Atomic coordinates ($\times 10^4$) and equivalent isotropic displacement parameters [Å$^2 \times 10^3$] for $Sb(N_3)_3$. U_{eq} is defined as one third of the trace of the orthogonalized U_{ij} tensor.

	x	y	z	U_{eq}
Sb1	6897(1)	6897(1)	6897(1)	21(1)
N1	8642(6)	6330(6)	3834(7)	22(1)
N2	7558(7)	7362(7)	2605(7)	24(1)
N3	6612(8)	8311(8)	1432(8)	39(1)

covalently bonded to the antimony atom that lies on a threefold rotational axis. The symmetry operations z,x,y and y,z,x for a rhombohedral setting for space group $R\bar{3}$ generate the remaining two azido groups, thus placing the antimony atom at the pivot of a propeller-shaped molecule. The Sb–N distance of 2.119(4) Å is shorter than the two Sb–N distances of 2.152(8) and 2.1444(7) Å found in the crystal structure of $SbCl(N_3)_2$.[8] The azido groups are almost linear with N-N-N angles of 178.3(5)°. As found for the $As(N_3)_3$ structure, the N_α–N_β distance of 1.233(6) Å is longer than the N_β–N_γ distance of 1.131(6) Å. However, in the case of $SbCl(N_3)_2$,[8] one of the azido groups has an "abnormal" N_α–N_β distance of 0.98(1) Å, which is shorter than the N_β–N_γ distance of 1.28(1) Å. This peculiarity has also been observed by us for mixed chloride/azide antimony(v) anions, $[Ph_4M]^+[SbCl_x(N_3)_{6-x}]^-$ ($x=2$–5; M = P or As) and the $Te(N_3)_5^-$ ion,[9] and by others for the structures of some azido derivatives of platinum,[10–12] vanadium,[13] and tantalum.[14] In our opinion, these unusually short distances are not real and are due to partial occupancy of some azide sites by other atoms, such as chlorine.

In $Sb(N_3)_3$ and $SbCl(N_3)_2$, the angles at the Sb atom are compressed from an ideal tetrahedral value of 109.5° to ~90°. This angle compression is caused by the increased repulsion from the sterically active free valence-electron pair on antimony. Because this effect increases with increasing size of the central atom, it is less pronounced for $As(N_3)_3$, which exhibits an N-As-N angle of 97.9°, and for isoelectronic $Te(N_3)_3^+$ in its SbF_6^- salt. The latter is significantly distorted from ideal C_3 symmetry due to crystal packing effects and fluorine bridging, and exhibits N-Te-N angles ranging from 91.9° to 97.3°.[15] Furthermore, the Sb-N-N angles of 115.8(3)° in $Sb(N_3)_3$ are smaller than those of ~120° found in $SbCl(N_3)_2$.[8] In accord with the requirements for C_3 symmetry, the torsion angles in $Sb(N_3)_3$ are all identical and, due to the almost linear azide group (178.3(5)°), the M-N-N-N torsion angles are poorly determined.

One of the most interesting consequences of the high symmetry of $Sb(N_3)_3$ is its crystal packing. Figure 7 shows aesthetically pleasing views down the z (111) axis. Each of the molecules has a threefold local symmetry, but the z axis also constitutes the crystallographic threefold axis. When no bonds are displayed, the nitrogen packing mimics the "Star of David". However, when all bonds are displayed, an inorganic pseudo[18]crown-6 evolves in which six antimony atoms form a perfect hexagon and encapsulate two $Sb(N_3)_3$ molecules located on a pseudo-S_6 axis passing through the center of the hexagonal cell. The two central $Sb(N_3)_3$ molecules are stacked with the lone pairs on antimony pointing away from each other and the three azido groups on each antimony being rotated by 60° from each other, forming a perfectly staggered structure. When viewed from the top, each individual $Sb(N_3)_3$ unit resembles the three legged "Isle of Man" emblem.

When viewed from the side (see Figure 8), the packing can be described as a sheet structure. Within each sheet, there are two $Sb(N_3)_3$ layers. The antimony atoms of each layer point in opposite directions and form triangular funnel-like holes. The antimony atoms of one layer are located deep inside the holes of the other layer and reside ~0.9 Å beyond the plane formed by the antimony atoms of the other layer. The resulting close contact between the two layers allows each antimony to form three close contacts of 2.844 Å with α-nitrogen atoms from three neighboring $Sb(N_3)_3$ units, thus creating two-dimensional sheets (see

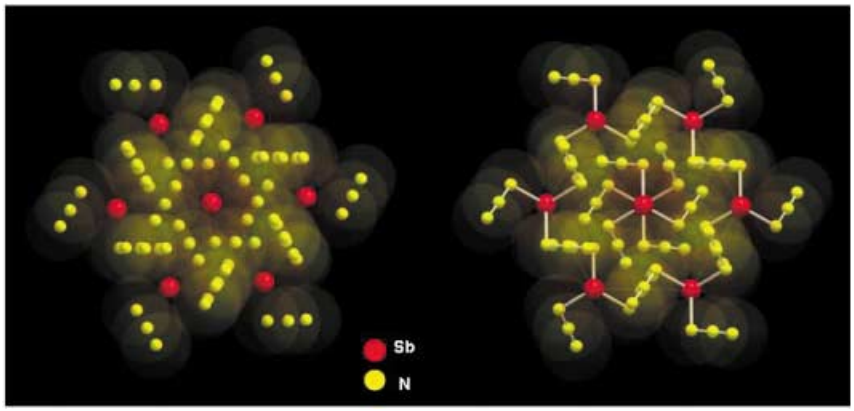

Figure 7. Packing diagrams of $Sb(N_3)_3$ viewed again along the z axis. The left-hand picture, in which the nitrogen atoms are highlighted in yellow forms a "Star of David" pattern, while in the right-hand picture, the addition of the connecting bonds emphasizes the six-fold high symmetry of the structure and gives the appearance of a crown made up from "Isle of Man" emblem subunits.

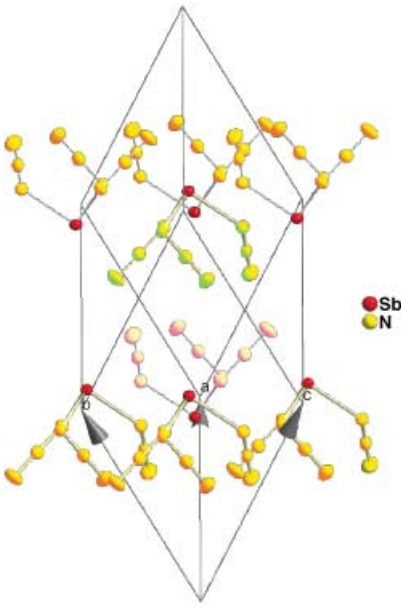

Figure 8. Side view of the $Sb(N_3)_3$ structure showing two sheets interconnected through staggered azido groups.

Figure 9). This gives antimony a total coordination number of seven (three equivalent azido ligands, three equivalent nitrogen bridges, and one sterically active, free valence-electron pair). Because of the increased repulsion from the free valence-electron pair of antimony, the angle between the Sb···N bridges is opened to 118.7°, while the N-Sb-N angle is compressed to about 90°. The Sb···N bridges result in the formation of three α-nitrogen-bridged, perfectly planar, four-membered rings around each antimony atom. A mean least-square plane analysis shows that they form angles of 76.6° with each other and are arranged in a fashion resembling the "Mitsubishi" emblem (see insert in Figure 9). The contacts between the sheets consist of staggered azido groups that are rotated by 60°with respect to each other.

The $Sb(N_3)_3$ and $As(N_3)_3$ packings have several features in common. In both structures, the central atoms have coordination numbers of seven with three azide ligands, three nitrogen bridges, and one sterically active free valence-electron pair. Furthermore, both molecules associate through the formation of N_α-bridged four-membered rings. However, in $Sb(N_3)_3$, all three N_α atoms participate equally in the bridge formation (see "Mitsubishi" insert in Figure 9), while in $As(N_3)_3$ only two N_α atoms and one N_γ atom are involved ("half-Mitsubishi", see Figure 10). This results in a ribbon-like structure for $As(N_3)_3$ and a sheet structure for $Sb(N_3)_3$. Also, the bridges in $Sb(N_3)_3$ are much stronger

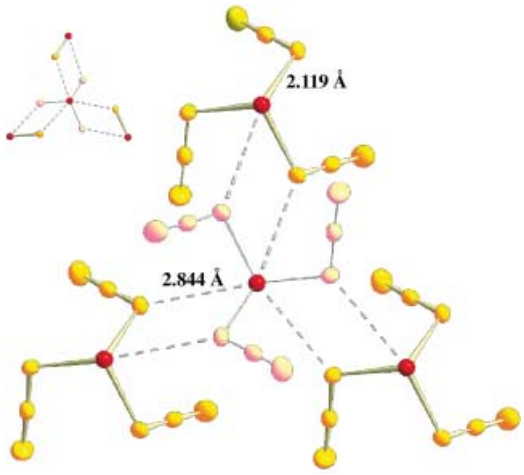

Figure 9. Nitrogen bridging within the $Sb(N_3)_3$ sheets. The insert shows the "Mitsubishi emblem" pattern of the bridging.

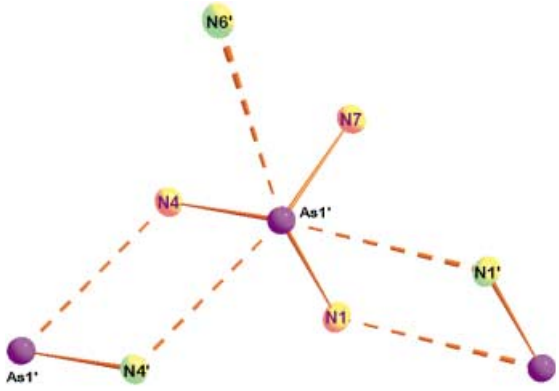

Figure 10. Nitrogen bridging within the $As(N_3)_3$ chains, showing a "Half-Mitsubishi" pattern.

(2.844 Å, while the sum of the covalent van der Waals radii is 3.66 Å) than those in $As(N_3)_3$ (2.970, 3.069, and 3.198 Å, while the sum of the covalent van der Waals radii is only 3.40 Å).

^{14}N NMR spectra: As expected for covalently bonded azides,[4] three well-resolved resonances were found for both compounds in their ^{14}N NMR spectra in CH_2Cl_2 at 25 °C. The $As(N_3)_3$ molecule shows a very broad signal at $\delta = -290$ ppm ($\Delta\nu_{1/2} = 300$ Hz) for the N_α atoms, a sharp signal at $\delta = -145.3$ ppm ($\Delta\nu_{1/2} = 14$ Hz) for the N_β atoms, and a medium-sharp resonance at $\delta = -175.9$ ppm ($\Delta\nu_{1/2} = 34$ Hz) for the N_γ atoms. This is in disagreement with the data previously reported for this compound, $\delta = -318.0$ (N_α), -131.1 (N_β), and -165.2 ppm (N_γ).[1,16] However, the observed ^{14}N NMR resonances for $Sb(N_3)_3$ of $\delta = -324.5$ ($\Delta\nu_{1/2} = 139$ Hz, N_α), -136.2 ($\Delta\nu_{1/2} = 18$ Hz, N_β), and -172.3 ppm ($\Delta\tilde{\nu}_{1/2} = 23$ Hz, N_γ) are in good agreement with the data reported previously.[2]

Theoretical calculations: Geometry optimizations were performed for $As(N_3)_3$ and $Sb(N_3)_3$ by using second-order perturbation theory methods (MP2, also known as MBPT(2)).[17,18] All stationary points were verified as local minima through diagonalization of the matrix of energy second derivatives with respect to nuclear displacements (i.e., the hessian matrix).

Four local minima were located for $As(N_3)_3$ (see Figure 11 and Table 5). Zero-point vibrational-energy corrections for these minima differed by less than 0.1 kcal mol^{-1}. In the most stable minimum at the MP2 level, (**3**, C_1), two azido ligands adopt an approximate *anti*-orientation relative to the stereochemically active lone pair on the As atom, with the remaining azido ligand in a *gauche*-like orientation. The second most stable isomer (**1**, C_3) is 0.4 kcal mol^{-1} higher in energy than **3** and has all three azido ligands in an *anti* orientation. The isomer with two *gauche* azido ligands and one *anti* azido ligand (**2**) has C_s symmetry and is 0.7 kcal mol^{-1} higher in energy than **3**. Finally, the least stable minimum (**4**) has all three azido groups in a *gauche* orientation (C_3 symmetry) and is 3.0 kcal mol^{-1} higher in energy than **3**. The observed crystal structure is best described as a somewhat distorted C_3 structure with the three azido ligands in an *anti* configuration. The calculated small energy differences can account for the ease with which this compound can distort from the ideal C_3 symmetry under the influence of crystal packing effects.

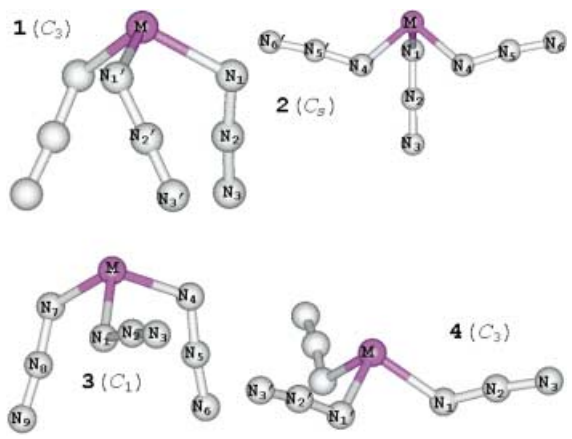

Figure 11. Local minima calculated for $As(N_3)_3$ (**1**–**4**) and $Sb(N_3)_3$ (**1** and **3**) at the MP2 level of theory. The values for the calculated bond lengths, bond angles, and torsion angles are given in Table 5.

Table 5. Calculated bond lengths [Å], bond angles [°], and torsion angles [°] for the local minima (**1**–**4**; see Figure 11) $As(N_3)_3$ (the values for $Sb(N_3)_3$ for minima **1** and **3** are given in parantheses) at the MP2 level of theory.

Compound **1**: $E = +0.4$ kcal mol^{-1} (0.0)			
M–N1	1.888 (2.069)	N2–N3	1.171 (1.196)
N1–N2	1.245 (1.267)		
N1-M-N1′	99.4 (96.2)	N3-N2-N1	175.0 (174.5)
N2-N1-M	117.6 (115.1)		
N3-N2-N1-M	164.9 (160.6)	N2-N1-M-N1′	81.7 (19.5)
Compound **2**: $E = +0.7$ kcal mol^{-1}			
M–N1	1.876	M–N4	1.877
N1–N2	1.246	N4–N5	1.246
N2–N3	1.170	N5–N6	1.171
N1-M-N4	99.9	N5-N4-M	117.9
N4-M-N4′	87.1	N3-N2-N1	174.6
N2-N1-M	117.2	N6-N5-N4	172.6
N3-N2-N1-M	180.0	N5-N4-M-N1	89.8
N6-N5-N4-M	180.0	N5-N4-M-N4	170.7
N2-N1-M-N4′	44.4		
Compound **3**: $E = 0.0$ kcal mol^{-1} (0.6)			
M–N1	1.893 (2.065)	N7–N6	1.246 (1.268)
M–N4	1.883 (2.063)	N2–N3	1.172 (1.199)
M–N7	1.865 (2.046)	N5–N6	1.171 (1.197)
N1–N2	1.243 (1.262)	N8–N9	1.169 (1.194)
N4–N5	1.245 (1.267)		
N1-M-N4	98.7 (95.3)	N8-N7-M	118.8 (117.2)
N4-M-N7	101.9 (98.2)	N3-N2-N1	173.6 (174.2)
N1-M-N7	92.5 (89.2)	N6-N5-N4	174.7 (174.7)
N2-N1-M	118.7 (120.5)	N9-N8-N7	173.6 (173.2)
N5-N4-M	118.0 (114.5)		
Compound **4**: $E = +3.0$ kcal mol^{-1}			
M–N1	1.871	N2–N3	1.171
N1–N2	1.245		
N1-M-N1′	93.4	N3-N2-N1	172.8
N2-N1-M	118.0		
N3-N2-N1-M	178.2	N2-N1-M-N1′	102.3

For $Sb(N_3)_3$, two local minima with C_3 and C_1 symmetry were located, with virtually identical zero-point vibrational-energy corrections. The C_3 structure has all azido ligands oriented *anti* with respect to the Sb lone pair. In the C_1 minimum, which is 0.6 kcal mol^{-1} less stable than the C_3 isomer, two azido ligands are *anti* and the third azide is *gauche* (see Figure 11 and Table 5). Our results are in reasonably good agreement with previous HF/6–31+G* and BLYP computations[19] for $As(N_3)_3$ and $Sb(N_3)_3$ and with the experimentally observed values (see above). The most significant difference

is the length of the terminal N–N bonds, which is overestimated in our calculations by about 0.05 Å.

Vibrational spectra: The infrared and Raman spectra of $As(N_3)_3$ and $Sb(N_3)_3$ are shown in Figures 12 and 13, respectively. Tables 6 and 7 summarize the computed and observed frequencies. The vibrational spectra of both compounds demonstrate the presence of covalently bonded azido ligands. The presence of more than one azido ligand results in in-phase and out-of-phase coupling, and the internal azido modes split into two components. For C_3 symmetry, the out-of-phase E modes are doubly degenerate and, in some cases, can be split due to a lifting of the degeneracy. The observation of extra bands in the 1350 to 1100 cm^{-1} region is attributed to Fermi resonance of ν_2 and ν_{10} with the appropriate combination bands or overtones.

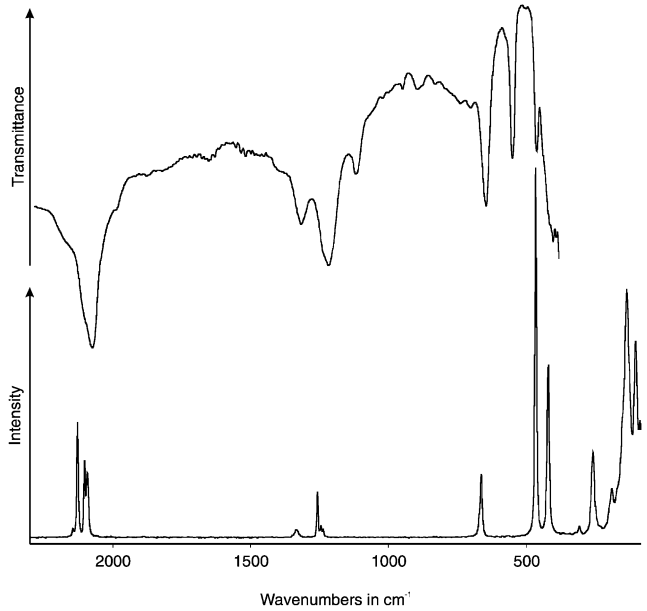

Figure 12. Infrared (upper trace) and Raman (lower trace) spectra of solid $As(N_3)_3$.

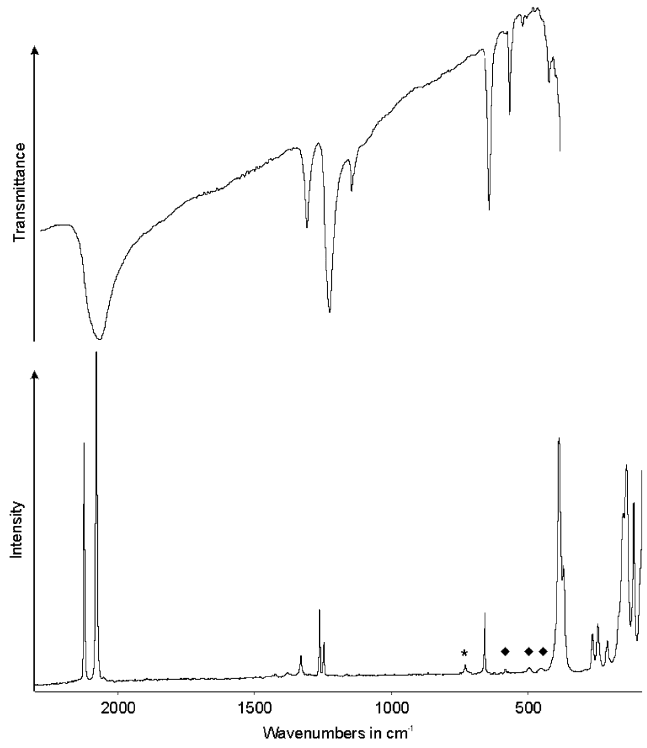

Figure 13. Infrared (upper trace) and Raman (lower trace) spectra of solid $Sb(N_3)_3$. The band marked by an asterisk is due to the FEP sample tube. Bands marked by ◆ are believed to be caused by a small amount of an unknown impurity.

For $As(N_3)_3$, the best fit between observed and computed frequencies is obtained for the C_3(**1**) isomer, in accord with the observed crystal structure. The fit between observed and calculated frequencies is good for both $As(N_3)_3$ and $Sb(N_3)_3$. As might be expected, the nitrogen bridging lowers the skeletal AsN_3 and SbN_3 stretching frequencies and increases those of the deformation modes. This effect is more pronounced for $Sb(N_3)_3$ because of the stronger bridging. The general agreement between the vibrational spectra of $As(N_3)_3$ and $Sb(N_3)_3$ is very good and supports our vibrational analysis. The only ambiguity is the observation of one weak Raman at 191 and 211 cm^{-1} in $As(N_3)_3$ and $Sb(N_3)_3$, respectively, which could not be accounted for in our assignments and were tentatively assigned to a stretching mode involving the nitrogen bridges.

Conclusion

The exact structures of the highly explosive $As(N_3)_3$ and $Sb(N_3)_3$ molecules have been determined for the first time. Both structures can be derived from an ideal C_3 symmetry with the azido ligands being bent away from the sterically active, free valence-electron pair of the central atom. Additional nitrogen bridging increases the coordination numbers of arsenic and antimony to seven. The basic motif for the nitrogen bridging are four-membered dimeric rings consisting of two As or Sb atoms and two α-nitrogen atoms from two azido ligands. For $As(N_3)_3$, only two of its three azido ligands participate in the association process, resulting in an infinite zigzag chain structure and destroying the perfect C_3 symmetry. For $Sb(N_3)_3$, however, all three azido ligands take part equally in the association and produce a highly symmetrical sheet structure, representing a case of perfect rhombohedral C_3 symmetry.

Experimental Section

Caution! *Arsenic and antimony azide compounds are potentially toxic and can decompose explosively under various conditions! They should be handled only on a scale of less than 2 mmol with appropriate safety precautions (safety shields, safety glasses, face shields, leather gloves, protective clothing, such as leather suits, and ear plugs). Teflon containers should be used, whenever possible, to avoid hazardous fragmentation. Ignoring safety precautions can lead to serious injuries.*

Materials and apparatus: All reactions were carried out in Teflon–FEP ampules that were closed by stainless steel valves. Volatile materials were handled in a stainless steel-Teflon-FEP or Pyrex glass vacuum line. All reaction vessels and the stainless steel line were passivated with ClF_3

Table 6. Comparison of observed and unscaled calculated MP2 vibrational frequencies [cm^{-1}] and intensities for C_3(**1**) $As(N_3)_3$.

Mode		Approx. mode description in point group C_3	Observed[a,g] IR	Raman	Calculated[b] (IR) [Raman]
A	ν_1	$\nu_{as}N_3$ in phase	2121 (vs)	2128 [3.1]	2255 (506.9) [6.7]
	ν_2	ν_sN_3 in phase	1251 (s,sh)[e]	1257 [1.2][e]	1293 (122.8) [22.1]
	ν_3	δN_3 in phase, in plane		663 [1.7]	681 (0.7) [16.6]
	ν_4	δN_3 in phase, out of plane			532 (0.2) [0.8]
	ν_5	ν_sAsN_3	480 (m)	465 [10.0]	507 (27.3) [23.4]
	ν_6	δAsN_3 in phase	[c]	307 [0.3]	325 (35.5) [0.4]
	ν_7	δAs-N-N in phase	[c]	102 [2.7]	94 (0.2) [1.0]
	ν_8	τ in-phase	[c]	[d]	57.4 (0.0) [8.6]
E	ν_9	$\nu_{as}N_3$ out of phase	2092 (vs)	2103 [2.1][e] 2093 [1.8][e]	2215 (298.3) [6.1]
	ν_{10}	ν_sN_3 out of phase	1231 (s)	1244 [0.3][e,f] 1237 [0.2][e,f]	1280 (92.8) [6.8]
	ν_{11}	δN_3 out of phase, in plane	664 (m)		673 (25.3) [2.4]
	ν_{12}	δN_3 out of phase, out of plane	568 (m)		532 (10.1) [0.7]
	ν_{13}	$\nu_{as}AsN_3$	420 (s)	419 [4.6]	459 (83.5) [4.7]
	ν_{14}	δAsN_3 out of phase	[c]	257 [2.3]	243 (8.8) [1.4]
	ν_{15}	δAs-N-N out of phase	[c]	135 [5]	113 (0.4) [5.9]
	ν_{16}	τ out of phase	[c]	[d]	44 (0.0) [4.4]

[a] Relative IR and Raman intensities given in parentheses and square brackets, respectively. [b] IR intensities given in km mol^{-1} and Raman intensities given in $Å^4 amu^{-1}$. [c] Not observed, IR spectrum recorded only between 4000 and 400 cm^{-1}. [d] Not observed, Raman spectrum recorded only between 4000 and 80 cm^{-1}. [e] Splittings caused by deviation from C_3 symmetry, resulting in lifting of the degeneracy. [f] These modes show the following Fermi resonance splittings: IR: 1337 cm^{-1} (m) ($\nu_3 + \nu_{11}$) (E); 1133 cm^{-1} (mw) ($\nu_5 + \nu_{11}$) (E); Raman: 1334 cm^{-1} [0.2] ($2\nu_3$ or $2\nu_{11}$) (A). [g] In addition to the listed bands, a Raman band at 191 cm^{-1} [1] was observed which was not assigned. It might represent a nitrogen-bridge stretching mode.

Table 7. Comparison of observed and unscaled calculated MP2 vibrational frequencies [cm^{-1}] and intensities for $Sb(N_3)_3$.

Mode		Approx. mode description in point group C_3	Observed[a] IR	Raman	Calculated[b] (IR) [Raman]
A	ν_1	$\nu_{as}N_3$ in phase	2121 (s,sh)	2123 [7.4]	2183 (631.9) [8.3]
	ν_2	ν_sN_3 in phase	1243 (vs)[d]	1263 [2.2] [d]	1243 (114.7) [37.8]
	ν_3	δN_3 in phase, in plane		660 [2.4]	653 (0.0) [20.7]
	ν_4	δN_3 in phase, out of plane			585 (0.2) [0.5]
	ν_5	ν_sSbN_3	[c]	386 [7.5]	456 (16.0) [39.9]
	ν_6	δSbN_3 in phase	[c]	289 [0.1]	258 (35.6) [0.8]
	ν_7	δSb-N-N in phase	[c]	115 [4]	91 (0.2) [1.4]
	ν_8	τ in-phase	[c]	[f]	78 (0.1) [7.5]
E	ν_9	$\nu_{as}N_3$ out of phase	2085 (vs)	2079 [10.0]	2140 (252.0) [14.5]
	ν_{10}	ν_sN_3 out of phase	1243 (vs) [d]	1248 [1.2] [d]	1231 (59.1) [5.7]
	ν_{11}	δN_3 out of phase, in plane	659 (s)		643 (7.0) [1.9]
	ν_{12}	δN_3 out of phase, out of plane	583 (m)		567 (3.3) [0.5]
	ν_{13}	$\nu_{as}SbN_3$	[c]	370 [3]	414 (70.7) [5.4]
	ν_{14}	δSbN_3 out of phase	[c]	264 [1.8] [e] 247 [1.5]	199 (9.0) [1.1]
	ν_{15}	δSb-N-N out of phase	[c]	153 [4][e] 141[6.0]	109 (0.2) [7.0]
	ν_{16}	τ out of phase	[c]	[f]	56 (0.1) [4.2]

[a] Relative IR and Raman intensities given in parentheses and brackets, respectively.[b] IR intensities given in km mol^{-1} and Raman intensities given in $Å^4 amu^{-1}$. [c] Not observed, IR spectrum was recorded only between 4000 and 400 cm^{-1}. [d] These modes show the following Fermi resonance splittings: IR, 1326 cm^{-1} (m), ($\nu_3 + \nu_{11}$) (E); 1162 cm^{-1} (mw), ($\nu_5 + \nu_{11}$) (E); Raman: 1331 cm^{-1} [1.2], ($2\nu_3$ or $2\nu_{11}$) (A). [e] Splitting due to lifting of the degeneracy. In the low-frequency region, the following additional bands were observed and tentatively assigned: IR: 442 cm^{-1} (mw) νSbN_3; RA: 211 cm^{-1} [0.9], corresponding to the 191 cm^{-1} [1] band in $As(N_3)_3$. These Raman bands might represent stretching modes of the nitrogen bridges. [f] Not observed, Raman spectrum recorded only between 4000 and 80 cm^{-1}.

prior to use. Nonvolatile materials were handled in the dry argon atmosphere of a glove box.

Infrared spectra were recorded in the range 4000–400 cm^{-1} on a Midac FT-IR model 1720 at a resolution of 1 cm^{-1}. Spectra of solids were obtained by using dry powders pressed between AgCl windows in an Econo press (Barnes Engineering Co.). Raman spectra were recorded in the range 4000–80 cm^{-1} on a Bruker Equinox 55 FT-RA spectrophotometer using a Nd:YAG laser at 1064 nm with power levels of 100 mw or less. Pyrex melting point tubes that were baked out at 300 °C for 48 h at 10 mTorr vacuum or Teflon–FEP tubes with stainless steel valves that were passivated with ClF_3 were used as sample containers.

^{14}N NMR spectra were recorded at 36.13 MHz on a Bruker AMX 500 spectrometer in CH_2Cl_2 in sealed standard glass tubes. Neat CH_3NO ($\delta =$ 0.00 ppm) was used as external reference for ^{14}N.

The $(CH_3)_3SiN_3$ (Aldrich) and AsF_3 (Ozark) were purified by fractional condensation prior to use. The SbF_3 (Alfa Aesar) was purified by sublimation. The SO_2 (Aldrich) was condensed into a bulb and dried over CaH_2.

Preparation of $As(N_3)_3$: On the stainless steel vacuum line, AsF_3 (0.23 mmol) was condensed at −196 °C into a Teflon–FEP ampule. The ampule was then attached to a glass vacuum line and after evacuation, SO_2 (3.3 mmol) was condensed in at −196 °C. The mixture was allowed to warm to ambient temperature. After all the AsF_3 had dissolved, the ampule was cooled back again to −196 °C, and $(CH_3)_3SiN_3$ (0.885 mmol) was added. The ampule was kept at −40 °C for 30 min and then slowly warmed to room temperature over a period of 4 h, resulting in a colorless solution. The volatile components were pumped off, leaving behind a white solid (0.045 g, weight calculated for 0.23 mmol $As(N_3)_3 = 0.046$ g). Further pumping at ambient temperature led to the sublimation of the crude product resulting in the formation of crystalline material on the walls of the reaction vessel. Inspection of the volatile material trapped at −196 °C by gas-FTIR spectroscopy showed SO_2 and $(CH_3)_3SiF$[20,21] as the only reaction by-products. The crystalline solid was identified as $As(N_3)_3$ by vibrational and NMR spectroscopy and its crystal structure.

Preparation of $Sb(N_3)_3$: A sample of SbF_3 (0.47 mmol) was loaded in the dry box into a Teflon–FEP ampule, followed by the addition of SO_2 (5.8 mmol) in vacuo at −196 °C. The

mixture was warmed to room temperature to suspend the SbF_5 in the SO_2, cooled back again to −196 °C, and $(CH_3)_3SiN_3$ (2.16 mmol) was condensed in. The ampule was kept at −40 °C for 30 min and then slowly warmed to ambient temperature over a period of 4 h. Volatile components were pumped off and collected at −196 °C, leaving behind a white solid residue (0.120 g, weight calculated for 0.47 mmol of $Sb(N_3)_3$ = 0.116 g). The only volatile byproduct, identified by gas-FTIR spectroscopy, was $(CH_3)_3SiF$. The crude $Sb(N_3)_3$ was vacuum sublimed in a sealed glass tube at 100–110 °C. The obtained colorless crystals were characterized by vibrational and NMR spectroscopy and their crystal structure.

Crystal structure determinations: The single-crystal X-ray diffraction data were collected on a Bruker three-circle platform diffractometer, equipped with a SMART CCD (charge coupled device) detector, with the χ axis fixed at 54.74° and with $Mo_{K\alpha}$ radiation ($\lambda = 0.71073$ Å) from a fine-focus tube. An LT-3 apparatus was employed for the low-temperature data collection by using controlled liquid nitrogen boil off. A few well-formed single crystals, prepared by careful sublimation of the amorphous solid, were selected in a glove box, by using a CCD camera microscope. The selected crystals were immersed in PFPE (perfluoropolyether) oil, contained in the cavity of a culture slide. A Cryoloop was used for picking a crystal and mounting it on a magnetic goniometer head. Cell constants were determined from ninety 10 s frames. A complete hemisphere of data was scanned on omega (0.3°) with a run time of 30 s per frame at a detector resolution of 512 × 512 pixels using the SMART software.[22] A total of 1271 frames was collected in three sets and a final set of 50 frames, identical to the first 50 frames, was also collected to determine any crystal decay. The frames were then processed on a PC running on Windows NT software. The SAINT software[23] was used to obtain the *hkl* file corrected for Lp/decay. The absorption correction was performed by using the SADABS program.[24] For $As(N_3)_3$, the intensity statistics, that is, E^2-1 values, indicated a centrosymmetric space group. Furthermore, the absence of $0k0$ (k = odd) and $h0l$ reflections ($h+L$ = odd) showed the presence of a 2_1 screw axis and a *c*-glide plane parallel and perpendicular to the *b* axis, respectively. The space group was thus unambiguously assigned as $P2_1/c$. For $Sb(N_3)_3$, the reciprocal lattice was initially indexed as a hexagonal cell with cell constants of $a = 7.2046$ (10), $c = 19.439(4)$ Å, $V = 873.8(2)$ Å^3, and $Z = 6$. An alternate setting with a smaller rhombohedral cell was obtained by using the transformation matrix $\{^2/_3, {}^1/_3, {}^1/_3, {}^{-1}/_3, {}^1/_3, {}^1/_3, {}^{-1}/_3, {}^{-2}/_3, {}^1/_3\}$ with cell constants of $a = 7.6998(9)$, $\alpha = 55.787(17)°$, $V = 291.26(6)$ Å^3, and $Z = 2$. The structures were solved by the Patterson method by using the SHELX-90 program[25] and refined by the least-squares method on F^2, SHELXL-97,[26] incorporated in the SHELXTL Suite 5.10 for Windows NT.[27] All atoms were refined anisotropically. For the anisotropic displacement parameters, the U_{eq} is defined as one third of the trace of the orthogonalized U_{ij} tensor. For generating the difference electron density contours the $F_o - F_c$ was calculated by using the "EDEN" feature of the SHELXTL program.[27] The difference $F(000)$ value of 2 was used to compute the lone pair contour. Further details of the crystal investigations can be obtained from the Fachinformationszentrum Karlsruhe, 76344 Eggenstein-Leopoldshafen, Germany (Fax: (+49) 7247-808-666; E-mail: crysdata@fiz-karlsruhe.de) on quoting the depository numbers CSD-413359 and CSD-413360 for $Sb(N_3)_3$ and $As(N_3)_3$, respectively.

Computational methods: Optimizations of all structures were performed by using second-order perturbation theory.[17,18] . For $As(N_3)_3$, the Binning and Curtis double-zeta valence basis set,[28] augmented with a d-polarization function[29] was used for arsenic and the 6–31G(d) basis set[30,31] for nitrogen. For $Sb(N_3)_3$, the Stevens, Basch, and Krauss effective core potentials and the corresponding valence-only basis sets were used.[32] The SBK valence basis set for nitrogen was augmented with a d-polarization function[31] and a diffuse s+p shell,[33] whereas only a d-polarization function[34] was added to the antimony basis set. Hessians (energy second derivatives) were calculated for the final equilibrium structures to determine if they are minima (positive definite hessian) or transition states (one negative eigenvalue). All calculations were performed with the electronic structure code GAMESS.[35]

Acknowledgement

We are grateful to the National Science Foundation, the Air Force Office of Scientific Research and Defense Advance Research Projects Agency for financial support. R.H. is grateful to the Deutsche Forschungsgemeinschaft for a stipend. A grant of computer time by the Department of Defense High-Performance Computing Modernization Program at the Aeronautical Systems Center (Wright-Patterson AFB, OH) and Army High Performance Computing Research Center (Minneapolis, MN) is gratefully acknowledged.

[1] T. M. Klapötke, P. Geissler, *J. Chem. Soc. Dalton Trans.* **1995**, 3365.
[2] T. M. Klapötke, A. Schulz, J. McNamara, *J. Chem. Soc. Dalton Trans.* **1996**, 2985.
[3] K. Karaghiosoff, T. M. Klapötke, B. Krumm, H. Nöth, T. Schütt, M. Suter, *Inorg. Chem.* **2002**, *41*, 170.
[4] For recent reviews, see W. Fraenk, T. M. Klapötke, in *Inorganic Chemistry Highlights* (Eds.: G. Meyer, D. Naumann, L. Wesemann), Wiley-VCH, Weinheim, **2002**; T. M. Klapötke, *Chem. Ber.* **1997**, *130*, 443.
[5] a) U. Mueller, H. Baernighausen, *Acta Crystallogr. Sect B* **1970**, *26*, 1671; b) W. Kolitsch, U. Mueller, *Z. Anorg. Allg. Chem.* **1974**, *410*, 21; c) M. A. Petrie, J. A. Sheehy, J. A. Boatz, G. Rasul, G. K. S. Prakash, G. A. Olah, K. O. Christe, *J. Am. Chem. Soc.* **1997**, *119*, 8802.
[6] S. F. Boys, *Quantum Science of Atoms, Molecules, and Solids* (Ed.: P. O. Lowdin), Academic Press, NY, **1966**, pp. 253–262.
[7] R. F. W. Bader, *Atoms in Molecules: A Quantum Theory*, Clarendon, Oxford, **1990**.
[8] T. M. Klapötke, H. Nöth, T. Schütt, M. Warchold, *Z. Anorg. Allg. Chem.* **2001**, *627*, 81.
[9] R. Haiges, J. A. Boatz, M. Gerken, S. Schneider, T. Schroer, K. O. Christe, *Angew. Chem.* **2003**, *115*, 6027; *Angew. Chem. Int. Ed.* **2003**, *42*, 5847.
[10] B. Neumüller, F. Schmock, S. Schlecht, K. Dehnicke, *Z. Anorg. Allg. Chem.* **2000**, *626*, 1972.
[11] M. Atam, U. Mueller, *J. Organomet. Chem.* **1974**, *71*, 435.
[12] S. Schroeder, W. Preetz, *Z. Anorg. Allg. Chem.* **2001**, *627*, 390.
[13] M. Herberhold, A.-M. Dietel, W. Milius, *Z. Anorg. Allg. Chem.* **1999**, *625*, 1885.
[14] M. Herberhold, A. Goller, W. Milius, *Z. Anorg. Allg. Chem.* **2001**, *627*, 891.
[15] J. P. Johnson, G. K. MacLean, J. Passmore, P. S. White, *Can. J. Chem.* **1989**, *67*, 1687.
[16] P. Geissler, T. M. Klapötke, H.-J. Kroth, *Spectrochim. Acta* **1995**, *51A*, 1075.
[17] a) C. Moller, M. S. Plesset, *Phys. Rev.* **1934**, *46*, 618b) J. A. Pople, J. S. Binkley, R. Seeger, *Int. J. Quantum Chem. S10*, **1976**, 1; c) M. J. Frisch, M. Head-Gordon, J. A. Pople, *Chem. Phys. Lett.* **1990**, *166*, 275.
[18] R. J. Bartlett, D. M. Silver, *Int. J. Quantum Chem. Symp.* **1975**, *9*, 1927.
[19] T. M. Klapötke, A. Schulz, *Main Group Met. Chem.* **1997**, *20*, 325.
[20] K. Licht, P. Koehler, H. Kriegsmann, *Z. Anorg. Allg. Chem.* **1975**, *415*, 31.
[21] H. Bürger, *Spectrochim. Acta* **1968**, *24A*, 2015.
[22] SMART V 4.045 Software for the CCD Detector System, Bruker AXS, Madison, WI, **1999**.
[23] SAINT V 4.035 Software for the CCD Detector System, Bruker AXS, Madison, WI, **1999**.
[24] SADABS Program for absorption correction for area detectors, Version 2.01, Bruker AXS, Madison, WI, **2000**.
[25] G. M. Sheldrick, SHELXS-90, Program for the Solution of Crystal Structure, University of Göttingen, Germany, **1990**.
[26] G. M. Sheldrick, SHELXL-97, Program for the Refinement of Crystal Structure, University of Göttingen, Germany, **1997**.
[27] SHELXTL 5.10 for Windows NT, Program library for Structure Solution and Molecular Graphics, Bruker AXS, Madison, WI, **1997**.
[28] R. C. Binning, Jr., L. A. Curtiss, *J. Comput. Chem.* **1990**, *11*, 1206.
[29] A d-function polarization exponent of 0.293 was used.

[30] W. J. Hehre, R. Ditchfield, J. A. Pople, *J. Chem. Phys.* **1972**, *56*, 2257.
[31] The exponent of the d-polarization function on N is 0.8; see P. C. Hariharan, J. A. Pople, *Theor. Chim. Acta* **1973**, *28*, 213.
[32] W. J. Stevens, H. Basch, M. Krauss, *J. Chem. Phys.* **1984**, *81*, 6026.
[33] The exponent of the diffuse s+p shell is 0.0639; see T. Clark, J. Chandrasekhar, G. W. Spitznagel, P. von R. Schleyer, *J. Comput. Chem.* **1983**, *4*, 294.
[34] The exponent of the d polarization function on Sb is 0.211; seeS. Huzinaga, J. Andzelm, M. Klobukowski, E. Radzio-Andzelm, Y. Sakai, H. Tatewaki, *Gaussian Basis Sets for Molecular Calculations*, Elsevier, Amsterdam, **1984**.
[35] M. W. Schmidt, K. K. Baldridge, J. A. Boatz, S. T. Elbert, M. S. Gordon, J. H. Jensen, S. Koseki, N. Matsunaga, K. A. Nguyen, S. Su, T. L. Windus, *J. Comput. Chem.* **1993**, *14*, 1347.

Received: August 27, 2003 [F5482]

APPENDIX K

"Improved Synthesis of CsN_3"
Z. Anorg. Allg. Chem., 628, 909 (2002)

This Page Intentionally Left Blank

Improved Synthesis of CsN_3

Michael Gerken [a], Stefan Schneider [a], Thorsten Schroer [a], Ralf Haiges[a], and Karl O. Christe[a,b,*]

[a] Los Angeles, CA / USA, Loker Hydrocarbon Research Institute, University of Southern California
[b] Edwards Air Force Base, CA / USA, Air Force Research Laboratory,

Received December 24th, 2001.

Dedicated to Professor Joachim Strähle on the Occasion of his 65th Birthday

Abstract. Cesium azide can conveniently be prepared from anhydrous CsF and $(CH_3)_3SiN_3$ in SO_2 solvent in high purity and yield. In this reaction, the initially generated SO_2F^- anion is converted in SO_2 solvent to solvated azide, $(SO_2)_nN_3^-$, which is labile and releases SO_2 under dynamic vacuum yielding pure CsN_3.
Keywords: Cesium azide; Fluorosulfite; Azidosulfite

Verbesserte Synthese von CsN_3

Inhaltsübersicht. Caesiumazid kann bequem durch die Reaktion von wasserfreiem CsF und $(CH_3)_3SiN_3$ in SO_2-Lösung in hoher Reinheit und Ausbeute dargestellt werden. In dieser Reaktion wird das zuerst gebildete SO_2F^--Anion in SO_2-Lösung zu dem solvatisierten Azid, $(SO_2)_nN_3^-$ umgesetzt, das im dynamischen Vakuum labil ist und unter SO_2-Verlust reines CsN_3 ergibt.

Sodium azide is a widely used reagent and is technically prepared form $NaNH_2$ and N_2O [1]. The heavier alkali metal azides are generally prepared starting from NaN_3. Two general methodologies for the preparation of heavier alkali metal azides such as CsN_3 have been employed. The most common preparative route utilizes an aqueous solution of HN_3 which is neutralized by the corresponding alkali metal hydroxide or carbonate [2–4]. Aqueous HN_3 is generally prepared from NaN_3 and H_2SO_4 [2]. In the second approach, cesium and rubidium azide have been prepared via ion exchange chromatography starting from aqueous NaN_3 [5]. Since the handling of HN_3 is potentially hazardous, a facile synthetic route to CsN_3 without the use of HN_3 is highly desirable. Circumventing the use of HN_3 and laborious chromatographic techniques, $[N(CH_3)_4][N_3]$ has been prepared from $[N(CH_3)_4][F]$ and $(CH_3)_3SiN_3$ in CH_3CN solvent [6]. In the present note, we present a new facile laboratory preparation of CsN_3 starting from $(CH_3)_3SiN_3$ and CsF in SO_2 solvent.

Results and Discussion

In analogy to the synthesis of $[N(CH_3)_4][N_3]$, the preparation of CsN_3 was attempted from anhydrous CsF and excess $(CH_3)_3SiN_3$ in refluxing CH_3CN solvent. The reaction in CH_3CN solvent was found to be slow and did not yield pure CsN_3 even after five days. The reaction of CsF with neat $(CH_3)_3SiN_3$ was also found to be slow; even after three days at temperatures close to the boiling point of $(CH_3)_3SiN_3$ (93 °C) significant amounts of CsF were still present. The sluggishness of these reactions is presumably a consequence of the insufficient solubility of CsF in CH_3CN and $(CH_3)_3SiN_3$. The removal of $(CH_3)_3SiF$ and addition of fresh $(CH_3)_3SiN_3$ did not result in a significantly faster conversion, indicating either the absence of an equilibrium reaction or a coating of the starting material by the product.

Anhydrous CsF reacts with SO_2 solvent to the fluorosulfite anion, SO_2F^- (eq. (1)) [7]. The reaction of $[Cs][SO_2F]$ suspended in SO_2 with excess $(CH_3)_3SiN_3$ results in complete azide-fluoride exchange within less than one hour yielding a clear, yellow solution of $[Cs][(SO_2)_nN_3]$ according to eq. (2).

$$CsF + SO_2 \longrightarrow [Cs][SO_2F] \quad (1)$$

$$[Cs][SO_2F] + (CH_3)_3SiN_3 + nSO_2 \xrightarrow{SO_2} [Cs][(SO_2)_{n+1}N_3] + (CH_3)_3SiF \quad (2)$$

Removal of the volatiles (SO_2 and $(CH_3)_3SiF$) at ambient temperature results in precipitation of yellow $[Cs][(SO_2)_2N_3]$ which is converted to $[Cs][SO_2N_3]$ and $[Cs][N_3]$ upon prolonged pumping [8,9]. Pure $[Cs][N_3]$ is obtained after SO_2 removal under dynamic vacuum at 55 °C yielding a white solid. Since $[Cs][SO_2F]$ does not lose SO_2 at 55 °C, the complete conversion of F^- to N_3^- can be verified by the absence of signals associated with the SO_2F^- anion in the Raman spectrum.

Experimental

Materials and Apparatus. All volatile materials were handled in a Pyrex vacuum line equipped with Kontes Teflon valves. Nonvolatile materials were handled in the dry argon atmosphere of a dry box. The solvents, CH_3CN (Baker) and SO_2 (Aldrich, >99.9%) were dried over P_4O_{10} and CaH_2 and were freshly distilled prior to use. The CsF (KBI) was fused in a platinum crucible, transferred while hot to the dry box, and finely powdered. Trimethylsilyl azide (Ald-

* Prof. K. O. Christe
Loker Hydrocarbon Research Institute, University of Southern California
University Park
Los Angeles, CA 90089-1661/ USA
FAX: 001-(213) 740 6679
E-mail: karl.christe@edwards.af.mil

rich, 95%) was purified by fractional condensation through cold traps held at −35 and −196 °C and using the −196 °C fraction.

Preparation of CsN_3. In a typical reaction, anhydrous CsF (2.952 g, 0.0194 mol) was suspended in 8.861 g SO_2 at room temperature inside a glass vessel equipped with a Kontes valve. Excess trimethylsilyl azide (2.754 g, 0.0239 mol) was condensed onto the frozen reaction mixture at −196 °C. Upon warming to room temperature, the solid phase turned yellow and dissolved in the liquid SO_2 within 40 min, yielding a two-phase system consisting of a lower yellow and an upper colorless layer. Volatiles were removed under dynamic vacuum at ambient temperatures for approximately 30 min. yielding a yellow solid. Further pumping at 50 to 55 °C for ca. 2 hours yielded pure, colorless $[Cs][N_3]$ (3.4 g; 0.0194 mol).

Acknowledgements. The work at USC was financially supported by the National Science Foundation and the Defense Advanced Research Project Agency. Two of us (S. S. And T. S.) thank the Alexander von Humboldt Foundation for Feodor-Lynen Fellowships, one of us (R. H.) thanks the Deutsche Forschungsgemeinschaft and one of us (M. G.) thanks the Natural Sciences and Engineering Research Council of Canada for a postdoctoral fellowship.

References

[1] A. F. Holleman, E. Wiberg, *Lehrbuch der Anorganischen Chemie*, Walter de Gruyter, Berlin 1995, p. 666.
[2] A. W. Browne, *Inorg. Synth.* **1939**, *1*, 79.
[3] R. Suhrmann, K. Clusius, *Z. Anorg. Allg. Chem.* **1926**, *152*, 52.
[4] G. Brauer, *Handbook of Preparative Inorganic Chemistry, 2nd Edition*; Academic Press, New York 1963, pp. 472-476.
[5] K. Landskron, E. Irran, W. Schnick, *Chem. Eur. J.* **1999**, *5*, 2548.
[6] K. O. Christe, W. W. Wilson, R. Bau, S. W. Bunte, *J. Am. Chem. Soc.* **1992**, *114*, 3411.
[7] A. Kornath, F. Neumann, R. Ludwig, *Inorg. Chem.* **1997**, *36*, 5570.
[8] A. Kornath, O. Blecher, R. Ludwig, *Z. Anorg. Allg. Chem.* **2002**, *628*, 183.
[9] K. O. Christe, J. A. Boatz, M. Gerken, R. Haiges, S. Schneider, T. Schroer, F. S. Tham, A. Vij, V. Vij, R. I. Wagner, W. W. Wilson, *Inorg. Chem.*, in Press.

AFRL-PR-ED-TR-2004-0041, Volume 2
Primary Distribution of this Report:

AFRL/PRSP (3 CD + 2 HC)
Dr. Ashwani Vij
10 E. Saturn Blvd.
Edwards AFB CA 93524-7680

AFRL/PRS (3 CD + 2 HC)
Dr. Robert Corley
5 Pollux Drive
Edwards AFB CA 93524-7048

ERC, Inc. (1 CD + 1 HC)
Dr. Angelo J. Alfano
10 E. Saturn Blvd.
Edwards AFB CA 93524-7680

ERC, Inc. (1 CD + 1 HC)
Dr. Karl O. Christe
10 E. Saturn Blvd.
Edwards AFB CA 93524-7680

Air Force Office of Scientific Research (AFOSR)
Dr. Michael R. Berman (1 CD + 2 HC)
4015 Wilson Blvd.
Arlington, VA 22203

Defense Advanced Research Projects Agency (DARPA)
Mr. Don Woodbury (1 CD + 2 HC)
3701 N. Fairfax Drive
Arlington, VA 22203-1714

AFRL/PR Technical Library (2 CD + 1 HC)
6 Draco Drive
Edwards AFB CA 93524-7130

Chemical Propulsion Information Agency (1 CD)
Attn: Tech Lib (Dottie Becker)
10630 Little Patuxent Parkway, Suite 202
Columbia MD 21044-3200

AFRL/PROI (Public Affairs) (1 CD + 1 HC)
Ranney Adams
2 Draco Drive
Edwards AFB CA 93524-7808

Dr. Alan Garscadden (1 CD + 1 HC)
AFRL/PR, Bldg 18A, 1950 Fifth Street
Area B
Wright-Patterson AFB, OH 45433-7251

Defense Technical Information Center
(1 Electronic Submission via STINT)
Attn: DTIC-ACQS (Pat Mawby)
8725 John J. Kingman Road, Suite 94
Ft. Belvoir VA 22060-6218